N-colour separation methods for accurate reproduction of spot colours

by

Kiran Deshpande

A thesis submitted in partial fulfilment of the requirements of the University of the Arts London for the degree of PhD

May 2015

Abstract

In packaging, spot colours are used to print key information like brand logos and elements for which the colour accuracy is critical. The present study investigates methods to aid the accurate reproduction of these spot colours with the n-colour printing process. Typical n-colour printing systems consist of supplementary inks in addition to the usual CMYK inks. Adding these inks to the traditional CMYK set increases the attainable colour gamut, but the added complexity creates several challenges in generating suitable colour separations for rendering colour images.

In this project, the n-colour separation is achieved by the use of additional sectors for intermediate inks. Each sector contains four inks with the achromatic ink (black) common to all sectors. This allows the extension of the principles of the CMYK printing process to these additional sectors. The methods developed in this study can be generalised to any number of inks. The project explores various aspects of the n-colour printing process including the forward characterisation methods, gamut prediction of the n-colour process and the inverse characterisation to calculate the n-colour separation for target spot colours. The scope of the study covers different printing technologies including lithographic offset, flexographic, thermal sublimation and inkjet printing.

A new method is proposed to characterise the printing devices. This method, the spot colour overprint (SCOP) model, was evaluated for the n-colour printing process with different printing technologies. In addition, a set of real-world spot colours were converted to n-colour separations and printed with the 7-colour printing process to evaluate against the original spot colours. The results show that the proposed methods can be effectively used to replace the spot coloured inks with the n-colour printing process. This can save significant material, time and costs in the packaging industry.

Acknowledgements

List of Publications

Deshpande, K., Green, P.J., MacDonald, L. and Bayley, T. (2009) Gamut prediction of *n*-colour printing processes, *Proc 11th Congress of the International Colour Association (AIC),* Sydney, Australia.

Deshpande, K. and Green, P.J. (2010) A simplified method of predicting the colorimetry of spot colour overprints, *IS&T/SID 18th Color Imaging Conference,* San Antonio, Texas, USA, 213-216.

Deshpande, K. and Green, P.J. (2011) Regression method for predicting the colorimetry of spot colour overprints, *Proc. 38th IARIGAI conf. Advances in Printing and Media Technology*, Budapest, Hungary.

Deshpande, K. and Green, P.J. (2012) Gamut comparison index: a metric for comparing colour gamuts, *AIC Interim Meeting*, Taipei.

Deshpande, K., Green, P.J. and Pointer, M.R. (2014a) Gamut evaluation of an *n*-colour printing process with the minimum number of measurements, *Color Res. Appl.* **40** (4), 408-415.

Deshpande, K., Green, P.J. and Pointer, M.R. (2014b) Metrics for comparing and analysing two colour gamuts, *Color Res. Appl.* doi: 10.1002/col.21930.

Deshpande, K., Green, P.J. and Pointer, M.R. (2014c) Characterisation of the *n*-colour printing process using the spot colour overprint model, *Optics Express*, **22** (26), 31786-31800, Dec. 2014.

Deshpande, K., Green, P.J. and Pointer, M.R. (2014d) Colour separation of *n*-colour printing process using inverse printer models, Proc. *IS&T/SID 22nd Color Imaging Conference,* Boston, Arizona, USA, 194-199.

Dedicated to my mother and father.

Table of Contents

List of Tables

List of Figures

Chapter 1 Introduction

"I don't know anything, but I do know that everything is interesting if you go into it deeply enough." – Richard Feynman, The Pleasure of Finding Things Out.

1.1 Background

The use of an *n*-colour printing process is growing in the printing industry especially in the packaging printing with the flexographic printing process. It is known by different names in the industry, for example, Expanded or Extended Colour Gamut (ECG) printing, Multi-Colour Process Printing (MCPP), High-Fidelity (Hi-Fi) colour printing etc.

Key benefits for the *n*-colour printing include: significant cost savings by reducing the make-ready times due to less wash-ups of the print units, reduction in wastage of materials, higher productivity and efficiency, no need to maintain inventory of special inks, more flexibility for print planning and scheduling. There are also environmental benefits from the reduction of solvent and ink usage and the combining of several jobs into one job to provide additional waste reduction.

1.2 Industrial application and significance

The main drivers for moving from conventional printing to the *n*-colour printing process are to replace spot colours with a fixed set of inks and to leverage the wider gamut to reproduce much brighter and pleasing images. Although the *n*-colour printing process is used in some sectors of the printing and packaging industry, the aim is usually to enhance the vividness of images rather than to replace existing spot colour libraries.
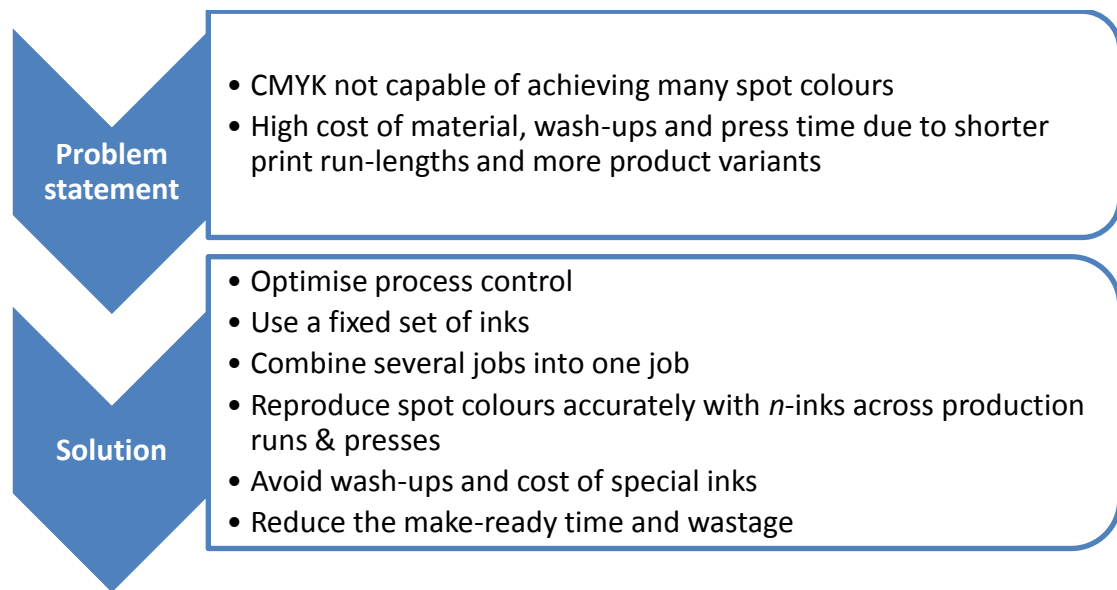
Figure 1.1 Overview of the problem and solution

This project is mainly focussed on the benefit of replacing the solid spot colours and special inks by using the *n*-colour printing process (Figure 1.1). The packaging printing industry is facing new challenges with the arrival of the digital age. Print run-lengths are getting shorter with more product variants like languages, product subcategories and flavours etc. At the same time, brand colour accuracy has become more important due to growing brand competition. This has increased the cost of printing due to more make-readies, wash-ups and materials. The use of *n*-colour printing, with suitable printing technology, can help to reduce the cost by reproducing accurate colours with *n* number of fixed inks.

The packaging printing industry traditionally uses CMYK process colours to reproduce photographic images and spot colours to reproduce large solid areas and critical brand information like logos. Different print jobs use different spot colours. Hence the special inks have to be changed frequently from job to job.

In contrast, *n*-colour printing uses a fixed ink-set consisting of *n* inks to reproduce all the elements in the given print job using a combination of different overprint tints. The spot colours are broken down into tints of process channels (Figure 1.2). This avoids hundreds of special inks, thus saving the ink costs, inventory management and storage in the pressroom. It also allows the combination of several print jobs into one job. This

leads to flexibility in the production planning and job scheduling process which traditionally depends on the job-specific spot colour portfolio, for example, jobs with common spot colours are scheduled together.

An artwork printed

with spot colours

The same artwork converted to

the *n*-colour printing process
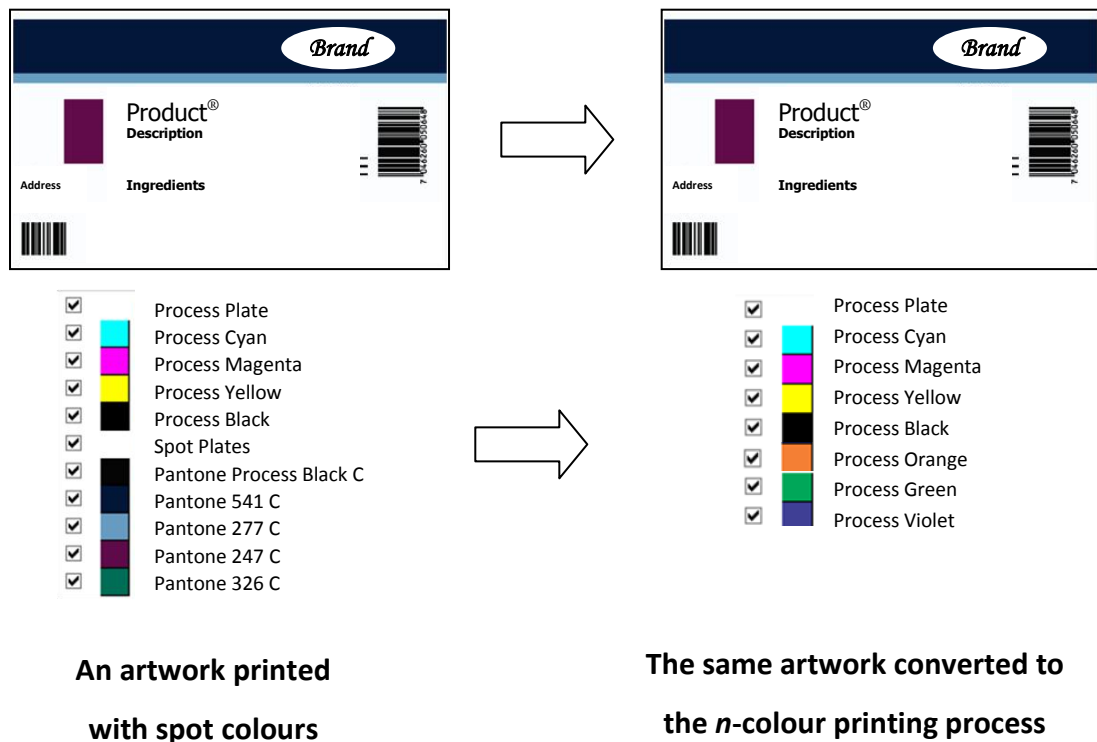
Figure 1.2 Converting a print job containing spot colours to *n*-colour separation

A colour matching system like the Pantone Formula Guides is a colour specification system in which a colour library is used to select colours which are then printed using special inks. They can provide effective communication of colours across the workflow. However, only a fraction of the colours can be reproduced with the traditional CMYK printing process due to its limited colour gamut. By the addition of supplementary intermediate inks to the CMYK set, for example, orange, green and violet, the colour gamut can be extended thus covering more spot colours from the colour matching system (Figure 1.3).

CMYKOGV gamut

CMYK gamut

A sample spot colour library
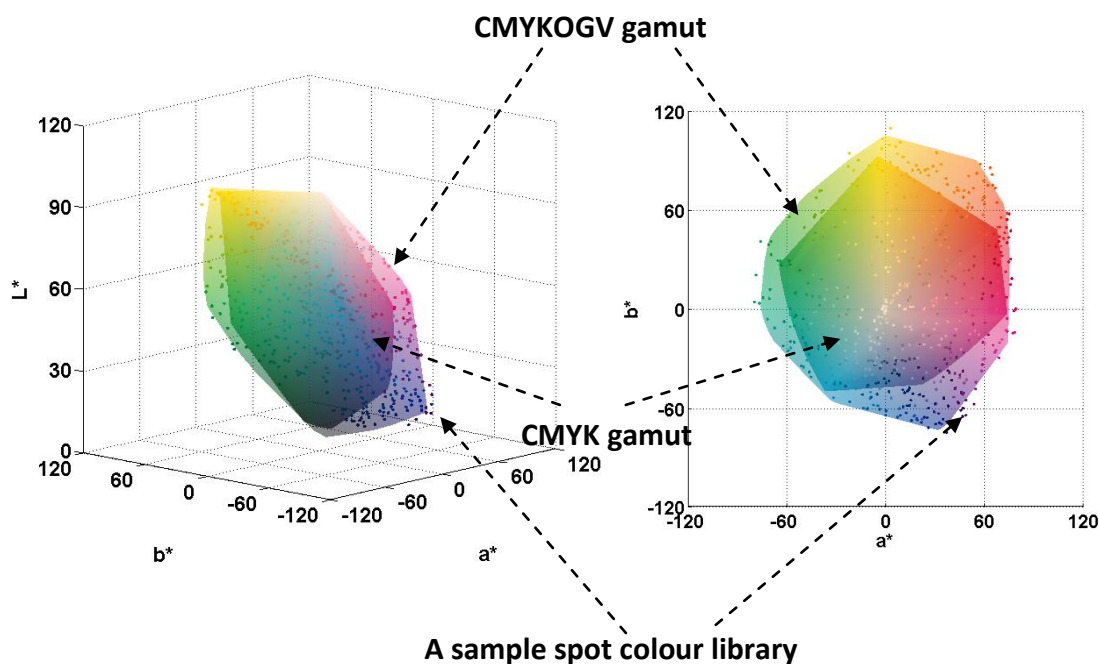
Figure 1.3 Example of the colour gamuts of CMYK and CMYKOGV with the spot colours

The *n*-colour printing process can be used with different printing technologies, for example, lithographic offset, flexography and various digital printing technologies including electrophotography and inkjet printing.

There are several challenges in implementing the *n*-colour printing process in a production environment. Key considerations for real-life implementation for the *n*-colour printing process are discussed in Section 9.2.

1.3   Theoretical context

Since the invention of the four-colour printing process, various problems related to colour separation and colour fidelity of the CMYK printing process have been studied, (Hunt, 1995). Although this conventional process is adequate in most of cases, the colour gamut of typical CMYK inks is restricted as compared with that of display devices.

Printers with just four process inks can produce only a relatively small colour gamut, limiting colour reproduction accuracy (see Figure 1.3). Also, it is very hard to achieve isomeric reproduction (see definition in Section 1.6) using conventional four-colour printing, or even obtain low levels of metamerism (see definition in Section 1.6) for matching colours. Because of the subtractive interaction of ink and incident light, the lighter shades of red, green and blue are hard to achieve with traditional CMYK inks. These lighter shades can however, be obtained by using single inks of the desired hue.

By increasing the number of inks the colour gamut of a printing device can be expanded. The use of additional inks also increases the number of degrees of freedom, thus enhancing the possibility of isomeric matching. These printing systems with additional inks are also referred to as high fidelity (Hi-Fi) colour printing systems. Typical *n*-colour printing systems consist of CMYK plus additional colours such as orange, green, violet, etc. Although adding these inks to the traditional set of CMYK inks increases the attainable colour gamut, the added complexity creates a challenge in generating suitable separations for rendering colour images. (Mahy, 1997a)

Several new colour printing processes have been proposed that use more than four standard inks. (Kueppers, 1989) (Ostromoukhov, 1993) (Boll, 1994) (Viggiano, 1998) (Mahy, 2011) (Morovič, 2012a). Kueppers (1989) suggested a model in which each colour is reproduced with a maximum of three inks (see Chapter 2, Section 2.4). Ostromoukhov (1993) provided an overview of the basic methods of widening a CMYK printing process to a CMYKRGB printing process by modelling the relationship between colour and ink. Boll (1994) used a method of selection of a primary colour to obtain a desired colour in a CMYKRGB system. His technique used a subdivision of the colorant space gamut into smaller subgroups.

In ICC-based colour management, when the number of primary inks is more than three, there is a usual colour management problem of one-to-many mapping. There are more inks than colorimetric co-ordinates: thus a given colour can be matched using more than one combination of inks. This problem has been addressed by dividing the inks into 3-ink subgroups or 4-ink subgroups. (Kueppers, 1989) (Tzeng, 2000). As the colour gamuts of subgroups overlap, it is difficult to find a single colorant combination. In

addition, smoothness of tonal gradations in an image is affected due to abrupt ink changes when the gradation crosses the colour gamut boundary of two subgroups.

Major attempts have been made to exploit spectral printer models (see definition in Section 1.6). Researchers have developed and evaluated spectral models using multiple printing inks to make a reasonable spectral match (Tzeng, 1998 & 1999) (Taplin, 2001) (Chen, 2004a & 2004b) (Zuffi, 2005) (Gerhardt, 2006). These models were based on criteria such as minimising metamerism and increasing colour constancy. The spectral models represent significant advancements in the multi-colour separation field, but they are complex and the inversions of the models are computationally expensive.

To find the relationship between colorant amounts and colorimetric quantities, a characterisation model has to be developed. However, it is difficult to derive a physical model that accurately predicts how arbitrary inks will interact when printed together using halftoning. In addition to optical effects, the model must take into account physical effects such as dot gain and trapping. Also the colour gamuts produced by multi-colour inks have irregular, non-convex shapes (Stollnitz, 1998b). Morovič (2007) proposed a method for computing a gamut of arbitrary n inks.

Most models of colour halftone printing are based on the equations of Neugebauer published in 1937. These physical models, for example, Neugebauer, Beer-Bouguer, Kubelka-Munk, and Clapper-Yule etc. have been well described by Green (2002).

Taplin (2001) tested the Yule-Nielsen modified spectral Neugebauer (YNSN) model. It has been shown that the YNSN model and its cellular extension can improve the model accuracy significantly (Rolleston, 1993) (Bastani, 1996). Tzeng (1999) used Kubelka-Munk turbid media theory for translucent inks printed on top of a highly scattering support. Emmel and Hersch (1999, 2002) introduced new models that describe the light scattering and ink spreading phenomena. They incorporated all physical phenomena into a single model using a mathematical framework based on matrices (see Chapter 2, Section 2.2.1.10 for more details).

The printer characterisation model provides the tristimulus values of colours as a function of the ink amounts; when computing colour separation it is necessary to find the ink amounts as a function of the tristimulus values that define the colour. This inversion is not a simple process, since the model is a non-linear function of the ink amount. In addition, it is more difficult for n-colour separation because there may be many ink amount values that yield the same colour. Thus a robust separation method for 'n' arbitrary inks is needed.

Ideally the n-colour separation should be context-aware and dynamic. For example, a colour separation strategy used for reproducing a company logo with a solid brand colour should be different from a strategy used for reproducing a photographic image. Depending on the range of tonal data in a graphic element, the n-colour separation algorithm should adopt the best suitable approach. This project aims to reproduce solid spot colours using a method of n-colour separation to provide an accurate colour separation algorithm.

The existing techniques of the n-colour separations are either not capable of reproducing the spot colours accurately and consistently or they are too complex and computationally expensive to be used in the print workflow. Hence a simpler and more robust solution is needed that gives effective reproduction of the spot colours.

In packaging, spot colours are predominantly used for printing solid elements like brand logos and identities rather than the tints and the overprints. The present study is mainly aimed at replacing the solid spot colours with the n-colour printing process (Figure 1.4). Although the tints and overprints are considered, the main focus is on reproducing the solid spot colours. This is a different use case from that of an image reproduction using the n-colour printing process, where other criteria emerge such as avoidance of contouring in blends. Contouring could be an issue in spot colour reproduction as well, if the designer has included such spot blends in the artwork. However, there are several market sectors within the packaging industry, where the spot colours are almost exclusively used for printing solid elements, for example, ethical pharmaceutical packaging.
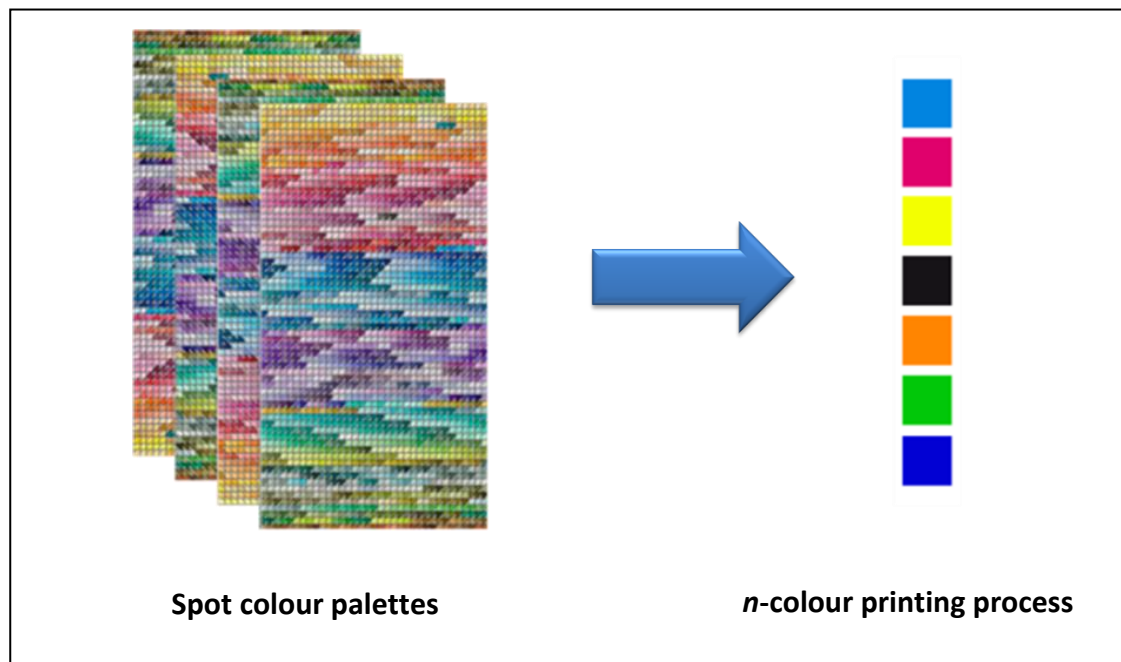
Figure 1.4 Objective of the project: to replace a potential palette of many spot colours with the *n*-colour printing process using a relatively small number of inks.

1.4   Thesis overview

The outline of the thesis is as follows. The second chapter presents an overview of the essential fundamentals of colour science; it presents method for the characterisation of the printing devices and also describes previous work related to *n*-colour separation. Chapter 3 describes the metrology, reproduction workflow, computation procedures and the process control requirements used in this study.

Chapter 4 discusses the implementation of the forward spectral printer models for the conventional 4-colour printing process and then the 7-colour printing process, along with their results. Chapter 5 explains the gamut prediction and analysis of the *n*-colour printing process using spectral printer models. A new set of metrics, including the Gamut Comparison Index (GCI) is proposed to quantify the difference between two gamuts. Chapter 6 describes the spot colour overprint model, which is proposed as a simplified printer model for forward characterisation.

Chapter 7 deals with the implementation of the inverse printer model to obtain 7-colour separation. Various approaches are compared to reproduce the spot colours using a 7-colour printing processes. In Chapter 8, the n-colour separation is evaluated using a number of real-life spot colours. This was done by quantitative evaluation using instrumentally measured colour difference values and qualitative evaluation using a psychophysical experiment. Finally Chapter 9 summarises the results and the contribution of this study. The key considerations for real-life implementation, the production strategies and the future work are discussed.

1.5   Key contributions

This study explores many facets of the n-colour printing process with the aim of reproducing spot colours using n-colour separation.

- Several spectral printer models were implemented and evaluated for the n-colour printing processes using different printing technologies.
- A new simplified printer model was developed for characterising printing devices. The spot colour overprint (SCOP) model was evaluated using the n-colour printing process. Due to lower computation cost, this model can be integrated into existing standard workflows in the printing industry
- The colour gamut of the 7-colour printing process was predicted using the minimum number of input measurements and used to obtain the colour separations. The methods used for gamut prediction and evaluation are useful when selecting the optimum ink-set for the n-colour printing process and to compare the n-colour printing gamut against the proofing system.
- The inverse printer models were evaluated to estimate the colour separation for the 7-colour printing processes. An algorithm consisting of modular functions was developed for deriving the colour separation for the target spot colours.
- A set of brand colours were converted to 7-colour separations using the algorithm and printed by lithographic offset printing. A psychophysical experiment was performed to determine the perceptibility and acceptability thresholds of the reproduced colours.

- Analysis showed that the proposed methods can be used successfully for accurate reproduction of brand colours using *n*-colour printing processes resulting in substantial cost savings in terms of the production time and materials.

1.6 Terminology

Colour separation – the process by which an original colour artwork or image is decomposed into individual single-colour components for printing using primary inks, for example, CMYK or CMYKOGV inks.

Colour gamut of printing system: the range of colours that can be reproduced by the printing system.

CMYK: a set of 4 inks – cyan, magenta, yellow and black – used traditionally as process inks for printing.

CMYKOGV – a printing process used as an example of the *n*-colour printing process that uses 7 inks – cyan, magenta, yellow, black, orange, green, violet. The methods described can be generalised to any *n*-colour printing process.

Forward printer characterisation model – a model defining the relationship between the colorant (ink) values and the colorimetric values (for example, CIELAB) of the measured printed colour.

Spectral printer model – A forward printer characterisation model which uses spectral reflectance instead of colorimetric values.

Gamut mapping: a method of mapping the colours lying outside the colour gamut of the printing system onto the colour coordinates that are within the colour gamut.

Intermediate inks – additional primary inks used in the *n*-colour printing process to supplement the CMYK process inks, for example, orange (or red), green and violet (or blue).

Inverse printer characterisation model – a model which provides a colour separation of an original colour artwork or image by mapping the device-independent colour values to ink values for a given viewing condition.

Isomeric reproduction – identical reproduction of the spectral reflectance curve of the original colour.

Metamerism – phenomenon of matching of colour stimuli which have different spectral reflectance curves.

***N*-colour printing process**: a printing process with more than 4 process inks usually with the intermediate hues like orange, green, violet etc. It is known by many names, for example, High-Fidelity (Hi-Fi) printing, Extended or Expanded Colour Gamut (ECG) printing, Multi Colour Process Printing (MCPP), fixed palette printing etc.

Printing process: a process of reproducing visual information like text and images by using colorants onto a substrate.

Printing system: a set of printing conditions including printing device, imaging method, substrate, inks and consumables.

Printing technology: different techniques of reproducing visual information by placing a colorant on to a substrate in a controlled manner. For example, lithographic offset printing, flexography, thermal sublimation printing, electrophotography, inkjet printing etc.

Simulated spot colours: spot colours reproduced using an *n*-colour printing process.

Special inks or spot coloured inks: inks used for printing spot colours.

Spot colour or brand colour: a colour printed with its own pre-mixed ink instead of the process inks. These are usually critical colours or brand colours used in packaging.

Chapter 2 Literature Review

2.1 Colorimetry and colour measurements

2.1.1 Human Vision

The human visual system is crucial to our understanding of the perception of colour. It depends on the stimulation of light sensitive cells, known as photoreceptors, in the eye. Light consists of electromagnetic radiation. The visible portion of the electromagnetic spectrum is in the wavelength range of approximately 380 nm to 780 nm. An image is formed in the human eye when light enters the pupil and is imaged onto in the retina, the location of the photoreceptors. These receptors generate signals which are transmitted to the brain via the optic nerve. There are two types of photoreceptors in the retina; rods and cones. Rods are active under low levels of illumination and do not provide wavelength discrimination; thus they provide monochromatic vision and record information about brightness. In humans, there are three types of cones. The cones which are sensitive to long wavelength light are called L cones, those sensitive to medium and short wavelength light are called M cones and S cones respectively.

2.1.2 Colour vision theories

The function of colour vision can be explained by two theories. Trichromatic theory, which is also known as Young-Helmholtz three-component theory (Gordon, 2004) suggests that there are three independent sets of receptors from which signals are transmitted directly to the brain i.e. the cones (L, M and S) are sensitive to (approximately) red, green and blue light. But this theory cannot explain many visually observed phenomena. A complementary theory, the opponent colour theory, was proposed by Hering in 1878 (Gordon, 2004). According to this theory, the human eye distinguishes colours based on pairs of two opponent colours, red-green, yellow-blue and black-white. These opponent colours cannot be perceived to occur together. Both trichromatic and opponent-colours theories are combined in modern opponent-colours theory to explain most visual phenomena.

2.1.3   Colorimetry and CIE system

Modern colorimetry is aimed at modelling the human perception of colour (Green, 2002). It provides the basis for predicting the visual match between two colour stimuli. In 1931, the CIE (Commission Internationale de l'Eclairage), the International Commission on Illumination, established a colour specification system. The 1931 CIE system is derived from a series of colour-matching studies to define a *standard observer*. Two scientists, Wright and Guild, performed quite separate colour-matching experiments to describe a series of colour stimuli in terms of the amounts of three matching stimuli required to match them (Berns, 2004). The trichromatic properties of human vision were characterised using these colour-matching experiments.

Figure 2.1 shows a simple set up of a colour-matching experiment. A small circular field is split into two parts. One half of this visual field is illuminated by a test colour and other half by a combination of primary colours (red, green and blue). The observer is asked to adjust the intensities of the three primary colours in order to obtain a visual match between test colour and the mixture of primary colours. A set of three curves derived from these experiments are called the RGB colour-matching functions denoted by $\bar{r}(\lambda)$, $\bar{g}(\lambda)$ and $\bar{b}(\lambda)$.
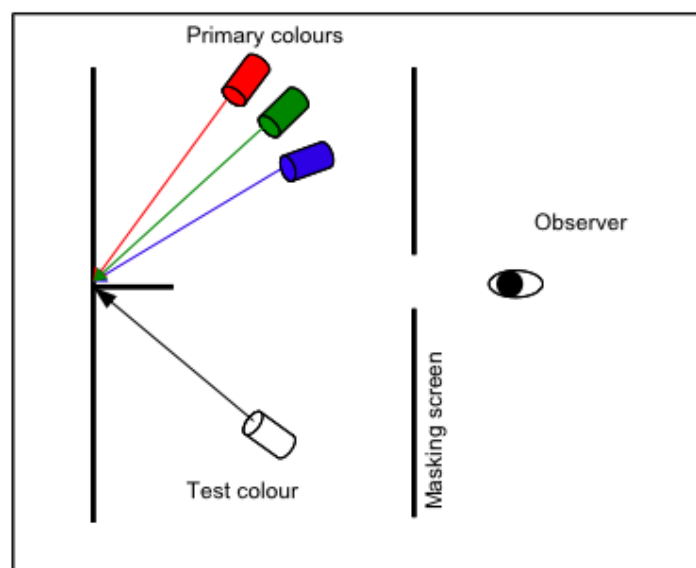
Figure 2.1 Colour matching experiment set-up

Some of the test colours had to be matched by adding one or more primaries to the test colour. The primary light added to the test colour is considered to be subtracted from the mixture of the primaries, thus resulting in negative tristimulus values. But there is no convenient way of accurately introducing the negative sensitivities in practice (Hunt, 2004). To avoid the negative values and to reduce the complexity, the RGB colour matching functions were mathematically transformed into all-positive colour matching functions $\bar{x}, \bar{y}$ and $\bar{z}$ (Figure 2.2). They are known as the CIE 1931 standard colorimetric observer for 2° angular sub tense of vision.
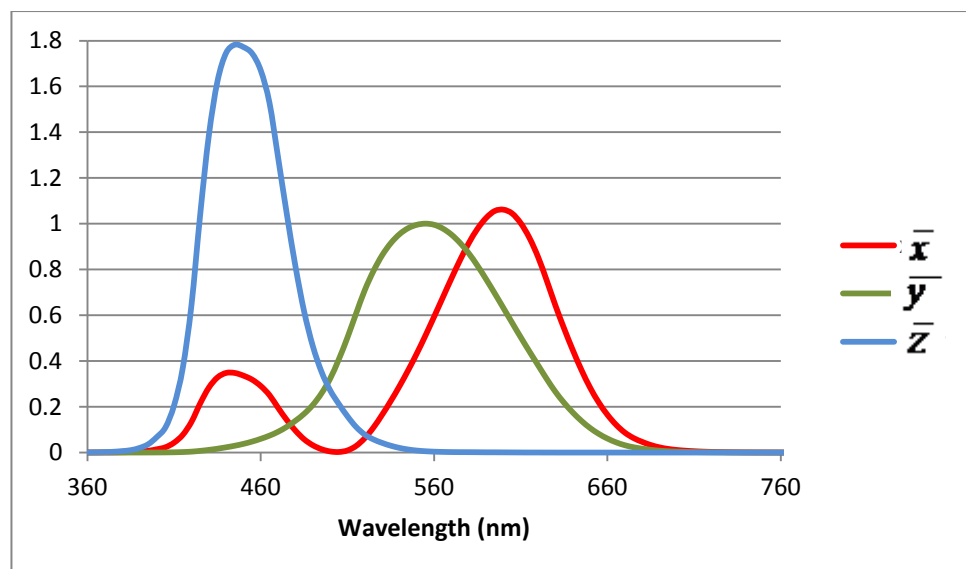
Figure 2.2 Colour matching functions for the CIE 1931 Standard Observer

The tristimulus values *X*, *Y* and *Z* are calculated by summing the product, with respect to wavelength, of the following three components: light source, object and colour-matching functions. The light source is represented by the spectral power distribution measured across the visible spectrum. Objects are characterised using spectral reflectance or transmittance. The CIE standard observer provides the colour-matching functions.

Thus a colour stimulus can be represented using tristimulus values (CIE, 1986) as follows:

$$X = k \sum_{\lambda=380}^{780} \bar{x}(\lambda)S(\lambda)R(\lambda)$$

$$Y = k \sum_{\lambda=380}^{780} \bar{y}(\lambda)S(\lambda)R(\lambda)$$

$$Z = k \sum_{\lambda=380}^{780} \bar{z}(\lambda)S(\lambda)R(\lambda)$$

(2.1)

where $S(\lambda)$ is the spectral power distribution of a light source, $R(\lambda)$ is the spectral reflectance (or transmittance factor $T(\lambda)$) of the colour stimulus and $\bar{x}, \bar{y}$ and $\bar{z}$ are the colour matching functions. k is a normalising constant given by

$$k = \frac{100}{\sum_{\lambda=380}^{780} \bar{y}(\lambda)S(\lambda)}$$

(2.2)

Tristimulus values *X*, *Y* and *Z* are loosely analogous to red, green and blue. A significance of CIEXYZ system is that the *Y* tristimulus value corresponds to the luminance factor of colour stimulus; thus it can be correlated to visual perceptual attribute lightness. For measuring light sources and self illuminating colours, if we set *k* = 683, then the *Y* tristimulus value is the luminance. This is because the maximum luminous efficacy of monochromatic radiation is 683 lumens/watt at 555 nm, which is the wavelength of the eye's maximum response. The luminance is expressed in units of candela per square meter (cd/m^2). The candela is defined as the luminous intensity in a given direction, of a source that emits monochromatic radiation of frequency 540×10^{12} hertz and that has a radiant intensity in that direction of 1/683 watt per steradian (Ohta, 2006). For measuring reflective colours, the value of *k* is chosen so that *Y* = 100 for the given reference white point.

The *XYZ* values can be normalised to derive chromaticity co-ordinates as follows:

$$x = \frac{X}{(X + Y + Z)}$$

$$y = \frac{Y}{(X + Y + Z)}$$

$$z = \frac{Z}{(X + Y + Z)}$$

(2.3)

From this it follows that the chromaticity of any colour sample is described by *x* and *y* values; value of *z* can be obtained using (1-*x*-*y*). To include the luminance (or luminance factor), colours are described using the *xyY* triplet. A chromaticity diagram (Figure 2.3) can be used to plot *y* versus *x* plot to provide a two-dimensional map of colour space.

The horseshoe-shaped outline is called as the spectrum locus which represents chromaticity of monochromatic light at different wavelengths sequentially through the spectrum. A straight line joining the end points of spectrum locus is called the purple boundary. These are purple colours which cannot be produced using a single wavelength of light.
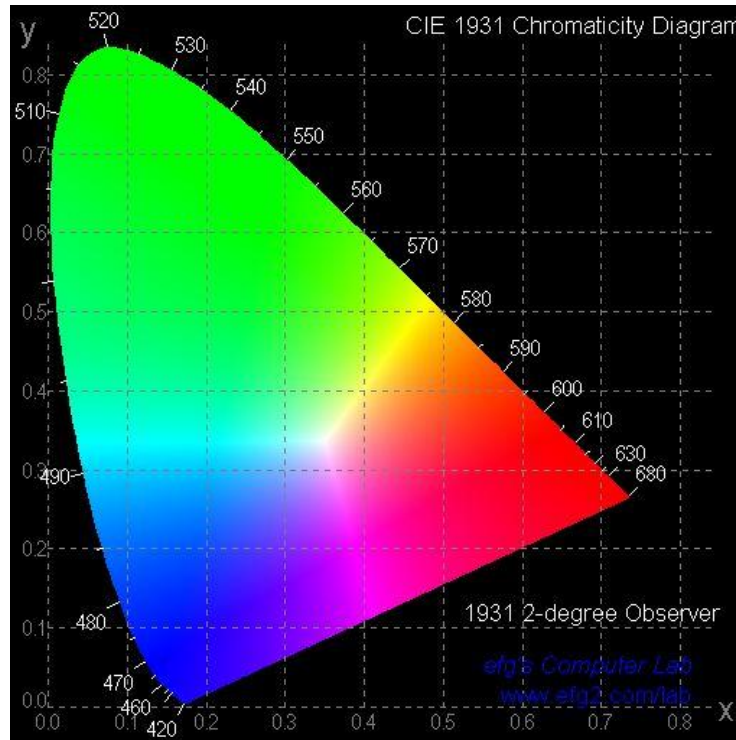
Figure 2.3 CIE 1931 Chromaticity diagram (Glynn, 2007)

A disadvantage of *XYZ* colour space is that it is not perceptually uniform. Colours with an equal perceptual difference are not equidistant in the chromaticity diagram. In 1976, CIE tried to develop a visually uniform colour space (UCS) by mathematical transformations of *XYZ*. These are known as CIE 1976 *L*u*v** colour space and CIE 1976 *L*a*b** or CIELAB colour space.

In CIELAB space (Figure 2.4), *a** and *b** are chromatic axes corresponding approximately to green-red and blue-yellow colours. Lightness is represented by *L** axis from white (100) to black (0). Chroma (*C**) and hue (*h**) can be calculated from *a** and *b** values. One of the benefits of the CIE system is that any CIE colour space can be converted to any other space because they are all based on CIE XYZ tristimulus values. Although, the CIE 1931 system simply predicts colours that match in a specified viewing condition, it is adequate for the purpose of this research. If two sets of tristimulus values match, the appearance is expected to match as long as the viewing conditions are identical (Hunt, 2004). Throughout this research, spot colours are assessed using ISO 3664 (2009) viewing conditions.

Though CIELAB colour space has better perceptual uniformity than CIE XYZ space, it is not completely perceptually uniform. It has been observed that CIELAB is non-linear in blue-purple region. Colours along a straight hue-angle line may not have a constant hue particularly in the blue region (Fairchild, 2005).

Figure 2.4 CIELAB 1976 colour space (MacEvoy, 2005)
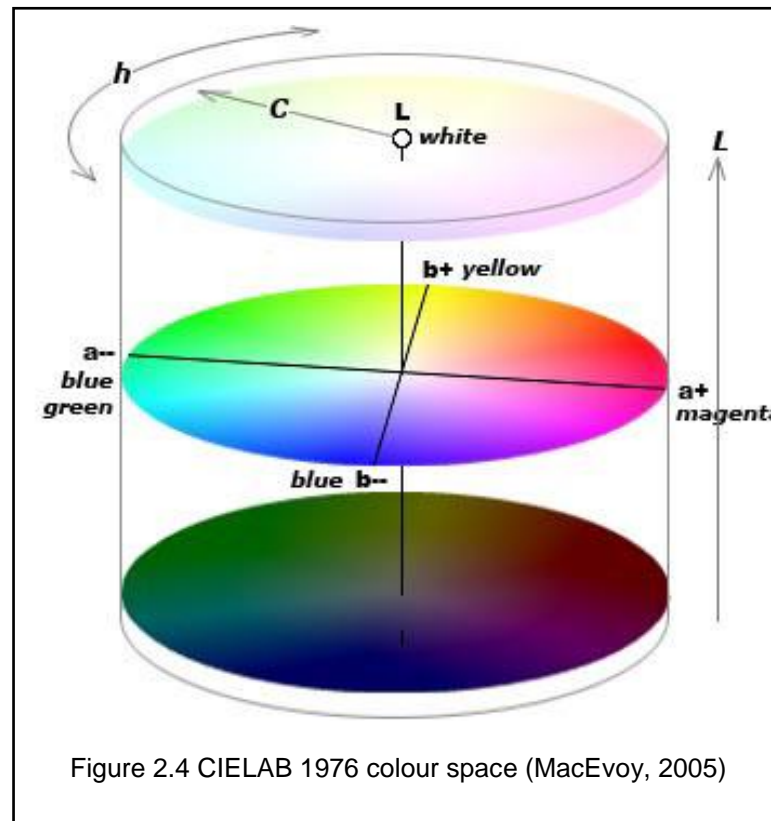
2.1.4   Colour Difference

The difference between two colours can be specified numerically using their *L*a*b** or *L*C*h** values. As the CIELAB colour space was designed to provide a perceptually uniform colour space, the Euclidean distance between two-colours in CIELAB space gives the colour difference ΔE^*_{ab}, as follows:

$$\Delta E_{ab} = \sqrt{((L_1 - L_2)^2 + (a_1 - a_2)^2 + (b_1 - b_2)^2)}$$

(2.4)

where L_1, a_1, b_1 represent the reference colour and L_2, a_2, b_2 represent the sample colour.

However, the uniformity of CIELAB space is not perfect. This colour difference ΔE^*_{ab} performs better in some parts of the colour space than in others. In order to correlate with the perceptual difference, the colour difference can be better represented as an ellipsoid rather than a sphere. Perceived colour difference is also influenced by viewing conditions as well as material characteristics, for example, gloss, texture etc.

To overcome the limitations of non-uniformity in the 1976 CIE spaces, new colour difference equations have been derived. These advanced equations are based on weighted components of the colour difference equation.

The Colour Measurement Committee (CMC) of the Society of Dyers and Colourists (SDC) used a colour difference metric ΔE^*_{CMC} based on the experiments of colour matching for the textile industry. The lightness and chroma weightings (*l* and *c*) were incorporated to improve the acceptability predictions (Clarke, 1984). The ratio of lightness to chroma weightings can be changed according to acceptability criteria.

CIE Technical Committee TC 1-29 proposed the new equation ΔE^*_{94} similar to ΔE^*_{CMC} (CIE, 1995). Weighting functions in this formula were found empirically from experiments with automotive paints. Parametric factors like illuminant, background, illumination, sample size, sample separations etc. were defined as references; but these could be changed to suit different parametric conditions.

A hue-chroma interaction term was added to ΔE^*_{94} to give a new equation CIEDE2000 also known as ΔE^*_{00} (Luo, 2001). Over-predictions of lightness differences in light and dark colours were accounted for in CIEDE2000 by varying the lightness weighting function according to the L^* value. This colour difference formula has been used throughout the project (see 3.1 and Appendix A: CIEDE2000 calculations).

The CIEDE2000 formula is more complex than other colour difference formulae particularly ΔE^*_{ab}, which is simple and conventionally used in industry. However, the CIEDE2000 formula provides a better correlation with perceived colour difference especially in the blue region of colour space (Luo, 2001) (Wang, 2012). The CIEDE2000 does not have its own colour space, but it is a local distortion of Euclidean

space, i.e. CIELAB colour space. It is only applicable for small colour differences (Sharma, 2005). This is a subject of ongoing research. Presently the CIEDE2000 offers significant improvement over other formulae.

Various studies were carried out to test these advanced colour difference equations (CIE, 1993) (Mahy, 1994) (Luo, 1996) (Guan, 1999). Some experiments investigated acceptability in colour difference (Green, 2000) (Song, 2000). It was found that the weighting functions derived from <u>perceptibility</u> data may not be linearly applicable for predicting <u>acceptability</u> limits.

The present research simply attempts to match colours using the *n*-colour printing process; hence colour appearance is not an issue. But acceptability in colour difference is considered as important. For example, whether a difference between the desired colour and the colour printed using *n*-colour separation is commercially acceptable or not. See Section 8.3 for more details.

2.1.5   Colour Measurement

The aim of colour measurement is to quantify the visual perception of colour in order to describe it objectively. A colour measuring instrument defines colour numerically in terms of colour attributes. Colour measurement plays a key role in colour management, for example, calibration and characterisation of a printing device, measuring colour difference between sample and proof, formulation of special inks, etc.

A colour perception phenomenon is based on three components: light source, object and viewer i.e. the human eye. Light consists of electromagnetic radiation having a wavelength range from approximately 380 nm to 780 nm. A colour is measured as an amount of radiation reflected or transmitted from a colour stimulus over the specified wavelength range. The tristimulus values can then be calculated by multiplying the spectral reflectance (or transmittance) factor of the colour sample by the spectral power distribution of the light source and the colour matching functions.

Several substrates used in practice exhibit fluorescence since they contain optical brightening agents (OBA). They absorb ultraviolet radiation at wavelength below 400 nm and emit light in the blue region of visible spectrum. Sometimes inks used for printing are fluorescent. Also the light sources used in viewing booths vary with respect to UV content. As a result the colour measurements become ambiguous and the perceived colour may look different. ISO 13655:2009 specifies four measuring conditions appropriate for different applications when substrates or ink (or both) fluoresce.

CIE has developed a number of standard illuminants based on their relative spectral power distributions. These illuminants can be described in terms of their correlated colour temperature (CCT). The CCT of an illuminant can be defined as the colour temperature of a black body radiator that appears to be the closest colour match to the illuminant. The relative spectral power distribution of an illuminant is related to its correlated colour temperature. Figure 2.5 shows the relative spectral power distributions of some recommended CIE illuminants including illuminant A representing a tungsten lamp operating at 2856K, D65 representing one of the phases of daylight with a CCT of 6500K. In the graphic arts industry, illuminant D50 (with a CCT of approximately 5000K) is the recommended viewing illuminant (ISO 3664:2009). One of the problems with the CIE illuminants is that they are not real light sources; in practice they have to be simulated (Hunt, 1998).
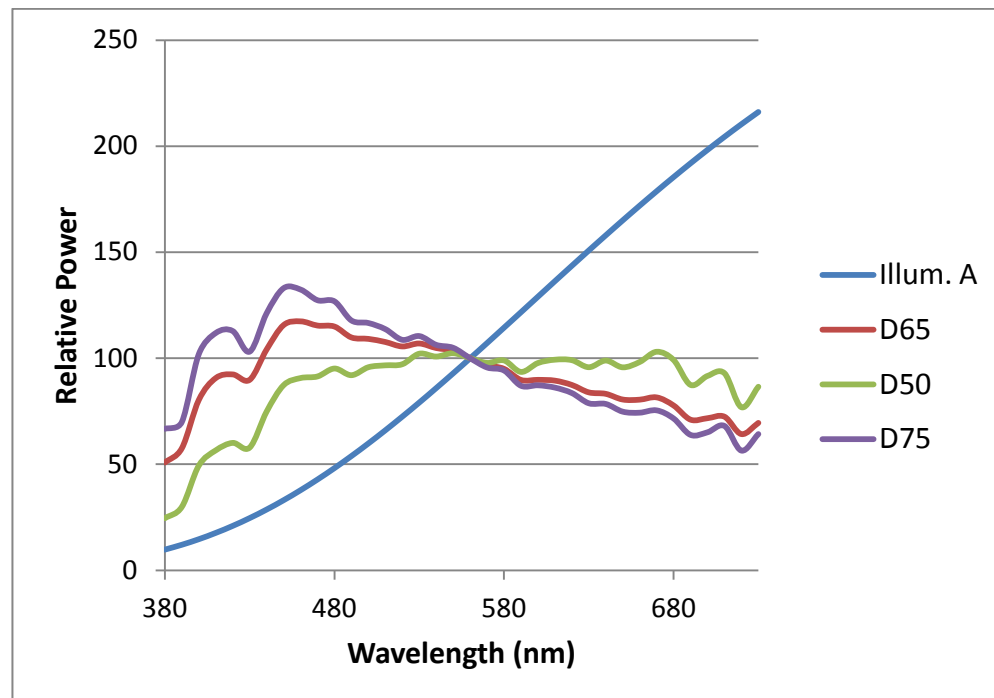
Figure 2.5 Relative spectral power distribution of different CIE illuminants

One important aspect of colour measurement is the geometry of the incident and reflected light and one of two geometries are most commonly used. If the sample is illuminated with a light source at 0° to the surface normal then the reflected light can be measured at 45° to the surface normal. The reverse geometry is equally applicable. These are denoted 0°:45° and 45°:0° geometry respectively. Another geometry is 0°: diffuse in which the sample is illuminated with a light source at 0°. The reflected light is then diffused by using a highly reflective sphere and this diffused light is sampled with a detector. In practice, 0° geometry is replaced by 8°. (Johnson, 1995)

Different types of instruments can be used for colour measurement: densitometers, colorimeters, spectrophotometers, spectroradiometers etc. Densitometers are used to measure density – the logarithm of opacity. In the case of reflectance measurement, density represents the degree to which light is absorbed by the sample. Although densitometers have a limited use in colour measurement, they have been conventionally used for calibration and process control in the pre-press and pressroom areas of the graphic arts industry.

A colorimeter works on a similar principle to the human eye. It has three filters which produce colorimetric values CIE XYZ, which can be converted to other spaces, for example, CIELAB. Though they are flexible, they do not measure spectral data and hence are inadequate for colour matching across different media as well as for spectral matching. A spectrophotometer measures the spectral reflectance across the entire visible spectrum by sampling the spectrum into a series of equally defined band pass, for example, 5 nm or 10 nm intervals. This is important for many applications, such as the assessment of metamerism and the calibration of a printing device for different illuminants. If two colours match one another but differ in spectral composition then it is called as a metameric match. If the spectral reflectance curves of the two colours are identical then it is called a spectral match (Hunt, 2004). For spot colour reproduction, spectral match is becoming more desirable.

A spectroradiometer explicitly measures the radiant power of a colour stimulus as a function of wavelength. Spectroradiometers can produce high colorimetric accuracy and are helpful for the measurement of colours on displays.

Among all these instruments, spectrophotometers are the most commonly used instruments in the graphic arts industry at present.

2.1.6 Uncertainty of colour measurement

Uncertainty in the measurement is inevitable and should not be ignored. ISO 15790 (2000) defines the measurement uncertainty as a parameter, associated with the result of a measurement, that characterises the dispersion of the values that could reasonably be attributed to the measurand.

Every measurement has an associated uncertainty, the causes of which include repeatability, reproducibility, accuracy compared with a calibrated set of measurements, wavelength errors, polarisation effects, geometry errors, etc. The main contributors to measurement uncertainty in any spectral instrument are the instrument repeatability, and the difference between the measurements of a set of calibrated artefacts compared with those obtained by a calibration laboratory.

Sources of variation in colour measurement can be classified into two categories: variations arising from the method of computation and those attributed to the instrument and the colour sample (Green, 2003). Sources related to the computation method are different data interpolation and abridgement techniques. Instruments can cause variation because of their different measurement geometries, bandwidths, wavelength ranges, aperture sizes etc. If the colour sample contains a fluorescence component then some of the incident light is absorbed and re-emitted at a different wavelength. In such cases, measurement is dependent on the amount of ultraviolet (UV) in the light source of the instrument as well as the quantity of optical brightener in the substrate and/or ink. Other sources of uncertainty include variation in specular reflection, polarisation, sample backing etc. Gardner (2000) derived an analytical expression for uncertainty in the measurement and provided a method of uncertainty analysis.

2.2   Characterisation of printing devices

For the conversion of a colour specification from one imaging device to another it is important to define a model of the relationship between CIE colour space and device colour space (Figure 2.6). Numerous methods have been developed for this colour space conversion process. These methods can be grouped into three categories as follows (Green, 2002):

Physical models: These describe the physical properties of the output device, for example, the reflectance, the absorbance of colorant and that of the substrate. Relatively few measurements are needed to predict the colour specifications.

Numerical Models: These are based on the correlation between colour spaces obtained through a set of simultaneous equations. A polynomial regression method is often used to derive the coefficients of the equations.

Three dimensional look-up tables (LUTs): A colour space is divided into small cells. The source and destination colour specifications are found empirically for all co-ordinate points. To locate a non-lattice point, interpolation is required.

These methods differ in terms of the number of input measurements required and the accuracy achieved. Usually the trade-off between the results of these methods is the amount of measurement required to populate the model against the accuracy it achieves.
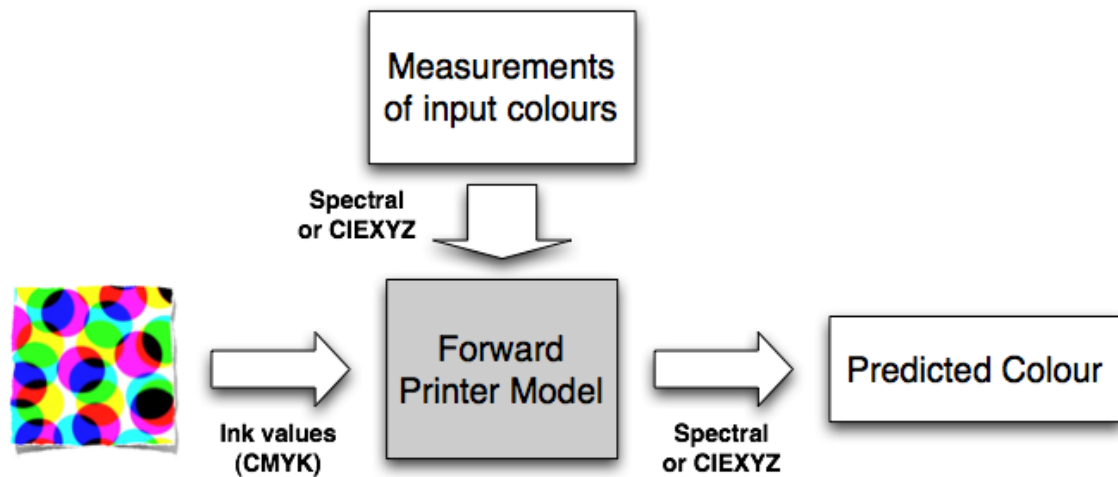
Figure 2.6 Forward printer characterisation model

2.2.1   Physical Models

Physical models for printers use the physical properties to predict colours for example, the reflectance, the absorbance and the scattering of the ink and the substrate. Some physical models represent the relationship between reflectance and dot area.

These models can be sub-divided into two types. Models based on the halftone printing process including the Neugebauer model, the Yule-Nielsen model, etc. and models based on the subtractive principle including the Beer-Bouguer law, Kubelka-Munk theories, etc. Normally an empirical component is required to use these models. Thus a number of colour patches are required to be printed and measured. The measured data can be used as input to facilitate the models.

2.2.1.1   The Murray-Davies Model

This physical model (Yule, 1967) derives the reflectance or output density from input dot area. In a unit area, if the reflectance of the solid ink is R_s, then the absorption by halftone dots is $(1-R_s)$ weighted by A, the dot area coverage. The reflectance factor of the halftone area, R is given by:

$$R = R_w - A(R_w - R_s)$$

(2.5)

where R_w is the reflectance of the paper. If the above equation is expressed in terms of density by using the relationship between density and reflectance, then the density of the halftone area is given by:

$$D = -\log(R)$$

(2.6)

Thus the area coverage can be written as:

$$A = \frac{(10^{-D_w} - 10^{-D})}{(10^{-D_w} - 10^{-D_s})}$$

(2.7)

where D_w is the density of the paper white and D_s is the density of the solid ink. If the density of paper white, D_w is normalised to 0 then this equation becomes

$$A = \frac{(1 - 10^{-D})}{(1 - 10^{-D_s})}$$

(2.8)

This equation is generally used to find the dot area by measuring the reflectance values of the solid and halftone area.

The spectral form of Murray-Davies equation can be represented as

$$R(\lambda) = R_w(\lambda) - A(R_w(\lambda) - R_s(\lambda))$$

(2.9)

where λ is a wavelength in the visible range.

This model is the basis for dot area calculation, which is an important step in the printer characterisation process.

2.2.1.2 The Neugebauer Model

Hans Neugebauer proposed a colour mixing model for halftone reproduction in 1937 (Yule, 1967). He found that for 3-colorant system, there are eight dominant colours - also known as the Neugebauer Primaries - which form the halftone print. For CMY these are: white, cyan, magenta, yellow, red, green, blue and black. These primaries correspond to the colorants, and two and three colour overprints of those colorants C, M, Y on to paper white (W).

This model considers the halftone reproduction as an additive process under which, the reflectance of a print is the sum of all eight colours weighted by the corresponding area coverage.

For a three-colorant (CMY) printer the Neugebauer equation defines the total reflectance, R as:

$$R = A_w R_w + A_c R_c + A_m R_m + A_y R_y + A_r R_r + A_g R_g + A_b R_b + A_k R_k$$

(2.10)

where A is the relative area covered by the indicated primary, R is the reflectance of the solid ink and suffixes w, c, m, y, r, g, b and k designate the paper white, the primary colours (cyan, magenta, yellow), the secondary colours (red, green, blue) and 3-colour overprint, respectively.

The Neugebauer model describes the colour mixing by predicting the resulting reflectance for any set of primaries, for example, tristimulus values *XYZ*:

$$X = A_w X_w + A_c X_c + A_m X_m + A_y X_y + A_r X_r + A_g X_g + A_b X_b + A_k X_k$$

$$Y = A_w Y_w + A_c Y_c + A_m Y_m + A_y Y_y + A_r Y_r + A_g Y_g + A_b Y_b + A_k Y_k$$

$$Z = A_w Z_w + A_c Z_c + A_m Z_m + A_y Z_y + A_r Z_r + A_g Z_g + A_b Z_b + A_k Z_k$$

(2.11)

Neugebauer used a model by Demichel (Yule, 1967) to determine the relative area of each of the eight component colours. According to Demichel's equations, these areas are obtained from the halftone dot areas of cyan, magenta and yellow as follows:

$$A_w = (1 - a_c)(1 - a_m)(1 - a_y)$$

$$A_c = a_c(1 - a_m)(1 - a_y)$$

$$A_m = a_m(1 - a_c)(1 - a_y)$$

$$A_y = a_y(1 - a_c)(1 - a_m)$$

$$A_r = a_m a_y(1 - a_c)$$

$$A_g = a_c a_y(1 - a_m)$$

$$A_b = a_c a_m(1 - a_y)$$

$$A_k = a_c a_m a_y$$

(2.12)

where a_c, a_m and a_y represents the fractional area coverage of the cyan, magenta and yellow inks respectively. A_w, A_c, A_m, A_y, A_r, A_g, A_b, A_k denote the relative areas of the substrate, cyan, magenta, yellow, red (magenta-yellow overlap), green (cyan-yellow overlap), blue (cyan-magenta overlap) and black (cyan-magenta-yellow overlap), respectively.

Demichel's equations assume that the probability of finding all inks at a given point is the product of their individual coverage fractions (Viggiano, 2005). These equations can be used if the dot placement on the substrate is statistically independent. In this case, the dot overlap is the product of the individual fractional coverages of inks. The Demichel model fails when the dot placements are at the same angle; it is valid for rotated halftone screen as is usually the case and for the frequency modulated (FM) screens.

In practice, it is more useful to obtain the amounts of CMY required to reproduce a desired colour (set of tristimulus value *XYZ*). This could be calculated by inverting the Neugebauer equations; however, because the equations are non-linear their inversion is non-trivial. Kang (1997) has described different attempts to invert the Neugebauer equations.

With the addition of black ink, the three-primary Neugebauer equations can be extended to four primaries to give 16 possible overlaps rather than 8. Now the analytical inversion is even more complicated as a greater number of unknowns are involved and, more importantly, there will be no unique solution. Due to the penetration and scattering of light into paper, the simple Neugebauer model does not perform well in practice (Green, 2002). As a result, several empirical modifications have been suggested for the model. They are discussed in following sections.

Spectral Extension

If narrow spectral reflectance data are used instead of the tristimulus values of the dominant colours, the spectral extension of Neugebauer equations can be obtained (Viggiano, 1990) as follows:

$$R(\lambda) = \sum_{i=1}^{N} w_i R_i(\lambda)$$

(2.13)

where $R(\lambda)$ is the predicted spectral reflectance as a function of wavelength for a given patch printed using *N* colorants.

$R_i(\lambda)$ is the spectral distribution of the patch printed with only the *i*-th Neugebauer primary, the weight w_i is the fraction of the *i*-th Neugebauer primary in the given patch. As compared to the Neugebauer model, this is a computationally expensive model and its inversion becomes even more complex.

2.2.1.3   The Yule-Nielsen modified Neugebauer equations

In the halftone process, the dot area measurement is affected by internal light scattering in the substrate resulting in optical dot gain and the Neugebauer model fails to represent this optical dot gain. Yule and Nielsen (1951) modified the Murray-Davies equation and later Yule and Colt (1951) extended this to the Neugebauer equations to take into account the optical dot gain for a single-colour halftone tint. They considered the effect of the penetration and scattering of light into the paper. To account for multiple internal reflections of light within the substrate and ink film, a power law expression was used. The equation for a single-colour (for example, black ink) can be given as:

$$R(\lambda)^{(1/n)} = w_k R_k(\lambda)^{(1/n)} + w_w R_w(\lambda)^{(1/n)}$$

$$(2.14)$$

where $R_k(\lambda)$ and $R_W(\lambda)$ are the spectral distributions of the black ink and white paper respectively. The factor *n* is called the Yule-Nielsen factor and is derived empirically for fitting the data.

Viggiano (1990) applied the Yule-Nielsen relationship to the spectral Neugebauer equations, and obtained the following *Yule-Nielsen modified Spectral Neugebauer model* (YNSN):

$$R(\lambda)^{(1/n)} = \sum_{i=1}^{N} w_i R_i(\lambda)^{(1/n)}$$

$$(2.15)$$

where *R* is the reflectance factor, λ represents the visible wavelength, *w* is the fractional

dot area and *n* is the Yule-Nielsen factor. This model showed a substantial increase in accuracy over the Neugebauer model by improving the fit of the model to a training data set. As defined by Yule and Nielsen (1951), the theoretical upper limit for *n* is 2. When defined empirically, the value of *n* is invariably close to, or above 2. This led to the development of another model by Clapper and Yule (1955).

2.2.1.4   The Clapper-Yule model

This model (Clapper and Yule, 1955) accounts for multiple scattering and internal reflections, which were not considered in Murray-Davies equations and Yule-Nielsen model. The model adds correction factors by characterising the multiple scattering, ink transmissions and the reflectance from the front surface. The total reflected light is calculated by adding all the light fractions that emerge after each internal reflection cycle. The halftone process can be analytically expressed by this model as follows:

$$R(\lambda) = K_s + \frac{xIr(1 - A + AT(\lambda))^2}{1 - r(1 - x)(1 - A + AT(\lambda)^2)}$$

(2.16)

where K_s = the specular component of the surface reflection

$T(\lambda)$ = the ink transmittance

I = amount of light incident in the medium

x = the fraction of light which is internally reflected

Ink area coverage and ink transmittance can be calculated using the Neugebauer equations.

2.2.1.5   The Cellular Neugebauer model

Heuberger (1992) suggested the cellular approach where the model is interpreted as interpolating between a numbers of grid-points specified by the primaries. This is a localised model where the colorant space is divided into cells and the Neugebauer model is used locally within them. This approach was found to be more accurate than the simple Neugebauer model as it reduces errors caused by interpolation; however, it

requires a greater number of measurements and additional computation (Bastani, 1996) (Hua, 1997). Agar (1998) used a cellular YNSN model to develop an iterative method for colour printer characterisation.

2.2.1.6   The Beer-Bouguer law

Colorant models define the subtractive nature of a colorant and the substrate. The Beer-Bouguer law describes the empirical relationship between the absorption of light and the concentration of the colorants and, as such, it is not applicable to media that exhibit scattering. The Law states that the transmittance of light through a medium is proportional to the distance travelled by that light through the medium (i.e. thickness of the medium) and its absorption coefficient. Absorbance A of the medium is given by:

$$A = \log\left(\frac{I}{I_0}\right) = \log\left(\frac{1}{T}\right)$$

(2.17)

where I = the light intensity after passing through the medium

I_0 = the light intensity before passing through a medium

T = transmittance

Absorbance can also be expressed as follows

$$A = \varepsilon(\lambda)wc$$

(2.18)

where $\varepsilon(\lambda)$ = spectral absorption coefficient of the medium

w = the thickness of the medium

c = the concentration of the medium

The spectral transmittance can be given as:

$$T(\lambda) = e^{-\varepsilon(\lambda)wc}$$

(2.19)

This law provides the basis for other colorant models described in the following sections. It, however, doesn't account for the scattering of the light by the colorant. Also proportionality failure and additivity failure at higher dye concentrations restricts the application of the Law. Nevertheless, this law is the basis of the masking equations (Kang, 2006).

2.2.1.7   Masking equations

This method attempts to quantify the relationship between original and reproduced colours using matrix transformation. The masking equations method was first suggested in 1938 by Yule. It assumes that the additivity and proportionality rules hold for ink densities of mixed colours. This gives a simple linear transformation to establish the amount of ink required to match the three colour intensities in the original copy. In practice, however, additivity failure and proportionality failure occur due to the halftone screen and turbidity of the media (Johnson, 1997). The first-order equations can be improved by including second-order and cross-product terms to increase the prediction accuracy (Clapper, 1961). The second order masking equations are given below.

$$D_r = a_1c + a_2m + a_3y + a_4c^2 + a_5m^2 + a_6y^2 + a_7cm + a_8cy + a_9my$$
$$D_g = b_1c + b_2m + b_3y + b_4c^2 + b_5m^2 + b_6y^2 + b_7cm + b_8cy + b_9my$$
$$D_b = c_1c + c_2m + c_3y + c_4c^2 + c_5m^2 + c_6y^2 + c_7cm + c_8cy + c_9my$$

(2.20)

where a_1, b_1 and c_1 are the coefficients which can be calculated using least-square fitting method. The red, green and blue colorimetric densities are calculated as follows:

$$D_r = \log{(X_0/X)}, \ D_g = \log{(Y_0/Y)}, \ D_b = \log{(Z_0/Z)}$$

(2.21)

The c, m and y values are the individual ink amounts for the combination of which the XYZ values are to be calculated. The X_0, Y_0, Z_0 is the reference white.

Higher order polynomials, such as third-order, may be used to reduce the prediction errors even further (Yule, 1967). Johnson (1997) pointed out that local maxima and minima resulting from the higher order masking equations can create artefacts for local regions of colour space. These effects can be reduced by linearising the data prior to applying the masking equations in such a way that the coefficients for the higher order terms are minimised.

2.2.1.8   Kubelka-Munk (KM) theory

Kubelka-Munk (KM) theory predicts the absorption and scattering of the light within the colorant and the theory was originally developed for both translucent and opaque media. The theory relates the total diffusely reflected light from a substrate as a function of the amount of light scattered by, and absorbed by, the substrate. The light incident on to a material is scattered in all directions. The light can be absorbed or scattered in two directions: the downward flux is an average of all light travelling in a downward direction and the upward flux is an average of all light travelling in an upward direction. Thus the theory is based on two light channels travelling in opposite directions (Kang, 1997). This assumes that, for a material of infinite lateral extension, the internal lateral scattering is irrelevant, i.e. no light escapes from the edges of the material due to lateral scattering.

In the single-constant KM model, the spectral reflectance for a sample of infinite thickness can be predicted as:

$$R(\lambda) = 1 + \frac{K(\lambda)}{S(\lambda)} - \sqrt{\left(\frac{K(\lambda)}{S(\lambda)}\right)^2 + 2\left(\frac{K(\lambda)}{S(\lambda)}\right)}$$

(2.22)

where $K(\lambda)$ is the absorption coefficient and $S(\lambda)$ the scattering coefficient.

The ratio $K(\lambda)/S(\lambda)$ of a 4-colour process (for example, CMYK) can be calculated by summing the ratios of all the components.

$$\frac{K(\lambda)}{S(\lambda)} = \left(\frac{K(\lambda)}{S(\lambda)}\right)_p + c_1\left(\frac{K(\lambda)}{S(\lambda)}\right)_1 + c_2\left(\frac{K(\lambda)}{S(\lambda)}\right)_2 + c_3\left(\frac{K(\lambda)}{S(\lambda)}\right)_3 + c_4\left(\frac{K(\lambda)}{S(\lambda)}\right)_4$$

(2.23)

$\left(\frac{K(\lambda)}{S(\lambda)}\right)_p$ = single-constant ratio of the paper (substrate)

$\left(\frac{K(\lambda)}{S(\lambda)}\right)_i$ = single-constant ratio of the i-th process ink (for example, Cyan)

c_i = concentration of the i-th process ink

The ratio $K(\lambda)/S(\lambda)$ for each ink can be calculated from the measured spectral reflectance of the ink as follows.

$$\left(\frac{K(\lambda)}{S(\lambda)}\right)_i = \frac{[1 - R_i(\lambda)]^2}{2R_i(\lambda)}$$

(2.24)

Equation (2.24) represents the specific case of an infinite layer of a thick sample. If the ink thickness and the spectral reflectance of the substrate are known, then the spectral reflectance of the sample can be calculated as:

$$R(\lambda) = \frac{1 - R_g(\lambda)\{\alpha(\lambda) - \beta(\lambda)\coth[\beta(\lambda)S(\lambda)x]\}}{\alpha(\lambda) - R_g(\lambda) + \beta(\lambda)\coth[\beta(\lambda)S(\lambda)x]}$$

(2.25)

where

$R_g(\lambda)$ = spectral reflectance of the substrate

x = ink layer thickness

$\alpha(\lambda) = 1 + K(\lambda)/S(\lambda)$

$\beta(\lambda) = [\alpha(\lambda)^2 - 1]^{1/2}$

The Saunderson correction (Emmel, 2003) is used to account for the reflection losses at the sample boundaries and for the internal reflection as follows:

$$R(\lambda) = \frac{R_m(\lambda) - K_1}{1 - K_1 - K_2 + K_2 R_m(\lambda)}$$

(2.26)

where $R_m(\lambda)$ is the measured spectral reflectance, K_1 is a constant representing the surface reflection and K_2 is a fraction representing internal reflections.

The KM theory had been extended by different authors. Emmel and Hersch (1999, 2001, and 2002) developed mathematical models based on KM theory that describe various light scattering and ink spreading phenomena. These models were found to predict the reflection spectra of halftone prints with better accuracy than physical models.

To correlate the subtractive theories with halftoning, an empirical spectral halftone correction factor was suggested by Kang (1993). This can be derived as:

$$h(\lambda) = Q_m(\lambda)/Q_c(\lambda)$$

(2.27)

where Q may be any parameter that has to be corrected, for example optical density, absorption coefficient K or scattering coefficient S; Q_m is the measured quantity and Q_c is the computed (predicted) quantity.

This correction factor is useful to minimise the difference between the computed and measured quantity and it can be applied to the Beer-Bouguer law as well as KM theory.

In another interesting study (Edström, 2004), the KM model was compared to DORT2002 model for optical modelling of paper. The DORT2002 model (Edström, 2005) is based on the radiative transfer theory, which describes the interaction of radiation with scattering and absorbing media. This model was found to be accurate, very fast and numerically stable. The DORT2002 model can be considered as a

generalisation of the KM model. Unlike the KM model, which is one-dimensional, radiative transfer solution is three-dimensional thus enabling the modelling of many physical processes, such as scattering, without approximation (Edström, 2004).

KM theory is widely used for colorant formulation in the colorant industries due to its accepted accuracy. It is used for colour gamut estimation of ink jet inks and the characterisation of continuous tone (thermal dye diffusion) printers. The theory is best suited for low absorption: it does not perform well for a high level of absorption. Van De Capelle (1997) investigated the KM theory and found that the coefficients K and S are heavily dependent on the substrate colour in the cases where the substrate does not approximate to white.

KM theory also neglects lateral scattering of the light; hence it is not strictly capable of depicting the optical properties of printed ink. Mourad (2001) adopted the KM theory to study this lateral light scattering for a halftone print and proposed an extended method for the accurate prediction of reflection.

Accurate determination of the parameters is complicated; some interactions between the colorant and substrate are not accounted for in KM theory, thus purely empirical methods are often used for printer characterisation (Sharma, 1997).

2.2.1.9 Combination of the KM and YNSN models

Finally, a combination of the KM and YNSN models can be used (Figure 2.7). First, the KM model is applied to derive the overprints of the primary inks from spectral measurements of the solid inks and the substrate. These overprints, along with the spectra of the primary inks, form the Neugebauer primaries which are then used as input to the YNSN model. This method has been used before to obtain an overall gamut of the *n*-colour printing process. (Deshpande, 2009 and 2014a).
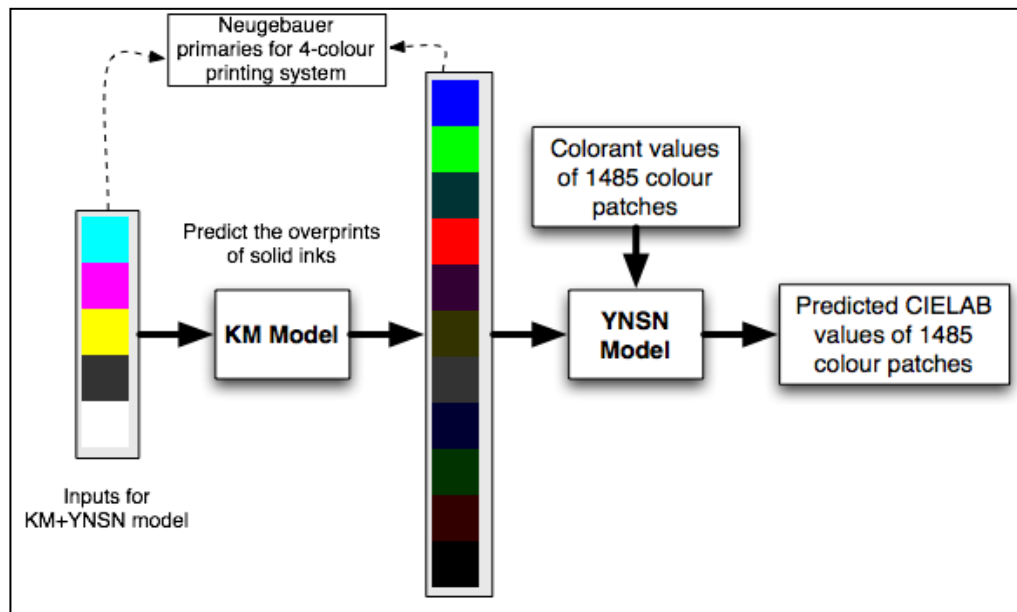
Figure 2.7 Combination of the KM and YNSN models

In another study (Abebe, 2011), this approach of combining the KM and YNSN model was evaluated against the traditional models using inkjet and laser printing devices. Slavuj (2014) estimated the Neugebauer primaries for a 7-colorant printer using DORT2002 model (Edström, 2005) and found that the DORT2002 model does not offer significant improvements over the KM model. However, a simple scattering model improved the estimation of the Neugebauer primaries. When the estimated primaries are used as inputs to the spectral Neugebauer model instead of the measured primaries, the model accuracy has been reported to be improved. (Abebe, 2011) (Slavuj, 2014)

2.2.1.10 The ink spreading enhanced YNSN model (EYNSN)

The YNSN model was extended by Hersch (2005) to account for the ink spreading phenomenon in the different ink superposition conditions. Ink spreads out differently according to the ink superposition condition, for example, when the ink halftone is printed alone on substrate or in superposition with one or more inks. The amount of dot gain changes depending on the ink superposition condition.

A model for calculating the effective area coverage i.e. physical coverage that accounts for ink spreading was developed (Hersch, 2005). The model assumes that when a halftone layer is printed either beneath or on top of a solid layer, its effective surface area coverage is changed due to the ink spreading phenomenon.

Suppose the printing process consists of cyan, magenta and yellow inks with their nominal area coverages c, m and y respectively and the tone reproduction functions of $f_c(c)$, $f_m(m)$ and $f_y(y)$ respectively. The tone reproduction functions map the nominal area coverages (c, m, y) to the effective area coverages (c', m', y'). There are three ink superposition conditions as follows: single ink halftone, single ink halftone superposed with one solid ink and single ink halftone superposed with two solid inks. To account for the ink spreading phenomenon, a separate ink spreading function is created to map the nominal area coverages to the effective area coverage for each superposition condition. The ink spreading functions for each superposition condition can be denoted as follows:

$f_{c/m}(c)$: cyan ink of coverage c superposed with solid ink magenta,

$f_{c/y}(c)$: cyan ink of coverage c superposed with solid ink yellow,

$f_{m/c}(m)$: magenta ink of coverage m superposed with solid ink cyan,

$f_{m/y}(m)$: magenta ink of coverage m superposed with solid yellow,

$y_{y/c}(y)$: yellow ink of coverage y superposed with solid ink cyan,

$y_{y/m}(y)$: yellow ink of coverage y superposed with solid magenta,

$f_{c/my}(c)$: cyan ink of coverage c superposed with solid magenta and yellow,

$f_{m/cy}(m)$: magenta ink of coverage m superposed with solid cyan and yellow,

$f_{y/cm}(y)$: yellow ink of coverage y superposed with solid cyan and magenta.

The ink spreading functions can be derived by fitting a training set of colour patches, for example, three colour patches of 25%, 50% and 75% nominal area coverages per ink spreading function. The effective area coverages (c', m', y') of a given colour halftone are derived by weighing the contributions of the corresponding ink spreading functions for each ink. The weights depend on the effective area coverage of each ink superposition condition.

The following system of equations is obtained by calculating the relative weight of each superposition condition (Hersch, 2005).

$$c' = f_c(c)(1 - m')(1 - y') + f_{c/m}(c)m'(1 - y') + f_{c/y}(c)(1 - m')y' + f_{c/my}(c)m'y'$$

$$m' = f_m(m)(1 - c')(1 - m') + f_{m/c}(m)c'(1 - y') + f_{m/y}(m)(1 - c')y' + f_{m/cy}(m)c'y'$$

$$y' = f_y(y)(1 - c')(1 - m') + f_{y/c}(y)c'(1 - m') + f_{y/m}(y)(1 - c')m' + f_{y/cm}(y)c'm'$$

$$(2.28)$$

It can be seen that the above system of equations is analogous to Demichel's equations (2.12). For example, the proportion of a halftone patch printed with cyan ink of coverage c on the substrate is $(1-m')(1-y')$. The proportion of the same patch printed in superposition with solid magenta ink is $m'(1-y')$, and so on.

To calculate the effective area coverages (c', m', y'), Eq.(2.28) can be solved iteratively, setting the initial values of c', m' and y' equal to the respective nominal area coverage c, m and y. After first iteration, new values of c', m' and y' are used for the next iteration. After a few iterations, the resulting area coverage values are stabilised. From the effective area coverages c', m' and y' the effective ink area coverages a_1', a_2', …, a_8' are obtained using Demichel's equations (2.12). A framework of the ink spreading enhanced spectral printer model is given in Figure 2.8.
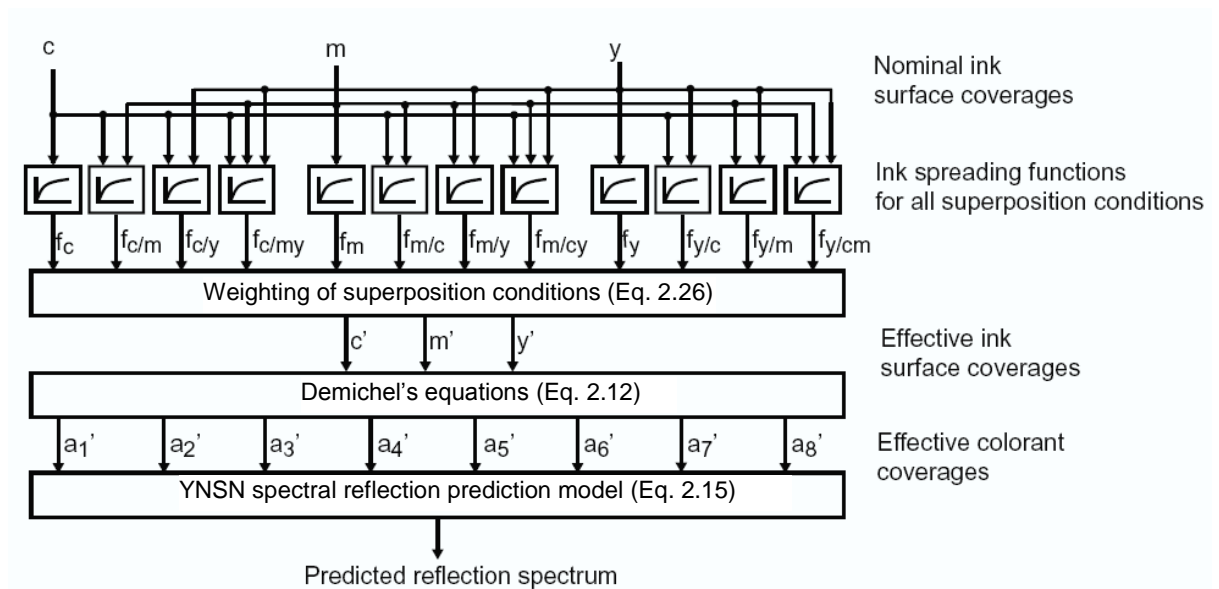
Figure 2.8 Spectral prediction model framework (Hersch, 2005) with the YNSN model and ink spreading in all superposition conditions

This model was implemented by Hersch (2005) using lithographic offset, thermal transfer and ink jet printing technologies using 3-ink combinations, C, M and Y inks, with different screen frequencies. The halftoning method was classical clustered-dot and the screen angles for inks were mutually rotated by 30°. For fitting the effective area coverages, three colour patches per ink were used: 25%, 50% and 75% nominal area coverages. The model was evaluated using a test set of 729 colour patches consisting of all nominal coverage combinations at 0%, 13%, 25%, 38%, 50%, 63%, 75%, 88% and 100%.

The results showed that the ink spreading model with all superposition conditions improved the prediction accuracy. In most of the cases (i.e. combinations of the printing technologies and the screen frequencies), the mean colour difference between the predicted and the measured spectra was below $1.00 \, \Delta E^*_{94}$ for the model with all superposition conditions. It was also noted that the ink spreading enhanced YNSN model works for the dispersed-dot and error-diffusion screening methods, but gives less prediction accuracy than that for the clustered-dot screening.

The ink spreading enhanced YNSN model was further extended (Rossier, 2010) by replacing the global Yule-Nielsen factor (*n*-factor) with the ink-specific *n*-factors. The optimal *n*-factors are computed for halftones consisting of multiple inks by weighing the ink-specific *n*-factors with a parabolic function of their area coverages. This extension accounts for the different optical properties of the inks. The standard EYNSN model was compared with the extended EYNSN model with the ink jet and electrophotographic printing technologies. For inks having very different optical or mechanical properties, for example, standard and daylight fluorescent inks of ink jet printer, prediction accuracies of the extended EYNSN model (1.25 mean ΔE^*_{94}) were improved as compared to the standard EYNSN model (1.08 mean ΔE^*_{94}). For electrophotographic normal toners, the prediction accuracies were slightly improved from 1.26 mean ΔE^*_{94} for the standard EYNSN model to 1.23 mean ΔE^*_9 for the extended EYNSN model.

2.2.1.11 Van De Capelle model

Van De Capelle (1997a, 1997b, 1999 & 2002) proposed a novel method of printer characterisation. This method defines each ink separately by printing solid and tints of the ink on three different backgrounds: the substrate, a grey background and a black background (Figure 2.9). The spectral reflectance of the given colour can be predicted as follows:

$$R_p(\lambda) = \left[1 - \alpha_p(\lambda)\right].R_{bg}(\lambda)^{\mu_p(\lambda)} + S_p(\lambda)$$

(2.29)

where p is a nominal surface coverage (%), α is the absorption parameter, μ is the interaction parameter, S is the scattering parameter, and R_{bg} is the spectral reflectance of the paper. The model parameters are calculated as follows:

$$S_p(\lambda) = R_{pik}(\lambda) - R_k(\lambda)$$

(2.30)

$$\mu_p(\lambda) = \frac{\log\big(R'_{piw}(\lambda)/R'_{pig}(\lambda)\big)}{\log\big(R_w(\lambda)/R_g(\lambda)\big)}$$

(2.31)

where

$$R'_{piw}(\lambda) = R_{piw}(\lambda) - S_p(\lambda)$$

$$R'_{pig}(\lambda) = R_{pig}(\lambda) - S_p(\lambda)$$

(2.32)

$$\alpha_p(\lambda) = 1 - \frac{R'_{piw}(\lambda)}{R_w(\lambda)^{\mu_p(\lambda)}}$$

(2.33)

where

$R_{piw}(\lambda)$ is the spectral reflectance of $p\%$ ink layer on white

$R_{pig}(\lambda)$ is the spectral reflectance of $p\%$ ink layer on grey

$R_{pik}(\lambda)$ is the spectral reflectance of $p\%$ ink layer on black

$R_w(\lambda)$ is the spectral reflectance of the white substrate

$R_g(\lambda)$ is the spectral reflectance of the grey background

$R_k(\lambda)$ is the spectral reflectance of the black background
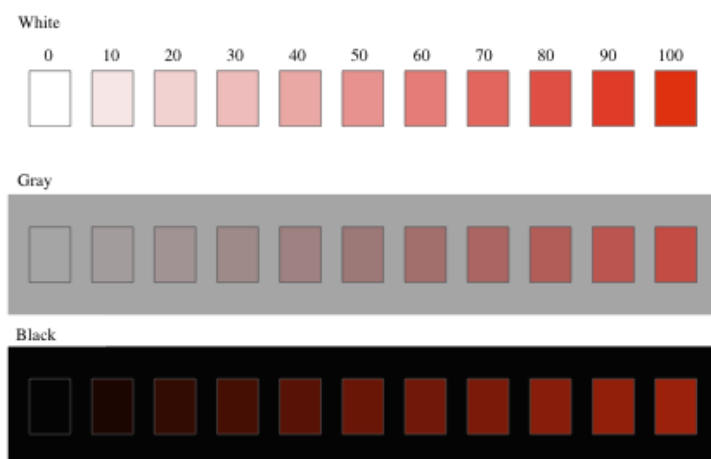
Figure 2.9 A test chart for characterising ink (Van De Capelle, 1997a)

2.2.1.12 Other studies

There have been several studies that have explored the various spectral printer models. Abebe (2011) evaluated a combination of the KM and YNSN models against the traditional printer models using inkjet and laser printing devices. A hybrid approach with mixed Neugebauer primaries was also tested by measuring half of the Neugebauer primaries and estimating half of the Neugebauer primaries. The results showed improved prediction accuracy of the model based on the hybrid approach with mixed Neugebauer primaries over the traditional model based on the measured Neugebauer primaries.

In another study (Berns, 2007), three different approaches to the single-constant simplification of the KM model – textile, paint and a hybrid of the paint and textile approaches – were compared. The three approaches were tested using tints made from a mixture of cobalt blue and titanium white acrylic emulsion artist paints. The differences between the textile and hybrid approaches were found to be insignificant, while the paint approach was found to be better than other two approaches.

2.2.1.13 Accuracy of different models

A number of investigations highlighted the poor accuracy of the basic Neugebauer model (Taplin, 2001). For example, Rolleston (1993) investigated the accuracy of different forms of the Neugebauer equations (See Table 2.1). They compared the performance of colorimetric and spectral Neugebauer equations. There was a significant improvement in accuracy when Yule-Nielsen factor was applied, and the YNSN model performed the best. Kang (1993) also compared the accuracy of the spectral Neugebauer, the YNSN model, the Clapper-Yule multiple internal reflections model, the Beer-Bouguer law and the (KM) theory (See Table 2.2).

Johnson (1997) compared masking models with the Neugebauer model and its extension; the performance of the modified Neugebauer model was found to be better than that of the Neugebauer model, but both these models performed poorer than the

masking models. The effects of using the cellular approach and including the Yule-Nielsen factor in the spectral Neugebauer equations were reviewed by Balasubramanian (1995 and 1999). Some of the studies involving the comparison of different models are described below.

Rolleston and Balasubramanian (1993)

In this study the focus was on forward characterisation. Different Neugebauer models were evaluated to predict the colorimetric behaviour of a Xerox 5775 printer. This is a CMYK printer and 16 primaries were used: w, c, m, y, k, cm, cy, ck, my, mk, yk, cmy, cmk, cyk, myk, cmyk.

The colorimetric response of the printer to samples of C, M, Y and K colorants was measured. Those dot areas were selected that minimised the perceived colour difference between the measured and the predicted colour.

Sixteen samples of each of C, M, Y and K inks (from 0 to 100%) were printed and measured. The colour of each patch was predicted using the Neugebauer model. The dot area was chosen to minimise the ΔE^*_{ab} value between the measured and predicted colour.

One thousand test patches, randomly distributed in CMYK space, were printed and measured. Each model was used to predict the *L*a*b** values of the patches. For the basic Neugebauer equation average colour difference was found to be 7.4 ΔE^*_{ab}, which is considered unacceptable.

In order to apply the Yule-Nielsen modified Neugebauer equation, a value of *n* (the Yule-Nielsen factor) was selected from 1.0 to 8.0 to minimise the error function $\Delta E(n)$ for the given value of *n*. The average colour difference including the Yule-Nielsen modification was found to be 4.5 ΔE^*_{ab}.

For the spectral Yule-Nielsen modified Neugebauer model, the spectral data measured over a wavelength range of 400 nm to 700 nm at 10 nm intervals was used. In this case,

the three broadband colour values (tristimulus values) were replaced by the sampling values of the reflectance curves; however, the weights of the Neugebauer equations were still the same. This model produced the significant improvement with the average colour difference to give a value of 2.7 ΔE^*_{ab}.

The cellular Neugebauer model was applied by partitioning CMYK space into cells and employing the Neugebauer equation within each cell. For this purpose, the combinations of 0%, 50% and 100% colorant values were used giving 81 sample points; also, the 0%, 25%, 50%, 75% and 100% colorant values and their combinations were used to yield 625 sample points. Under the cellular Neugebauer model, two approaches were explored: the Cellular Neugebauer broadband equation and Cellular Spectral Neugebauer equation.

In the Cellular Neugebauer broadband equation, the dot area values *c*, *m*, *y*, *k* were normalised to be in a range of 0 to 1. The Yule-Nielsen modified Neugebauer equation can be obtained for *X*, *Y* and *Z* using 16 co-ordinates of the cell in 4 space (CMYK). The average colour difference values were found to be 3.1 and 2.6 ΔE^*_{ab} for 81 nodes and 625 nodes respectively (Table 2.1).

Table 2.1 Accuracy of various models found by Rolleston and Balasubramanian (1993)

Model	ΔE_{avg}	ΔE_{max}
Basic Neugebauer	7.41	15.52
YN modified Neugebauer with n=2.5	4.53	11.47
Spectral Neugebauer	7.41	15.52
YNSN with n=5.5	2.7	9.71
Cellular Neugebauer 3^4 cells	4.19	11.16
Cellular YN modified Neugebauer 3^4 cells, n=7.0	3.06	9.49
Cellular Neugebauer 5^4 cells	2.85	8.76
Cellular YN modified Neugebauer 5^4 cells, n=6.0	2.6	8.4
Cellular Spectral Neugebauer 3^4 cells	4.19	11.16
Cellular YNSN 3^4 cells, n=7.0	3.07	10.05
Cellular Spectral Neugebauer 5^4 cells	2.85	8.76
Cellular YNSN 5^4 cells, n=6.0	2.62	8.71

For the Cellular Spectral Neugebauer equation, the spectral measurements were used to predict the colour using Eq. (2.15). The average values of colour difference were found to be 4.2 and 2.8 ΔE^*_{ab} for 81 nodes and 625 nodes respectively.

It was observed that for non-cellular models, the accuracy strongly depended on the value of *n*. As the number of cells increased the value of ΔE^*_{ab} was found to decrease. In the case of spectral models, the dependence of ΔE^*_{ab} on *n* decreases as the number of cells increases. It was concluded that a reasonably accurate printer model can be developed with only a few spectral measurements. Overall, the results showed that either the cellular model with sufficient number of cells or the YNSN model with an optimised value of *n*, produces the same level of accuracy. This is because both are correcting the same error and hence, using one of these approaches should be adequate.

Kang (1993)

Kang (1993) examined five different models by applying them to the characterisation of a xerographic printer and an ink jet printer. The Neugebauer equations, the YNSN model, the Clapper-Yule modification, the Beer-Bouguer law and the KM model were compared, along with the empirical extension of the Beer-Bouguer law and KM theory. The spectral modelling of the printers were particularly investigated.

To test 3-colour and 4-colour mixing, colour patches of known CMY and CMYK were printed on a Canon Colour Laser Copier 500 (CLC-500) printer. These colour patches include halftone tints of the primary colours from 0% to 100%. Multi-level intensity wedges of the primary colours were printed to determine halftone correction factors. The printed colour patches were measured using a spectrophotometer and CIE colorimetric coordinates calculated using CIE illuminant D50 and the CIE 2° standard observer.

For a continuous ink jet printer, the following five 8-level halftone wedges were printed: 5% C + 95% M; 90% C + 10% M; 40% C + 60% Y; 15% M + 85% Y; 90% M + 10% Y. The printed colours were again measured to obtain the spectral reflectance data and CIE colorimetric coordinates calculated.

Three metrics were used to evaluate all the models: the mean colour difference (mean ΔE^*_{ab}), the RMS colour difference (ΔE^*_{rms}) and the spectral RMS error (Δr_{rms}) each between the calculated and the measured spectral data. The following four parameters were adjusted for the different models in order to find the best fit to the data: the surface reflection (r_s), the Yule-Nielsen factor (n), a constant representing the surface reflection (f_s) and a constant representing internal reflections (f_i).

Results of the 3-colour mixing model for the CLC-500 printer are shown in Table 2.2. The Neugebauer equation produced values of mean colour difference of 12.33 and 13.24 ΔE^*_{ab} for $n = 2.0$ and $n = 2.7$ respectively. The YNSN model gave mean ΔE^*_{ab} values approximately 8; the surface reflection (r_s) didn't have any significant effect on colour difference. The range of mean ΔE^*_{ab} values for the Clapper-Yule model was between 7.51 to 10.02 ΔE^*_{ab}; the accuracy was found to be improved with higher values of n as well as f_i. The Beer-Bouguer model showed similar performance to the Neugebauer model (mean $\Delta E^*_{ab} = 12.27$) whereas the KM models had the worst accuracy with mean ΔE^*_{ab} values from 30 to 36. However, the halftone correction factors improved the accuracy of these models significantly to produce means values of 5.01 to 8.01 mean ΔE^*_{ab}.

Three models, the YNSN, the corrected Beer-Bouguer and the Saunderson corrected KM – were used to model a 4-colour process. It was found that the empirically corrected KM model performed the best among the three models but all models showed higher colour differences (by approximately 2 mean ΔE^*_{ab}) than those obtained for the 3-colour models.

For the ink jet printer, all models performed poorly giving higher values of mean ΔE^*_{ab} i.e. from 7.4 for the single-constant KM (KM1) to 18.34 for the Saunderson corrected single-constant KM (KM1S). Halftone correction methods produced lower colour differences among all models.

Kang (1993) concluded that the spectral Neugebauer model, the Beer-Bouguer law and the KM theory were inappropriate for these two printers due to poor accuracy (see Table

2.2). The halftone corrected models were found to give a better fit to the experimental data, giving better predictions for the CLC-500 printer than for the ink jet printer, and a better fit for the 3-colour printing than 4-colour printing. It was particularly observed that the printer variability (toner density variations) limits the accuracy of the models. Other factors affecting the results were the choice of Yule-Nielsen factor (n), the multiple internal reflections, the accuracy of area coverage and the surface reflections. As the empirical correction factor directly accounts for the behaviour of an individual printer, it reduces the colour difference irrespective of the printing process, unlike the analytical models.

Table 2.2 Accuracy of various models found by Kang (1993)

Model	n	r_s	f_s	f_i	ΔE_{avg}	ΔE_{max}
Neugebauer	2	-	-	-	12.33	14.86
Neugebauer	2.7	-	-	-	13.24	-
Yule-Neilsen	2	0	-	-	7.93	9.09
Yule-Neilsen	2	0.01	-	-	8.01	9.3
Yule-Neilsen	2	0.02	-	-	8.25	9.8
Yule-Neilsen	2.7	0	-	-	7.85	9.3
Yule-Neilsen	2.7	0.01	-	-	7.78	9.31
Yule-Neilsen	2.7	0.02	-	-	7.81	9.55
Yule-Neilsen	2.7	0.04	-	-	8.69	10.98
Clapper-Yule	2	0.04	0.01	0.4	10.02	11.15
Clapper-Yule	2	0.04	0	0.4	9.4	10.27
Clapper-Yule	2	0.04	0	0.5	8.61	9.41
Clapper-Yule	2.7	0.04	0.01	0.35	9.11	10.3
Clapper-Yule	2.7	0.04	0.01	0.4	8.58	9.7
Clapper-Yule	2.7	0.04	0.01	0.45	8.19	9.3
Clapper-Yule	2.7	0.04	0.01	0.5	7.91	9.03
Clapper-Yule	2.7	0.04	0.01	0.55	7.72	8.85
Clapper-Yule	2.7	0.04	0.02	0.5	8.52	9.93
Clapper-Yule	2.7	0.04	0	0.5	7.54	8.44
Clapper-Yule	2.7	0.03	0	0.5	7.53	8.43
Clapper-Yule	2.7	0.02	0	0.5	7.52	8.43
Clapper-Yule	2.7	0.01	0	0.5	7.51	8.42
Beer-Bouguer	-	-	-	-	12.27	13.28
KM2	-	0	-	-	36.47	40.45
KM1	-	0	-	-	30.61	32.72
KM1S	-	-	0	0.6	32.62	34.75
Corrected BB	-	-	-	-	7.14	8.6
Corrected KM1-1	-	0	-	-	8.01	9.73
Corrected KM 1-2	-	0	-	-	5.83	7.12
Corrected KM 1-3	-	0	-	-	5.01	6.05

Taplin (2001)

In order to find a good candidate model for a 6-colour printing system, Taplin (2001) compared different halftone (physical) models and continuous tone (colorant) models for a 2-colour process. He used the following models: Neugebauer, YNSN, Cellular Neugebauer, Cellular YNSN, Single constant KM and Cellular KM.

A 6-colour printer (CMYKOG) was used with 15 possible combinations of 2-colours. For each 2-colour combination, a test chart of 81 colour patches (9-by-9 grids) was printed. Digital counts for these grid points were selected in steps of approximately equal area coverage using the inverse Murray-Davies equation (Yule, 1967). The printed colour patches were measured using a GretagMacbeth Spectrolino spectrophotometer. Colour difference (ΔE^*_{94} and ΔE^*_{00}) and root-mean-square spectral error were used as a goodness metric for evaluating the performance of the model.

Matlab code was generated to apply the above mentioned printer models. The performance of each was assessed by calculating the colour difference between the colorimetric coordinates calculated from the measured and the model-predicted reflectance spectra of all the colour patches: CIE illuminant D65 illuminant and the CIE 2° standard observer were used. For the Neugebauer model and its extensions, two types of transfer function were used: the theoretical area coverage and the effective area coverage. Theoretical area coverage is defined as the digital count for a given dot divided by the maximum digital count. Effective area coverage was obtained by constructing a look-up table (LUT) populated with values of area coverage calculated by linear regression using dot area for the single ink ramps.

The Neugebauer model (theoretical area coverage) produced poor colorimetric accuracy for all 2-colour combinations with average $\Delta E^*_{94} = 12.12$ and average $\Delta E^*_{00} = 10.16$ (Table 2.3). It showed systematic error shifts that could be associated with the poor prediction of the effective area coverage. The accuracy of this model improved significantly by using a look-up table for area coverage levels (mean $\Delta E^*_{94} = 2.58$ and mean $\Delta E^*_{00} = 2.64$); however, prediction of the spectral curve shape was poor.

Table 2.3 Accuracy of various models found by Taplin (2001)

Printer Model	n-value	transfer function	Mean ΔE^*_{94}	Max ΔE^*_{94}	Mean ΔE^*_{00}	Max ΔE^*_{00}
Neugebauer		AC theoretical	12.12	25.89	10.16	24.79
YN-Neugebauer	6	AC theoretical	4.53	11.47	3.98	10.41
Neugebauer		AC effective	2.58	7.79	2.64	9.91
YN-Neugebauer	6	AC effective	1.32	4.96	1.31	4.88
Cellular Neugebauer		AC theoretical	3.39	14.83	3.12	14.13
Cellular YN-Neugebauer	6	AC theoretical	1.4	7.08	1.31	7.07
Cellular Neugebauer		AC effective	0.84	3.18	0.83	4.59
Cellular YN-Neugebauer	6	AC effective	0.55	3.04	0.53	3.1
Continuous tone			1.71	12.72	1.77	14.32
Continuous tone cellular			0.75	9.53	0.76	10.53

With the addition of the Yule-Nielsen factor (n), better accuracy was achieved for the YNSN model with the mean values: $\Delta E^*_{94} = 1.32$ and $\Delta E^*_{00} = 1.31$. The optimal value of n (= 6) was determined by iterative testing with incremental n values and plotting the spectral and colorimetric error values against the n-value. Again, the systematic error shift similar to that for Neugebauer model was noticed though with the reduced magnitude.

The colorimetric error was further reduced by using the Cellular Neugebauer model i.e. $\Delta E^*_{94} = 3.39$ for theoretical area coverage. But the maximum colour difference was large: maximum $\Delta E^*_{94} = 14.83$. The cellular YNSN model performed better than the cellular Neugebauer model with $\Delta E^*_{94} = 1.40$ for theoretical area coverage and $\Delta E^*_{94} = 0.55$ for effective area coverage.

The single constant KM model was found to be inaccurate in terms of predicting the 2-ink overprints. Although the average colour difference was small i.e. 1.71 ΔE^*_{94}, the maximum colour difference was found to be unacceptable i.e. 12.72 ΔE^*_{94}. A systematic error shift was observed towards the full overprint region. Similarly the cellular KM model gave large values of maximum colour difference with only small improvements over the single constant KM model.

Finally the YNSN model with the effective area coverage look-up table was selected for modelling the 6-colour process. Though the cellular YNSN model proved to give the best performance, it required the largest number of primaries and complex implementation.

2.2.2 Empirical methods using lookup tables

Printing devices can also be characterised by using empirical methods, for example, numerical models using regression methods and lookup table-based techniques using lattice-based interpolation. These methods are described in detail by Green (2002), Balasubramanian (2003) and Kang (2006).

The device space, for example CMYK, is usually sampled to generate a test chart of known device values. This test chart is printed and all samples are measured using a spectrophotometer. The characterisation model is derived using data-fitting and interpolation techniques to find the correlation between the device values and the device-independent colour values, for example, CIELAB. The samples in the test chart should be carefully selected so as to adequately represent the device space.

The lookup table based approach is used widely to characterise printing devices. A multi-dimensional lookup table is used to define the relationship between the source and destination values in the lattice points while non-lattice points are interpolated. This method can be implemented in three steps: packing, extraction and interpolation.

2.2.2.1 Packing

In the first step, a device space is divided into a lattice and the sample points are populated to build the lookup table. The lookup table is typically uniformly spaced with an equal step sampling along each axis of the device space. For a three-dimensional lookup table, if the number of levels along each axis is p then there will be p^3 lattice points and $(p-1)^3$ cubes. The device-independent colour values of the samples are measured to formulate the lookup table.

Uniformly spaced lookup tables are simple and they implicitly provide information about lattice points and cells. They allow the quick location of a query point and its adjacent neighbours resulting in significant savings in computational overhead. The packing can also be non-uniform with unequal sampling.

2.2.2.2 Extraction

This step finds the location of the non-lattice input point and extracts the colour values of the nearest lattice point. The speed of the extraction depends on how well the packing is done in the first step: a well-packed device space provides quicker and simpler searches. If the packing is non-uniform with unequal sampling then a series of comparisons are required to locate the nearest lattice points. Depending on the interpolation method, further search within the cell may be required. For example, most of the geometric interpolation methods require a search mechanism to find the subdivided structure where the point is located (Kang, 2006).

2.2.2.3 Interpolation

Finally interpolation is performed to calculate the device-independent colour values of the input point using the extracted lattice points. Different interpolation techniques can be used, for example, geometric interpolation or cellular regression. Geometric interpolation methods include trilinear, prism, pyramid and tetrahedral.

Trilinear interpolation is an extension of a linear interpolation to three-dimensional space using the eight lattice points of a cube. In prism interpolation, a cube is divided diagonally into two halves and extraction is performed to locate the query point. Pyramid interpolation cuts the cube into three parts each consisting of a pyramid. For tetrahedral interpolation the cube is divided into six tetrahedra each with a triangular base and four vertices.

Sequential interpolation

Although a regular grid facilitates simple interpolation methods, it uses the available colour space inefficiently and it is not flexible in the placement of control points in multidimensional colour space (Figure 2.10). The large space outside the gamut of the given printing device would not be used for performing interpolations. Sequential interpolation provides additional freedom by optimally allocating grid points based on the characteristics of the printer gamut.

Sequential interpolation is a simple extension or generalisation of a regularly spaced lattice interpolation. It automatically tracks the gamut of the printing device by placing all the lattice points inside the gamut (Kang, 2006).

This can be done as a two-stage interpolation process. Consider a breakdown of the *m*-dimensional space into two subspaces of dimensions *p* and *q*. For example, a three-dimensional CMY space can be considered as a group of two-dimensional CM lattice, corresponding to different levels of the third-dimension Y. The *m*-dimensional lattice L^m can be decomposed into two sub-lattices L^p and L^q. In a conventional regular lattice each *p*-dimensional lattice is identical and we have $L^m = L^p \times L^q$. In sequential interpolation, we let the *p*-dimensional lattice structure vary as a function of the remaining *q* dimensions. For example, the CM lattice structure is allowed to change as a function of Y (Balasubramanian, 2003).
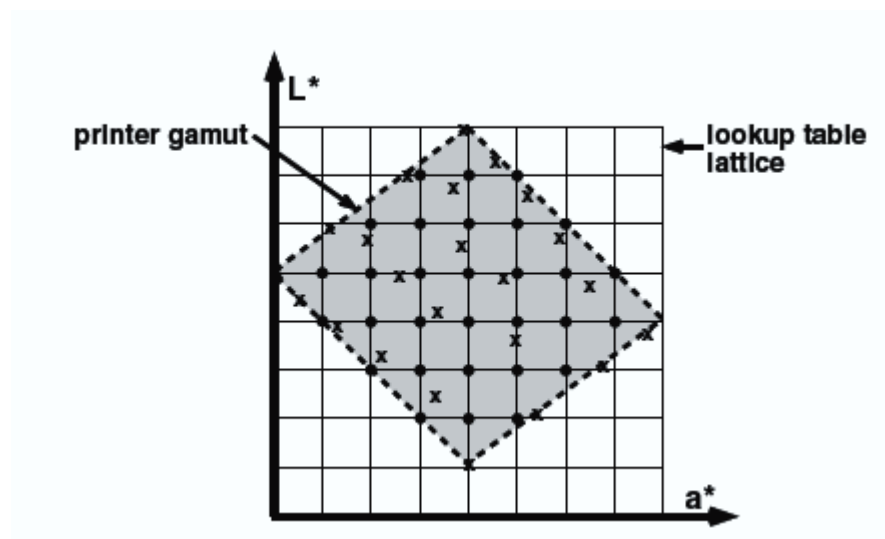
Figure 2.10 Multi-dimensional lookup table in CIELAB (Balasubramanian, 2003)

2.2.2.4   Accuracy of the lookup table based methods

Lookup table based methods were evaluated in many studies to characterise the printing devices. Kang (2006) tested several three-dimensional lookup table packings with different levels, for example, 5-level, 9-level and 17-level equally spaced lookup tables

with 125, 729 and 4913 lattice points respectively. The 5-level and 9-level unequally spaced lookup tables were also compared.

Table 2.4 shows the mean colour difference (ΔE^*_{ab}) of the interpolation techniques under five different conditions using 3072 test samples. As expected the interpolation error reduces with the increasing number of levels (sampling points across each axis). Non-uniform lookup tables with unequal spacing show better accuracy than the uniform lookup tables.

Table 2.4 Comparison of interpolation accuracies (Kang, 2006) in terms of the average ΔE^*_{ab} using 3072 data points

LUT level	5-level	9-level	17-level	5-level	9-level
LUT packing	Equal spacing	Equal spacing	Equal spacing	Unequal spacing	Unequal spacing
Cubic (Trilinear)	5.81	2.50	0.92	1.74	0.46
Prism	6.38	2.77	1.02	1.81	0.47
Pyramid	6.29	2.74	1.01	1.76	0.45
Tetrahedral	6.84	2.99	1.11	1.86	0.49

For the given packing of the lookup table, the interpolation accuracies are similar for different geometric methods. For higher lookup table sizes, these accuracies are very close. For example, a 9-level unequal spacing packing gives the best accuracy of 0.46 ΔE^*_{ab} for trilinear interpolation and the least accuracy of 0.49 ΔE^*_{ab} for tetrahedral interpolation.

Balasubramanian (2003) compared the lattice sizes of 4, 6, 8 and 10 in 3-colour CMY space by building uniformly spaced lookup tables. An independent test target of CMY samples was used. Target data were processed through the calibration functions and printed on a Xerox DocuColor 12 laser printer. A set of three-dimensional lookup tables was generated mapping the device values (CMY) to the device-independent CIELAB values. Finally the test CMY samples were processed through each lookup table to estimate the resulting CIELAB values. Colour difference between the estimated and the measured CIELAB values were calculated.

Although the accuracy increases with the increasing number of lattice size, there is no appreciable improvement obtained by increasing the lattice size above 8 (Figure 2.11). Considering the computational cost and the accuracy requirements, usually there is a trade-off between the number of samples and the associated accuracy.
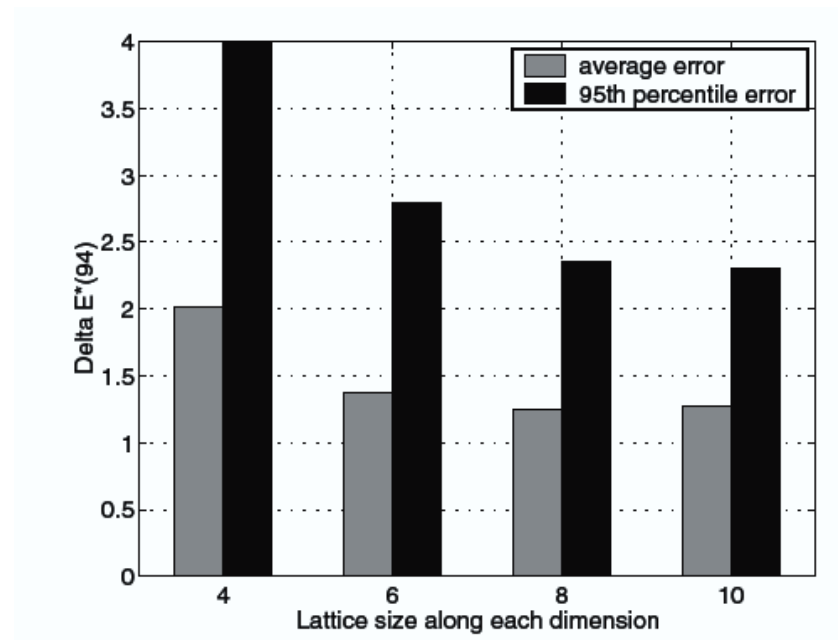
Figure 2.11 Accuracy of the lookup tables for different lattice sizes, Balasubramanian (2003)

2.3 Inverse characterisation – colour separation

Inverse characterisation maps the colorimetric values for a given viewing condition to the colorant amounts, for example, CMYK providing the colour separation for the target CIELAB values. Before applying the inverse characterisation it is important to derive the printer gamut boundary. If the target colour coordinates are outside the gamut of the printing device then these colours should be mapped to the gamut boundary using a gamut-mapping technique. Once all target colours are within the gamut then the inversion model can be used to derive the colour separation.

Balasubramanian (2003) has described a generic process of inversion as follows. First the forward characterisation function is applied to create a distribution of samples for a

training set in the device space and their corresponding coordinates in device-independent space. And then the inverse function is derived either by use of data-fitting techniques or interpolation methods.

Unlike the forward characterisation of the printing devices, the inverse characterisation is not trivial due to the nonlinear relationship between the device values and the device-independent colour values. Two approaches can be used: inverting the physical model using a constrained optimisation method or inversion based on a lookup table using an empirical method.

2.3.1 Constrained optimisation

A multi-dimensional data fitting method can be used for inverting a physical printer model through constrained optimisation. A common approach is to define and minimise the objective function, such as the root mean squared (RMS) spectral error between the predicted colour and the target colour.

If a set of T samples is generated in a device space and the corresponding device-independent coordinates obtained, for example CIELAB values, for all samples, then the mapping function f can be given as:

$$ f_{opt} = \arg \min_f \frac{1}{T} \sum_{i=1}^{T} \|R_\lambda(c) - r_\lambda\|^2 $$

(2.34)

where c is a colorant combination in device space, for example CMYK, $R_\lambda(c)$ is the estimated spectral reflectance for a combination of device values based on the forward physical model such as the YNSN model and r_λ is the target spectral reflectance to be achieved.

Different optimisation techniques can be used to minimise the objective function using an iterative process. For each step, a colorant combination is calculated to give a closer estimation of the target colour. A descent direction, the step length in the device space and the termination criteria can be defined for each technique.

Various methods have been proposed and investigated by researchers. For example, linear regression iteration (Urban, 2006), constrained nonlinear minimisation (Taplin, 2001), the Newton-Raphson method (Tzeng, 1999) and weight inversion (Alsam, 2005).

Most of the techniques are computationally expensive and take a long time to process the typical image files used in the graphic arts industry.

2.3.1.1   Optimisation process

As mentioned above, the optimisation process is iterative. It starts with an initial estimate of the optimal value of the variables and generates a sequence of improved estimates until the solution is reached (Nocedal, 2006). Optimisation algorithms differ in the strategy they use from one iteration to the next.

Typical criteria for selecting the optimisation algorithm are described by Nocedal (2006) as follows: the algorithm should give robust performance on different optimisation problems in its class. It should be efficient in order to avoid too much computational time and storage. Finally it should be accurate enough to produce a precise solution without being too sensitive to errors in the data. Tradeoffs between conflicting requirements, for example, robustness and speed, is critical in optimisation process.

A general form of a constrained optimisation is given below (MathWorks, 2014)

$$\min_x f(x)$$

$$subject\ to\ \begin{cases} g_i(x) = 0, & i = 1, \dots, m_e \\ g_i(x) \le 0, & i = m_e + 1, \dots, m \end{cases}$$

(2.35)

where x is an n-dimensional parameter vector, $f(x)$ is the objective function, $g_i(x)$ is the constraint function, while $g_i(x) = 0$, $i = 1, \dots, m_e$ have m_e equality constraints and $g_i(x) \le 0$, $i = m_e+1, \dots, m$ have m inequality constraints. The objective function and the constraint faction are assumed to be smooth.

Solution points x^*, for example local minima or maxima, of this problem depend on the characteristics of the objective function and the constraints. If the objective function and all the constraints are linear functions of x, then the problem is called as a linear programming (LP) problem. If the constraints are linear but the objective function is quadratic, then it is called as a quadratic programming (QP) problem. When the objective function and the constraints are nonlinear functions of x, then the problem becomes the nonlinear programming (NP) problem. As compared to the LP and QP problems, the NP problem is more complex. Usually it requires an iterative procedure to establish a direction of search at each iteration (MathWorks, 2014).

Many optimisation algorithms search for a local solution, a local point where the objective function is smaller than at all other viable points in its neighbourhood. The best of all such local minima, known as the global solution, is usually difficult to locate, but is required in many applications. In case of the LP problems, there is a special case in which all local solutions are also global solutions; but the NP problems may have local solutions that are not global solutions (Nocedal, 2006).

Lagrange multiplier

For the objective function $f(x)$, a local minima or maxima can be determined by finding a point at which the gradient of the objective function $\nabla f(x)$ is zero i.e. each of the partial derivatives are zero. Lagrangian multiplier method finds the local minima or maxima of the objective function that is subject to the equality constraint function $g(x)$. Basic idea is: the gradients of the objective function and the constraint function are parallel to each other at the local minima or maxima. The Lagrange function or Lagrangian is formally defined as follows.

$$\mathcal{L}(x, \lambda) = f(x) + \lambda g(x)$$

(2.36)

where λ variable is Lagrange multiplier.

To find local minima which satisfy the constraints, we can find solution points at which the gradients of $f(x)$ and $g(x)$ are parallel to each other. This can be given as:

$$\nabla f(x) = -\lambda \nabla g(x)$$

(2.37)

where

$$\nabla f(x) = \frac{\partial f}{\partial x}, \qquad \nabla g(x) = \frac{\partial g}{\partial x}$$

(2.38)

Now we can solve Eq.(2.36) for points at which

$$\nabla \mathcal{L}(x, \lambda) = 0$$

(2.39)

The partial derivatives with respect to x recover Eq.(2.37), whereas the partial derivative with respect to λ recovers the constraints $g(x) = 0$.

Karush-Kunh-Tucker (KKT) conditions

The Lagrange multipliers method, which allows only equality constraints, is generalised by the Karush-Kunh-Tucker (KKT) conditions by allowing inequality constraints. Suppose x^* is a local minimum of the objective function. Then there exists a Lagrange multiplier λ_i^* such that the following conditions are satisfied.

$$\nabla f(x^*) + \sum_{i=1}^{m} \lambda_i^* \nabla g_i(x^*) = 0$$

$$subject\ to \begin{cases} \lambda_i^* g_i(x^*) = 0, & i = 1, \dots, m_e \\ \lambda_i^* \geq 0, & i = m_e + 1, \dots, m \end{cases}$$

(2.40)

The above conditions in Eq. (2.40) are known as the KKT conditions. The KKT conditions play an important role in optimisation. There are many optimisation algorithms based on the numerical solution of the KKT system of equations (Boyd, 2004).

The optimisation algorithms used in this project are described below in Sections 2.3.1.2 and 2.3.1.3.

2.3.1.2 Active set algorithm

This is based on the KKT conditions as given in Eq. (2.40), which cancels the gradients between the objective function and the active constraints at the local minima. Lagrange multipliers λ_i^*, $i = 1, \ldots, m_e$ are required to balance the deviations in magnitude of the objective function and constraint gradients. The constraints that are not active are not included in the cancelling operation. Hence the Lagrange multipliers are 0 (MathWorks, 2014).

2.3.1.3 Sequential quadratic programming (SQP) algorithm

The sequential quadratic programming (SQP) algorithm is similar to the active-set algorithm with some differences. Every iterative step in the SQP algorithm is taken in the region constrained by bounds. If any iteration fails, the algorithm tries to take a smaller step to find the solution thus making it more robust than other algorithms. If the constraints are not satisfied, the algorithm combines the objective function and the constraint function into a merit function and attempts to minimise this merit function (Spellucci, 1998 and Tone, 1983). But this can slow the computation speed since it now involves more variables.

For a general problem described in Eq. (2.35), the SQP algorithm defines a sub problem based on a quadratic approximation of the Lagrange function (MathWorks, 2014). The Lagrange function for the general problem is given as:

$$\mathcal{L}(x, \lambda) = f(x) + \lambda^T g(x)$$

(2.41)

where λ is a Lagrange multiplier and the superscript T denotes the transpose of a matrix.

To define the sub problem, both the inequality and equality constraints in Eq. (2.35) can be linearised as follows.

$$\min_d \frac{1}{2} d^T H_k d + \nabla f(x_k)^T d$$

$$subject\ to \begin{cases} \nabla g_i(x_k)^T d + g_i(x_k) = 0, & i = 1, \ldots, m_e \\ \nabla g_i(x_k)^T d + g_i(x_k) \leq 0, & i = m_e + 1, \ldots, m \end{cases}$$

(2.42)

Where x_k is an iterate and a search direction d_k is defined at an iterate x_k. H_k is a Hessian matrix, which is a second-order partial derivative of the Lagrange function given by:

$$H_k = \nabla_{xx}^2 \mathcal{L}(x_k, \lambda_k)$$

(2.43)

The sub-problem in Eq (2.42) can be solved by using any QP algorithm at each iteration. A new iterate is then obtained by

$$x_{k+1} = x_k + d_k$$

(2.44)

A sequence of iterations is generated until Eq. (2.44) converges to the solution point x^*.

The active set algorithm and the SQP algorithms were used in this project to invert the forward printer characterisation model. The results are given in Chapter 7 (Section 7.3).

2.3.2   Lookup table with interpolation

Inversion methods based on a lookup table are commonly used for mapping from the colorimetric values to colorant amounts. Lookup tables and interpolation methods have already been introduced in Section 2.2.2.

For a 3-color printing process, for example, CMY, a unique inverse mapping exists and any interpolation method can be applied to find out the inverse characterisation function from a training set. Note that if the device space is uniformly spaced, with equally spaced lattice points, then the device-independent colour space will not be uniformly sampled due to the nonlinear relationship between the device values and the colour values. Hence remapping to an equally spaced packing in the colour space is usually required (Kang, 2006).

The size of the lookup table and the number of measurements required to derive the inverse function affect the inversion accuracy. A large number of measurements of samples can provide better accuracy at the cost of a higher computational overhead. A trade-off between the number of measurements and the accuracy is required (Balasubramanian, 2003). This is particularly important for the *n*-colour printing process where the number of measurements may be prohibitively large depending on

the division of the device space. For the perceptually uniform space, the 3-dimensional lookup table between 6 and 16 levels in each axis are sufficient (Johnson, 1995). In another study, Balasubramanian (2003) found that a lookup table size beyond 16 uniformly spaced nodes in each dimension does not afford a noticeable gain in accuracy. The ISO 12640-1 (2007) test target provides adequate information to sample the device space of 4-colour printing process for characterisation.

Another important factor is the packing of the lookup table. Instead of the uniform spacing in all dimensions of colour space, non-uniform packing is more efficient for inversion. This reduces much of the waste by limiting the valid data to the fraction of the total space belonging to the printer gamut (Kang, 2006).

For typical conventional printing processes, for example, lithographic offset, it is important to measure multiple prints over a period and average the measurements to get representative performance of a printing process over time (Green, 2002).

2.4   Methods for the *n*-colour printing process

The number of Neugebauer primaries increases exponentially (2^n) with the number of colorants (*n*) used. Thus for 4 colorants 16 primaries, for 6 inks 64 primaries and for 7 inks 128 primaries are needed. Kueppers (1989), and Boll (1994) characterised a 7-colour printing using a model based approach. Ostromoukhov (1993) generalised the compound Neugebauer model to a 7-colour printing system. Stollnitz (1998a) developed a model to predict the overprints from measurements of the individual inks.

2.4.1   Kueppers

Kueppers (1989) introduced 3 additional colours to the conventional CMYK process in order to expand the colour gamut. The following 7 inks were used in his study: magenta-red (M), orange-red (O), yellow (Y), green (G), cyan-blue (C), violet-blue (V), black (K). If the substrate is coloured then 'white' can be printed as the 8th ink. These 8

fundamental colours correspond to three primary colours perceived by the human eye (R, G, B); this is shown in Table 2.5. Kueppers proposed an empirical algorithm in which each colour can be printed with a maximum of 3-inks: one ink from CMY, one adjacent ink from OGV and the black ink.

Table 2.5 Relationship between the primary inks and the chromatic colour sensation of the human eye (Kueppers, 1989)

	R	G	B
W	✓	✓	✓
Y	-	-	✓
M	✓	-	✓
C	✓	✓	-
V	✓	-	-
G	-	✓	-
O	-	-	✓
K	-	-	-

In his method, the given image is divided into tiny geometric sub-surfaces of equal size, for example, squares, rectangles, equilateral triangles, hexagons, etc. Each sub-surface is further divided into a maximum of four sub-surfaces.

Individual sub-surfaces are inked with one of the 8 colours. An achromatic sub-surface is inked by elemental surfaces of white and black. Highly chromatic colours are inked by elemental surfaces of two juxtaposed chromatic colours. In order to reproduce tertiary colours, a maximum of 4 elemental surfaces can be used in one sub-surface: two juxtaposed chromatic inks and the elemental surfaces of white and black. A laser recording (scanner) was used to generate the colour separations in order to provide 0-100% for corresponding elemental surface or sub-surfaces.

For example, a colour shade defined by the combination of (R, G, B) = (92%, 80%, 45%) can be achieved using the individual sub-colour quantities of the fundamental colours as follows. The common factor of 45% for all three primary colours can be attributed to achromatic white. Then a 35% colour quantity is common to R and G, for which the common fundamental colour is C (Table 2.3.1). The additional quantity of 12% is formed by the violet blue (V) and the remaining 8% by the black colour. This is illustrated in Figure 2.12.
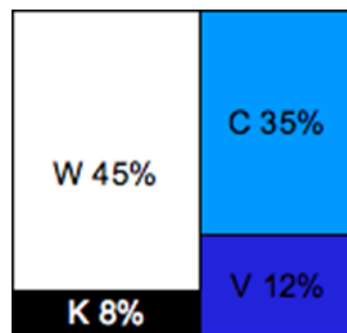
Figure 2.12 The percentage colour surfaces in a sub-surface for Kueppers' method

This method claims to have no trapping problems because only one ink layer is present at every location of the colour surface. This may reduce the drying problems resulting in smaller drying systems. It also claims to give moiré-free printing with expanded gamut to include high chromatic colours.

As the white ink can be used in this method, the colour of the substrate is not important. It can lead to higher tolerances because variations in individual inking have lower influence on appearance of the printed image. However this method may not be adequate for the offset printing process. It is not practical to print areas that do not overlap and are not visually noticeable. This method also restricts the gamut of 7-inks by printing only 3-inks for any given colour.

2.4.2   Ostromoukhov

Ostromoukhov (1993) proposed a model for expanding the conventional 4-colour printing process to a 7-colour (heptatone) printing process. In his method, the Neugebauer equation is extended to develop the compound Neugebauer model for 7-colour printing. This is done by partitioning CIEXYZ space and modelling the relationship between the colour and the ink. This process is claimed to be applicable for any ($2n+1$) colour printing where $n = 2, 3, 4...$

Compound Neugebauer model

First, CIEXYZ colour space was subdivided into multiple divisions each consisting of 3-inks and a generalised Neugebauer equation applied to each partition. This gives a prediction of 3-primary inks in terms of *XYZ* values for each partition; thus the relationship between the colour and the ink is obtained. For a printing process with ($2n+1$) primary inks, the colour gamut of the process is subdivided into $2n$ partitions. For each partition of 3-colours the compound Neugebauer equations can be applied as follows:

$$XYZ = A_w(XYZ)_w + A_1(XYZ)_1 + A_2(XYZ)_2 + A_3(XYZ)_3 + A_{12}(XYZ)_{12} + A_{23}(XYZ)_{23} + A_{31}(XYZ)_{31} + A_{123}(XYZ)_{123}$$

(2.45)

where $(XYZ)_w$, $(XYZ)_i$, $(XYZ)_{ij}$, $(XYZ)_{ijk}$ are the tristimulus values of the corresponding Neugebauer primaries.

$$A_w = (1 - a_1)(1 - a_2)(1 - a_3)$$
$$A_1 = a_1(1 - a_2)(1 - a_3)$$
$$A_2 = a_2(1 - a_1)(1 - a_3)$$
$$A_3 = a_3(1 - a_1)(1 - a_2)$$
$$A_{12} = a_1a_2(1 - a_3)$$
$$A_{23} = a_2a_3(1 - a_1)$$
$$A_{13} = a_1a_3(1 - a_2)$$
$$A_{123} = a_1a_2a_3$$

(2.46)

where a_1, a_2, a_3 are the dot areas of the primary inks. The total gamut of the printing process is the sum of all (2*n*) partitions. This method enables one-to-one mapping between colorant space and colour space.

Gamut

For each partition, *XYZ* tristimulus values of all primary colours (W, C1, C2, C12, K) were measured. The compound Neugebauer equation was used to compute the sub-gamut of the partition and all of the sub-gamuts for (2*n*) partitions were combined to produce the entire gamut of the printing process. The partitioned *XYZ* values were converted to a 7-colour separation by using a three dimensional relationship between the device space and CIEXYZ space by use of a look-up table (LUT) method with tri-linear interpolation.
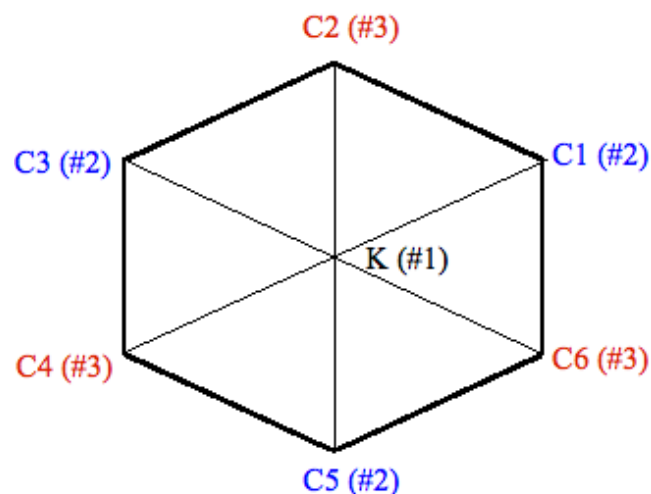
Figure 2.13 Black-White axis projection of 7-colour separation by Ostromoukhov (1994); The # number in bracket shows the order number of the screen angle/frequency pair.

Screen angles

For conventional halftone screening in the CMYK process, each primary colour was printed with a different screen angle to minimise the low-frequency interference pattern known as moiré. In this method for heptatone printing, only 3 different screen angles were used.

Alternate vertices or primaries of the hexagon use the same screen angle and frequency (Figure 2.13). A total of three screen angles was required for any even number of inks. This method claims that 7-colour printing is simpler than CMYK for reducing the moiré effect.

Results

The gamut of the 7-colour process was significantly larger than that of the CMYK printing process especially in violet and green regions. As the reproduction is restricted to only 3 inks for any given colour, the full potential of the 7-colour printing process may not be utilised. Thus some dark colours which could be achieved using more than 3 inks cannot be printed using this method. It should also be noted that discontinuities may occur on the boundaries of any two partitions.

2.4.3   Boll

In this method, Boll (1994) supplemented the CMYK process with additional RGB inks to expand the gamut of the printing process particularly in the darker region, for example for three-quarter tones. The CMYKRGB ink-set of 7-inks was subdivided into a series of 4-ink subsets. Each subset of 4-inks was characterised and the ink-table was generated in order to perform transformations from colour to ink.

An ink-table consists of a three-dimensional look up table (LUT) which generates halftone separations. It requires CIEXYZ or CIELAB values as an input; ink levels for 7 inks are produced as an output thus performing the colour-to-ink transformation for in-gamut colours. This method assumes that the ink-set (CMYKRGB) has already been chosen and the following steps were described to achieve the final colour separation.

The CMYKRGB ink-set was split into 6 subsets of 4-inks each containing 3 chromatic inks and black ink. For each 4-ink subset, a colour target was generated, printed and measured. A forward model for ink-to-colour transform was created to give a sub-gamut for each subset. All sub-gamuts were combined to construct a super-gamut i.e. a gamut

of the 7-ink process. An inverse model for each 4-ink subset was derived by defining the ink-table grid-points and compressing out-of-gamut colours (grid-points) to the super-gamut. Inverse models yield ink levels (separations) for each colour through a colour-to-ink transform.

Subsets

The following 6 subsets consisting of 4 inks were used: GYRK, YRMK, RMBK, MBCK, BCGK and CGYK. Within any 3 chromatic ink grouping, the central ink bordered by its adjacent inks is called as the dominant ink. The subsets can also be referred to by their dominant inks i.e. 'Yellow' (Y) ink which sits in the middle of red (R) and green (G) in case of the GYRK subset. In his study, Boll used the Cromalin proofing process along with an Agfa SelectSet 5000 image setter to produce separations for the Cromalin process.

Colour targets

Each of the six colour targets consisted of 625 patches having all combinations of 4 inks from 0% to 100% dots at an interval of 5% i.e. 0%, 5%, 10%, ..., 95%, 100%. This ensures reasonable sampling of colours across the colorant space.

Forward model

A forward model for each subset was constructed that related 4-ink combinations to colorimetric values. This was obtained by fitting experimental data to formulate a mathematical transform. The colour difference between the measured colours and model-predicted colours was calculated for each of the 6 forward models (Table 2.6). The maximum colour difference values lie between 4.82 and 7.10 ΔE^{*}_{ab} with values of standard deviation in the range 0.66 to 2.14.

Table 2.6 Accuracy of forward models of Boll (1994)

Forward Model	Maximum ΔE^*_{ab}	Standard Deviation
1GYRK	6.82	2.02
2YRMK	7.10	2.14
3RMBK	6.28	0.79
4MBCK	5.20	0.78
5BCGK	4.82	0.66
6CGYK	5.76	1.88

Gamuts

For each subset, a sub-gamut, which is a part of the overall super-gamut of 7-inks was constructed in CIELAB colour space. For constructing the gamut, the lightness (L^*) range was quantised into 128 levels and for each L^* level, the hue angle (h) was quantised. Further, for each L^* and h level, maximum chroma (C^*) value was determined to describe the gamut boundary.

By combining all 6 sub-gamuts, a super-gamut was obtained to represent the gamut of the CMYKRBG inks. As the adjacent sub-gamuts have 3 inks in common between them, there is a high degree of overlap. All sub-gamuts join at the neutral axis.

In order to map the colours which are outside the super-gamut, gamut mapping was applied. An out-of-gamut colour was mapped to the nearest points on the boundary of the super-gamut.

Inversion Model

Inverting a forward model is not straightforward; an inversion model was obtained by using the optimisation method of Nelder-Mead (1965) or the root finding algorithms of Newton-Raphson (Dennis, 1983).

A term called '*paired component replacement*' (PCR) was coined by Boll to represent an equivalent of grey component replacement (GCR) of the CMYK process. In the case of a 4-ink subset, a combination of dominant ink and black ink was replaced by two subordinate inks, for example, in the GY̲RK subset, YK may be replaced by GR. If the dominant ink is one of the CMY set then subordinate inks will largely replace black ink (K). If the dominant ink is in one of the RGB set then subordinate inks will replace most of the dominant ink., for example, in the case of CG̲YK, the dominant ink is G; C and Y inks will replace more G than K.

For a 7-colour printing process, any given colour can be reproduced by many possible combinations of inks. The criterion used by Boll for selecting the inks was to maximise the dominant ink. If the inking is based on maximisation of the dominant ink then this can help to smooth the transition of black ink between chromatic and achromatic colours. It also reduces the number of inks used for printing a specific colour. Black ink alone can be utilised to print neutral colours. Paired Component Replacement (PCR) assumes a colorimetric equivalency between a pair of dominant ink and black and a pair of subordinate inks. For example, in case of CGYK, monotonic variation in value of GK pair required CY pair to vary inversely. Hence the use of maximum dominant ink implies maximisation of black ink.

Because of the significant overlap between two adjacent sub-gamuts, any arbitrary colour is covered by two sub-gamuts. The ink combination which gives the closest match to the predicted inking was selected based on the maximisation of the dominant ink.

Inter-model errors

In practice, the forward models of adjacent sub-gamuts may not yield the same colour for values of inks common to both sub-gamuts. If forward models are highly inconsistent with each other then discontinuities of ink transitions may be unacceptable. Forward models for all subsets were evaluated to determine inter-model errors.

Sub-gamuts of GYRK, YRMK and CGYK showed a high level of agreement whereas RMBK, MBCK and BCGK sub-gamuts revealed variations in the darker regions. Sources of these errors could be measurement uncertainties and variation in toner density or print density.

Printing was carried out using the following screen angles: C and R – 15°; M and G – 75°; Y and B – 90°; K – 45°. Screen frequencies used was 150 lpi for the C, M, Y, K, R, G and 200 lpi for the B ink.

The Boll method utilises the full potential of a 7-ink gamut by using 4-ink subsets and maximising the dominant ink for the ink selection. This results in a larger gamut of CMYKRGB than that obtained from a 3-ink subset approach. The PCR technique can be particularly useful for dealing with the *n*-colour printing process. The constraint of maximising the dominant ink also ensures that a given colour can be printed with as few inks as possible.

At the same time, it requires 6 colour targets with a large number of colour patches to be printed and measured for constructing the forward and inverse models. Overlapping of two adjacent sub-gamuts results in the printing of redundant colour patches.

2.4.4   Halftone Area Neugebauer Separation (HANS) model

Morovič (2010 and 2012a) proposed a new colour separation method called as the halftone area Neugebauer separations (HANS) method. Instead of using traditional colorant space, this method uses the Neugebauer Primary (NP) space for colour separation by specifying the relative area coverages of the printer's Neugebauer primaries.

Consider a 2-ink printing system with cyan (C) and magenta (M) inks. Suppose that the printing system is bi-level where the number of levels of ink deposited at a given location is 2. With the conventional approach, the CM colorant space is accessible

(Figure 2.14a). The colorant space is restricted by the individual ink limits (m_C and m_M) as well as the total ink limit (m_T) to avoid the print artefacts, such as ink bleeding.
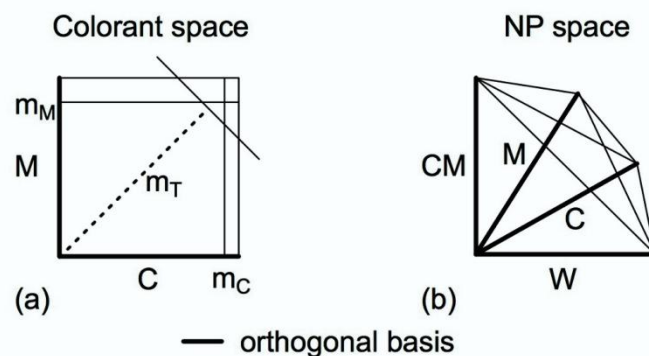
Figure 2.14 Print control spaces for a 2-ink bi-level printing system (Morovič, 2010): (a) the colorant space and (b) the Neugebauer Primary space

There are four Neugebauer primaries: W (the paper white), C, M and the 2-ink overprint CM. In case of the NP space, a k^n-dimensional simplex is accessible where k is the number of levels per ink and n is the number of inks. For example, the 2-ink bi-level printing system has the 100% area coverages of the W, C, M and CM Neugebauer primaries as the vertices of the simplex (Figure 2.14b). With the ink limitations in place, this accessible part of the NP space is restricted to the intersection of the simplex with half-planes defined by m_C, m_M and m_T.

The HANS approach gives access to all patterns formed by a printing system's NPs. Conventional halftoning process itself relies on the NPs. However, the HANS method exercises direct control over the NPs. This was illustrated with an example of a colorant combination of 50% cyan and 50% magenta. This can be expresses as an ink vector: $[c_C, c_M] = [0.5, 0.5]$ in a colorant space. Each ink vector corresponds to a continuum of NP area coverage vectors.

Thus the ink vector in the above example has the following constraints.

$$a_C + a_{CM} = c_C$$

$$a_M + a_{CM} = c_M$$

<div align="right">(2.47)</div>

where a_X is the area coverage of NP X and c_Y is the area coverage of ink Y.

The halftone patterns matching the above mentioned ink vector is shown in Figure 2.15. Note that the NPac vectors of these halftone patterns are different. When these were printed using an inkjet printer (HP Designjet Z3100) on a Hahnemühle Smooth Fine Art paper, the colours between the extremes of the NPac range showed 25 CIEDE2000 colour difference (Morovič, 2010).
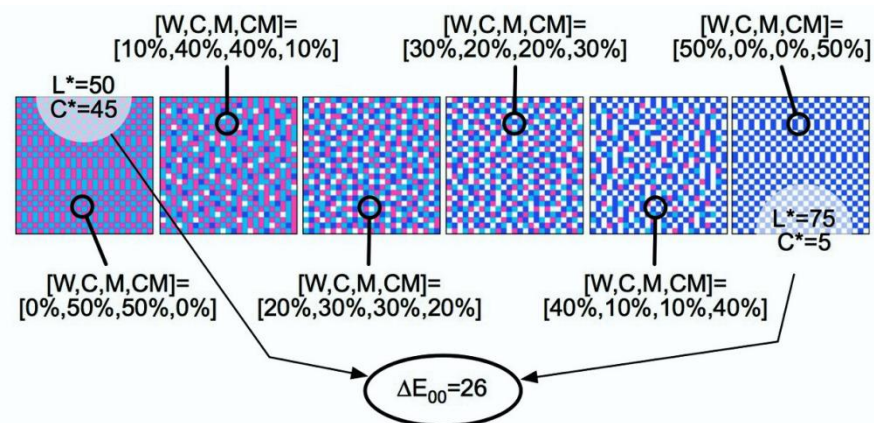
Figure 2.15 Continuum of halftone patterns corresponding to single ink vector $[c_C, c_M]$ = [0.5, 0.5] (Morovič, 2010)

For a conventional method based on a colorant space the halftoning gives one of the patterns shown in Figure 2.15, whereas the HANS method can access the entire range. Even for a 2-ink combination, this model can access metamers – the halftone patterns which are different from each other but still result in the same colour under a specific viewing condition. In case of the conventional colour separation, metamers are accessible with more than three inks.

A colour separation to NP area coverage (NPac) space can be computed as follows (Morovič, 2010). All NPs are printed and measured. A convex hull of all NPs is computed in the CIEXYZ space and then sampled. For each sample, the corresponding metamer set is computed. From each metamer set, the optimal NPac is selected for the given print attributes. As a result, a set of CIEXYZ coordinates is obtained spanning the full colour gamut. Each coordinate has NPac assigned to it.

Morovič (2010) implemented the HANS model using a HP Designjet L65500 latex large format signage printer with CMYKcm inks (where c and m represent light cyan and light magenta, respectively) on Avery Glossy Self-Adhesive Vinyl substrate. The HANS model was compared against the ICC pipeline configurations, first with the default colour separation configuration and then with the maximum GCR (grey component replacement) configuration. The HANS model showed 34% saving in ink use as compared to the ink used by the default ICC colour separation configuration and 20% saving in ink use as compared to the ink used by the maximum GCR configuration without affecting an image quality. It was also found that the HANS model gives around 10% increase in a colour gamut as compared to the ICC configuration.

The HANS approach gives access to all printable patterns that extend over the Neugebauer Primary area coverage, resulting in a larger gamut while using less ink as compared to existing ICC method which is based on the colorant space. HANS method is also independent of the ink set, for example, it can be used for colour separation of duotone, CMYK, CMYKOGV etc.

The HANS colour separation was optimised using a 3-ink (CMY) printing system (Morovič, 2011). In this case, the HANS approach provides significant metamer sets that lead to variety in print attributes, whereas the colorant space based methods provide unique solutions. It shows that the HANS approach can be used for direct optimisation of print attributes, for example, ink usage, colour constancy and grain, because the set of NPac metamers that map to the same colorimetry may vary in these print attributes.

In another use case, the HANS approach was applied for simplifying the print colour formation by combining only eight basic colour patterns (Morovič, 2013). This approach allows the printing system to be characterised using eight halftone patterns and the system's dot gain. This was tested using a HP Designjet Z6200 inkjet printer with pigmented CMYK inks on HP Coated Paper. A test chart consisting of 512 colour patches was printed and all colours were measured to calculate the CIEDE2000 between the measurements and the predictions. The results showed a mean of 1.59, a 95th percentile of 3.96 and a maximum of 5.54 CIEDE2000 between the measured and the predicted colours. Although this approach does not use the full gamut of a printing system, but in many cases the theoretical constraints represent very little loss ((Morovič, 2013).

2.4.5   Mahy

Mahy (2011) proposed a CMYK printing process complemented with opponent colours, for example, orange (O) and green (G). Colour separation process is divided into partial 4-colorant processes, for example, CMYK, OMYK and CGYK. From the CMYK process, if a chromatic colour is replaced by its opponent colour, then we get another partial process. For example, C in CMYK is replaced by its opponent colour O to get OMYK partial process. Similar approach was described by Deshpande (2009 and 2014a) and it has been used throughout this project (see details in Chapter 3, Section 3.2.1).

Each of these partial print processes has its colour gamut (Mahy, 2011). The colour gamuts of the partial colorant processes sharing only two inks do not overlap. For example, the OMYK and the CGYK share all possible combinations of Y and K. Hence the YK maps to a common surface that separates the gamuts of OMYK and CGYK processes showing no overlap between the colour gamuts of these two partial processes. However, the colour gamuts of the partial colorant processes sharing three inks show considerable overlap. For example, the CMYK and the OMYK share all combinations of the M, Y and K inks. Furthermore, some combinations including O in OMYK process may also be achieved using a CMYK combination.

Mahy (2011) assumed that for the CMYK process, separating a given colour with a larger amount of K ink results in a decrease of the CMY inks and vice versa. Similarly for the OMYK process, the variation of amount of an O ink can be exchanged for an opposite variation of the MYK inks. A forward printer characterisation model and the model inversion of the 4-colorant model are assumed to be continuous.

Continuity of the colorant amounts across the gamut boundaries is achieved by using specific constraints to reproduce the given target colour. For example, if a colour is within the gamut of a first partial print process (say, OMYK), it is achieved using the maximum magnitude of a first colorant i.e. O. If a colour is within the gamut of a second partial print process (say, CMYK) but not to the OMYK colour gamut, it is achieved using the minimum magnitude of the opponent of the first colorant i.e. C. This method allows extending the CMYK framework to other 4-colorant processes.

The continuity between colorant components is obtained by creating a curve that defines the amount of an opponent colorant with regard to the minimum and maximum possible magnitudes to render a given colour. This is achieved using weight factors for calculating the amount of an opponent colorant as a function of a minimum and maximum magnitude (Mahy, 2011).

2.4.6   Other methods

Viggiano (1998) proposed two criteria to select ink-sets for the six-colour lithographic printing process: the gamut volume of the printing device and the number of pixels within an image whose colours are inside the gamut of the device.

Viggiano used a spectral model to predict the overprints of two or more colorants. A convex hull method was used to derive the gamut of the printing process. The first criterion i.e. the volume of the gamut, is independent of the images whereas the second criterion is image-dependent.

The substrate colour and the colours of the inks printed on the substrate were considered as first-order factors due to their high effect on the gamut size. The colours of the

overprints (secondary, tertiary etc. colours) were treated as second-order factors, which were less significant than first-order factors. The behaviour of the inks between the gamut-limiting colours was considered as a higher-order factor, which was modelled instead of taking measurements.

Stollnitz (1998b) investigated the problems faced in colour reproduction using custom inks. The gamut model was based on the KM and the spectral Neugebauer models with modifications for trapping and dot gain. Colour separations were computed based on a multi-resolution algorithm. This algorithm computes for each pixel the colorant amounts that produce the right colour and are as close as possible to the colorant amounts of the entire surrounding neighbourhood. The algorithm is based on image pyramids which are defined recursively by finding a larger neighbourhood.

2.5   Psychophysics

Psychophysics is defined as a scientific method of studying the relationship between a physical stimulus and the perception evoked by the stimulus (Gescheider, 1997). Different types of techniques are used for measuring perception of the physical stimulus, for example, scaling and threshold techniques. More details on psychophysics and experimental methods can be found in Fairchild (2005), Gescheider (1997), Torgerson (1967), Engeldrum (2000) and Bartleson (1984).

2.5.1   Scaling techniques

Scaling experiments are used to derive a relationship between physical and perceptual magnitudes, for example, to correlate objective measurements of image quality to the subjective correlates of quality. Engeldrum (2000) defines psychometric scaling as the generation of scales of the image quality and attributes (also termed as "nesses") by human measurements. The basic scales used in psychometric scaling are – nominal, ordinal, interval and ratio.

Nominal scales are used to scale stimuli simply by names or labels. They are not very useful since no mathematical operation can be performed with them. Ordinal scales represent orders with respect to the attribute being assessed. Labels or numbers are used to represent the ascending or descending rank order of the samples. Mathematical operations like greater-than and less-than can be performed with these scales, but the magnitude of the difference can be large or small. Interval scales add the property of distance to ordinal scale. The distances have equal intervals. Operations like addition and subtraction can be performed with interval scales. Ratio scale adds zero point or origin to the interval scale. In addition to equal intervals they have equal ratios. Operations like addition, subtraction, multiplication and division can be performed with these scales. Following methods are used for measuring psychophysical scales.

Paired comparison method uses pairs of stimuli, for example reference and sample. For each pair, the observers are asked to choose the stimulus having greatest amount of attribute or image quality. This method can be used to generate an interval scale with few assumptions.

Rank order method can be considered as an alternative to the paired comparison method since it produces similar relative scores. The observer is asked to rank the samples in order of ascending or descending magnitudes of an attribute. This method produces an ordinal scale, but the ranking data can be transformed into an interval scale with some assumptions and additional analysis.

Category judgement method is based on the Law of Categorical Judgement by Torgerson (Fairchild, 2005) which assumes that the psychophysical continuum of the subject can be divided into multiple categories. The observers are given samples to judge against a reference and asked to separate each sample in different categories. Data obtained from the experiment can be used for generating an ordinal and interval scale. This method needs fairly large number of judgements.

2.5.2   Threshold techniques

Threshold techniques are used to find out a just-noticeable difference (JND) which is the difference in the stimulus observed as just perceptible or just acceptable. Threshold experiments are designed to measure the observers' sensitivity to changes in stimuli, for example, to define visual tolerances for perceived colour difference.

There are different techniques for threshold experiments. For example, the observers can adjust the stimulus magnitude such as the difference to the reference stimulus is just perceptible or just acceptable. In another technique the stimuli with discrete magnitude levels are presented to the observer in ascending or descending order. The observers are then asked to respond if they perceive the difference ("yes") or not ("no").

2.5.3   Other techniques

There are other types of psychophysical experiments. For example, memory matching experiment in which the observers produce a match to a previously memorised colour (Fairchild, 2005). These experiments produce data for testing colour appearance models. In magnitude estimation technique, the observers have to give a numerical response in proportion to the perception of colour attributes like lightness, chroma and hue. The observer assigns numbers to the stimuli according to the magnitude of the perception. This can be used to obtain ratio scales.

2.5.4   Observers

Observers usually fall into two categories – expert observers and average observers. Expert observers do have experience in judging the colour and image quality. They can make fine distinction of the attribute that they are judging. Their scaling may be more critical than the scaling by an average observer depending on the scaling task and a specific attribute used in the experiment. For example, in category scaling the expert observers can distinguish among categories that average observers may not (Engeldrum,

2000). For the applications which require fine categorisation of the colour difference values, such as packaging printing, the experienced observers are needed for the scaling task.

Observer training might be necessary to familiarise the observer with performing the psychophysical task. To avoid a bias to the experimental results, the observers should not be given hints or taught to follow any specific way of judgement. The observers should be allowed to interpret the concepts of colour attributes according to their own ideas.

A large number of observers increases the precision of the collected responses reducing the error in the scale value. The number of observers mainly depends on their availability. According to Engeldrum (2000), the number of observers from 10 to 30 is usually recommended.

Observer performance should be evaluated to know the uncertainty involved in the experiment. The consistency of each observer's judgement can be checked by analysing the observer repeatability, for example, by randomly presenting the same stimulus twice in a session and calculating the absolute difference between the two responses.

In this project, we used category judgements with verbally defined category labels to derive the perceptibility and acceptability thresholds (see 8.3). The observers were given various samples to judge against a reference stimulus and asked to separate each sample in different predefined categories. This method is better than the "pass-fail" method where the observers can respond "yes" or "no" to the stimuli. The categories allow collecting more information about the stimuli to analyse data with several thresholds. Also for the packaging print environment it is useful to assess the correlation between the measured colour differences and the visually perceived colour differences in terms of perceptibility and acceptability thresholds.

2.6 Conclusion

This chapter has summarised the previous research applicable to *n*-colour separation, including the characterisation methods of printing devices. Forward characterisation methods including physical models and empirical methods are discussed and the results of previous studies are summarised to compare the accuracy of the different models.

Inverse characterisation methods to obtain the colour separation are described. These include the inversion of forward printer models using data-fitting techniques and lookup table based inversion using interpolation methods.

Existing methods of deriving the *n*-colour separation are explained. The different approaches used by researchers to address the challenges to the *n*-colour separation are discussed.

Printer models described were evaluated and the prediction accuracy results of different models are compared in Chapter 4 (forward characterisation), Chapter 5 (gamut prediction of the *n*-colour printing process), Chapter 6 (spot colour overprint model) and Chapter 7 (inverse characterisation).

Chapter 3 Methods

This chapter describes the methods and procedures used throughout the project. It includes the metrology for colour measurements, the reproduction workflow, the computation procedures and the process control requirements for the *n*-colour printing processes.

3.1   Metrology

The principles of colour measurement are explained in Section 2.1.5. Different spectrophotometers were used to measure the various coloured test charts during the project, for example, an X-Rite i1 Pro 2 and an X-Rite SpectroEye. These spectrophotometers were compared in terms of their repeatability, accuracy and inter-instrument agreement.

To assure the consistency of colour measurements, the following measurement conditions were used throughout the project and they are referred to as the 'reference measurement conditions': CIE illuminant D50, CIE 2° standard observer, 45°:0° measurement geometry with a white backing material. These conditions resemble the measurement condition M0 specified in ISO 13655 (2009). A UV absorbing filter fitted to the instrument was used to remove the UV component of the lamp spectral power distribution. All substrates and colorants (inks) were non-fluorescent. Both factors ensured that there were no variations in the measurements due to florescence.

For all measurements, the spectral reflectance data of the colours of each test chart were measured. Wherever possible, multiple measurements (typically three) of the same test chart were made and the average values used for data analysis.

Metrics used for evaluating the printer characterisation models were the CIEDE2000 colour difference and spectral RMS error between the model-predicted colours and the measured colours. The CIEDE2000 colour difference formula, the latest formula recommended for use by CIE, was selected due to its high correlation with visual

100

observations. Several studies have showed that the CIEDE2000 formula reduces the perceptual non-uniformity of CIELAB colour space and is better than other colour difference formulae (Luo, 2001) (Sharma, 2005) (Wang, 2012). Various international standards for the graphic technology support the use of the CIEDE2000 colour difference formula (ISO 12647-2:2013, ISO 13655:2009). The following lightness, chroma and hue weighting factors were used: $k_L = k_C = k_H = 1$ respectively (see Appendix A: CIEDE2000 calculations for more details).

The mean, 95th percentile and the maximum value were used as statistical metrics throughout the project. The mean value provides a simple measure of the central tendency, but if the error distribution is not normal, as is usually the case for colour difference data, then the mean value is not a reliable central tendency. The maximum value represents the worst performance, but it is not robust if there are few outliers. The 95th percentile value indicates that the 95% of the population is below this value. It gives information about the distribution of values. These three statistical metrics are complementary and together they provide a good overview of the results.

Colour difference data sets are usually chi-squared distributions with three degrees of freedom (Dolezalek, 1994). For a non-symmetric distribution, the median is the best unbiased estimate of central tendency. It would have been better to have used the median as the measure of central tendency.

3.2   Reproduction workflow

3.2.1   Approach – colorant space division

Printing systems that consist of 7 process inks were used. These were Cyan, Magenta, Yellow, Black, Orange, Green and Violet. The colorant space was divided into sectors of 4-inks each: CMYK, OMYK, CGYK and CMVK (Figure 3.1). Every sector contains an achromatic channel (K) so as to provide a balanced division. In addition to CMYK, three sectors were defined based on the secondary colour as a dominant colour of the sector. For example, OMYK is the orange-sector with orange as a dominant colour, magenta and yellow as primary colours and black as an achromatic colour.
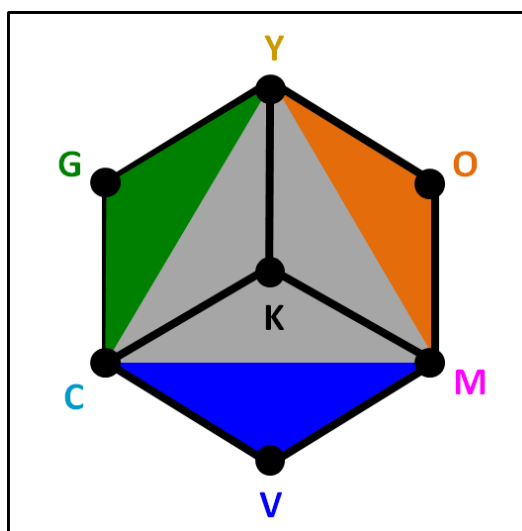
Figure 3.1 Four sectors of CMYKOGV colorant space – CMYK, OMYK, CGYK and CMVK

This method can be generalised for any *n*-colour printing process. For example, in the case of an 8-colour printing there will be five sub-sets of 4-inks containing black as a common ink and three chromatic inks in each sub-set.

This approach is similar to another method (Boll, 1994), in which the seven inks were split into six sets of 4-inks. The proposed method uses only four sets. With six sectors of 4-inks, there are more overlaps between the adjacent sectors adding to the complexity. In case of four sectors of 4-inks, the adjacent sectors of orange, green and violet have only two inks in common between them.

3.2.2   Printing technologies

Several printing technologies were used in this project, for example, offset lithography, flexography, thermal sublimation and inkjet printing (Figure 3.2). Substrates used were as follows: coated gloss paper for the lithographic offset and the thermal sublimation printing, white film for the flexographic printing and semimatte proofing paper for the inkjet printing. Considering the range of printing processes and the scope of this project, it was not possible to control the halftone algorithm. Amplitude modulation (AM) screening with 150 lines per inch (lpi) screen frequencies was used for all printing technologies except inkjet. For inkjet printing, a frequency modulated screening with 720 dpi was used.
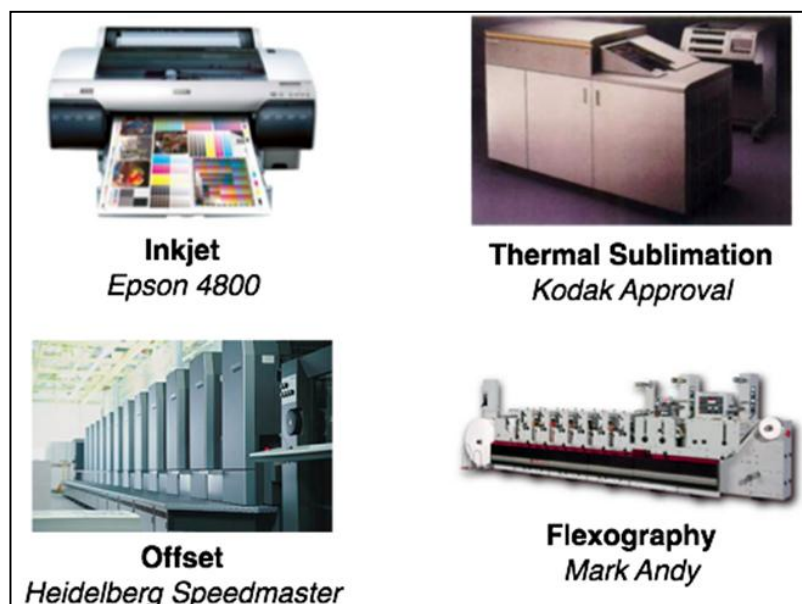
Figure 3.2 Printing technologies used in this project

Unlike conventional 4-colour printing, for *n*-colour printing, the screen angles should be carefully assigned to all the inks. Complementary colours were assigned the same screen angle and the following screen angles used: Cyan and Orange = 15°, Magenta and Green = 75°, Yellow and Violet = 90° and Black = 45°. The typical ink lay-down order (sequence) was Black – Violet — Cyan — Green — Magenta — Orange – Yellow. This was based on reducing the tack order from the first ink to the last.

Repeatability of each printing system was evaluated by printing a colour strip consisting of 20 patches. The colour strip was printed 10 times with a time interval of 15 minutes on each printing system. The printed colours were measured using X-Rite i1 Pro 2. For each colour patch, the mean values of L*, a* and b* were calculated. A colour difference between the mean L*a*b* and each individual L*a*b* values was calculated resulting in 10 values of CIEDE2000 for each patch. Average of these 10 values can be calculated as the 'mean colour difference from mean' or MCDM. The mean, maximum and 95th percentile values of MCDM were calculated (see Table 3.1).

Table 3.1 Repeatability of the printing systems

Printing Process	Repeatability in MCDM (CIEDE2000)		
	Mean	95th percentile	Max
Inkjet	0.76	0.89	1.02
Thermal Sublimation	0.52	0.79	0.98
Offset	1.24	1.92	2.38
Flexography	0.98	1.34	1.96

3.2.3   Calibration

Each printing system was calibrated to adjust its behaviour to known desired conditions. For example, the offset lithographic printing process was calibrated by matching the tone value curves (ISO 10128). Tone values for Cyan, Magenta and Yellow were adjusted to achieve the required tone value increase (TVI) targets of "curve A" specified in ISO 12647-2 (2007). Tone values for Black, Orange, Green and Violet were adjusted to achieve the tone value increase (TVI) targets of "curve B" specified in ISO 12647-2 (2007). Similarly for the flexographic printing process the ISO 12647-6 (2006) aim values were used with the tone value increase curve for the substrate type 4 (Film/Foil).

3.2.4   Test charts

For each 4-ink sector, the ECI2002 test chart (ISO 12642-2:2006) was generated and printed using the different printing processes. These charts were used to evaluate the printer models. Each test chart contained 1485 colour patches. By combining all ink sectors, there were a total of 5940 colour patches representing the overall 7-colour printing process. Each test chart contained the same colorant values (dot areas). For example, in the OMYK chart, all values of cyan (C) ink in the CMYK chart were replaced by orange (O) ink. Figure 3.3 shows the randomised test charts for all sectors.
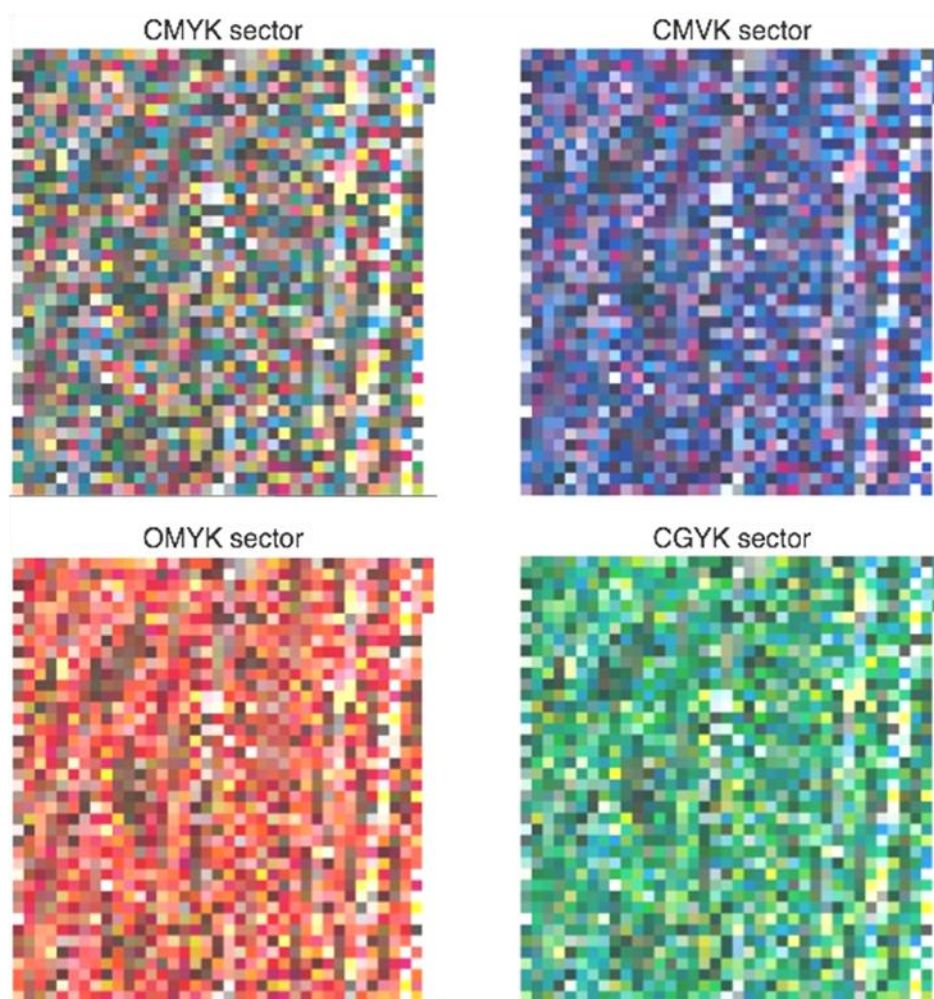
Figure 3.3 Printed 4-colour test charts for each sector of the 7-colour printing process

The colour patches in each test chart were measured using an X-Rite i1 Pro 2 spectrophotometer with the reference measurement conditions described in Section 3.1. Measurements for all ink sectors were collated to form a data set for each different printing process.

Although, *n*-colour printing represents any printing system with more than 4 inks ($n > 4$), a 7-colour printing ($n = 7$) was chosen because it supplements the conventional CMYK process with three additional inks, which are complementary to C, M and Y chromatic inks. These additional inks are red (R) or orange (O), green (G) and blue (B) or violet (V).

While a 7-colour printing process was used as an example, the method described below can be generalised to any *n*-colour printing process by having sub-sets of 4-inks each containing a common black ink and three chromatic inks.

For implementing the cellular Yule Nielsen modified Spectral Neugebauer (YNSN) model, the X-Rite MeasureTool application was used to generate the test charts for input colour patches. This is explained in detail in Chapter 4 (Section 4.2.4)

3.3   Computation procedures

MathWorks Matlab was used as the main tool for all computations and image processing. Matlab was preferred because of its suitability for the colour science algorithms particularly the matrix calculations. It has a collection of subprograms called M-files, which are useful for many computations. Matlab can also construct two-dimensional and three-dimensional graphics very easily. The algorithms (Matlab codes) written are included in Appendix B: Matlab codes for the spectral printer models.

A modular toolbox containing different Matlab functions was developed during the project. These functions mainly consist of the spectral printer models, gamut prediction methods and inversion models. For basic colorimetric calculations the Colour Engineering toolbox (Green, 2003b) was used.

The colour measurement data were acquired through X-Rite ColorPort and Esko ColorEngine by exporting the colour measurements as a Colour Exchange Format (CxF) file. These measurement data files were imported into Matlab.

3.4   Process control requirements

Process control is an essential part of any print production system and for the *n*-colour printing process it becomes more important because of the complexity of the additional inks. Spot colours are normally printed with special inks. When a spot colour is converted to an *n*-colour separation and printed with *n* colorants, the printing process should be controlled tightly to assure print stability and consistency throughout production runs.

This can be achieved by standardising the print production workflow from file delivery to the press output. For example, the reprographic or pre-press standardisation may include calibration of all devices, artwork specifications and plate-making standardisation. In the press room, the consumables, for example, substrate, inks, pressroom chemicals, blankets etc should be optimised for the given printing process. Press maintenance is another important aspect, where the roller settings and dryer settings should be set to the press manufacturer's recommendations. Press room conditions, for example, temperature and relative humidity, play a crucial role in process control. For visual assessment of colours, ISO 3664:2009 viewing conditions were used throughout the project.

For all the print tests in this project, the process control parameters were recorded. Below is an example of the partial list of parameters recorded for the lithographic offset process (Table 3.2).

Table 3.2 Process control parameters for the lithographic offset printing workflow

Press room	
Press	Komori 640
Substrate	Incada Exel
Substrate type	Coated Gloss
Substrate grammage	265 GSM
Ink sequence	K - V - C - G - M - O - Y
Fount solution pH	5.2
Fount solution conductivity	2130 mS
Fount solution temperature	10.4 °C
Fount dosage	4%
IPA dosage	4%
Run length	3000 sheets
Press speed	14000 sheets per hour
Press maintenance verified	Yes
Pre-press	
Halftone screen type	AM
Halftone screen ruling	150 lpi (lines per inch)
Halftone dot shape	Round
Screen angles (K-V-C-G-M-O-Y)	45-90-15-75-75-15-90
CTP calibration verified	Yes

3.5 Conclusion

This chapter outlines the metrology used throughout the project including the colour measurement specification, the choice of evaluation metrics and the statistical measures used for evaluating the printer characterisation models.

This provides a background for the remaining chapters which include the forward printer characterisation models (Chapter 4), colour gamut evaluation of the *n*-colour printing process (Chapter 5), a new simplified printer characterisation model (Chapter 6) and the inverse printer characterisation models (Chapter 7).

The colorant division approach is explained. This forms the basis for the characterisation, gamut prediction and the colour separation of the *n*-colour printing process.

Printing technologies used during the project are discussed. They include traditional printing techniques such as lithographic offset printing and flexographic printing, as well as relatively new printing techniques such as thermal sublimation and inkjet printing. The calibration methods for these printing technologies are mentioned. Typical test charts used for characterising the *n*-colour printing process are described.

Data acquisition of the colour measurements and the computational procedures using Matlab are given. Finally the significance of the process control is highlighted with the process control requirements for print production.

The next chapter deals with the implementation and evaluation of different printer characterisation methods for the 4-colour and the 7-colour printing processes.

Chapter 4 Implementation of the forward printer models

4.1   Introduction

The *n*-colour printing process is usually considered as an extension of the traditional 4-colour printing process i.e. CMYK. Before characterising the *n*-colour printing system, it is essential to implement the forward printer characterisation models to the 4-colour printing process. Printer models discussed in the literature (Chapter 2, Section 2.2) represent an important set of models for characterising printing devices. A printer model establishes a relationship between the colorant values and the corresponding colorimetric values of the measured printed colour. A forward model requires colorant values as input and predicts the resulting printed colour as the output.

In this project, several printer models were applied to different 4-colour printing systems, for example, offset, flexography and the inkjet printing processes. The accuracy of the forward model was evaluated by comparing the colours predicted by the models with the equivalent measured colours.

The following printer models were used in this study: the Neugebauer model, the Yule-Nielsen modified Neugebauer model, the Yule-Nielsen modified Spectral Neugebauer (YNSN) model, the Cellular YNSN model, the KM model with Saunderson correction, a combination of the KM and the YNSN model and the Van de Capelle model. Due to the scope of the project, especially the range of printing technologies and time constraints, it was not possible to implement all the models described in Chapter 2, Section 2.2.

All models were evaluated using the ECI2002 test chart (Figure 4.1) containing 1485 colour patches of different combinations of cyan, magenta, yellow and black inks. This test chart was printed using various printing systems. The printed colours were measured using an X-Rite i1 Pro 2 according to ISO 13655:2009 measurement condition M0 with CIE illuminant D50, CIE 2° observer, 45°:0° measurement geometry and a white backing material.
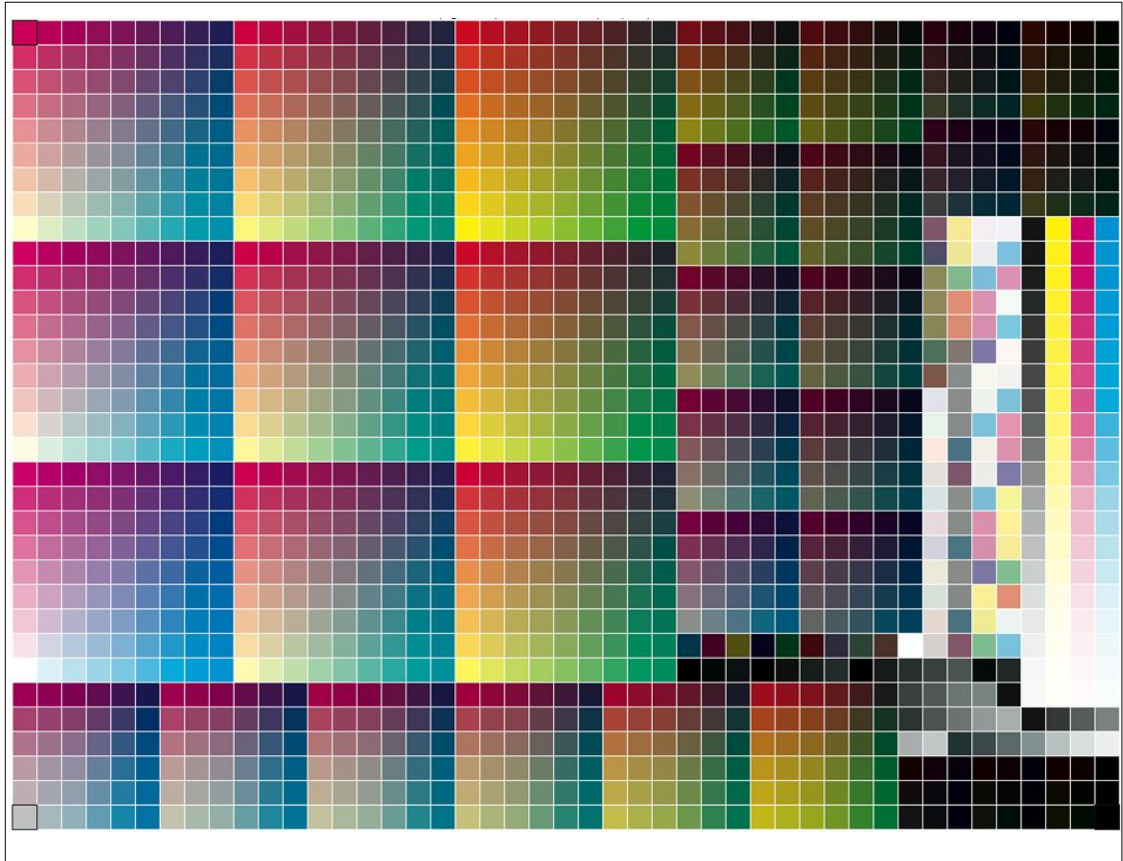
Figure 4.1 ECI2002 chart (visual layout) with 1485 colour patches

Each model required a set of colour patches to be printed and measured to act as an input training set to the model. This is described for each model in the respective sections below.

MathWorks Matlab was used as a programming language to implement all of the printer models (see Appendix B: Matlab codes for the spectral printer models). The printer characterisation models have been described in the literature review (Chapter 3). Here, each model is evaluated for the 4-colorant process (CMYK) in terms of the mean, 95th percentile and the maximum values of CIEDE2000 by comparing the model predicted colours with the measured colours. This is described in detail in Section 4.2.

Printing processes

The various printing processes used to evaluate printer models were as follows: inkjet, thermal sublimation, lithographic offset and flexography. Specifications for these printing systems are given below in Table 4.1. Each printing system was calibrated to adjust its behaviour to known desired conditions (see Chapter 3, Section 3.2.3).

Table 4.1 Printing systems used for evaluating printer models

Printing Process	Printing System	Substrate
Inkjet	Epson Stylus Pro 4800	Proofing papers – Semimatte & Luster
Thermal Sublimation	Kodak Approval	Gloss Coated paper
Lithographic Offset	Heidelberg Speedmaster	Gloss Coated paper
Flexography	MarkAndy Comco C2	White Film

4.2   Forward characterisation of a 4-colour printing process

4.2.1   The Neugebauer model

This was one of the first attempts to model the halftone printing process in terms of mathematical equations (2.2.1.2). Any printed colour can be considered as an integration of Neugebauer primaries, i.e. solid inks and their overprints. For a printing system with n inks, there are 2^n Neugebauer primaries. Thus in the case of a 4-colour printing process (CMYK), there are 16 Neugebauer primaries as follows:

Plain Substrate – white (no inks)
Solid colours — cyan (C), magenta (M), yellow (Y), black (K),
Two-ink overprints — C+M, C+Y, C+K, M+Y, M+K, Y+K.
Three-ink overprints — C+M+Y, C+M+K, C+Y+K, M+Y+K.
Four-ink overprint — C+M+Y+K

These 16 colour patches were printed on different printing devices. The printed colours were measured using the spectrophotometer to provide tristimulus values (CIEXYZ) and these measurements were used as the input to the model. To evaluate the model, ECI2002 chart was printed and measured.

To calculate the model predictions of the colours of the ECI2002 test chart, the colorant values (dot areas of C, M, Y and K) for each patch were used as input to the model algorithm. The model predicted the tristimulus values of the printed colours. Colour difference values between the predicted and the measured colours were then calculated using the CIEDE2000 colour difference formula. The results for all the printing processes are shown in Table 4.2. The mean and the 95th percentile CIEDE2000 values are above 5 and 8 respectively. None of these values are satisfactory.

Table 4.2 Accuracy of the Neugebauer model

Printing Process	CIEDE2000		
	Mean	95th percentile	Max
Inkjet	6.78	12.88	18.36
Thermal Sublimation	7.19	11.67	15.53
Offset	5.03	8.37	12.63
Flexography	7.56	14.06	18.25

4.2.2   The Yule-Nielsen modified Neugebauer (YNN) model

This model requires the same inputs as the Neugebauer model. This model introduces the Yule-Nielsen value (n) to the wide-band Neugebauer model to account for internal light scattering in the substrate. A value of $n = 1$ represents no light scattering in the substrate and the model reduces to the basic Neugebauer model. In this study, the Yule-Nielsen value (n) was treated as a correction factor to optimise the fit of the model to the empirical data.

The model is applied iteratively with increasing values of *n* with the objective function to minimise the mean colour difference between the predicted and the measured colours of ECI2002 chart. Figure 4.2 shows the relationship between the mean colour difference values (ΔE^*_{ab} and CIEDE2000) and *n*-values.
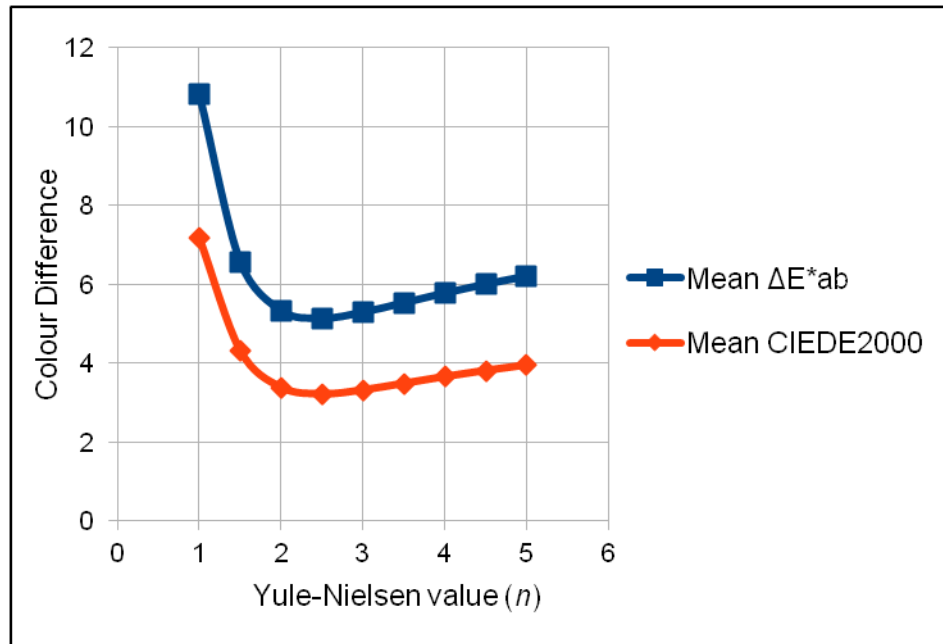
Figure 4.2 Effect of *n*-value on colour difference for the wide-band Neugebauer model

The accuracy of the Yule-Nielsen modified Neugebauer model is shown in Table 4.3.

Table 4.3 The accuracy of the Yule-Nielsen modified Neugebauer model, expressed in terms of values of CIEDE2000 colour difference, for 4 printing processes.

Printing Process	Optimised *n*-value	CIEDE2000		
		Mean	95th percentile	Max
Inkjet	1.57	4.83	10.04	14.73
Thermal Sublimation	2.46	3.21	5.70	8.65
Offset	1.78	2.36	4.43	7.71
Flexography	2.46	3.87	7.39	19.79

4.2.3 The Yule-Nielsen modified Spectral Neugebauer (YNSN) model

Now, the Yule-Nielsen correction was applied to the spectral model, instead of to the tristimulus values (Chapter 2, Section 2.2.1.3). This requires the measurements of the reflectance spectra of 16 Neugebauer primaries as described above. The YNSN model was applied to all colour patches of ECI2002 chart.

The mean colour difference values were plotted against *n*-values in Figure 4.3. This figure shows a similar trend as that shown for the Yule-Nielsen modified Neugebauer model (see Figure 4.2) except the sharp dip, indicating reduced values of colour difference, is more pronounced for the spectral model.
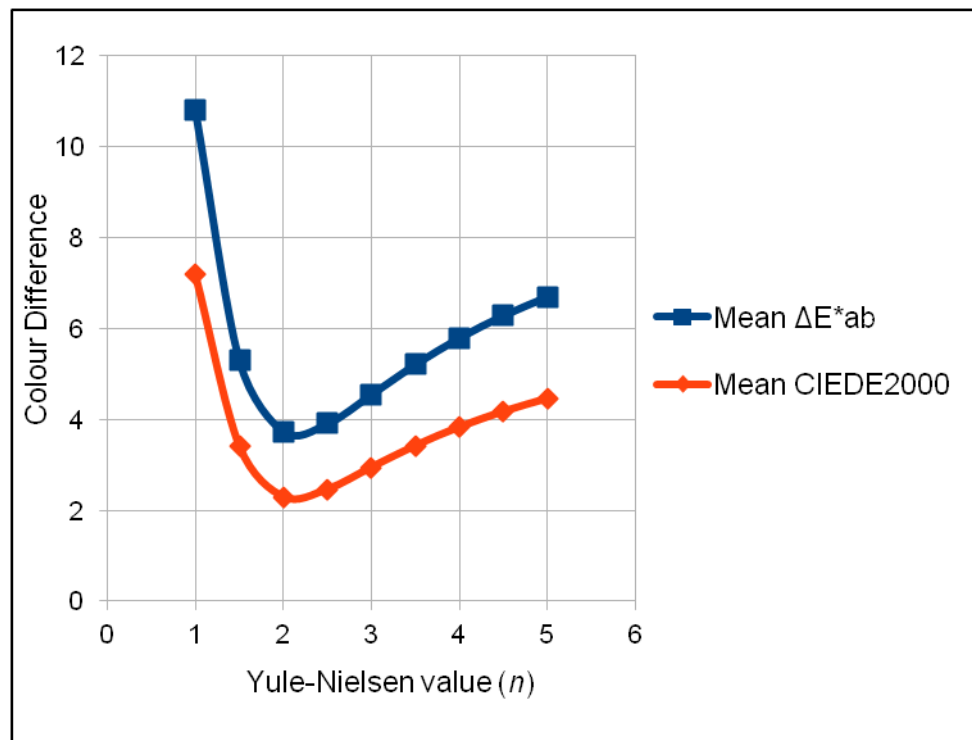
Figure 4.3 Effect of *n*-value on colour difference for the spectral Neugebauer model

The accuracy of the YNSN model, with optimised values of *n*-values for the four printing processes, is shown in Table 4.4. Comparison with Table 4.3 shows that the accuracy is improved from the wide-band to the spectral model. For example, the mean CIEDE2000 values for inkjet, thermal sublimation, lithographic offset and flexographic printing processes are decreased from 4.83, 3.21, 2.36 and 3.87 to 4.40, 2.26, 1.75 and

3.19, respectively. However, lithographic offset and thermal sublimation printing processes show more improvement than inkjet and flexographic printing processes, especially the maximum CIEDE2000 values.

Note that the YNSN model provides a simple n-factor to account for internal reflections of light within the substrate and ink film. This simplified approach may not be sufficient to handle some printing conditions, for example, white film in case of flexographic printing and the frequency modulated screening for inkjet printing. The results in Table 4.4 also agree with those found by other researchers including Taplin (2001), Rolleston (1993) and Kang (1993).

Table 4.4 The accuracy of the Yule-Nielsen modified spectral Neugebauer model, expressed in terms of values of CIEDE2000 colour difference, for 4 printing processes.

Printing Process	Optimised *n*-value	CIEDE2000		
		Mean	95th percentile	Max
Inkjet	1.52	4.40	9.77	14.32
Thermal Sublimation	2.12	2.26	3.76	5.02
Offset	1.66	1.75	3.40	5.85
Flexography	2.06	3.19	6.36	19.00

4.2.4   The Cellular YNSN model

In the case of a 4-colour printing process, the YNSN model requires $2^4 = 16$ Neugebauer primaries as input colours. For each colorant, there are two nodes, 0% and 100% dot areas. It is possible to include intermediate dot areas to increase the number of nodes along each colorant dimension (Chapter 2, Section 2.2.1.5). For example, if 3 nodes, 0%, 50% and 100%, are used for each colorant, then the number of Neugebauer primaries increases to $3^4 = 81$. This represents the cellular YNSN model with 3 nodes and it is necessary to print and measure all 81 primaries to provide input to the model.

In this study, the cellular YNSN model with 3, 4, 5 and 6 nodes was applied to evaluate the model accuracy for the inkjet printing system. Input colour patches (Neugebauer primaries) were generated using the X-Rite MeasureTool application. Figure 4.4 shows the input colour chart for 6 nodes with 1296 patches.

The accuracy of the model is shown in Table 4.5. Compared with the models described earlier, the mean colour difference values are shown to reduce with the increased number of nodes. The cellular model with 4 nodes seems to be sufficient, since any further increase in the number of nodes does not improve the colorimetric accuracy significantly. These results are in agreement with the results given by Rolleston and Balasubramanian (1993) and Taplin (2001).
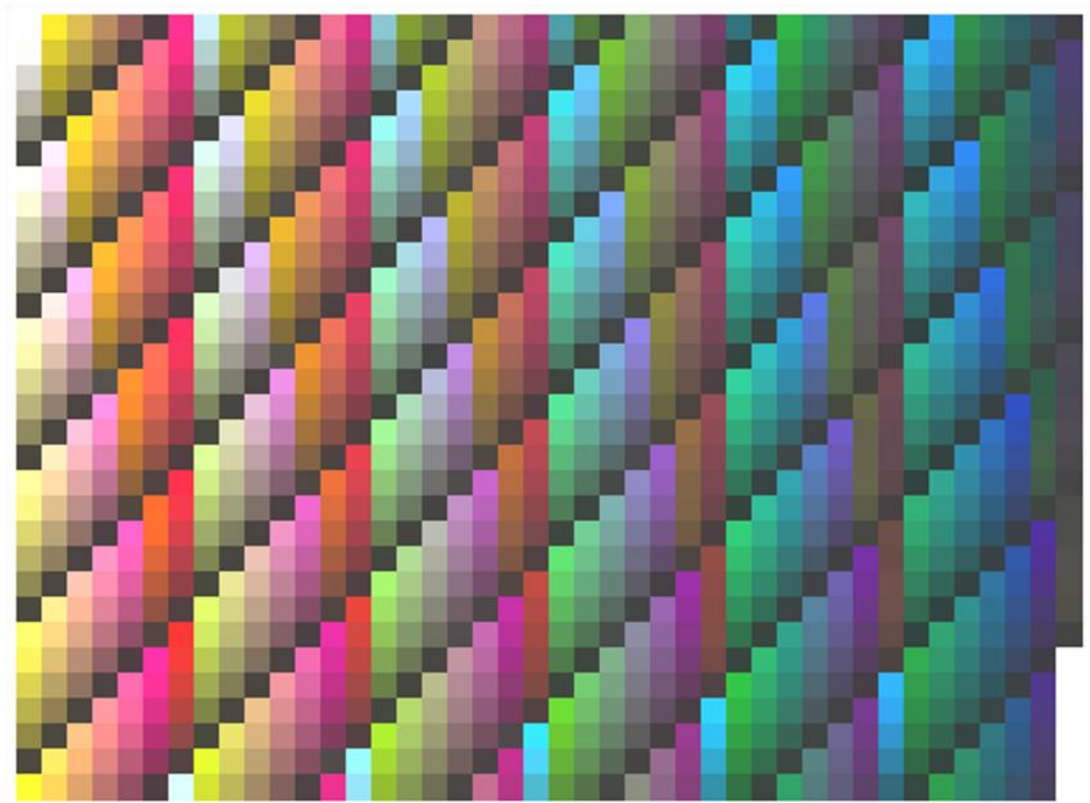
Figure 4.4 Input colour patches for the cellular YNSN model with 6 nodes (1296 patches)

Table 4.5 The accuracy of the cellular YNSN model with different numbers of nodes, expressed in terms of values of CIEDE2000 colour difference, for the inkjet printing process.

Number of nodes	Number of Neugebauer primaries	Optimised *n*-value	CIEDE2000		
			Mean	95th percentile	Max
2	16	1.52	4.40	9.75	14.32
3	81	1.35	1.79	3.96	6.39
4	256	1.45	0.97	2.17	4.18
5	625	1.55	0.92	2.09	5.27
6	1296	2.18	0.64	1.30	4.06

As the number of nodes in colorant space is increased, the number of input colour patches required increases exponentially (Figure 4.5). If the number of inks is increased too much then the number of inputs required could be prohibitive. For example, a 7-colorant printing system with 6 nodes requires $7^6 = 117\ 649$ input colour patches.
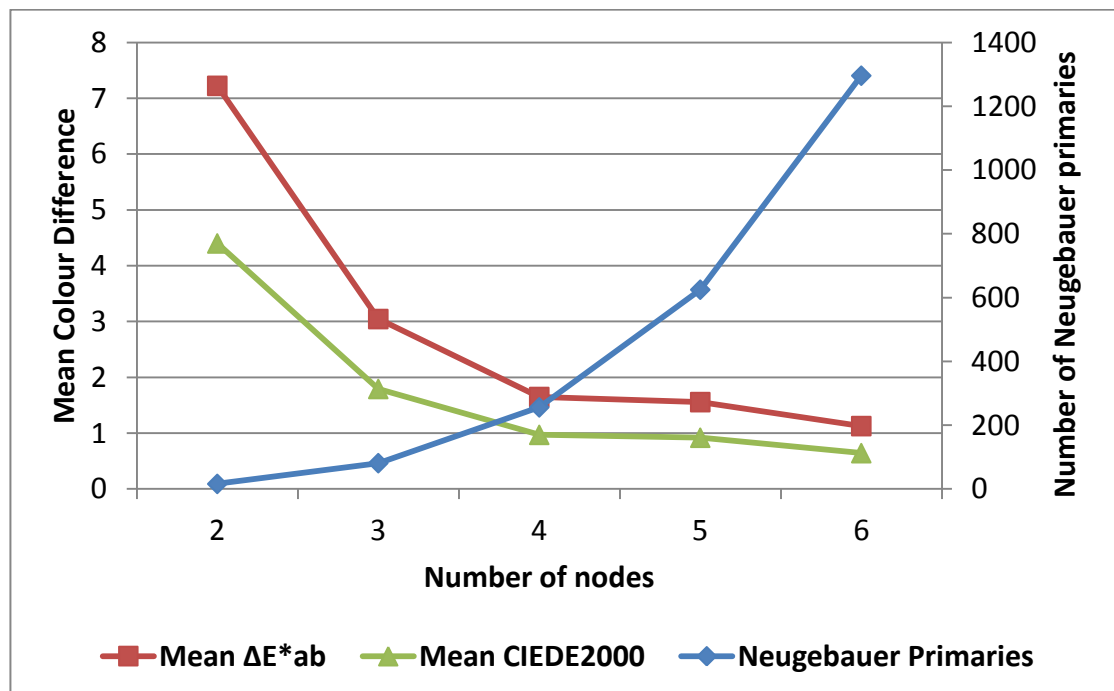
Figure 4.5 Cellular YNSN model results - mean colour difference values and Neugebauer primaries for a 4-colour printing system.

4.2.5 The single-constant KM model

The single-constant KM model as described in the literature review (Chapter 2, Section 2.2.1.8) was applied to all printing systems. The optimised values of the Saunderson correction factors in Eq. (2.26), K_1 and K_2, were 0.03 and 0.60, respectively. The values of K_1 and K_2 were treated as variables. The measured spectra of the solid primary inks and the substrate were used as a training set for optimising the values of *K1* and *K2*. The Kubelka-Munk model was applied to predict the spectra of the patches in the training set. The values of *K1* and *K2* were optimised by minimising the spectral RMS error between the measured and the predicted spectra of the patches in the training set.

The accuracy of this model was found to be poor with mean values of CIEDE2000 colour difference greater than 17 for all models (Table 4.6). Since the single-constant KM model assumes infinite thickness of the medium, the model accuracy should increase for more opaque substrates and colorants. These results for the KM model are consistent with the model accuracy found by Kang (1993).

Table 4.6 Accuracy of the single-constant KM model, expressed in terms of values of CIEDE2000 colour difference, for four printing processes.

Printing Process	CIEDE2000		
	Mean	95th percentile	Max
Inkjet	18.59	32.89	40.48
Thermal Sublimation	18.61	33.92	39.84
Offset	19.86	35.01	39.69
Flexography	18.65	33.26	40.02

4.2.6 A combination of the KM and the YNSN models (KM + YNSN)

The YNSN model requires Neugebauer primaries as inputs. These primaries contain solid inks as well as all solid overprints of 2-inks, 3-inks and 4-inks. In practice, it is sometimes desired to characterise the printing system without printing any overprints of inks. This is more appropriate for *n*-colour printing, where the best set of *n* inks is to be selected from a large ink database and it is not practical to print and measure the

Neugebauer primaries for all combinations of *n*-inks. A printer model must be found which requires the spectra of only the solid inks without the need for measuring the solid overprints.

To solve this problem, the KM model can be used to calculate the spectra of the overprints of the solid inks (Chapter 2, Section 2.2.1.9). These overprints, along with the spectra of solid inks, act as the Neugebauer primaries for the YNSN model. Thus, instead of printing and measuring all Neugebauer primaries, it is only necessary to print solid inks and then derive all Neugebauer primaries using the KM model. For *n*-colour printing, it requires only *n*+1 inputs (*n* solid inks and the plain substrate).

After calculating the spectra of the Neugebauer primaries, the *n*-value is optimised for each printing system. Optimisation of *n*-value is described in the Section 4.2.3. The predicted spectra of 2-ink overprints (part of the Neugebauer primaries) are compared with their measured spectra for the inkjet printing system in Figure 4.6. It should be noted that the prediction accuracy of the KM model depends on transparency of the ink and the substrate.
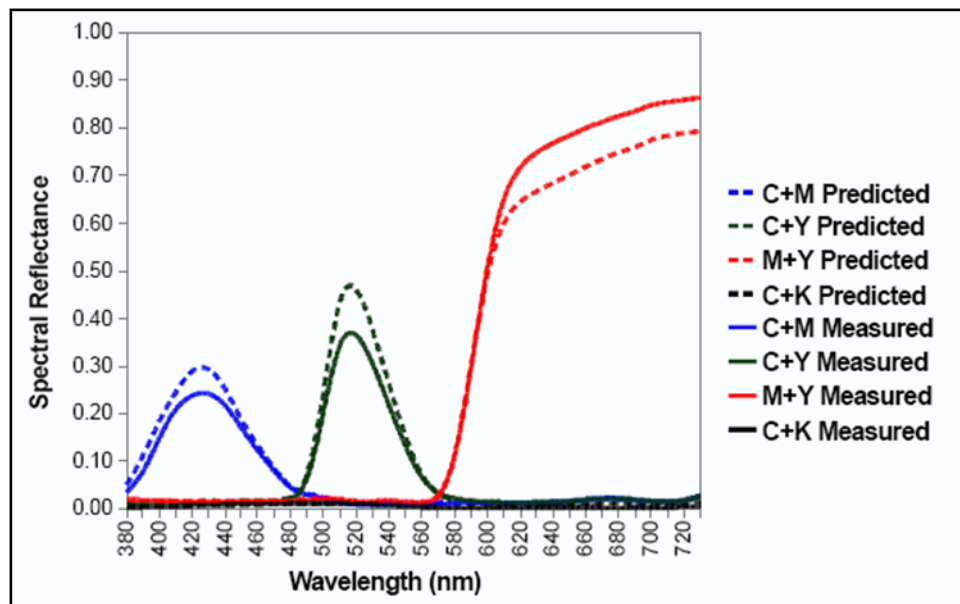
Figure 4.6 Comparison of the measured and the KM-predicted spectra of 2-ink overprints using an inkjet printing system.

Table 4.7 Accuracy of a combination of KM and YNSN model, expressed in terms of CIEDE2000 colour difference and for 4 printing systems.

Printing Process	Optimised *n*-value	CIEDE2000		
		Mean	95th percentile	Max
Inkjet	1.50	4.28	6.85	12.85
Thermal Sublimation	2.43	1.90	4.23	6.17
Offset	1.69	1.78	3.88	6.97
Flexography	2.24	3.52	6.41	19.38

Considering that the model needs a small number of inputs, the model accuracy is reasonably good (Table 4.7). This is particularly applicable for *n*-colour printing, since the number of inputs does not increase exponentially. Also, there is no need to print any combinations of overprints and thus this revised process can significantly reduce the time and cost of printing and materials for *n*-colour printing. The above results do not assume fixed ink opacity. The inks used had different opacities.

4.2.7 The Van de Capelle model

This model represents a unique approach in which each colorant is defined individually by printing solid and halftone dots on three different backgrounds: white, grey and black (Chapter 2, Section 2.2.1.11). The input colour chart for one ink is shown in Figure 4.7.
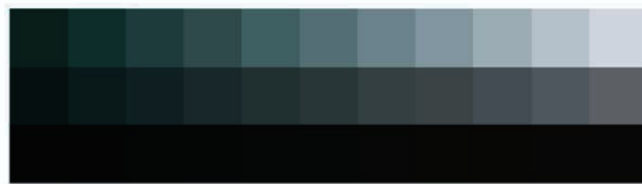
Figure 4.7 Input chart for one ink – Van De Capelle model

The results of the model accuracy for different printing systems are given below (Table 4.8). Although its accuracy is comparable to that of KM+YNSN model, the maximum values of CIEDE2000 are not acceptable, for example, 30.03 for inkjet, 11.45 for thermal sublimation, 13.48 for lithographic offset and 20.51 for flexographic printing.

Table 4.8 Accuracy of the Van De Capelle model, expressed in terms of CIEDE200 colour difference, for 4 printing systems.

Printing Process	CIEDE2000		
	Mean	95th percentile	Max
Inkjet	2.98	7.46	30.03
Thermal Sublimation	4.05	8.15	11.45
Offset	5.36	8.78	13.48
Flexography	3.54	8.42	20.51

Unlike the YNSN model, the Van De Capelle model characterises each ink independently without the need of any ink-overprints. This is advantageous for *n*-colour printing with larger number of process inks, for which the YNSN model requires a substantial number of inputs.

4.2.8   Summary

Figure 4.8 summarises the accuracy of each model for different printing systems in terms of the mean CIEDE2000 values.
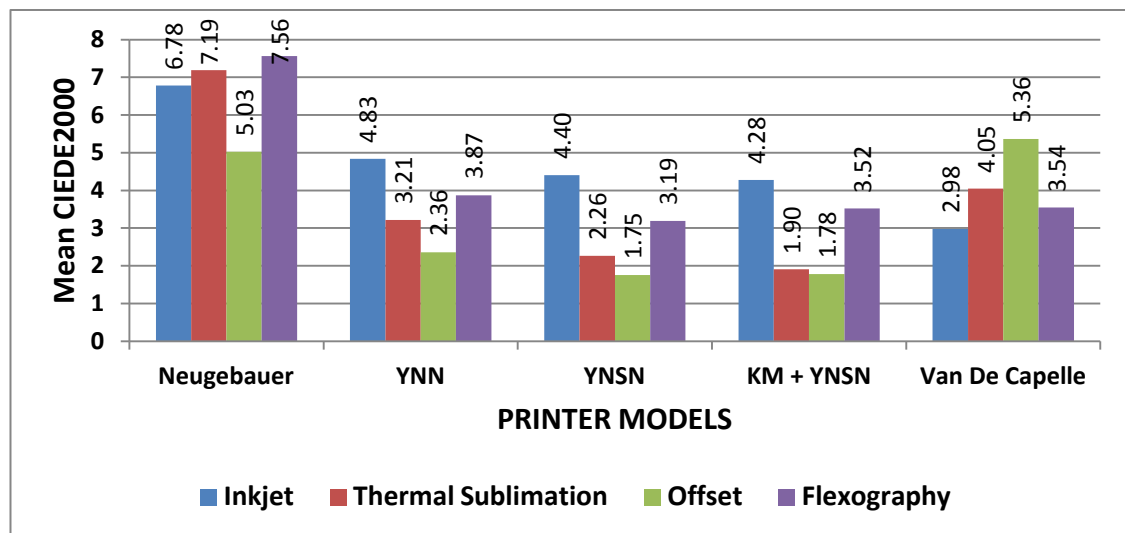
Figure 4.8 Overall performances of models for all printing processes – mean CIEDE2000 values

The KM model has the worst accuracy for all printing processes with the mean CIEDE2000 values greater than 18, hence it is not shown in Figure 4.8. Applying the Yule-Nielsen correction to the wide-band Neugebauer model has significantly increased the accuracy. Extending this to the spectral Neugebauer gave further improvement in the accuracy (YNSN model). For example, the mean CIEDE2000 value for lithographic offset printing process was 5.03 for the Neugebauer model. This was improved to 2.36 for the YNN model and further improved to 1.75 for the YNSN model. In case of the flexographic printing process, the mean CIEDE2000 value for the Neugebauer model was 7.56, which was decreased to 3.87 for the YNN model and 3.19 for the YNSN model.

A combination of the KM and the YNSN models gave similar accuracy as the YNSN model. For example, the mean CIEDE2000 values of 1.78 and 3.52 for lithographic offset and flexographic printing respectively. In fact, it showed better accuracy than the YNSN model for the inkjet and the thermal sublimation printing process. The YNSN model gave 4.40 and 2.26 mean CIEDE2000 values whereas a combination of the KM and the YNSN models gave 4.28 and 1.29 mean CIEDE2000 values for the inkjet and the thermal sublimation printing processes respectively. Considering that the KM+YNSN model requires very few inputs, these results are very encouraging. A similar trend was observed by Abebe (2011) using inkjet printing devices.

The Van De Capelle model gave the mean CIEDE2000 values of 2.98, 4.05, 5.36 and 3.54 for the inkjet, thermal sublimation, lithographic offset and flexographic printing process respectively.

Although most of these models were originally proposed for traditional printing processes using the halftone method, they can be applicable for new printing processes including inkjet and thermal sublimation printing. Among all printing processes, offset and thermal sublimation printing showed better results than flexography and inkjet printing. The YNSN model and the KM+YNSN model showed better accuracy than the rest of the models. A combination of KM and YNSN requires very few inputs: only the spectra of solid colours of process inks and this makes it more suitable for *n*-colour printing.

Though the cellular approach gained accuracy over the YNSN model, it requires an exponentially increasing number of inputs with the increase in the number of nodes or cells. The Van De Capelle model is another promising model, which doesn't require any overprints of process inks. To optimise the n-value of the YNSN and the KM+YNSN models, it is necessary to have the spectral measurements of the evaluation chart, whereas the Van De Capelle model requires the spectral measurements of the only the ink gradation charts, to calculate the model parameters.

Based on the accuracy of the printer models for a 4-colour printing process, the following printer models were selected to characterise the 7-colour printing process: YNSN, KM+YNSN and Van De Capelle. The KM model and Neugebauer model showed poor accuracy, whereas the cellular YNSN needs too many input measurements to be practical for an n-colour printing process and so these models were not used for the 7-colour printing process.

4.3   Implementation of printer models to 7-colour printing systems

In the previous section, different printing systems with 4-colorants were characterised by using the several printer models. These models were extended to characterise n-colorant printing systems. Here, the forward model is applied to 7-colour printing systems to predict the spectra and the CIELAB values of colours from the colorant values. Three different printing technologies were used: lithographic offset, flexographic and thermal sublimation printing. Chapter 3 (Section 3.2) describes the associated colorant space division, calibration of the printing process and test charts used for characterising the 7-colour printing process.
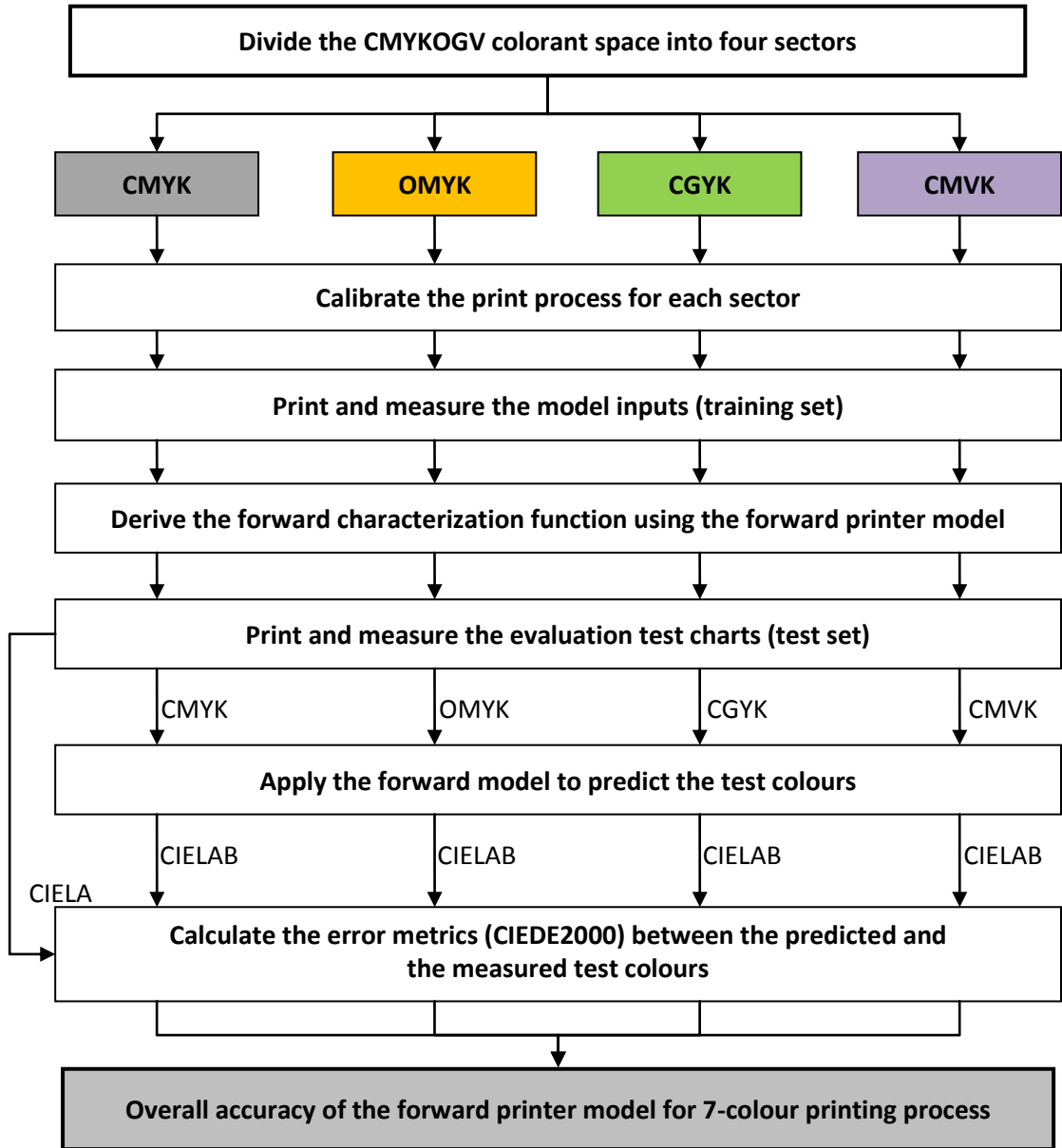
Figure 4.9 Implementation of the forward printer characterisation model to the 7-colour printing process.

The flow diagram for implementing and evaluating the forward printer characterisation model for the 7-colour printing process is shown in Figure 4.9. Each printing process was first calibrated (Chapter 3, Section 3.2). The colour patches of a training set, with known colorant values, were printed on each of the calibrated printing systems. The printed colours were then measured using a spectrophotometer (Chapter 3, Section 3.1).

The training set was used to provide the input values to each printer model to optimise the forward characterisation function for the given model. This function predicts the colorimetric values (for example, CIELAB) for the given colorant values (for example, CMYK). The inputs required for each printer model are explained in the next section (Section 4.3.1).

The evaluation test charts (Section 4.3.2) with known colorant values were printed and all colours were measured. These were considered as a test set for evaluating the model accuracy. The forward characterisation model was applied to the test set using the colorant values of the evaluation test charts. The model output consisted of the predicted colorimetric values of all patches in the evaluation test charts. The predicted colours were compared with the original measured colours to calculate the error metrics, the CIEDE2000 colour difference values between the predicted and the measured colours.

4.3.1   Model inputs

Table 4.9 shows the minimum number of input spectra required for each model. These are the training sets used to derive the forward characterization function. Note that these inputs are for a printing system with 7 process inks. Although extra intermediate colours can be added to improve the model accuracy, the goal was to find the minimum number of input measurements.

Table 4.9 Inputs required for various models for 7-colour printing process.

Models	Input spectra Required	Minimum number of colour patches to be measured
KM	Solid inks (7) and a substrate	8
YNSN	Neugebauer primaries (16) for each of the four sectors	40
Van De Capelle	A solid and one tint of each ink on two backgrounds (28) + 3 backgrounds	31
KM+YNSN	Solid inks (7) and a substrate	8

For the KM model and the combination of the KM and YNSN models, the spectral measurements of the solid patches of the process inks were required along with that of the substrate white.

For the YNSN model, all the Neugebauer primaries (16 for each sector) needed to be printed and measured for each sector. Many of the Neugebauer primaries from the CMYK sector are shared with other sectors. For example, in case of the CGYK sector it is necessary to measure one primary (G) and seven overprints (C+G, G+Y, G+K, C+G+Y, C+G+K, G+Y+K and C+G+Y+K); other inputs required for this sector were already measured from the CMYK sector. Thus there were 16 inputs for the CMYK sector and 8 inputs for each of the remaining sectors leading to a total of 40 input measurements.

For the Van De Capelle model, each ink needed to be profiled separately. Thus solid inks and at least one tint (for example, 50%) had to be printed on each of two backgrounds. Spectral values of the substrate white, grey and black patches representing the three backgrounds were measured. For each ink, 100% and 50% patches were printed and measured on a white and a black background and then interpolated for a grey background. Thus, for a 7-ink process, the input spectra of 31 patches were required.

In addition to the solid inks, the density values of the 40% and 80% patches for each ink were measured for calibrating the printing process. Thus a total of 14 patches were measured. However, calibration is required irrespective of the printer model used. Hence these patches were not considered as inputs when analysing the prediction accuracy and the number of input measurements for all models.

4.3.2   Test chart for evaluating the printer models

The printer model was applied to each ink-sector separately to evaluate the model accuracy for that sector. For each ink-sector, the variant of ECI2002 test chart was generated and printed (Chapter 3, Section 3.2). Each test chart contained 1485 colour patches similar to the ECI2002 chart. Thus, a total of 5940 colour patches were printed and measured for to evaluate the printer models.

Each test chart contains the same colorant values (dot areas). For example, in the CGYK chart, all values of the magenta (M) ink in the CMYK chart are replaced by the green (G) ink. Figure 3.3 shows the test charts for all sectors.

The colour patches in each test chart were measured using an X-Rite i1 Pro 2 spectrophotometer using the measuring conditions specified in Chapter 3 (Section 3.1). The colour measurement data of all sectors were collected to form a data set for each printing technology.

These measurements were then compared to the model predictions for each sector to evaluate the model accuracy for that sector. The overall accuracy of the model for the 7-colour printing process was determined by calculating the average colour difference values between the measured and the predicted colour values from all sectors.

4.4   Results

The overall colorimetric accuracy of the 7-colour printing process was computed from the accuracy of individual 4-ink sectors as described above. Results for three models for each printing process are given below. Each model was applied to four sectors to calculate the mean CIEDE2000 values between the predicted and the measured colours. The results for each sector of the offset printing process are shown in Table 4.10. The results for the CMYK sector for the offset printing process are included (See Table 4.4, Table 4.7 and Table 4.8) to compare them against the remaining sectors.

The Yule-Nielsen value (n-factor) was treated as a free empirical parameter and its value was optimised for each sector. The optimised value of n for each sector is different, because each sector contains different combinations of inks. Although three inks are common between adjacent two sectors, the optimised n-values are disparate.

For the given sector, the optimised n-values of the YNSN model and the KM+YNSN model are similar. For example, the optimised values of n for the CMYK sector using the YNSN and the KM + YNSN models are 1.66 and 1.69 respectively. Some sectors, for example, CMYK and OMYK, are predicted more accurately than others.

Table 4.10 Accuracy of three models for each sector of the offset printing process

Model	Ink sector	Optimised *n*-value	Mean CIEDE2000
YNSN	CMYK	1.66	1.75
	OMYK	1.68	1.34
	CGYK	1.54	2.85
	CMVK	1.74	2.15
	Overall	-	**2.02**
KM+YNSN	CMYK	1.69	1.78
	OMYK	1.65	2.01
	CGYK	1.6	2.67
	CMVK	1.83	2.41
	Overall	-	**2.22**
Van De Capelle	CMYK	-	5.36
	OMYK	-	4.97
	CGYK	-	5.59
	CMVK	-	6.39
	Overall	-	**5.58**

The overall accuracy of three models for all printing processes with 7 inks is shown in Figure 4.10. The mean CIEDE2000 values between the predicted and the measured colours were calculated for a total of 5940 colour patches. These include four sectors, each containing 1485 colour patches of 4-ink combinations.

Both the YNSN and the KM+YNSN models showed good colorimetric accuracy with similar values of the mean CIEDE2000 for all printing processes.
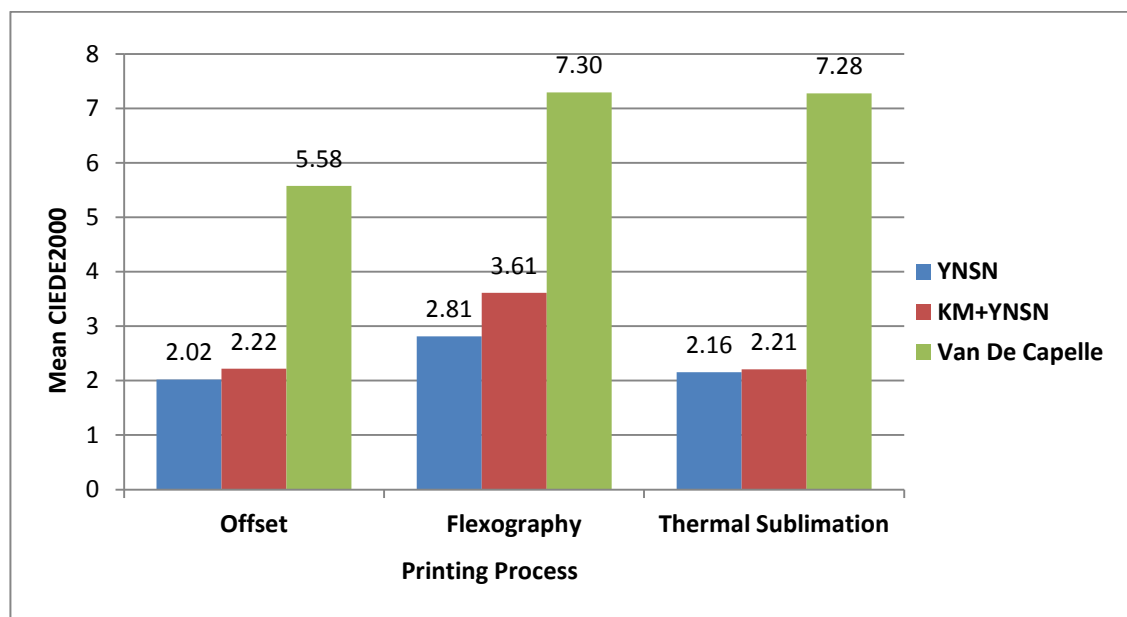
Figure 4.10 Overall colorimetric accuracy of three models for all printing processes

The KM+YNSN model requires only eight input measurements: spectra of all inks and the plain substrate. On the other hand, the YNSN model requires a total of 64 input measurements: spectra of all Neugebauer primaries for all sectors. In spite of this difference in input data requirements the prediction accuracy of the KM+YNSN model is very close to that of the YNSN model.

4.5   Conclusion

Forward printer characterisation for different printing technologies was performed using various physical printer models to predict the device-independent colour values from the device-dependent colorant values. Initially the models were implemented for 4-colour printing processes and then extended to 7-colour printing processes. The colorant space of 7-colour printing process was divided into sectors of 4-inks each as follows: CMYK, OMYK, CGYK and CMVK. This method can be generalised to any n-colour printing process.

The YNSN and a combination of the KM and YNSN models performed well for all printing processes. The latter requires only a low number of inputs, but still gives reasonably good prediction accuracy. Although most of these physical models were developed for traditional printing processes based on halftone screening, they can be successfully used for other printing processes, for example inkjet. Other models not evaluated as part of this work have been reported as giving good results, such as EYNSN (Hersch, 2005).

In the next phase of the project, the colour gamuts of the n-colour printing processes are predicted and analysed using the forward printer characterisation models (Chapter 5). This will lead to the inverse printer characterisation models in Chapter 7 to derive the colour separations for given spot colours.

Chapter 5 Gamut evaluation of the *n*-colour printing process

5.1 Introduction

The forward printer characterisation models were discussed in the previous chapter. The colour gamut of a printing system is an important component of the colour characterisation process, particularly the gamut boundary which is used in gamut mapping (Balasubramanian, 2003). A colour gamut represents the volume of colours physically achievable by the printing system in three-dimensional colour space. This chapter describes the gamut prediction and evaluation of the *n*-colour printing process. The results described in this chapter have been published in Deshpande (2009 and 2014a).

The main purpose of an *n*-colour printing process is to increase the colour gamut of a traditional four-colour printing process by the use of additional inks. There are many reasons to derive the gamut of an *n*-colour printing process, for example, to perform gamut-mapping before deriving the inverse characterisation function to obtain a colour separation, to select the optimum ink-set for *n*-colour printing and to compare the *n*-colour printing gamut with that of the proofing system.

An *n*-colour printing system uses CMYK inks plus additional inks of intermediate hues, for example, orange, green, violet, etc. The increase in the attainable colour gamut however, is at the cost of added complexity, which creates a challenge for generating colour separations for these ink sets. Models for *n*-colour printing have been discussed in the literature review (Chapter 2, Section 2.4).

The gamut of a printing system is typically found by using a numerical model to predict coordinates on the gamut surface. This can be done by printing a set of colour patches, calculating their colorimetric co-ordinates from spectral measurements, deriving a model and using this model to calculate the 3D gamut boundary in a uniform colour space such as CIELAB. Several methods of calculating gamut boundaries have been

proposed, for example, by Braun (1997), Balasubramanian (1997), Morovič (2000) and Green (2001). For printing processes with more than four inks (*n*-colour printing), the number of colour patches required to determine the gamut boundary using any of these approaches can become excessively complex because the sample combinations required for *n*-channels at the sampling density *d* is d^n.

The gamut boundary can also be predicted from an analytical model using a smaller sample of colours (Mahy, 1996b and 1997b). Classical approaches include physical printer models such as that of Neugebauer and that based on KM theory. Previous studies have dealt with the analysis and visualisation of the colour gamuts of printing devices, for example, Reel (1999) and Perales (2009). In addition, several printer models were used for predicting the colour gamut of a 7-colour printing system in a study by Deshpande (2009).

It is possible to calculate the gamut volume by determining the coordinates of colours on the gamut boundary using one of several methods, for example, the convex hull (Barber, 1996), SM-GBD (Morovič, 2008), the curve-face model (Guyler, 2001) and alpha-shapes (Cholewo, 1999). Although the gamut can be considered as a convex hull (Barber, 1996), this representation assumes there are no concavities in the gamut surface (Morovič, 2008). To account for any such concavities, the gamut volumes can be calculated using alpha-shapes with a radius (alpha parameter). The optimum value of the alpha parameter can be found by visualising a 3-dimensional gamut based on the criterion that the gamut should not have any voids. Beyond the optimum value of the alpha parameter, if the gamut is visualised in a 3-dimensional space like CIELAB, there are some regions in a gamut that cannot be accessed from the outside (Cholewo, 1999).

To compute the gamut volume, a surface triangulation is applied using a set of triangles which completely covers the gamut, for example *n*-dimensional Delaunay triangulation (de Berg, 2008). A list of triangle faces is generated to determine a set of tetrahedra that fill the gamut volume. Finally the total gamut volume can be obtained by computing the volume of each tetrahedron and summing the individual volumes.

There have been some previous studies related to gamut comparison (Reel, 1999 and Doll, 2001), but they did not provide an objective method for the comparison of gamuts. A set of objective metrics was proposed by CIE (2005) for evaluating the extended-gamut colour encodings, for example, sYCC (IEC 61966-2-1/Amd:2003) and ROMM RGB (ANSI/13A IT10.7666:2002). These metrics measure the sizes of the colour gamuts of different colour encodings and compare their ability to encode the target colours, for example, real-world surface colours and CRT colours as defined by sRGB (IEC 61966-2-1:1999). Thus a target colour gamut was compared to a colour encoding gamut.

These metrics can be used to compare two gamuts that are intended to be a good match, but they do not provide a single number which quantifies the similarity between two gamuts. To address this issue, a new metric called the Gamut Comparison Index is proposed (Deshpande, 2012). This metric is mainly aimed at real-world colour gamuts rather than theoretical gamuts like the optimal surface colour gamut and the legal colour gamut comprising all colours within the given colour space as described in the CIE Technical Report (2005).

5.2   Gamut of the *n*-colour printing process

For the *n*-colour printing, it is desirable to know the colour gamut of the given set of inks without having to print a large number of test patches. Here, the aim is to predict the colour gamut of the *n*-colour printing process from a minimum number of measured colour patches.

Four different printer models were used to characterise a 7-colour printing process: Kubelka-Munk (KM), Yule-Nielsen modified Spectral Neugebauer (YNSN), Van De Capelle model and a combination of the KM and the YNSN models. These printer models are described in detail in Chapter 2 (Section 2.2.1).

The colorant space was divided into sectors each containing four inks (Section 3.2.1). For each printer model, the colour gamut of the given sector was predicted, and this predicted gamut was then compared with the actual gamut obtained by measuring the printed test-chart. The gamut volume alone is not a good indicator of the gamut prediction accuracy, since two gamuts may have the same volume but not be coincident in colour space. To overcome this problem, new gamut metrics are introduced to aid the comparison of colour gamuts. These metrics are discussed in detail in the next section.

5.3   Method

In this project, a 7-colour lithographic offset printing system was used with the following process inks: Cyan, Magenta, Yellow, Black, Orange, Green, and Violet (CMYKOGV). The substrate used was a gloss coated paper. The printing process was calibrated to adjust its behaviour to known desired conditions (see Chapter 3, Section 3.2.3). Tone values for Cyan, Magenta and Yellow were adjusted to achieve the tone value increase (TVI) targets of "curve A" specified in ISO 12647-2 (2007). Tone values for Black, Orange, Green and Violet were adjusted to achieve the tone value increase (TVI) targets of "curve B" specified in ISO 12647-2 (2007).

The colorant space was divided into 4-ink sectors of CMYK, OMYK, CGYK and CMVK (see Figure 3.1). Black is common across all sub-sets, whereas each of the chromatic colours (C, M and Y) is replaced by its complementary colours (O, G and V respectively). Each of these sub-sets of 4-inks has a colour gamut. The full colour gamut of the *n*-colour printing process can be calculated by using all colours that are part of all sub-gamuts. This method can be generalised for any *n*-colour printing process. For example, in case of an 8-colour process there will be five sub-sets of 4-inks containing black as a common ink and three chromatic inks in each sub-set.

The printer model was applied to each sector to predict the sector-gamut of the separate 4-colour processes (Figure 5.1). All colours forming the sector-gamuts were then combined to form an overall gamut for the complete 7-colour process.

```
┌─────────────────────────────────────────────────────────────────────────┐
│  ┌───────────────────────────┐      ┌───────────────────────────┐        │
│  │ Print and measure input   │      │ Print & measure all test  │        │
│  │ spectra for the           │      │ charts                    │        │
│  │ calibration of the        │      │                           │        │
│  │ printer model             │      └───────────────────────────┘        │
│  └───────────────────────────┘                  │                        │
│              │                                   ▼                        │
│  ┌───────────────────────────┐      ┌───────────────────────────┐        │
│  │ Apply the printer model   │      │ Use the measured colours  │        │
│  │ to each sector and        │      │ from all sectors and      │        │
│  │ predict a larger number   │      │ derive the overall        │        │
│  │ of colours                │      │ measured gamut            │        │
│  └───────────────────────────┘      └───────────────────────────┘        │
│              │                                                            │
│              ▼                                                            │
│  ┌───────────────────────────┐                                           │
│  │ Use the colours predicted │                                           │
│  │ from all sectors and      │                                           │
│  │ derive the overall        │                                           │
│  │ predicted gamut           │                                           │
│  └───────────────────────────┘                                           │
│                    │                    │                                 │
│                    └──────────┬─────────┘                                 │
│                               ▼                                           │
│              ┌───────────────────────────┐                               │
│              │ Compare the predicted     │                               │
│              │ gamut to the measured     │                               │
│              │ gamut                     │                               │
│              └───────────────────────────┘                               │
└─────────────────────────────────────────────────────────────────────────┘
```

Figure 5.1 Flowchart for the gamut prediction and evaluation process for the 7-colour printing process.

For each 4-colour sector, the IT8.7/4 test chart (ANSI IT8.7/4, 2005) was generated containing 1617 colour patches and printed using a conventional offset printing process on to the gloss coated paper. Thus a total of 6468 colour patches were printed. The spectral reflectance values of all the colour patches in each test chart were measured using the measuring conditions specified in Chapter 3 (Section 3.1).. The 1617 measurements for each sector were used to determine the sector gamuts. The 6468 colours forming all sector gamuts were used to derive the overall measured CMYKOGV gamut. All the gamut boundaries were computed in Matlab using the alpha-shapes method (Lundgren, 2010) with a radius of 40 CIELAB units.

To obtain the boundary points, a surface triangulation is applied to a set of all points P in the CIELAB colour space such that no tetrahedron contains a point of P in its circumsphere. This gives a set of all convex combinations of its points and triangle faces. A list of triangle faces is generated. Each triangle face on the gamut boundary creates a tetrahedron along with the fixed centre point inside the gamut (Green, 2013). Figure 5.2 illustrates this.
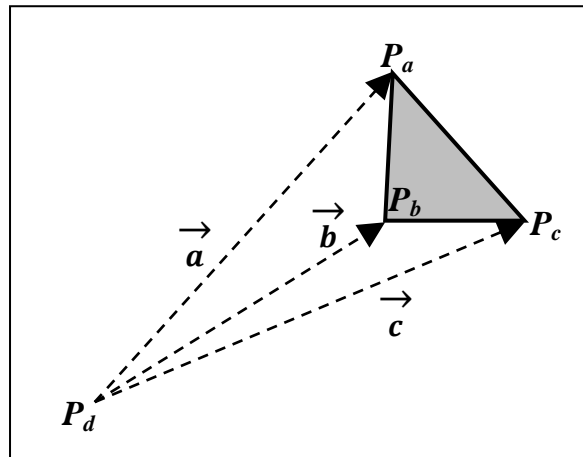
Figure 5.2 Individual tetrahedron with the triangle face and the fixed point inside the gamut

Using the list of triangle faces, a set of tetrahedra that fill the gamut volume is determined. One method of calculating the volume of each individual tetrahedron is described below.

$$V = \frac{1}{6}|a.\,(b \times c)|$$

(5.1)

where *a*, *b* and *c* are the vectors connecting each of the three vertices of the triangle on the gamut boundary to a fixed centre point inside the gamut. Note that the term $a \cdot (b \times c)$ is a scalar triple product.

Finally the total gamut volume is computed by summing the volumes of all individual tetrahedra. If the CIELAB colour space is used for calculating the gamut then the gamut volume is measured in cubic CIELAB units.

If the gamut is considered as the convex hull then the gamut volume can be computed in CIELAB co-ordinates from the Delaunay triangulation, using for example the Qhull algorithm (Barber, 1996). The convex hull provides an approximation of a gamut solid, but it has been noted elsewhere (Morovič, 2008) that it has limited accuracy as it does not represent the curvature of a gamut and any concave regions.

In this study, the convex hull method was compared to the alpha-shapes method (Cholewo, 1999) to evaluate the difference in the gamut volume using the same data-set of measured CIELAB values. A lithographic offset printing system with CMYK inks was calibrated. Using the measured data-set of all colours in the test chart, a colour gamut was derived, first using the alpha-shapes method and then using the convex hull method.

For the optimised value of the probe radius (α), the alpha-shapes gamut volume was 336330 cubic CIELAB units as compared to the convex hull gamut volume of 355001 cubic CIELAB units. Thus the gamut volume difference was 18671 and the ratio of the volume of the alpha-shapes gamut to that of the convex hull gamut was approximately 0.95. Considering the concavity of the gamut boundary, the gamut volumes are calculated using alpha-shapes in this project using a radius (alpha parameter) of 40 CIELAB units. This optimum value of alpha parameter is found experimentally by visualising a 3-dimensional gamut based on the criterion that the gamut should not have any voids i.e. all tetrahedra should be included in the alpha-shape.

For the CMYK sector of the offset printing process, the boundary of the measured gamut consisted of 600 vertices (colours) forming the triangular faces on the surface of the gamut. A 3-dimensional mesh plot of the CMYK sector gamut in the CIELAB colour space is shown in Figure 5.3. For these 600 colours on the gamut boundary, the CIEDE2000 colour differences between the measured and the predicted colours were calculated for each printer model. The average of these values was then used to compare the model predictions.
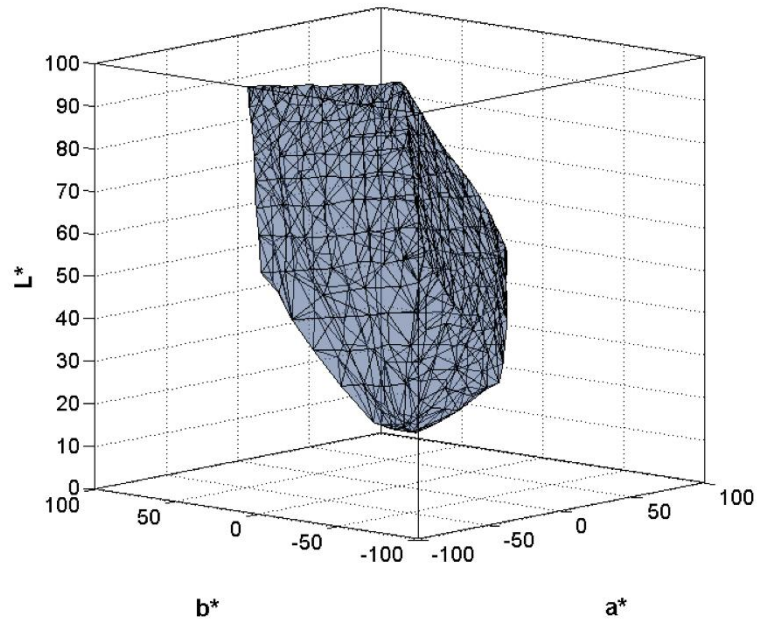
Figure 5.3 CMYK sector gamut for the offset printing process as a 3D mesh in CIELAB colour space

5.4 Results

The measured colour gamut of each sector is shown below in the $a*$ - $b*$ projection of CIELAB space (Figure 5.4). All the gamut boundaries were computed using the alpha-shapes method with a radius of 40 CIELAB units. The upper-left graph shows the colour gamut of the CMYK sector and the other graphs indicate successive addition of other sector-gamuts. The overall gamut of the 7-colour printing process (CMYKOGV) can be considered as the combined gamut of all sector-gamuts.
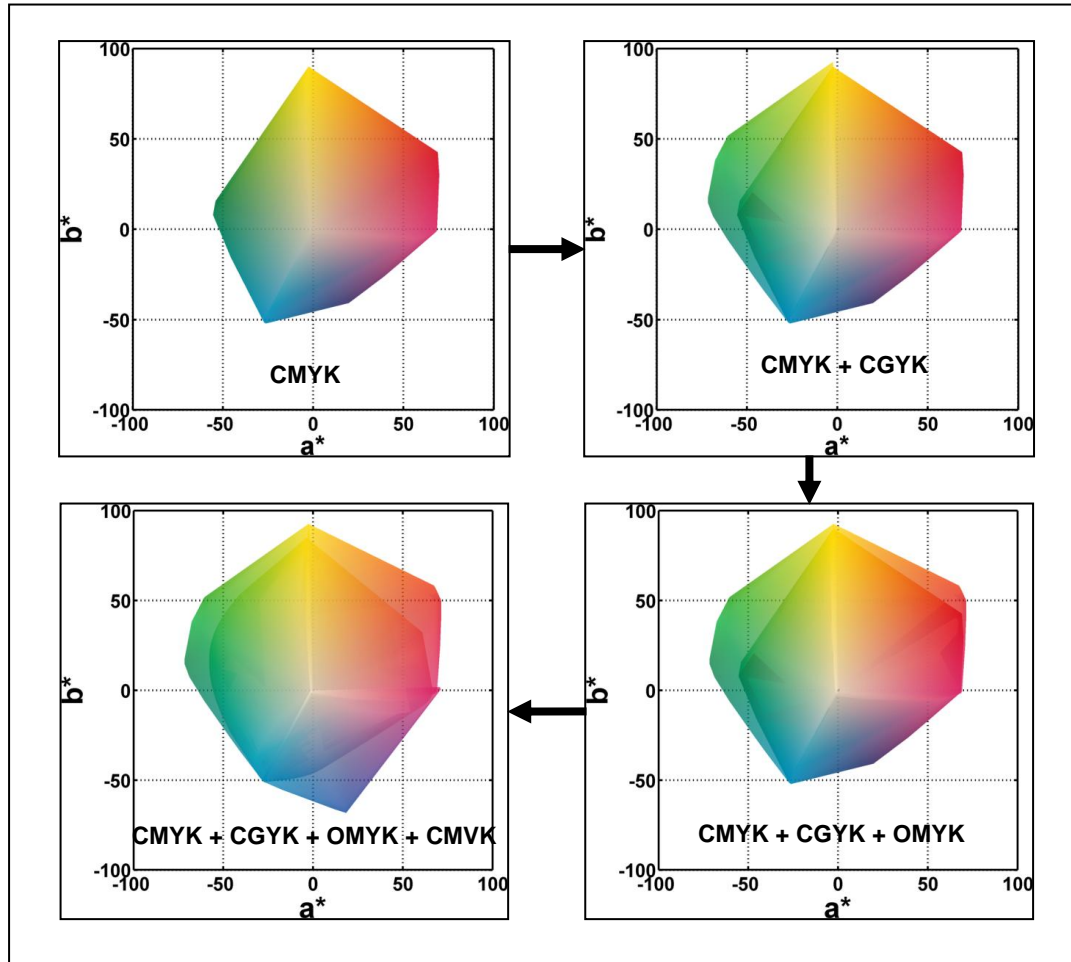
Figure 5.4 Combined gamuts of all sectors in the a* - b* plane.

Figure 5.5 shows the mean CIEDE2000 colour difference between the measured and the predicted colours on the primary vertical axis and the percentage volume difference between the measured gamut and the predicted gamut on the secondary axis. The mean CIEDE2000 values for the CMYK sector were calculated for two sets of colours – the boundary colours representing the gamut boundary of the measured gamut (600) and all colours (6468) populating the colour space, and including the boundaries. Although the KM model has the worst (highest) value of CIEDE2000, it has better performance than the KM+YNSN model in terms of the percentage gamut volume difference. This supports the concept that the gamut volume difference is not by itself a good metric for comparing gamuts (see Section 5.5).
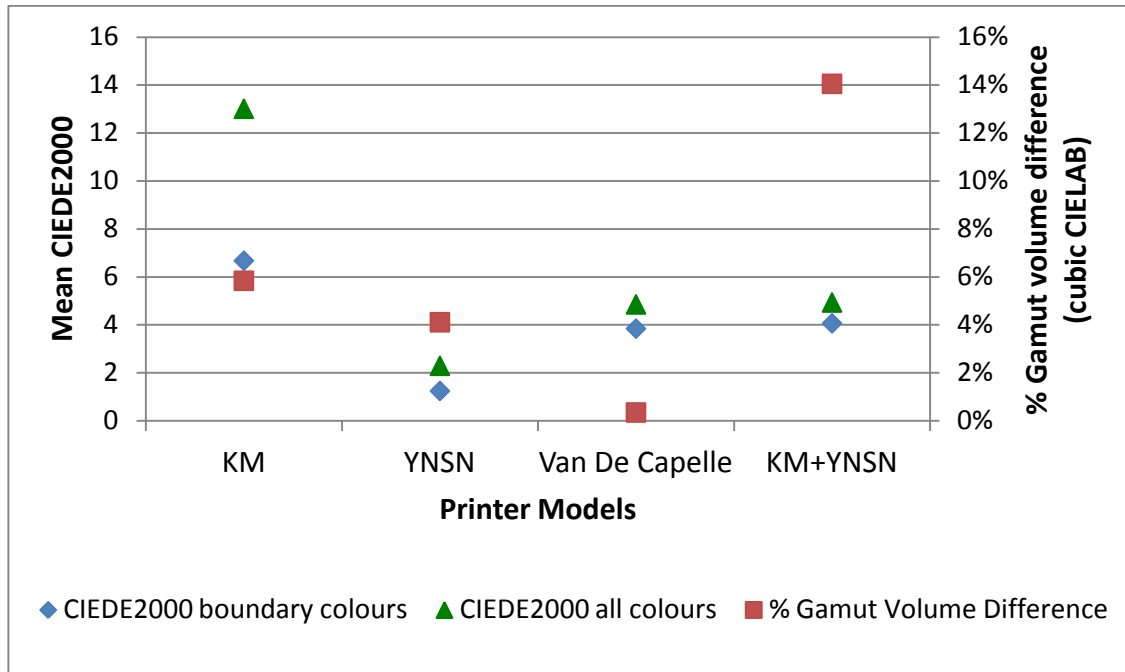
Figure 5.5 Gamut volume difference between the measured and the predicted gamuts.

Figure 5.6 shows histograms of values of CIEDE2000 colour difference between the measured and the predicted colours. The KM model performed the worst and the YNSN performed the best in terms of colour difference values. This is shown by all values of CIEDE2000 colour difference being below a value of 5 for the YNSN model; for the other models the data exhibit long tails that include relatively high values of colour difference, up to 20 units for the KM model, which would usually be considered unacceptable in practice.
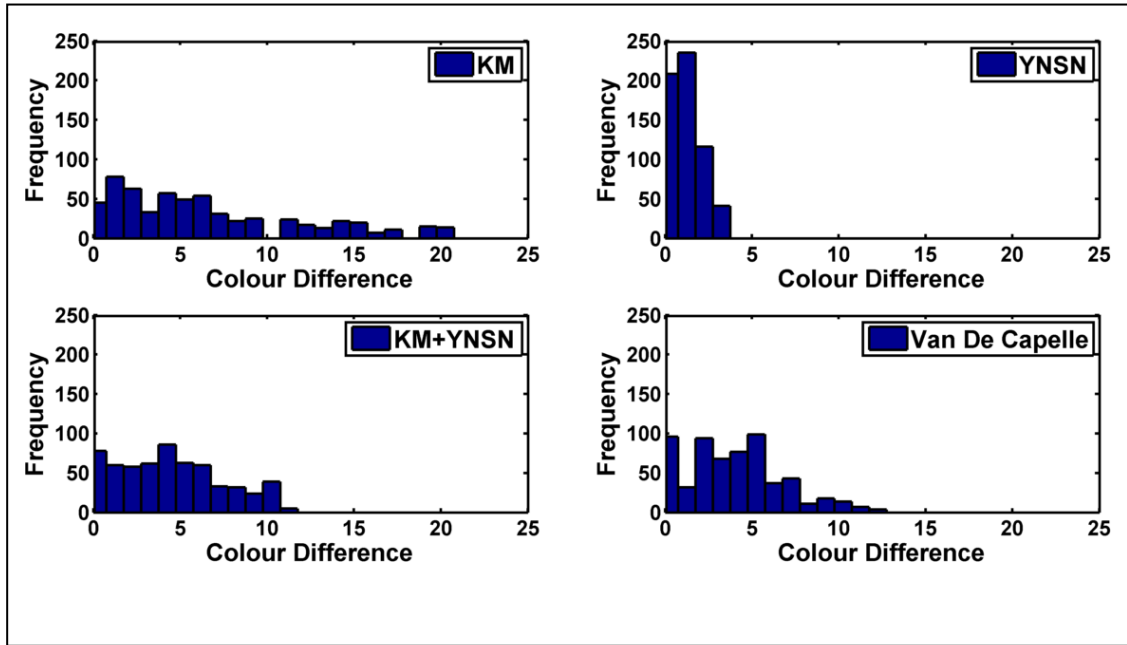
Figure 5.6 Histograms of colour difference values (CIEDE2000) for all models.

These results still cannot tell how closely the predicted gamut matches to the measured gamut. For example, both gamuts could have similar volume, but might not coincide in CIELAB colour space. The gamut volume alone enables a comparison of the size of the gamut, but not whether the gamuts intersect sufficiently to have a good match. To address this issue, the Gamut Comparison Index (GCI) metric which includes both relative volume and intersection was used (Deshpande, 2012 and 2014b).

5.5   Gamut Comparison Index (GCI) and other metrics

The predicted overall gamut for each printer model was compared with the measured overall gamut using a Gamut Comparison Index (GCI), which serves to better indicate how closely the predicted gamut matches the measured gamut.

Consider two colour systems, x and y with gamut volumes V_x and V_y respectively. A gamut comparison index (GCI) between these two systems can be calculated by the following equations.

$$GCI = \left(\frac{V_i}{V_x}\right)\left(\frac{V_i}{V_y}\right)$$

$$GCI = \frac{V_i^2}{V_x V_y}$$

(5.2)

where V_i is the volume of intersection of the two gamuts ($V_i = Vx \cap V_y$). The term (V_i / V_x) indicates how much of the gamut x is outside the intersection of the gamuts, while (V_i / V_y) indicates how much of gamut y is outside the intersection (Figure 5.7).
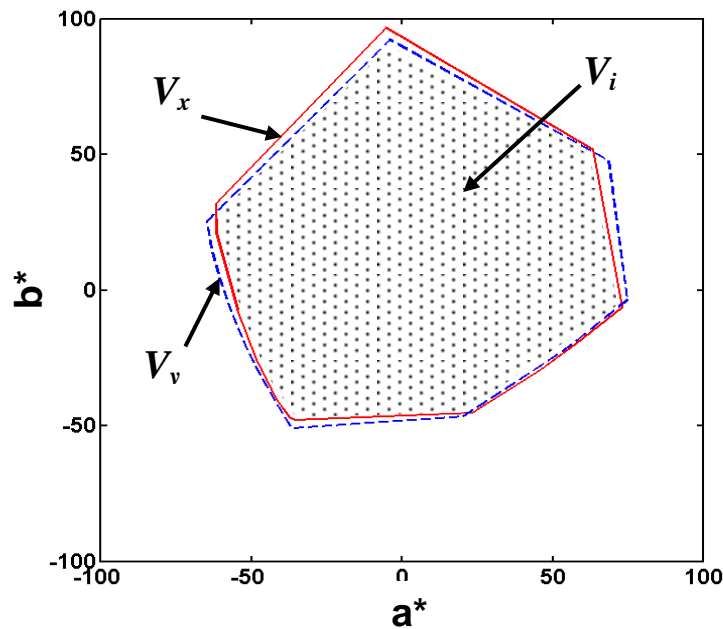
Figure 5.7 Projection of the 3-dimensional gamuts *x* and *y* on to the a* - b* plane

The value of GCI between two gamuts indicates how closely they match. The value ranges from 0 for no match to 1 for an exact match: for a perfectly matched gamut, $V_x = V_y = V_i$ and the value of GCI is equal to unity. If these two gamuts have the same volume ($V_x = V_y$), but they don't intersect fully with each other, then the value of GCI will be less than 1. If the two gamuts do not intersect at all ($V_i = 0$), then $GCI = 0$. Where gamut V_x completely encloses gamut V_y, then $V_i = V_y$. The GCI can be used

when the objective is to match a source gamut to the target gamuts, for example, matching the model-predicted gamut to the actual device gamut.

The intersection of two gamuts can be derived by finding a set of points common to both gamuts. First, a set of all vertices and tetrahedra forming the first gamut volume is identified. Similarly another set of all vertices and tetrahedra forming the second gamut volume is identified. Now we can determine a list of vertices from the first gamut that are inside the second gamut. Similarly we can also find a list of vertices from the second gamut that are inside the first gamut. This provides a set of the surface points which make up the intersection of two gamuts. These intersection points are then used to compute the volume of intersection by calculating the gamut volume as described above (Section 5.3).

Note that using CIELAB colour space will over-predict differences in high-chroma regions (Sharma, 2012). Ideally a colour space having more perceptual uniformity than the CIELAB colour space is desirable. Also note that gamuts are affected by viewing conditions (Morovič, 2008).

5.5.1   Other gamut metrics

In addition, the following metrics are useful for further analysis of two gamuts.

Gamut volume ratio: compares the sizes of two gamuts without considering their intersection. They show which of the two gamuts has the bigger volume. If x is a reference gamut and y is a test gamut, then a gamut ratio can be calculated as follows.

- $[V_x / V_y]$: ratio of the volume of gamut x to that of gamut y

This ratio can be inverted to obtain another gamut ratio, V_y / V_x.

Out-of-gamut volume: gives the fraction of one gamut volume lying outside of another gamut.

- $[(V_x - V_i) / V_x]$: the volume of gamut x outside gamut y

Similarly the out-of-gamut volume for gamut *y* can be obtained by replacing V_x with V_y in the above ratio. These metrics especially are valuable for evaluating the proportion of one gamut outside a second gamut, which is important when performing gamut mapping and re-targeting an image to different reproduction media.

Simple representation of gamuts using the Venn diagram

A colour gamut is usually represented in a three-dimensional colour space such as CIELAB and Figure 5.8 shows two gamut volumes plotted in that space. The first gamut is shown as a solid volume and the second gamut as a wireframe. Although this representation makes it possible to visualize the relationship between the two gamuts, precise quantification of this relationship is not available from inspection of the figure.
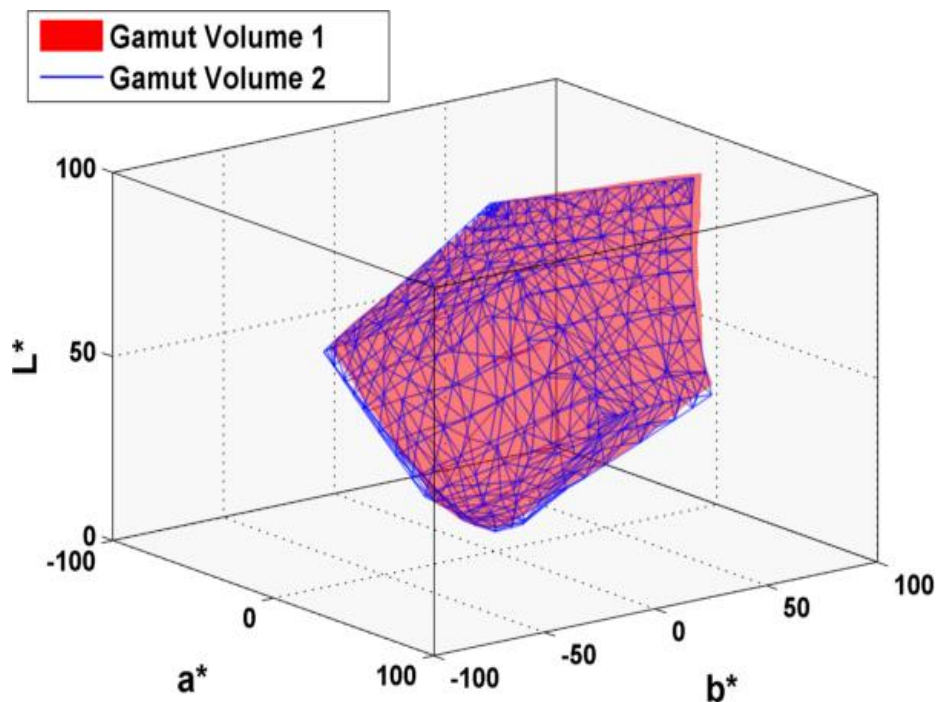
Figure 5.8 Visualisation of two gamuts in the CIELAB colour space.

This comparison can be simplified by representing the gamuts in two dimensions (Figure 5.7), but as these are projections of the 3-dimensional gamuts on to the 2-dimensional plane, they do not represent the relative volumes of the gamuts and the volume of their intersection.

As a supplement to the gamut metrics, it is easier to visualise the two gamuts in a simple two-dimensional illustration depicting the relative volumes of these gamuts and the volume of intersection. A simple representation of two gamuts using the volume-proportional idealised projection illustrated in Figure 5.9 is proposed. One gamut is a reference printing condition RPC3 and another gamut is a reference printing condition RPC4 specified in ISO 15339-2 (2012).
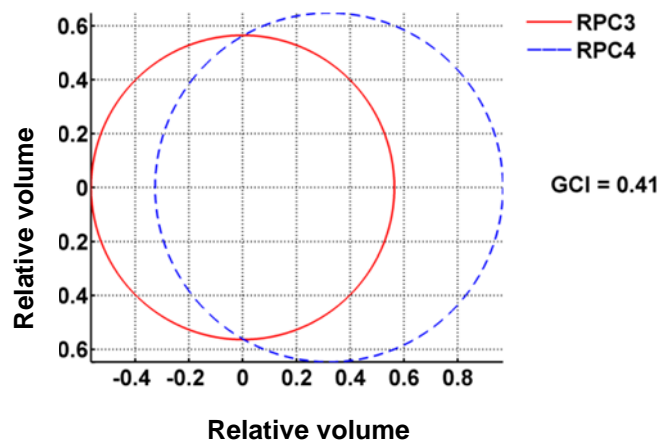
Figure 5.9 Representation of two gamuts as a volume-proportional idealised projection.

(all volumes are in cubic CIELAB units)

Each circle in this diagram represents the volume of an individual gamut, and the areas of these circles are proportional to the volumes of the respective gamuts. The intersection area of the two circles is also proportional to the volume of intersection of the two gamuts. Thus the volume-proportional idealised projection depicts the relative volumes of two gamuts together with the volume of their intersection. The gamut volume is measured in cubic CIELAB units. Note that the volume-proportional idealised projection does not represent the shapes of the gamuts or the projections of the gamuts on to the 2-dimensional plane, for example the *a** - *b** plane.

5.6 Evaluation of predicted gamuts using gamut metrics

The following Table 5.1 compares results obtained for all models in terms of gamut volume difference, GCI values, the proportion of the measured gamut lying outside the predicted gamut and vice versa. Note that the range of the gamut index is from 0 to 1 and lower values of the gamut index indicate a poorer match to the target colour gamut. For two identical colour gamuts, the gamut index has a values of unity.

The YNSN model gave the best results followed by the Van De Capelle model with the GCI values of 0.93 and 0.87 respectively. These models also showed lower average values of CIEDE2000 than those of the remaining models (Figure 5.5). The KM model had the worst performance with a gamut comparison index of 0.64.

All the predicted gamuts had less volume than that of the measured gamut; however, this does not mean that the predicted gamuts lie entirely inside the measured gamuts.

Table 5.1 Evaluation of the printer models using gamut metrics.

Description	KM model	YNSN model	Van De Capelle model	KM + YNSN model
Volume of the measured gamut	455256	455256	455256	455256
Volume of the model predicted gamut	428690	436563	453700	391296
Volume of intersection	353645	429995	423677	381968
GCI (Gamut Comparison Index)	**0.64**	**0.93**	**0.87**	**0.82**
Fraction of the measured gamut lying outside the predicted gamut	0.22	0.05	0.07	0.16
Fraction of the predicted gamut lying outside the measured gamut	0.17	0.01	0.07	0.02
Percentage difference between gamut volumes	5.84%	4.11%	0.34%	14.05%

Note: All volumes are measured in cubic CIELAB units.

Figure 5.10 shows the volume-proportional idealised projection for each model. This is a simple representation of the measured gamut and the predicted gamut showing the relative volumes of two gamuts and the relative volume of their intersection. Each circle represents the volume of an individual gamut and the area of the circle is proportional to the volume of that gamut.
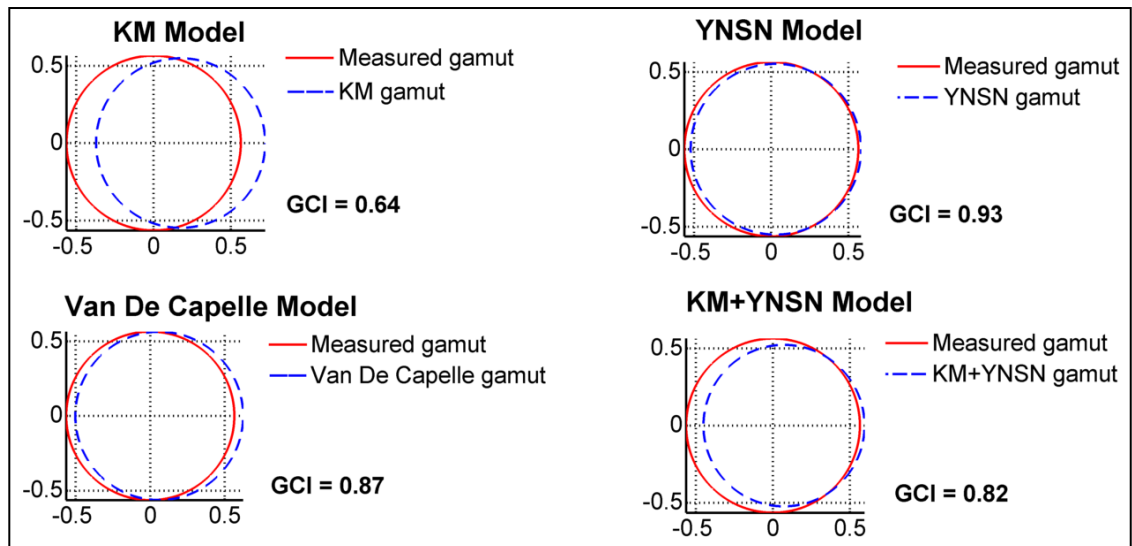
Figure 5.10 Volume-proportional idealised projections of the gamut pairs.

(Measured gamut and the model predicted gamut)

Figure 5.11 includes the GCI values on the primary vertical axis and the percentage gamut volume differences on the secondary vertical axis. Considering the GCI values, the YNSN model gives the best gamut match among all models followed by the Van De Capelle, KM+YNSN and KM models. The GCI values are in agreement with the CIEDE2000 values in Figure 5.5. However, in terms of the gamut volume difference, the Van De Capelle model performs the best followed by the YNSN, KM and KM+YNSN models. As discussed above, the volume difference metric does not account for the intersection of the gamuts, making it inappropriate for evaluating the prediction accuracy (see Figure 5.5 and Figure 5.11).
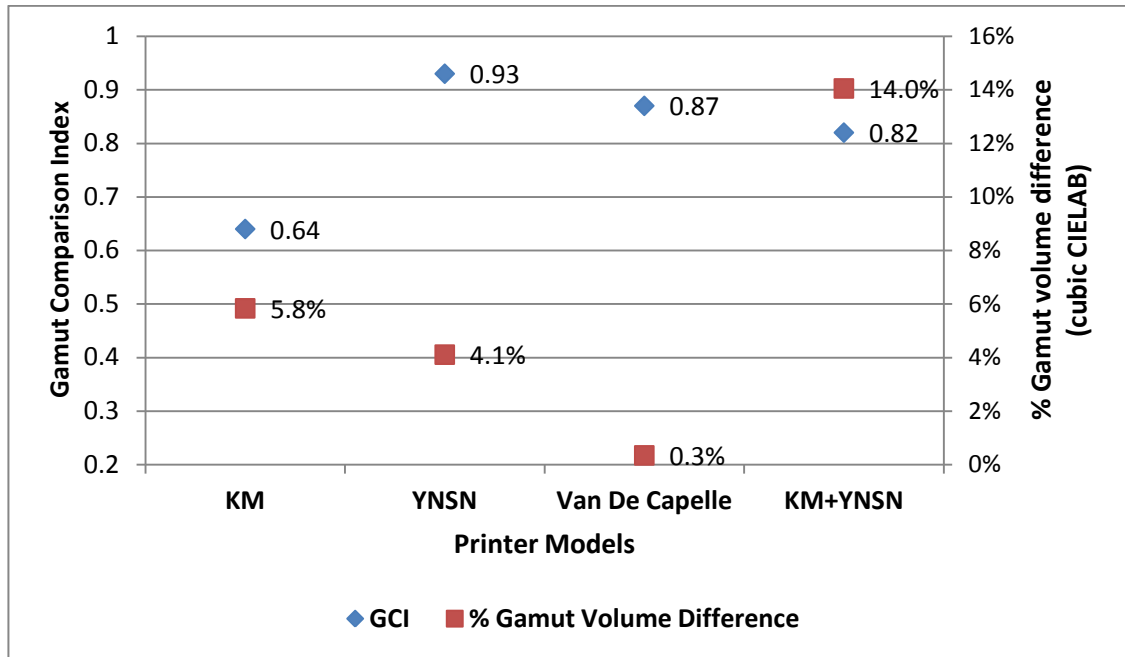
Figure 5.11 GCI and gamut volume difference between each model and the measured gamut.

For *n*-colour printing, it is also important to consider the number of input measurements required for the given printer model. As mentioned in Section 5.1, the number of colour patches required to determine the gamut boundary of the *n*-colour printing process can become excessively high as the number of inks (*n*) increases. The printer models usually try to seek a trade-off between accuracy and the number of inputs. The number of input measurements is also important when selecting an optimum ink-set from a large number of inks, for the *n*-colour printing process. The selection process may require analysing the colour gamuts of several combinations of inks. Printing and measuring the colour patches for these combinations of inks becomes prohibitive.

For each printer model, the GCI value was plotted against the minimum number of input measurements required (Figure 5.12). These are the minimum number of colour patches that need to be measured to apply the given printer model to the 7-colour printing process (see Chapter 4, Section 4.3.1).

Ideally, a model is needed which requires the least number of inputs and gives high-accuracy (top-left corner of the graph). But, in reality, all printer models try to seek a balance between accuracy and the number of inputs.
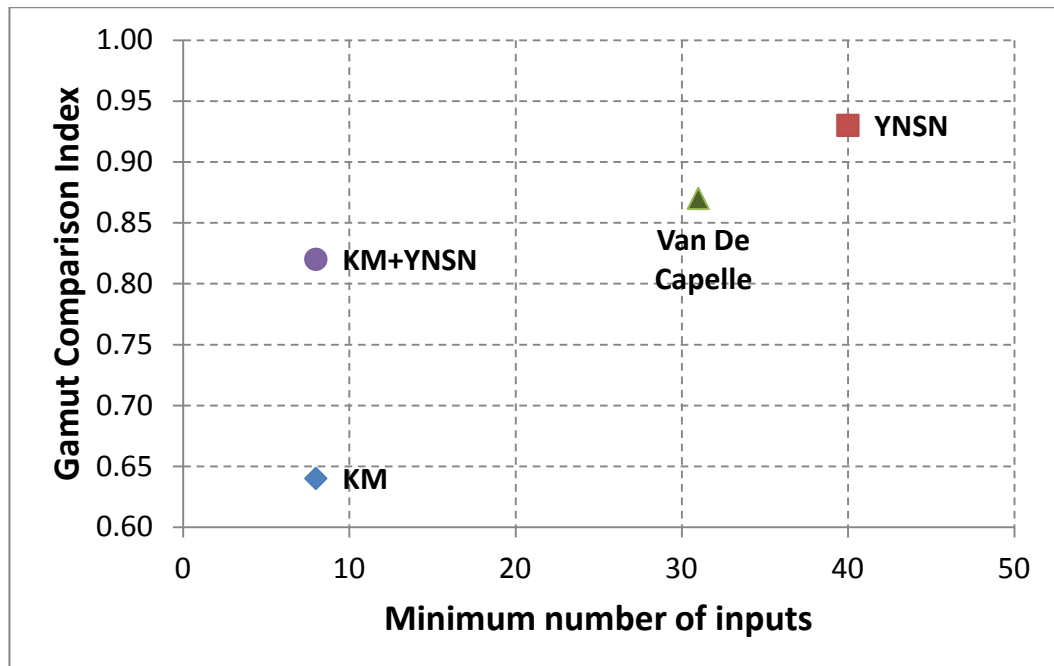
Figure 5.12 Gamut index versus minimum number of inputs for each model.

The KM+YNSN model gives a significantly better match (GCI = 0.82) than the KM model alone (GCI = 0.64), although these two models require the same number of inputs i.e. 8 colour patches. The Van De Capelle method gives good results (GCI = 0.87) with a lower number of inputs (31 colour patches) than the YNSN model (GCI = 0.93 with 40 colour patches). Note that the YNSN model requires overprints of inks in addition to the solid inks; however, the Van De Capelle model does not require any overprints since it characterises each ink separately. This is advantageous for a printing system with a higher numbers of process inks, for which the YNSN model requires a substantial number of inputs.

In addition the YNSN and the Van De Capelle models were also evaluated with a larger number of input colour patches. For the YNSN model, a subset of 60 colour patches from the ECI2002 test chart was selected which includes the 16 Neugebauer primaries. This set was used as a training set for optimising the Yule-Nielsen factor for each ink-sector. Thus a total of 240 colour patches were printed and measured. For the Van De

Capelle model, a full ink-profiling chart consisting of 11 patches (0%, 10%, 20%,…, 90%, 100%) on three backgrounds was used. Thus each ink requires 33 input patches resulting in a total number of 231 colour patches as input measurements.

The CIEDE2000 values between the measured and the predicted colours were calculated for the 600 boundary colours of the CMYK sector gamut (Section 5.4). Table 5.2 shows the mean colour difference values and the GCI values for the two models.

Table 5.2 Colour difference and the GCI values with the increased number of input measurements.

Models	Number of input colour patches	Mean CIEDE2000 for boundary colours	GCI
YNSN	240	1.01	0.95
Van De Capelle	231	1.63	0.90

Both models show improvements in the value of the mean colour difference and the GCI values. However this is at the cost of the increased number of inputs and the computational speed. As a future work the colour gamuts of several combinations of inks for the *n*-colour printing process will be analysed. For a large number of ink-sets and their colour gamuts, printing and measuring the minimum number of colour patches is practical. Conversely for a limited number of ink-sets, it is useful to have a greater number of input patches to get more accurate prediction of the colour gamut.

5.7 Conclusion

An *n*-colour printing process was characterised using each of four printer models and the resulting colour gamuts analysed. Since it might be expected that the model accuracy would increase with the number of input measurements, the challenge was to find a trade-off between accuracy and the number of inputs. This requirement is particularly significant as the number of colorants increases, because the colorant space is *n*-dimensional.

A 7-colour printing process was used as an example, but the method described here can be generalised to any *n*-colour printing process by having sub-sets of 4-inks each containing a common black ink and three chromatic inks.

A combination of the KM and the YNSN models gave a reasonable prediction of the gamut of an *n*-colour process, when using spectral reflectance measurements of the primary inks alone. This procedure can significantly reduce the time and cost of printing and materials for *n*-colour printing, particularly when there are several ink-sets to be analysed. However, the accuracy of gamut prediction is lower than for the YNSN and the Van De Capelle models which showed better performance at the cost of more input measurements than other models. In future work, the YNSN model will be utilised for further consideration for evaluation of *n*-colour printing processes.

Once the gamut volumes and their intersection are calculated, the GCI can be calculated. Additional gamut metrics are also used for further analysis of two gamuts. The GCI and other gamut metrics are supplemented by a simple volume-proportional idealised projection showing the relative volumes of two gamuts and the volume of their intersection.

The gamut metrics can be used in various scenarios, for example, comparing the colour gamuts of different imaging devices; comparing the model-predicted gamut to the real gamut of the imaging device and guiding the reproduction process by analysing the image gamut against the standard colour encoding gamuts, for example, sRGB.

The results in this chapter are derived using colorimetry, but the spectral printer models (like YNSN, Van De Capelle etc.) require spectral data, which may not be always available in practice. The spectral printer models are difficult to integrate into the existing standards like ICC and PDF/X workflow due to the complexities of the models (Deshpande, 2014c). The next chapter introduces a new model based on tristimulus data to provide a simplified method that can be easily implemented for characterising the printing devices.

Chapter 6 Spot colour overprint (SCOP) model

The results described in this chapter have been published in Deshpande (2010 and 2011). For a typical reproduction workflow in the printing and packaging industry, the printer models discussed in the previous chapters (Chapter 4 and Chapter 5) are relatively complex and computationally expensive. They are based on spectral data, which may not be readily available throughout the pre-press and print production process. A simpler method based on CIELAB or CIEXYZ data is necessary but without compromising the colour accuracy.

In this chapter, a new simplified numerical method is proposed as a forward printer characterisation model. Although this model was initially developed to estimate the spot colour overprints, it was extended to be used as a generic forward characterisation model for *n*-colour printing process.

A background for the spot colour overprint (SCOP) prediction is given followed by the description and implementation of the spot colour overprint model. The main objective was to offer a simple and computationally inexpensive model which can be incorporated within the current ICC and PDF/X workflow.

Finally the SCOP model was extended to the 7-colour printing process. The model was evaluated for the same data-sets used in Chapter 4 to compare its accuracy against the existing printer models, for example, the YNSN model, the Van De Capelle model etc.

6.1 Need for a simple model

Conventional printing process uses four process inks i.e. CMYK. For packaging and some other applications, additional inks are used to print critical brand colours. These are known as spot colours and printed with special inks. These inks are also useful for maintaining the colour consistency throughout the print-run.

As discussed earlier, the *n*-colour printing process consists of more than four inks, where all inks are process inks. Thus, all inks are printed in combination to constitute an image. On the other hand, the spot coloured ink is usually printed as a single ink-channel to print individual elements like company logos, corporate colours, etc. But, a spot coloured ink can also be printed in combination with process inks (CMYK) or another spot coloured ink. This can be considered as an *n*-colour printing process. Figure 6.1 illustrates a real-world example of an artwork consisting of two spot colours printed in combination.
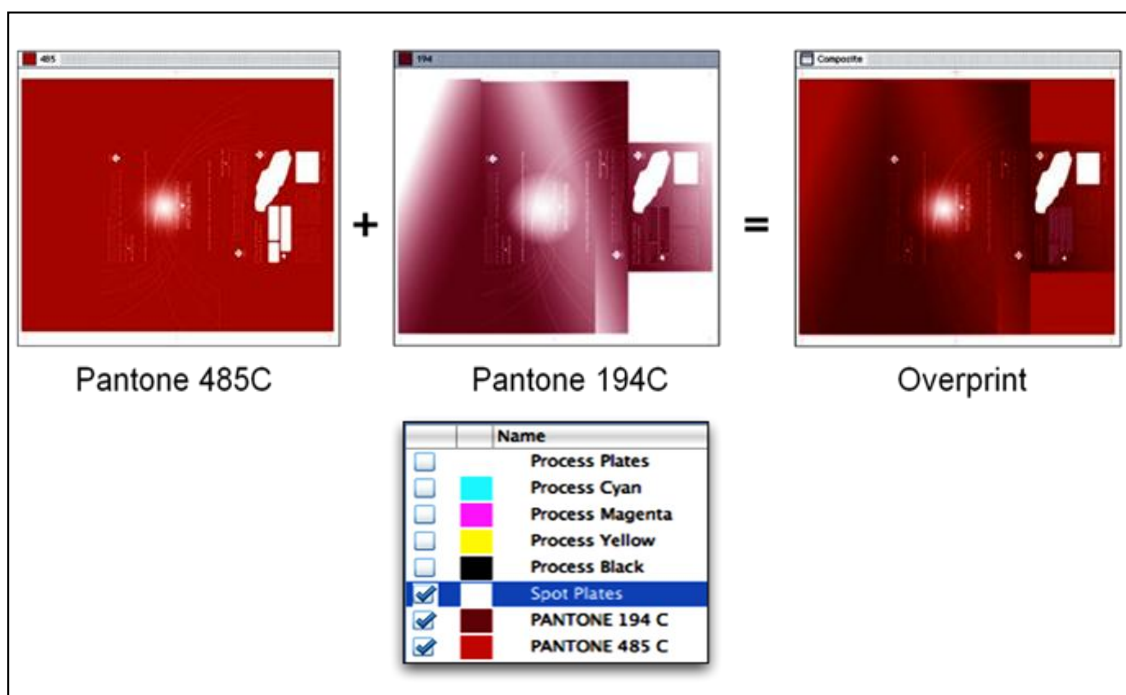
Figure 6.1 A print job containing the overprints of two spot colours with tints.

In order to predict the colours printed by a combination of process inks and spot coloured inks, an ICC profile has to be generated. An ICC profile describes the colour behaviour of an imaging device and helps to translate colour data between devices. It is a file containing look-up tables that define the relationship between device values (for example, CMYK or RGB) and colorimetric values (for example, CIELAB). The ICC profile for a printing device can be generated by printing a profile target, for example IT8.7/4 test chart (ANSI IT8.7/4, 2005), and measuring all colours from this chart. However, it is not practical to print a profile target and generate an ICC profile for all

inks in combination (Deshpande, 2010c). Ink properties, such as opacity, are not defined; this makes it difficult to predict the resulting colour for different ink-sequences.

Recently there have been some attempts to predict the overprints of spot colours. Viggiano (2008) used various ink trapping equations to predict the overprint colour. The YNSN based spectral model was used by Sigg (2011) to predict the spot colour overprint with an acceptable accuracy. Chung (2008) found that the display-to-print match fails completely for spot colour overprints and there is a colour management gap in the ability of pre-press software to predict spot colour overprints accurately between display and print.

Although methods exist for predicting the colour of a spot colour ink when it overprints another ink, there is a need for a simplified model for the purpose of previewing that can be used during document creation.

As described above, spectral printer models are available for characterising the four-colour printing system. These models try to depict the complex interaction between light, paper and ink. Some of these models include: KM model, Yule-Nielsen modified Neugebauer model (Viggiano, 1990), Van De Capelle and Meireson model patented by EskoArtwork (Van De Capelle, 1997 & 2002), Enhanced Yule-Nielsen modified Neugebauer (EYNSN) model to account for ink spreading in different ink superposition conditions (Hersch, 2004 & 2005). Although these models were not developed for spot colours, they can be used to predict the colour of ink combinations of spot colours.

Some of these models require an extensive number of inputs and an optimisation process. Furthermore, these are relatively complex models and they cannot be easily integrated into the existing standards like ICC profiles and PDF/X.

The YNSN model requires printing all combinations of primary inks. For a 6-ink printing system, it needs 64 colour patches. The packaging industry uses a large number of spot colours. For example, the Pantone Plus Solid Coated Formula Guide contains 1617 spot colours and it is not practical to print and measure all possible combinations of all inks.

Morovič (2012b) compared spectral reproduction against colorimetric reproduction of the spot colours and fine art using *n*-colour inkjet printing system with 11 inks. For the fine art reproduction on glossy substrate, spectral print reproduction showed significant improvement as compared to the colorimetric reproduction. But for the spot colour proofing on matte substrate, there was no significant improvement suggesting that driving a printer spectrally would be unnecessary. This means that the current systems along with the printing conditions (for example, inks and substrates) are well tuned for colorimetric reproduction and also perform well in terms of the spectral domain (Morovič, 2012b).

The proposed SCOP model (Deshpande, 2010 & 2011) is *not* an attempt to generate a more accurate prediction than these established methods, but to provide a simplified method that can be easily implemented and that is free of existing intellectual property. It characterises each spot colour individually and predicts the colour of overprinting solids and halftones by linearly combining the reflectances of two colours. Each ink is defined separately in terms of its opacity, and relatively few measurements are required to predict the resulting colour of the overprint.

The model was initially based on a linear regression method, but the model accuracy was further improved by using a power regression method. Power regression is the regression on the logs of the powers of the independent variables. The assumption made in this method is that at each wavelength the reflectance factor of an overprint approximates the product of the reflectance factors of the two inks measured independently. When this reflectance product is modified by using power regression, the approximation is often a good prediction of the actual reflectance. Since CIEXYZ is a linear transform of reflectance, the same approach can be adopted for CIEXYZ tristimulus values.

The SCOP model was evaluated for three different substrates. A 6-colour test chart, containing a total of 4550 patches of different combinations of C, M, Y, K and two spot colours, was printed using the offset printing process.

The overprint model was applied to predict the resulting colours. Model predictions were compared to the measured data in terms of Δ*L**, Δ*a**, Δ*b** and CIEDE2000 colour difference. The following method is used to apply the proposed simplified model.

6.2 Method

A 6-colour test chart (Figure 6.2) was designed to evaluate the SCOP model, which is described in the next section. A basic set of the IT8.7/3 chart (CMYK), consisting of 182 colour patches, was selected to represent the background objects. Two spot colours, Pantone 157C (Spot1) and Pantone 330C (Spot2), were used in addition to Cyan, Magenta, Yellow and Black inks. These specific two spot colours were selected because they have very different spectral reflectances. Spot1 is a representative of pastel colours and Spot2 is a dark colour. Thus, light and dark spot colours were covered to evaluate the model.

On each of the 182 patches of CMYK, solid and tints of each spot colour (0%, 25%, 50%, 75% and 100%) were printed. This gives a set of 25 colour patches for each CMYK basic colour, resulting in a total of 4550 patches. Figure 6.3 shows one of the four parts of the 6-colour test chart.
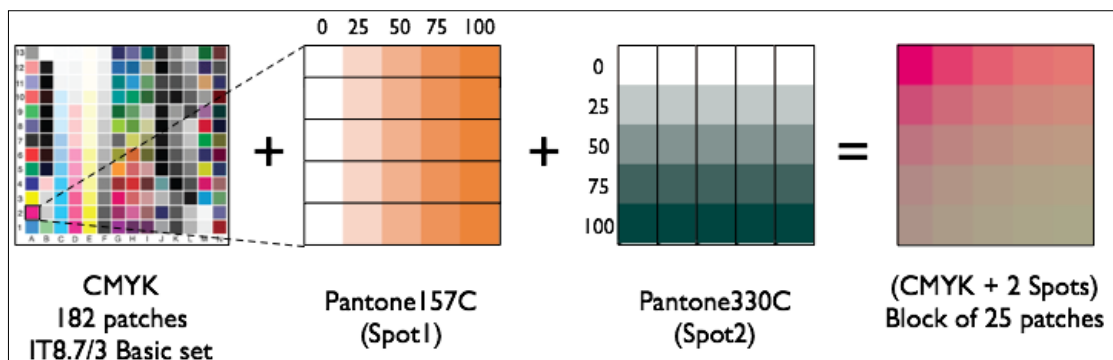
Figure 6.2 Design of the 6-colour test chart.
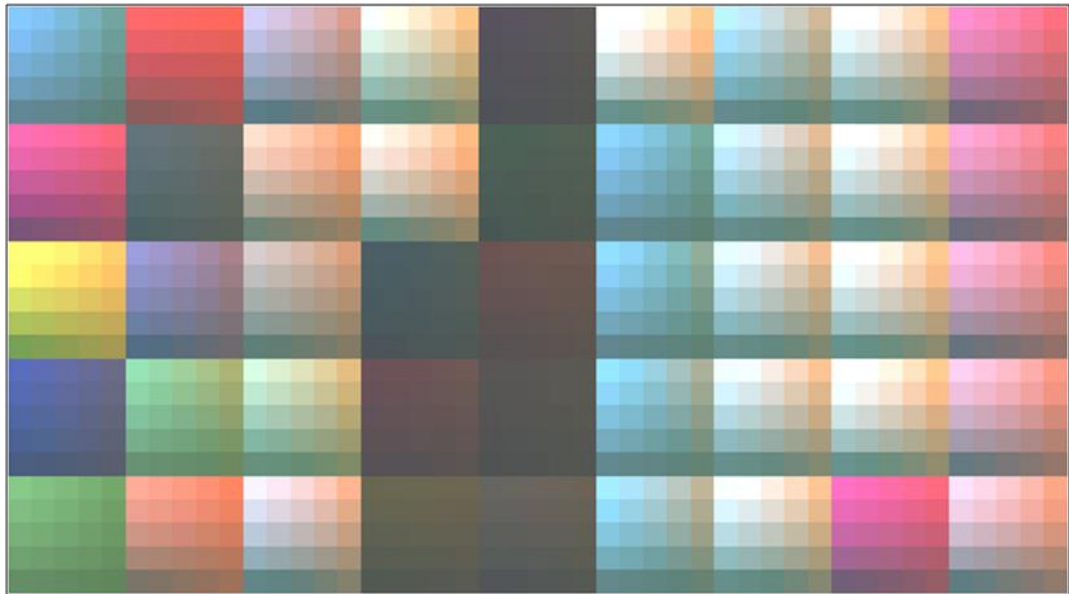
Figure 6.3 One of the four parts of the 6-colour test chart.

To define each spot coloured ink individually, an ink characterisation chart was used. This consists of ramps of inks from 0% to 100% printed over the substrate, over the grey backing (50% black ink) and over the black backing (solid black ink). Thus there were three similar ramps consisting of 11 steps, printed over white (i.e. substrate), grey and black backings (see Figure 6.4). This is similar to Van De Capelle's method (Van De Capelle, 1997 & 2002). Spectral measurements of the ink characterisation chart provide ink reflectance characteristics. The model coefficients are derived from the ink step-wedge chart of the foreground colour (see Section 6.4.2).
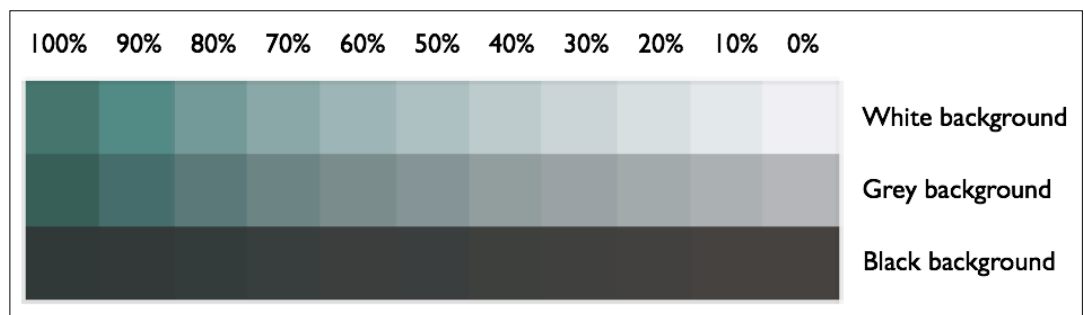
Figure 6.4 Ink characterisation chart for Spot2 (Pantone 330C).

Figure 6.5 shows spectra of solid colours (Spot1 and Spot2) over white and black backings.
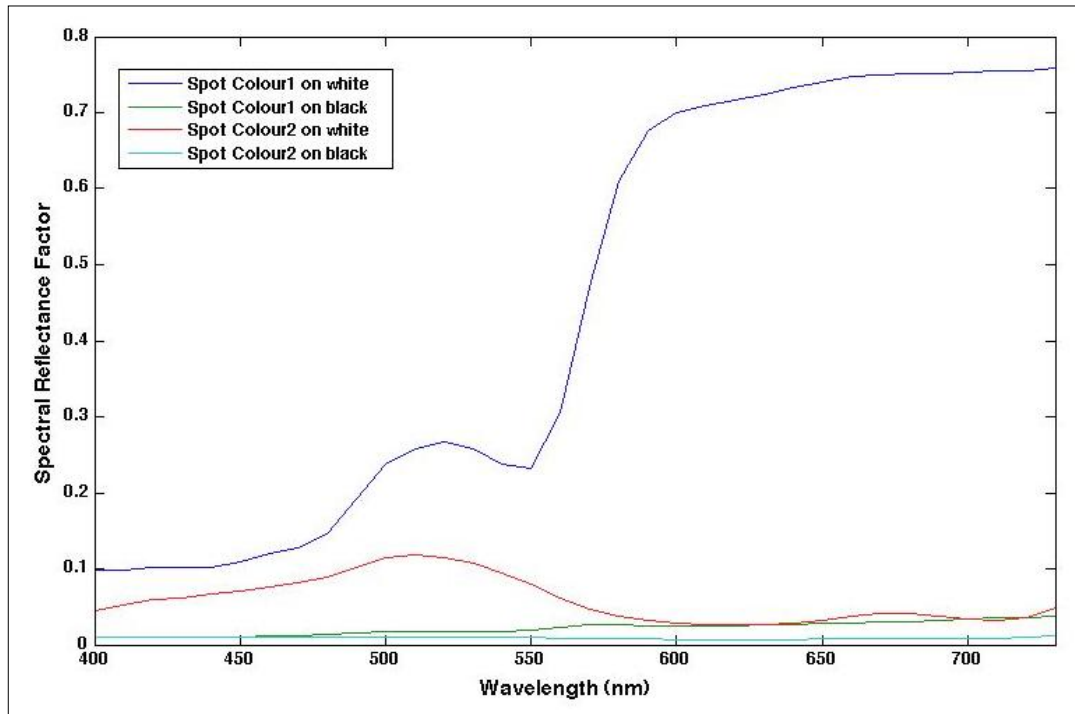
Figure 6.5 Spectra of two spot colours on white and black backing.

The printing process used in this study was the lithographic offset printing process on three different substrates: Mitsubishi Paper MYU Coat NEOS, Hokuetsu Paper Pearl Coat N and Nihon Paper Be-7 (Table 6.1). Toppan standard inks were used with the following sequence: K – C – M – Y – Spot1 (PMS 157C) – Spot2 (PMS 330C). All inks were printed with 150 lpi (lines per inch) screen ruling and the following screen angles: K = 45, C = 15, M = 75, Y = 90, PMS 157C = 30 and PMS 330C = 60. The test charts and ink characterisation charts were measured using an X-Rite i1 Pro 2 using the measuring conditions specified in Chapter 3 (Section 3.1).

Table 6.1 Substrate specifications.

Substrate	Weight (gsm)	L*	a*	b*	Whiteness
Mitsubishi "MYU Coat NEOS"	157	94	1	-1	86
Hokuetsu "Pearl Coat N"	127.9	94	1	-1	84
Nihon "Be-7"	122	96	1	-1	89

The model coefficients were calculated from the ink step-wedge chart for the foreground colour. Power regression was applied to predict the overprint colours. Model predictions were compared to the actual measured tristimulus values of the overprint colours.

The proposed model was compared to following existing models: KM model with Saunderson correction, YNSN model, Van De Capelle model. These models were applied for the above mentioned 6-ink printing system.

6.2.1   Linear regression

Consider an overprint colour obtained by printing ink on top of another ink. Since each ink reflectance spectrum represents the absorbance of light across the spectrum, the reflectance of an overprint can be approximated by simply convolving the two reflectances wavelength by wavelength. A spectral product of the individual inks can be used to predict the spectrum of the overprint colour. The error is typically an underestimate of the reflectance.

Scaling the spectrum by a single parameter often gives an acceptable reflectance. Thus, the spectral reflectance product of two inks can be modified numerically by a correction factor. This correction factor depends on the colorant opacity, the ink sequence and the dot area of the overprint colour.

Figure 6.6 shows a spectral reflectance curve of the overprint colour, obtained by printing yellow ink on top of magenta. The spectral product of magenta and yellow inks is also shown as a grey curve. It is an underestimate of the real overprint. When a correction factor is applied to this spectral product, the resulting spectrum (dashed curve) is closer to the actual measurement of the overprint colour.
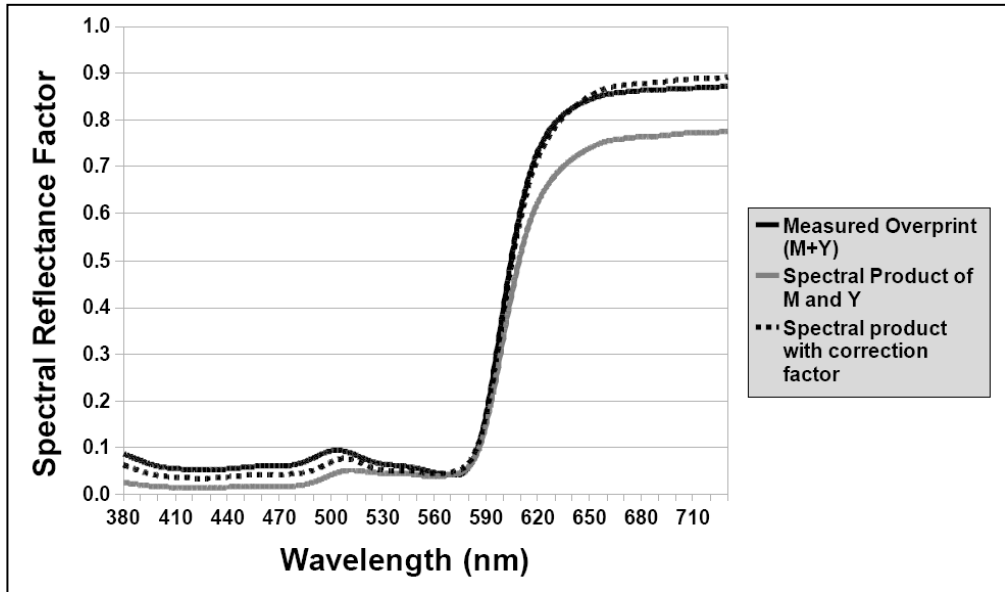
Figure 6.6 Spectral product of individual inks with correction factor.

However, the spectral data is usually not available in PDF and in ICC profiles. Therefore, a trichromatic-based approach (CIEXYZ or CIELAB) is required. Since XYZ is a linear transform of reflectance, the same approach is applicable to XYZ.

Where a spot colour is printed over another colour (say 40% Spot1 and 30% Spot2), the first-printed underlying colour (40% Spot1) can be considered as a background object and the overprinted spot colour (30% Spot2) as a foreground object as shown in Figure 6.7. The background and the foreground objects are obtained from the ink characterisation charts as shown in Figure 6.4 (tints printed on the white backing). The missing dot percentages are derived by interpolating the existing measurements.
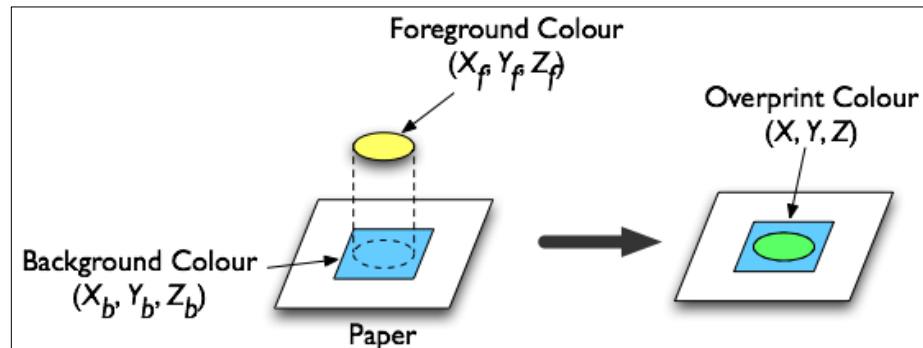
Figure 6.7 Spot colour overprint – background and foreground colours.

The overprint model assumes that a resulting colour (X_r, Y_r, Z_r) is correlated to the multiplicative function of the background colour (X_b, Y_b, Z_b) and foreground colour (X_f, Y_f, Z_f). The resulting colour (X_r, Y_r, Z_r) is predicted as follows:

$$X_r = j_x(X_b X_f) + k_x$$
$$Y_r = j_y(Y_b Y_f) + k_y$$
$$Z_r = j_z(Z_b Z_f) + k_z$$

(6.1)

where

$[X_b\ Y_b\ Z_b]$: tristimulus values of background colour

$[X_f\ Y_f\ Z_f]$: tristimulus values of foreground colour

$[j_x\ j_y\ j_z]$: scaling factors of foreground colour

$[k_x\ k_y\ k_z]$: constants of foreground colour

The scaling factors and constants are calculated from the ink characterisation chart. Colour patches on all three backings (white, grey and black) are used to derive these coefficients. The linear least squares method was sufficient to derive the scaling factors (j_x, j_y, j_z) and constants (k_x, k_y, k_z).

6.2.2 Power regression

It was found that power regression was a better choice than linear regression for predicting the spot colour overprints. Figure 6.8 depicts a strong correlation between the measured overprint colour and the product of the background and the foreground colours, with a correlation coefficient 0.99.
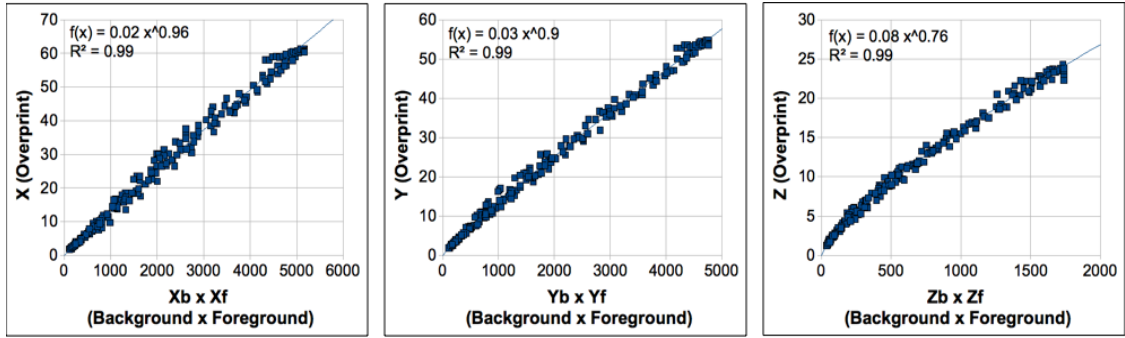
Figure 6.8 Data fitting – measured overprint colours vs. the product of background and foreground colours.

The overprint model predicts a resulting colour (X_r, Y_r, Z_r) from the product of the background colour (X_b, Y_b, Z_b) and the foreground colour (X_f, Y_f, Z_f) as follows:

$$X_r = j_x (X_b X_f)^{k_x}$$
$$Y_r = j_y (Y_b Y_f)^{k_y}$$
$$Z_r = j_z (Z_b Z_f)^{k_z}$$

(6.2)

where

$[X_b\ Y_b\ Z_b]$: tristimulus values of background colour

$[X_f\ Y_f\ Z_f]$: tristimulus values of foreground colour

$[j_x\ j_y\ j_z]$: scaling factors of foreground colour

$[k_x\ k_y\ k_z]$: exponents of foreground colour

Taking the natural logarithm of both sides of the above equations (6.2), we have the following equivalent set of equations.

$$\ln(X_r) = \ln(j_x) + k_x \ln(X_b X_f)$$
$$\ln(Y_r) = \ln(j_y) + k_y \ln(Y_b Y_f)$$
$$\ln(Z_r) = \ln(j_z) + k_z \ln(Z_b Z_f)$$

(6.3)

This equation has the form of linear regression as shown in Eq. (6.1) and can be referred to as a log-log regression. Thus power regression is a form of linear regression.

Note that the variable names [k_x k_y k_z] used in Eq. (6.2) are the same as those used in Eq. (6.1) to maintain consistency. The SCOP model is mainly used with power regression i.e. Eq. (6.2) for the rest of this thesis. The coefficients (scaling factors and exponents) are dependent on the foreground colour. They can be calculated from the ink step-wedge chart of the foreground colour. This is explained in detail in the implementation section (6.4). The above equation can be used recursively to calculate the colour printed by multiple inks, for example 3-inks, 4-inks and so on.

6.3   Results

6.3.1   Linear regression

Table 6.2 shows the CIEDE2000 colour difference values between the predicted and the measured colours for CMYK + Spot1 combinations on all papers. All CIEDE2000 values are below 3. It can be seen that ΔL* values have contributed less that the Δa* and Δb* values to colour difference values.

Table 6.2 Overall accuracy of the overprint model for Spot1.

Substrate	Average				Max
	CIEDE2000	ΔL*	Δa*	Δb*	CIEDE2000
Be-7	2.89	1.30	2.40	2.07	14.82
MYU Coat NEOS	2.90	1.50	2.40	2.35	15.26
Pearl Coat N	2.92	1.51	2.42	2.35	15.10

A histogram of CIEDE2000 values is shown in Figure 6.9. This is for MYU Coat Paper and combinations of CMYK and Spot1. Most of the values are below 5. Despite being a simple linear model, it gives relatively good accuracy.
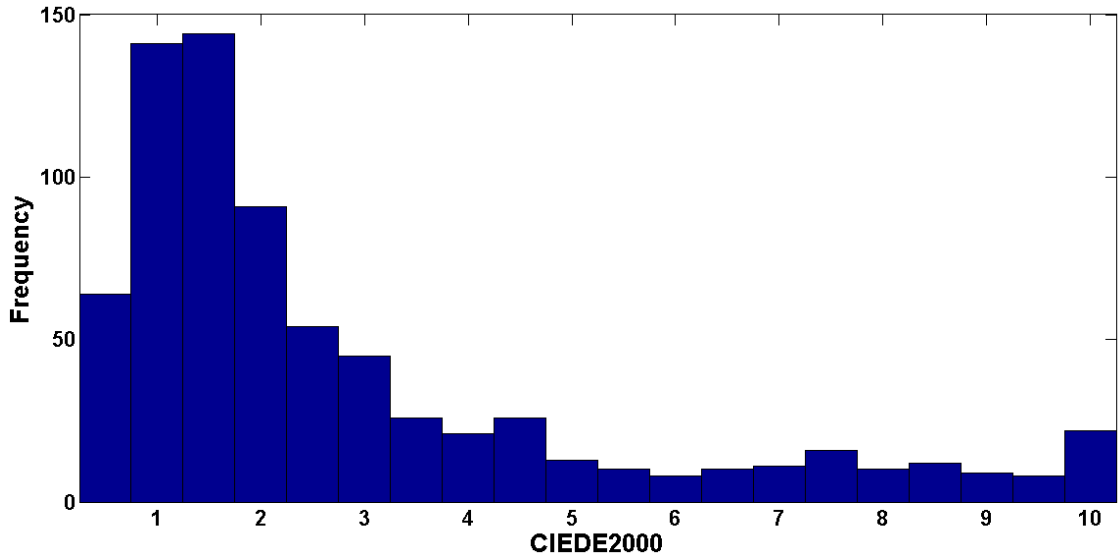
Figure 6.9 Histogram of CIEDE2000 – CMYK + Spot1 for MYU Coat paper

Colour difference results for CMYK + Spot2 combinations on the same substrate are given in Table 6.3. The accuracy achieved is similar to that for Spot1.

Table 6.3 Overall accuracy of the overprint model for Spot2.

Substrate	Average				Max
	CIEDE2000	ΔL^*	Δa^*	Δb^*	CIEDE2000
Be-7	2.49	1.28	2.22	1.35	13.06
MYU Coat NEOS	2.51	1.41	2.44	1.42	16.72
Pearl Coat N	2.48	1.39	2.43	1.48	16.40

Table 6.4 shows the scaling factors (j_x, j_y, j_z) and constants (k_x, k_y, k_z) for the Nihon Paper Be-7 for each spot coloured ink. For the given paper, scaling factors remain the same, but constants change.

166

Table 6.4 Scaling factors and constants for Spot1 and Spot2 inks for Paper Be-7.

Ink	Model Coefficients					
	j_x	k_x	j_y	k_y	j_z	k_z
Spot1	0.01	0.74	0.01	1.17	0.01	1.25
Spot2	0.01	1.06	0.01	1.10	0.01	0.98

To further investigate the robustness of scaling factors and constants, the overprint model was applied separately to different dot percentages of spot colour, for example, 25%, 50%, 75% and 100%. Table 6.5 shows the accuracy for these dot percentages for the paper MYU coat NEOS and Spot1.

Table 6.5 Accuracy of the overprint model for different dot percentages of Spot1.

	Average				Max
	CIEDE2000	ΔL^*	Δa^*	Δb^*	CIEDE2000
CMYK + 25% Spot1	1.22	0.51	1.02	0.89	1.96
CMYK + 50% Spot1	2.07	1.27	4.89	1.68	4.35
CMYK + 75% Spot1	2.84	1.44	2.45	2.30	5.27
CMYK + 100% Spot1	3.68	1.73	4.38	3.11	12.98

Colour difference values are increasing with the dot percentages of spot colour. This indicates that the model works better for highlights and mid-tones than for shadows. Note that the average CIEDE2000 value of 2.90 in Table 6.2 shows an average of all combinations of CMYK + Spot1; whereas Table 6.5 shows average CIEDE2000 for each dot % of Spot1 e.g. 25%, 50%, 75% and 100% Spot1 on top of CMYK. The average CIEDE2000 value of 3.68 is for a combination of CMYK and 100% Spot1.

The following Table 6.6 compares the accuracy of different models for a combination of Nihon Paper Be-7 and 6-inks (K, C, M, Y, Spot1, Spot2). KM theory showed the worst performance (mean CIEDE2000 of 14.74), whereas the YNSN model gave the least values of mean colour difference (mean CIEDE2000 of 2.72). The proposed simplified model showed moderate accuracy (mean CIEDE2000 of 4.01). Considering the

simplicity of this model, these results can be considered acceptable for displaying a preview of spot colour overprints.

Despite being a spectral model, the Van De Capelle model performed worse than the SCOP model. The Van De Capelle model uses completely different set of equations and coefficients than the SCOP model. Also the Van De Capelle method has shown similar results in Chapter 4 (see Section 4.2.7).

Table 6.6 Comparison of the models for a 6-inks printing system (overprint of Spot1 and Spot2).

Models for 6-ink system (Spot1 and Spot2)	CIEDE2000		
	Mean	95th Percentile	Max
KM model	14.74	31.03	34.68
YNSN model	2.72	6.85	19.19
Van De Capelle model	5.35	11.77	23.83
KM+YNSN model	4.60	13.74	24.54
SCOP model	4.01	10.04	16.44

6.3.2   Power regression

Figure 6.10 shows the model accuracy of linear regression and power regression for CMYK + Spot1 combinations on all papers. It is evident that power regression has improved the accuracy of the predictions.
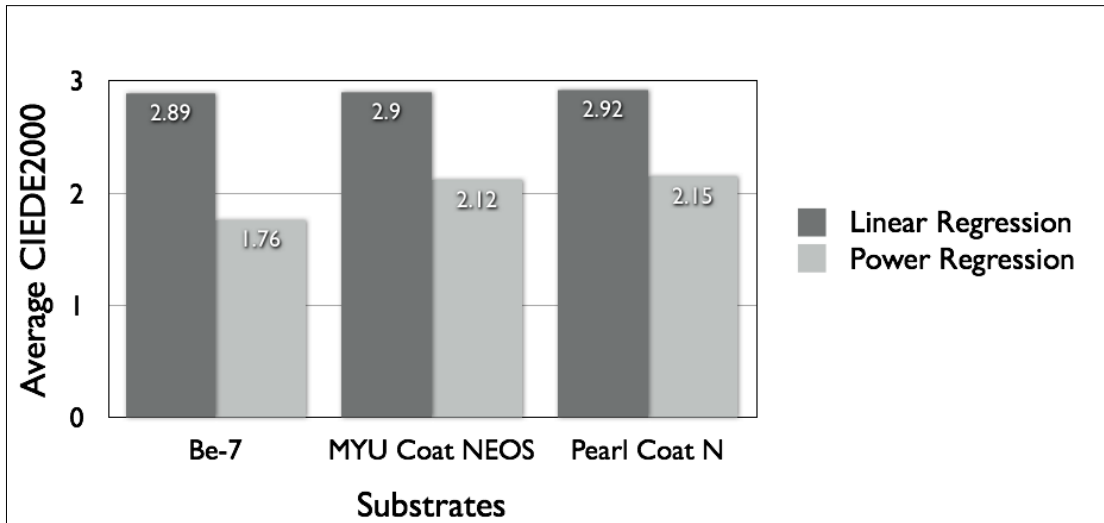
Figure 6.10 Improvement in model accuracy using power regression.

The 6-colour test chart was printed on three substrates. Average CIEDE2000 values between the measured and the predicted overprint colours were calculated for three different combinations: Spot1 + Spot2, CMYK + Spot1 and CMYK + Spot2. Results for each substrate are shown in Figure 6.11. Model accuracy is acceptable with all average CIEDE2000 values below 2.5.
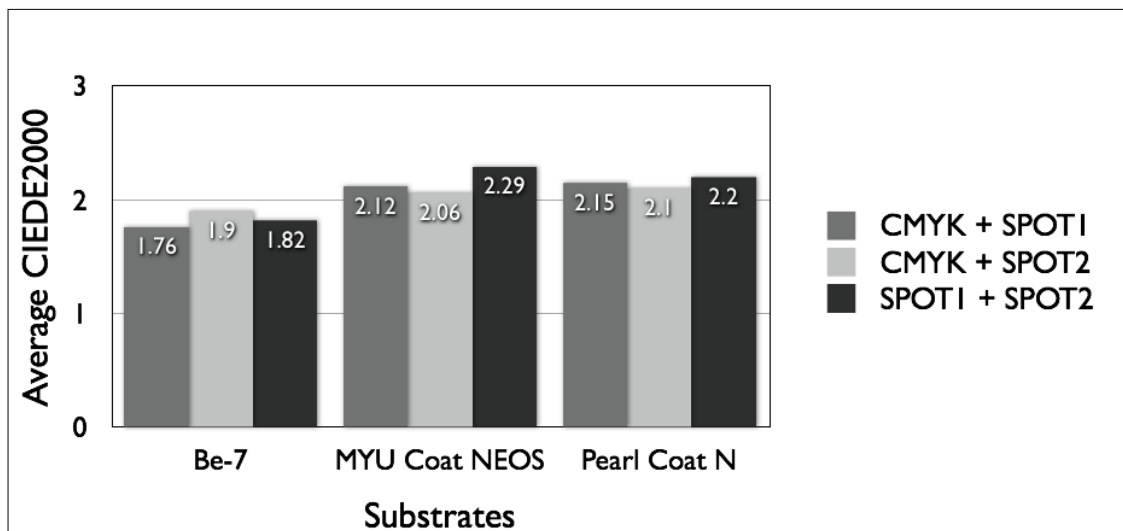
Figure 6.11 Summary of results for power regression method.

Since every ink is defined separately by printing the ink step-wedge chart, there is no need to print combinations of individual inks. For a given library of spot colours, once the ink step-wedge chart for each ink has been measured and the model coefficients *j* and *k* are calculated, it is possible to predict the overprint colour resulting from any combination of inks in the library.

6.4   Implementation

This section includes step-by-step guidelines for those who want to implement the SCOP model for predicting the colour of a 2-ink overprint (see Figure 6.14). It can be easily extended to more than 2-ink overprint.

As an example, assume the requirement is to print two special inks with the following ink sequence: Spot1 – Spot2, and it is necessary to predict the overprint colour resulting from a combination of 40% Spot1 and 60% Spot2. Here, the background colour is 40% Spot1 and foreground colour is 60% Spot2. The overprint colour can be predicted as follows.

6.4.1   Print and measure the ink step-wedge chart

Print the ink step-wedge charts for Spot1 and Spot2. This chart should include the following minimum number of colours: the substrate, solid black, solid ink printed over white, grey and black backgrounds and at least one tint patch of the ink printed over white, grey and black backgrounds. For example, the ink step-wedge chart in Figure 6.12 consists of ink ramps of 0% to 100% in 11 steps over a white background (the plain substrate), a grey background (50% black) and a black background (solid black). Each patch of the ink step-wedge charts is then measured to obtain the tristimulus values (*X*, *Y*, *Z*).

6.4.2   Calculate the overprint coefficients for the foreground colour

Calculate the overprint coefficients ($j_x, j_y, j_z, k_x, k_y, k_z$) for the foreground colour, which is the 60% Spot2 ink. This is done by applying the model equations to the ink step-wedge chart of the Spot2 ink as follows.

Obtain the measured tristimulus values (X, Y, Z) of all the patches in the ink step-wedge chart for the foreground colour (Spot2) as described in Section 6.4.1 above. This gives the measurements of the 60% Spot2 over white, grey and black backgrounds. By applying the overprint model to these patches it is possible to calculate the coefficients. These patches (marked as 1, 2 and 3 in Figure 6.12) are treated as the resultant overprint colours.
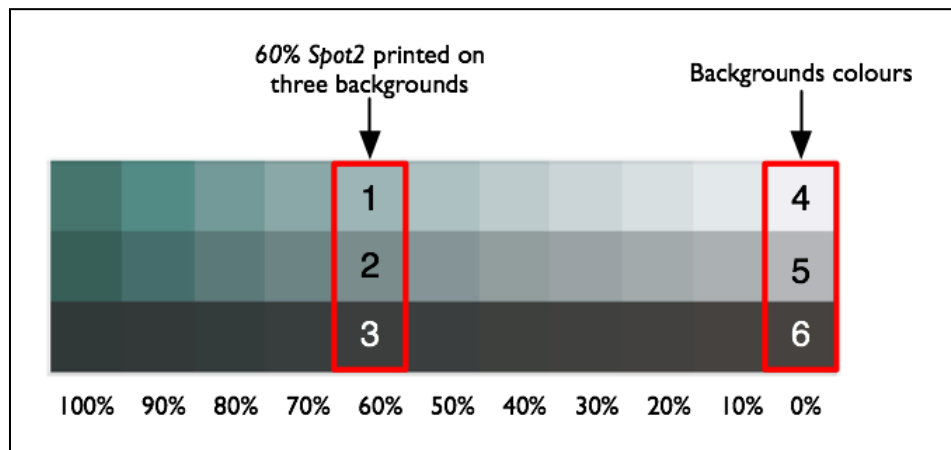
Figure 6.12 Ink step-wedge chart – Spot2 ink printed on three backgrounds.

Table 6.7 Background and foreground colours for each overprint colour.

Overprint Colour [X, Y, Z]	Background Colour [X_b, Y_b, Z_b]	Foreground Colour [X_f, Y_f, Z_f]
60% *Spot2* over white (Patch 1)	Substrate (Patch 4)	60% *Spot2* over white (Patch 1)
60% *Spot2* over grey (Patch 2)	Grey (Patch 5)	60% *Spot2* over white (Patch 1)
60% *Spot2* over black (Patch 3)	Solid Black (Patch 6)	60% *Spot2* over white (Patch 1)

Table 6.7 defines the background colour and foreground colour for each of three overprint colours. For example, consider a 60% Spot2 on a grey background (X, Y, Z) i.e. Patch 2. In this example, the background colour (X_b, Y_b, Z_b) appears grey, which is patch number 5 in Figure 6.12, and the foreground colour (X_f, Y_f, Z_f) is the 60% Spot2 printed over white, which is patch number 1 in Figure 6.12. Similarly, the background and the foreground colours for the remaining two overprint colours can be found.

This provides the measured tristimulus values of all three resulting overprint colours and their background and foreground colours and these can be used in the models to calculate the coefficients.

6.4.3 Calculate the overprint coefficients for the required dot area

Using a set of three patches for 60% Spot2, power regression is applied to calculate the scaling factors (j_x, j_y, j_z) and constants (k_x, k_y, k_z) as shown in Eq. (6.2).

All tristimulus values can be obtained from the measurements of the ink step-wedge chart as described above. If a 60% dot area is not printed in the ink step-wedge chart of Spot2, then the tristimulus values of 60% Spot2 can be obtained by interpolating the existing measurements. For example, the tristimulus values of 60% Spot2 over white can be calculated by interpolating the existing measurements of the ink ramp over the white background. Using this method the model coefficients for any intermediate dot area can be calculated.

Once the overprint coefficients are calculated, the next step is to find the product of the background colour 40% Spot1 and the foreground colour 60% Spot2.

6.4.4 Calculate the product of background colour and foreground colour

The tristimulus values of the background colour, 40% Spot1, can be obtained from the measurements of the ink step-wedge chart of Spot1 ink (40% Spot1 printed on plain substrate). Similarly, the tristimulus values of the foreground colour, 60% Spot2, can be obtained from measurements of the ink step-wedge chart of Spot2 ink (60% Spot2 printed on a plain substrate). If the required dot area, for example 24%, is not printed in the ink step-wedge chart, then it can be obtained by interpolating the available measurements. This assumes that the dot area is linear with X, Y and Z values. Figure 6.13 shows how the measured values of X, Y and Z change with the dot area for one of the inks printed over white background.
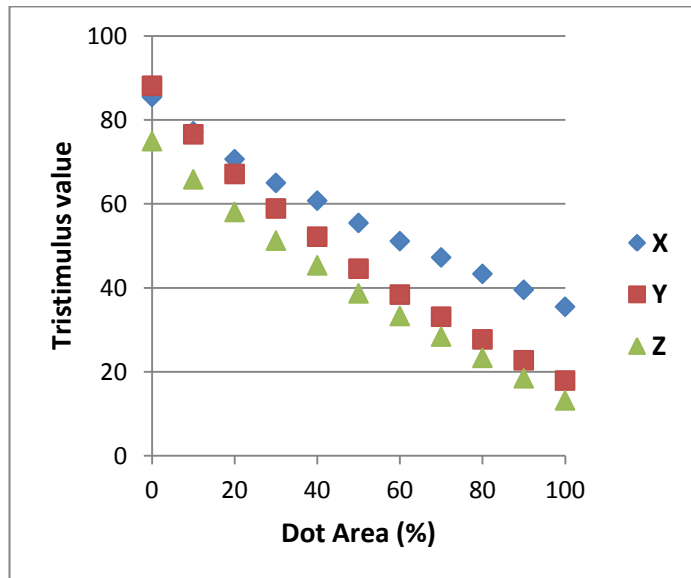
Figure 6.13 *X, Y* and *Z* values for different dot areas for an ink printed over white background.

If the tristimulus values of the background colour are $(X_b\ Y_b\ Z_b)$ and those of foreground colour are $(X_f\ Y_f\ Z_f)$, then the product of two colours is given by: (X_bX_f), (Y_bY_f), (Z_bZ_f).

6.4.5   Calculate the resulting colour

Apply the model equations Eq. (6.2) to calculate the resulting colour *XYZ* using the overprint coefficients ($j_x, j_y, j_z, k_x, k_y, k_z$) obtained in Section 6.4.2.

An overview of the implementation of the SCOP model for the 2-ink combination is shown in Figure 6.14.
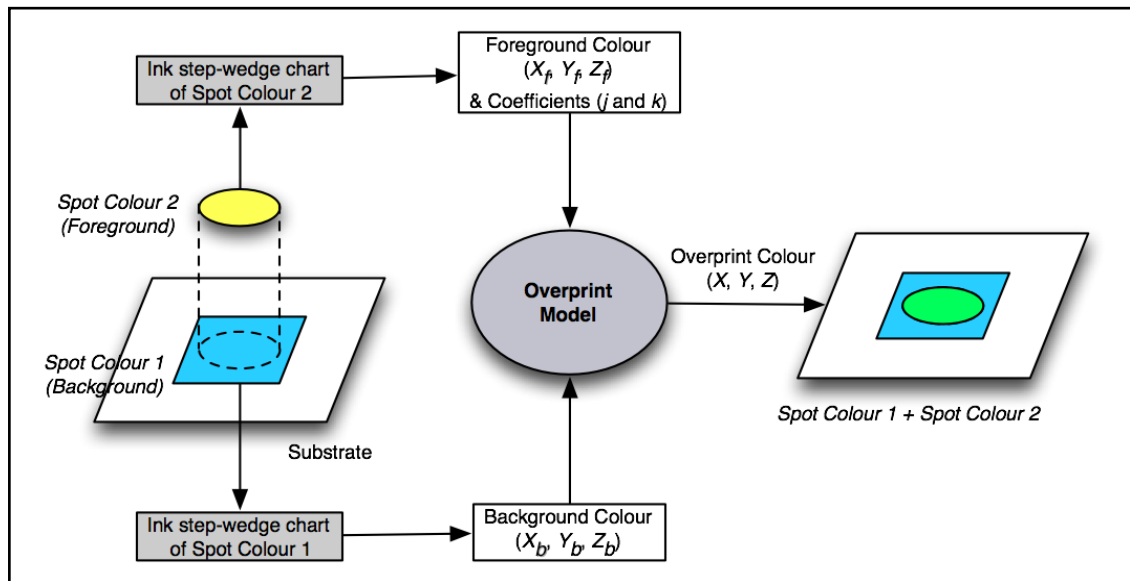
Figure 6.14 Implementation of the overprint model for 2-inks combination.

6.5   Applications

In a colour managed document, the tristimulus values of background colour (comprising C, M, Y, K ink-combinations) can be calculated using the *A2B* tag of the output intent ICC profile as shown in Figure 6.15 (Deshpande, 2010). The tristimulus values of the foreground colour (i.e. the spot coloured ink) can be derived from the measurements of the ink characterisation chart (colours on the white substrate). The tristimulus values of the resulting colour (X_r, Y_r, Z_r) can be predicted by applying Eq (6.2). Finally for reproducing the resulting colour on a proofing device, the *B2A* tag of the proofer's ICC profile can be used to estimate the colorant percentages.
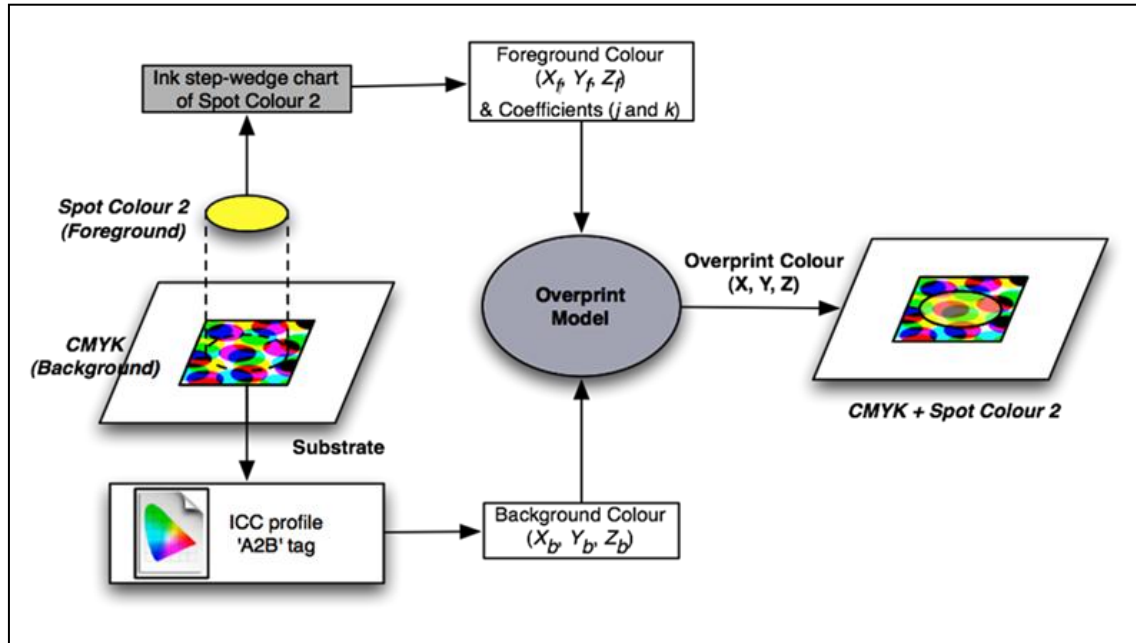
Figure 6.15 Implementation of the overprint model for CMYK + spot colour.

For a printing system using multiple spot inks printed on top of each other, Eq (6.2) can be applied recursively to predict the resulting colour of any given combinations of inks (Figure 6.16). There is no need to measure overprints of different combinations of inks; each ink only need be characterised individually.
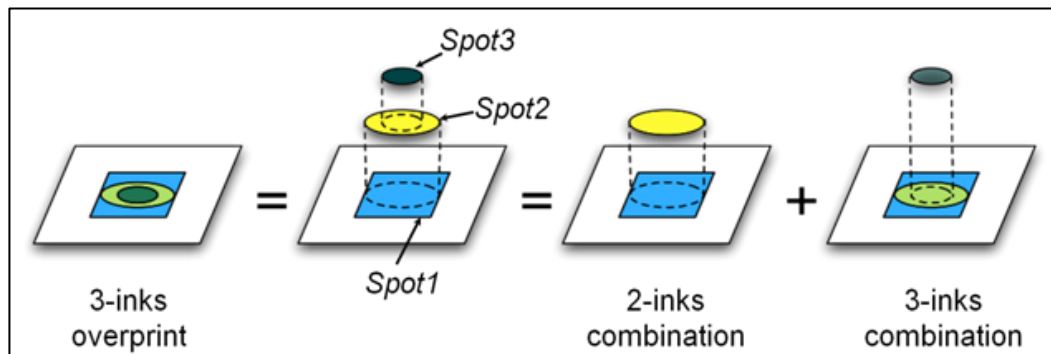
Figure 6.16 Implementation of the overprint model for 3-inks combination.

6.6   The SCOP model as a forward characterisation model

In the earlier sections of this chapter, the SCOP model was used for predicting the overprints of spot colours. Here the model is extended as a generic characterisation model for 4-colour and n-colour printing with process inks. In Figure 6.16, if the spot colours are replaced with process colours, the method becomes a generalised forward characterisation model for printing devices. The SCOP model given in Eq (6.2) can be recursively applied to a printing system consisting of *n*-inks. If the coefficients ($j_x, j_y, j_z, k_x, k_y, k_z$) are calculated separately for each dot area of the foreground colour, the model accuracy increases. Thus the coefficients depend on the dot area of the foreground colour. The SCOP model was evaluated using the same method and data which were used for evaluating other printer models in Chapter 4, for example, the YNSN, the KM and the Van De Capelle models.

The 7-colour lithographic offset data-set was used. Calibration, workflow parameters and the printing conditions were identical to those described in Chapter 3 (3.2). The ECI2002 test chart was printed for each ink-sector and all colour patches were measured using an X-Rite i1 Pro 2 spectrophotometer. The main criterion for the ink-sequence was printing the black ink first before the chromatic inks, for example, K − C − M − Y. This allows extracting the model coefficients for each chromatic ink on three different backgrounds, namely black, grey (50% black) and white (0% black).

The training set used for deriving the model coefficients consisted of the following colours: 4 colour patches per primary ink − solid and 50% ink printed on white (plain substrate) and black (100% black) backgrounds. In addition, the plain substrate, 50% black and 100% black colour patches were measured to represent 0% of inks on white, grey and black backgrounds respectively. Thus for a 7-colour printing process, a total of 31 colour patches were used to provide input measurements for the model. The training set was derived from the ECI2002 test chart.

The remaining colour patches from the test chart were used as a test set for evaluating the model accuracy.

6.6.1   Method

In Section 6.4 of this chapter, the implementation of the SCOP model for 2-ink combination has been explained. The same method was extended to a 4-inks combinations for each ink-sector (Figure 6.17) and then to a 7-inks combination using four ink-sectors. A modular framework of Matlab functions was developed to implement the model (see Appendix B: Matlab codes for the spectral printer models).

For each ink, the tristimulus values of all dot areas were calculated using one-dimensional linear interpolation of the colour measurements from the training set. For example, it is possible to calculate the tristimulus values of 1%, 2%, …., 98%, 99% cyan from the measured tristimulus values of the solid (100%) and 50% of cyan ink on a white background by interpolating X, Y and Z values separately. These tristimulus values were required as the background and foreground colours for the next step. Similarly it is possible to calculate the tristimulus values of all dot areas of each ink for the grey and black backgrounds using the training set. The set of all the tristimulus values were denoted as the 'Ink Step-Wedge Data'.

Since the black ink was printed first, it is not necessary to calculate the model coefficients for this ink. For each chromatic ink, the model coefficients (j_x, j_y, j_z, k_x, k_y, k_z) were calculated using Eq (6.2) for the solid, 50% and 0% over three backgrounds using the training set (see Section 6.4.2). The model coefficients for the remaining dot areas (1%, 2%, …., 98%, 99%) were calculated by interpolating the known values. This set of all coefficients is denoted as the 'Coefficients Data'.
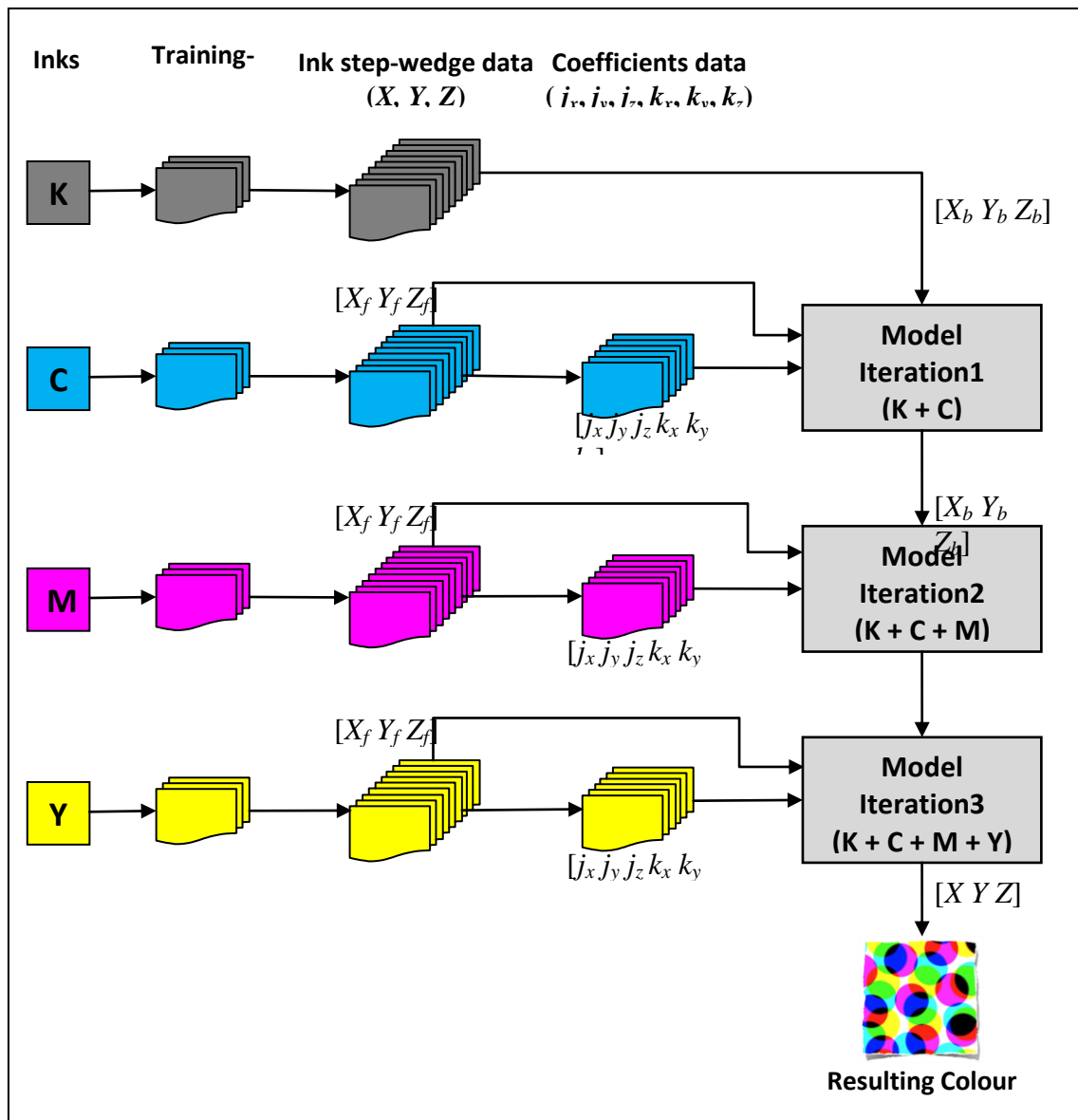
Figure 6.17 Framework for implementing the SCOP model to 4-colour printing process.

For each ink-sector, there is a test set of 1485 colorant values for which predictions of the CIELAB values are required. For the first iteration, for example, cyan printed over black (K + C), for each patch in the test set, the tristimulus values of the background colour and the foreground colour can be obtained from the 'Ink Step-Wedge Data' of the cyan ink. The model coefficients for the foreground colour were obtained from the 'Coefficients Data'. Using these inputs, Eq (6.2) can be applied to calculate the resulting colour of the first iteration.

The next iteration contains the third ink, for example, the magenta ink printed over the black and cyan inks (K + C + M). The resulting colours from the first iteration become the background colours. The tristimulus values of the foreground colours of all the patches in the test set were obtained from the 'Ink Step-Wedge Data' of magenta ink. Similarly the model coefficients for the foreground colour were obtained from the 'Coefficients Data' for magenta ink. The resulting colours of this iteration were calculated using Eq (6.2).

Finally the last iteration follows the same methodology as described for the previous iteration by adding yellow ink as the foreground colour. This gives the resulting colour of the 4-inks combination (K + C + M + Y).

The above mentioned steps describe four iterations which were also applied for the remaining ink sectors – orange, green and violet – to predict the colours of 1485 patches in each sector. The predicted colours were compared to the colour measurements to calculate the CIEDE2000 colour difference values.

6.6.2   Results

Table 6.8 shows the prediction accuracy of the SCOP model for all ink sectors of the 7-colour offset printing process. The mean CIEDE2000 values between the predicted colours and the measured colours for all sectors are between 2.80 and 3.52. A histogram of the CIEDE2000 values is shown in Figure 6.18. The maximum CIEDE2000 values range from 11.87 for the CGYK sector to 15.75 for the CMVK sector. Although the maximum values are high, they are less than the maximum CIEDE2000 values for the KM model (Table 4.6) and the Van De Capelle model (Table 4.8).

Table 6.8 Accuracy of the SCOP model for each ink-sector of the offset printing process.

CIEDE2000	CMYK	OMYK	CGYK	CMVK
Mean	2.80	3.20	3.09	3.52
95th percentile	7.67	8.52	6.96	9.04
Max	15.33	14.09	11.87	15.75
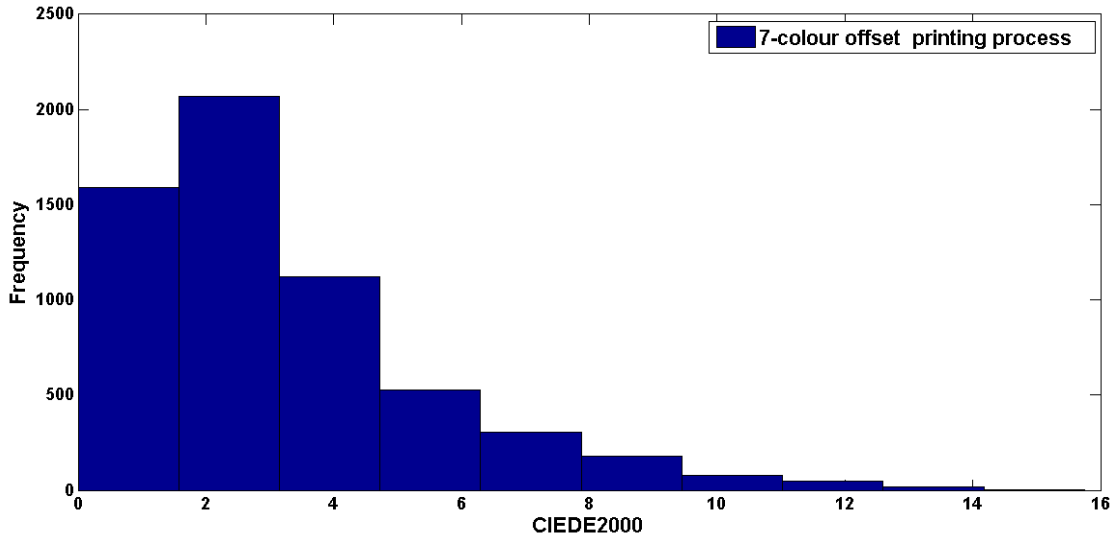
Figure 6.18 Histogram of the CIEDE2000 between the model-predicted colours and the measured colours for the 7-colour offset printing process.

The SCOP model was also implemented for the 7-colour flexographic and thermal sublimation printing processes. The results for each ink sector using these processes are given in Figure 6.19. The mean CIEDE2000 values are below 5 except for the orange sector of the flexographic printing process (mean CIEDE2000 of 5.10) and the violet sector of the thermal sublimation printing process (mean CIEDE2000 of 7.14).
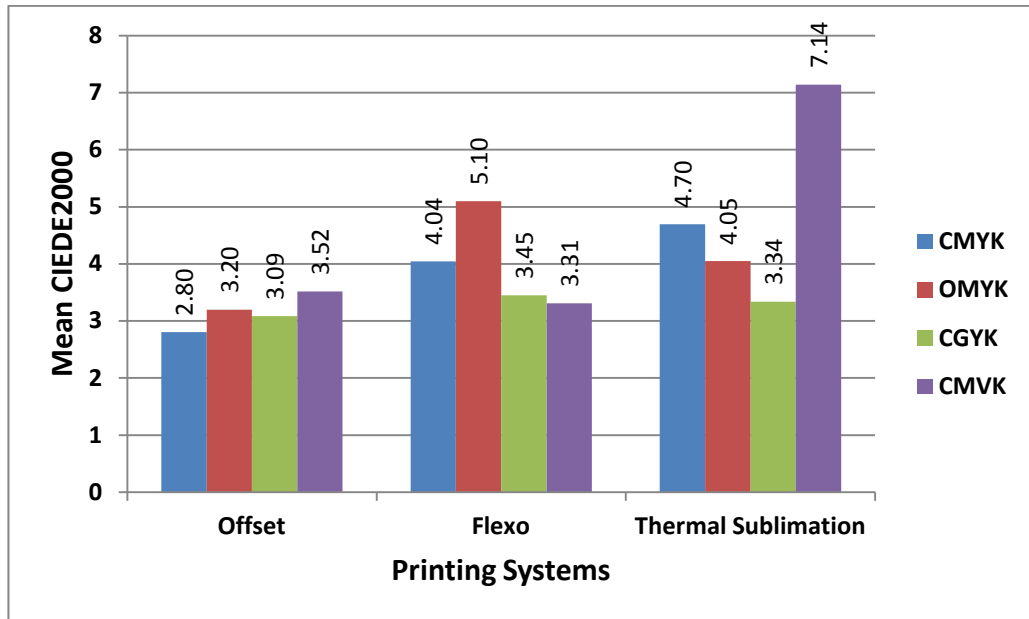
Figure 6.19 Performance of the SCOP model for each sector of the 7-colour printing processes.

The overall performance of the SCOP model is compared to the performance of other printer models in Figure 6.20 and Figure 6.21 (see Section 4.4).
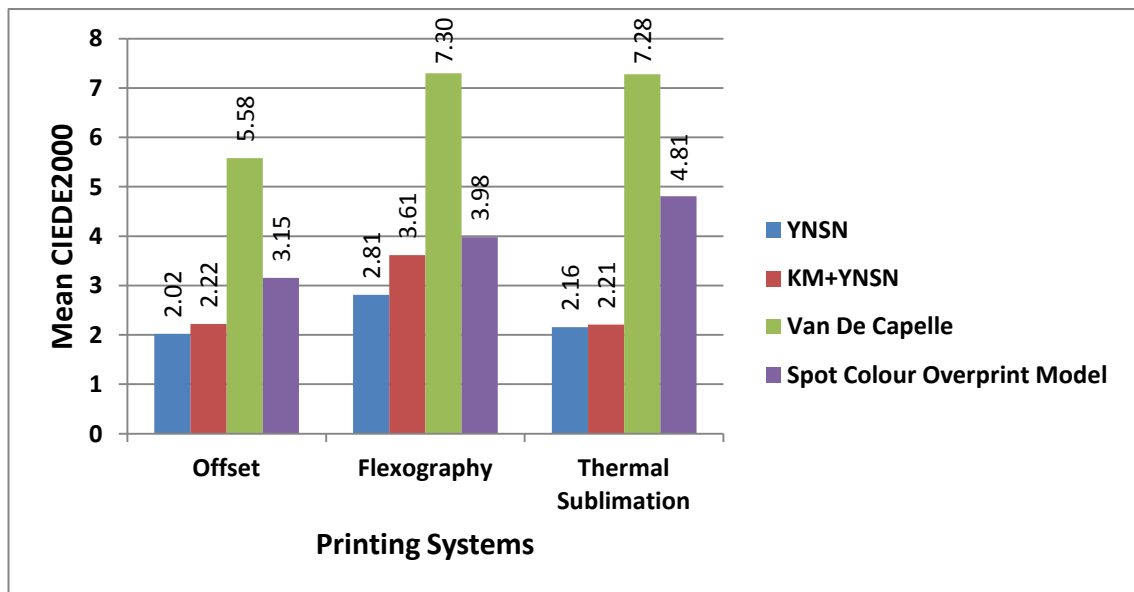
Figure 6.20 Overall performance of the SCOP model (mean CIEDE2000) for the 7-colour printing processes compared to that of other models.
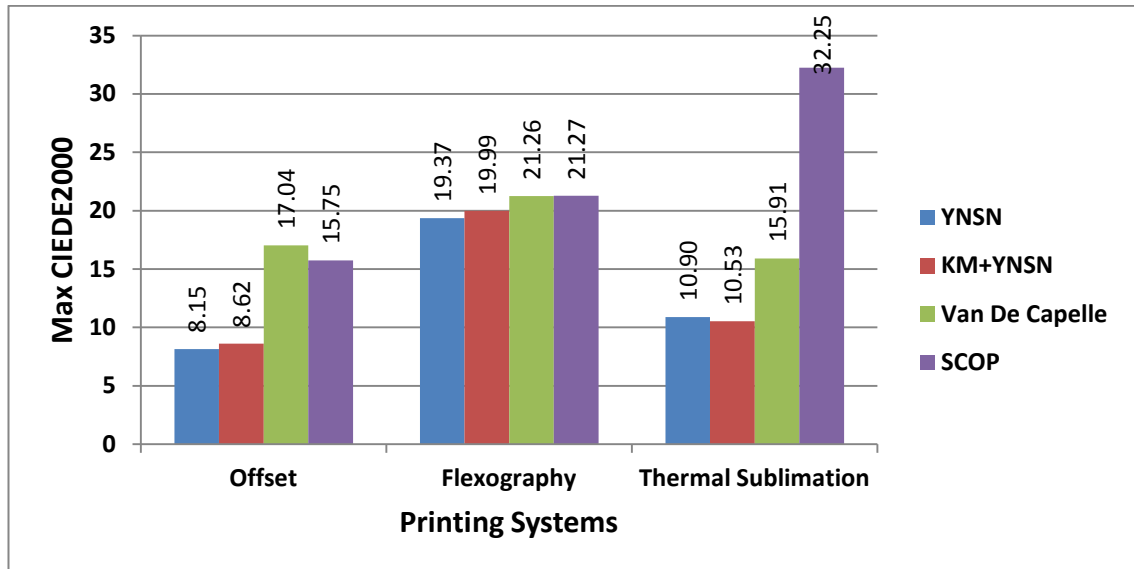
Figure 6.21 Overall performance of the SCOP model (maximum CIEDE2000) for the 7-colour printing processes compared to that of other models.

The model performed better than the Van De Capelle model but worse than the YNSN and KM+YNSN models. For example, the SCOP model gave the mean CIEDE2000 colour difference value of 3.15 for the lithographic offset, as compared to 2.02 (YNSN model), 2.22 (KM+YNSN model) and 5.58 (Van De Capelle model). Considering that the model uses only the CIEXYZ colour space unlike the other models which rely on spectral data, these results are encouraging.

6.7 Conclusion

In spite of there being several spectral printer models available for printer characterisation, there is a lack of a simple model for characterising the *n*-colour printing process. The spot colour overprint (SCOP) model is proposed as a forward printer characterisation model to provide such a tristimulus based model.

This model is relatively simple to use and computationally inexpensive. It calculates the resulting colour in CIEXYZ space rather than in the spectral domain. This makes it suitable to be incorporated in an ICC workflow and PDF/X documents. It characterises each ink separately and both solid and halftone overprints can be predicted.

The model was initially developed for predicting solid and halftone overprints of spot colours. It uses a regression method for calculating the model coefficients to predict the resulting colour of different combinations of spot colours. The model was evaluated using a 6-colour test chart containing CMYK and two spot colours. It showed very good accuracy for 2-ink overprints with mean CIEDE2000 values between the predicted and the measured overprint colours of less than 2.5.

The SCOP model was extended to an *n*-colour printing process. It was implemented and evaluated for the 4-colour and the 7-colour printing processes with different printing technologies including lithographic offset, flexographic and thermal sublimation printing. Although it showed performance that was worse than the YNSN and KM+YNSN models, the accuracy was better than that of the Van De Capelle model.

The next stage of the project includes an investigation into inverse printer characterisation methods to obtain the colour separations for the *n*-colour printing process. The YNSN model and the SCOP model will be used as forward characterisation models to implement the inversion models. Trade-off between spectral and colorimetric measurements means that viewing conditions must be fixed.

Chapter 7 Implementation of the inverse printer model – colour separation

7.1 Introduction

The results described in this chapter have been published in Deshpande (2014d and 2014e). The inverse printer model derives colorant amounts from colorimetric values like CIELAB for a given viewing condition. If the forward relationship from colorant values to colour values is defined by a physical printer model then the inversion is possible using search-based optimisation methods. Due to the inherent nonlinearity of the printing process, inversion is often difficult. Previous studies, using spectral models for printer characterisation, include those by Mahy (1996a), Stollnitz (1998a), Tzeng (2000), Taplin (2001), Cholewo (2001), Agar (2001) and Urban (2006).

The inversion process generally involves using the forward characterisation method to find the device-independent colour values for the given colorant values and then deriving the inverse function using data-fitting or interpolation methods (Balasubramanian, 2003).

For a 3-colour process, the inversion is trivial since there is a unique combination of colorants to achieve any given colour. For a 4-colour process, where a black ink is used in addition to three chromatic inks, there are many combinations of colorants that can result in the same colour. For an *n*-colour process with more than 4 inks this one-to-many mapping issue becomes much more complex. By dividing the colorant space of the *n*-colour process into sectors each of 4 inks, the inversion model can be restricted to the 4-colour process of each sector.

This chapter describes different methods of implementing the inverse printer model to obtain colour separation for *n*-colour printing processes. A constrained nonlinear optimisation method and look-up table based inversion methods are discussed. These methods were implemented for the 3-colour and the 4-colour printing process and then extended to *n*-colour printing with an example of a 7-colour printing process (Deshpande, 2014d). To achieve good accuracy of inversion model, it is important to

use a precise forward model. Since the YNSN model performed the best in terms of forward characterisation (Chapter 4), this model was used for colour separation. Also, the spot colour overprint (SCOP) model was used, due to its simplicity, as a forward characterisation model to populate the lookup tables and to obtain the colour separations.

In addition to the accuracy, it is desirable to minimise the computational cost or to increase the computational speed. Sometimes it is necessary to perform the calculation at run-time rather than store pre-computed results in lookup table. Depending on the resolution of the artwork file it could take long time to compute the inversion. In a live production environment, this is not desirable. Hence the speed performance is also analysed.

7.2   Experiment

The 7-colour printing process was used with the following printing technologies – lithographic offset, flexographic and thermal sublimation printing. The approach, division of colorant space, pre-press parameters, calibration and test charts are described in Chapter 3 (Section 3.2). These are briefly summarised below.

Figure 7.1 gives an outline for the implementation of inverse printer characterisation for the 7-colour printing process.

The colorant space of the CMYKOGV inks was divided into sectors of 4-inks each – CMYK, OMYK, CGYK and CMVK. The printing conditions and calibration methods are described in Chapter 3 (Section 3.2.2 and Section 3.2.3).
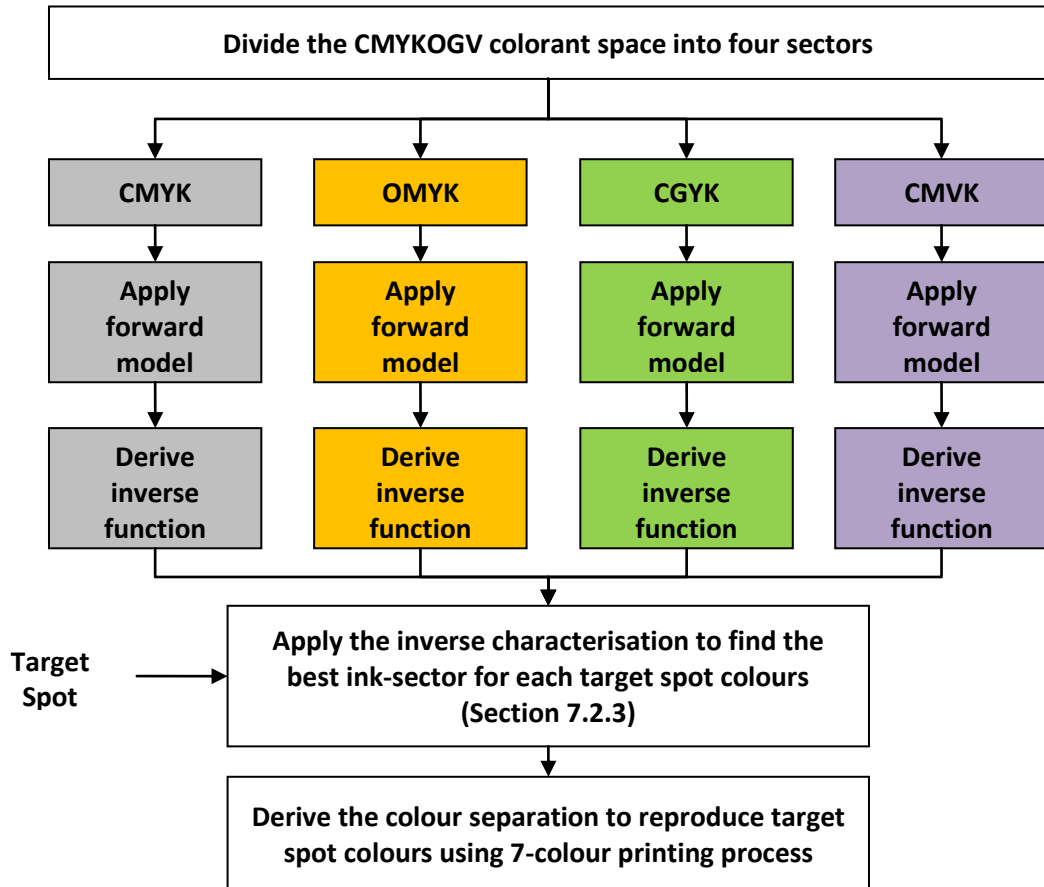
Figure 7.1 Overview of implementing the inverse printer characterisation model to 7-colour printing process.

The ECI2002 test chart was printed for each 4-ink sector. Each chart contained 1485 colour patches resulting in a total of 5940 colour patches for the 7-colour printing process. All colour patches were measured using the measuring conditions specified in Chapter 3 (Section 3.1). The colour measurement data of all sectors were collected to form a data set for each printing technology, for example, lithographic offset printing.

For the YNSN model, a subset of 60 colour patches from the ECI2002 test chart was selected. This subset includes the 16 Neugebauer primaries and it was used as a training set for optimising the Yule-Nielsen factor for each ink-sector. Thus a total of 240 colour patches were printed and measured.

The training set for the SCOP model consisted of the following colours: 33 colour patches for each primary chromatic ink – 11 patches (0%, 10%, 20%,…, 90%, 100%) printed on white (plain substrate), grey (50% black) and black (100% black) backgrounds. A total of 198 colour patches were used to provide input measurements to cover all sectors for the SCOP model.

The main difference between the inputs required for two models was that the YNSN model needed to have overprints of multiple inks whereas the SCOP model used the inputs derived from each ink separately without the need for any overprints.

The remaining colour patches from the ECI2002 test chart were used as a test set for evaluating the inverse printer models..

7.2.1   Forward characterisation

The forward printer characterisation using the YNSN model was discussed in Chapter 4 (4.2.3). The YNSN model was applied for the forward characterisation of each ink sector. In a 4-colorant printing system, there are 16 different colours formed by the solid colours and their overprints. The YNSN model introduces the Yule-Nielsen value (n) to the wide-band Neugebauer model to account for internal light scattering in the substrate. In this project, the Yule-Nielsen value (n) was treated as a correction factor to optimise the fit of the model to empirical data. The forward YNSN model was applied iteratively with increasing values of n. The optimised Yule-Nielsen value was obtained when the mean colour difference between the predicted and the measured colours of the training set was minimised. For each 4-ink sector, the Yule-Nielsen value was optimised and used when applying the forward printer model.

The SCOP model was discussed in Chapter 6 (6.6). This model was used as a forward printer characterisation model to each ink sector using Eq (6.2). The implementation of the model for a 7-colour printing process was described in section 6.6.

7.2.2   Gamut mapping

Before applying the inverse printer models, gamut mapping was performed. A colour gamut for each sector was determined as described in Chapter 5, Section 5.3). The coordinates lying outside the sector gamut were first mapped to the gamut surface using the minimum ΔE clipping method (Morovič, 2008), which is based on Euclidean distance. Each colour was evaluated to check if it was inside the gamut or not. If it was outside the gamut, the nearest coordinate on the gamut boundary was found. The desired colour was then replaced by the nearest point on the gamut boundary.

Figure 7.2 shows the gamut mapping where the source colours are mapped onto the destination gamut boundary colours in a plane of constant hue angle. This minimises the colour difference between the target colour and the reproduced colour. All colours lying inside the gamut were not affected by the gamut mapping. For reproducing tonal data, overprints and images, this may not be the best strategy. However, the main focus was on reproducing solid spot colours and hence the minimum ΔE clipping method should provide reasonable results.
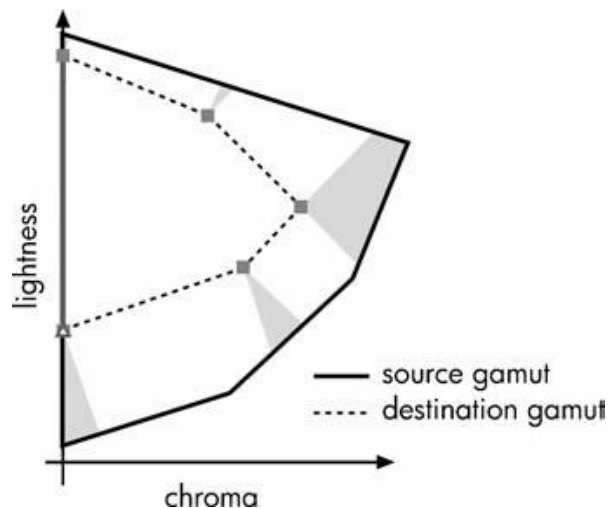
Figure 7.2 Gamut mapping with the minimum ΔE clipping method in a plane of constant hue angle (Morovič, 2008).Grey regions indicate the colours from source gamut mapped on single boundary colours from destination gamut.

Another candidate for the gamut mapping is HPminDE (CIE, 8-03) – hue preserving minimum ΔE method. In this method, the hue angle is preserved and minimum distance to the destination boundary is determined. This method applied in a perceptual space (for example, CIECAM02) would be appropriate for the spot colour reproduction. This will be considered as a future work (Section 9.4).

7.2.3   Inverse characterisation

Inverse characterisation methods for a 4-colour printing process are explained in Section 7.3 and 7.4. The aim was to achieve the colorimetric reproduction of the target spot colour using a 7-colour printing process. Any given colour can be reproduced using a maximum of 4 inks belonging to the corresponding ink-sector. Finding the best sector for the target colour is described in Figure 7.3.

First, the forward characterisation was applied to each sector using methods described in Chapter 4 (Section 4.2). All sector-gamuts and the colorimetric coordinates of the target colour are located in 3-dimensional CIELAB colour space. The target colour is then checked against the colour gamut of each sector to find if the colour is inside the gamut or not. This can be achieved as follows.

Build a Delaunay triangulation from the CIELAB values of all colour patches which form the sector-gamut. For each target colour, try to find the enclosing simplex of the Delaunay triangulation. If the enclosing simplex exists then the target colour is inside the sector-gamut. If the enclosing simplex doesn't exist then the target colour is outside the sector-gamut.

If the target colour is inside a single sector-gamut, then this becomes the best sector for reproducing the target colours. If the target spot colour is inside multiple sector-gamuts, for example the CMYK and the OMYK sector-gamuts, then the inverse model is applied to each of those sectors. The CIEDE2000 error metric between the model-estimated colour and the target colour is calculated and the sector which gives the least CIEDE2000 between the target colour and the model predicted colour is selected as the best sector. For the continuous tone image, this may seem like a random criterion. But

the objective here is to reproduce a target spot colour. If there are 2 sectors which can reproduce the target spot colour, then the sector which gives the least CIEDE2000 would be better choice.

```
┌──────────────────────────────────────────────────────────────────┐
│ Derive the sector-gamuts using forward characterisation (Section 5.3) │
└──────────────────────────────────────────────────────────────────┘
                              │
              ┌────────────────────────────────────────────┐
              │ Locate the target spot colour in CIELAB colour space │
              └────────────────────────────────────────────┘
                              │
              ┌────────────────────────────────────────────┐
              │ Compare the target spot colour against each sub-gamut │
              └────────────────────────────────────────────┘
                              │

Yes – inside                                        Yes – inside only
multiple sector-          ◇ Is the target colour inside        one sector-gamut
            │               any of the sector-gamuts? ◇                │
            │                          │ No                            │
┌──────────────────┐    ┌──────────────────────┐                      │
│ Apply inverse model │  │ Calculate distance between │                     │
│ for those sectors  │  │ the target colour and the │       ┌──────────────┐
└──────────────────┘    │ closest boundary point on │       │ Apply inverse │
            │            │ each sector-gamut        │       │ model for that │
┌──────────────────┐    └──────────────────────┘       │ sector        │
│ Calculate CIEDE2000 │              │                   └──────────────┘
│ between the target  │  ┌──────────────────────┐               │
│ colour and the estimated │ Find the sector which has │          │
│ colour              │    │ the closest boundary point │         │
└──────────────────┘    │ to the target colour     │            │
            │            └──────────────────────┘               │
┌──────────────────┐              │                             │
│ Find the sector which │    ⬡ Best sector ⬡ ◄─────────────────┘
│ gives the least CIEDE2000 │─►
└──────────────────┘              │
                    ⬭ Derive the colour separation for target colour using the best sector ⬭
```

Figure 7.3 Derive the best sector for reproducing the given target colour.

If the target colour is not inside any of the sector-gamuts, then the distance between the target colour and the closest point on the surface (boundary) of each sector-gamut is calculated. The best sector is then the one which has the closest boundary point to the target colour, that is, the least distance between the target colour and the boundary point. Once the best sector is obtained, the colour separation for that target colour can be calculated by applying the inverse characterisation model to the best sector.

The overall accuracy of the inversion model for the 7-colour offset printing process was calculated by combining all colours in all ink-sectors. Each ink-sector had 1485 colour samples resulting into a total of 5940 target colours for the overall 7-colour process. The next two sections (7.3 and 7.4) describe a constrained optimisation and a lookup table based inverse characterisation methods.

7.3   Constrained optimisation

For a typical 4-colour printing process, direct analytical inversion of the forward YNSN model is not possible. One solution is to use constrained nonlinear optimisation by minimising the objective function, such as the colour difference between the desired colour and the predicted colour. Cholewo (2000) used constraint optimisation with the conjugate gradient approach. Taplin (2001) assessed different techniques of nonlinear optimisation for a 6-colour inkjet printer characterisation. Urban (2006) proposed linear regression, an iteration method for inversion of the YNSN model.

A general description of the problem can be considered as follows.

$$\min_{x} F(x)$$

(7.1)

where

$$F(x) = \|R_\lambda(x) - r_\lambda\|_2^2$$

(7.2)

with the constraints

$$x_i \in [0,1] \; for \; i = 1, \dots, n.$$

(7.3)

where *x* is an ink combination for *n* inks, $R_\lambda(x)$ is the estimated spectral reflectance for the ink combination *x* derived from the YNSN model and r_λ is the desired or the target spectral reflectance. Theoretical background of the constrained optimisation is discussed in Chapter 2 (Section 2.3.1).

In this study, various optimisation algorithms were used to invert the YNSN model and the accuracy of each algorithm was evaluated. Nonlinear constrained optimisation was performed for each sector using different optimisation algorithms by minimising the spectral root mean squared (RMS) error between the predicted spectra and the measured spectra. The constraints for the effective area coverage were set as 0 to 1 corresponding to 0% to 100% ink coverage and the maximum number of iterations allowed was 1000. The termination tolerance on the objective function value was set to 10^{-6} to stop the iterative process. The Matlab optimisation toolbox was used to perform the constrained optimisation and the following two algorithms were tested: the active-set algorithm and the sequential quadratic programming (SQP) algorithm. An overview of each of these algorithms is given in Chapter 2 (Sections 2.3.1.2 and 2.3.1.3).

The active set method was selected for its efficiency since it takes large steps, increasing the speed of computations. This method is usually very effective for small-scale to medium-scale optimisation problems (Nocedal, 2006). The sequential quadratic programming (SQP) method was selected for its robustness. Its strength lies in solving problems with significant nonlinearities. The SQP based method had been tested and

compared with other methods and it performed better than others in terms of accuracy and proportion of successful solutions (Schittkowski, 1985)

7.3.1   Results

Two optimisation algorithms were evaluated using the 7-colour offset printing process and, for each of the 4-ink sectors, the ECI2002 test-chart (ISO 12642-2:2006) was used to test these algorithms. The spectral RMS error and CIEDE2000 colour difference between the model predictions and the measured colours of 1485 colour patches were calculated. Mean values, 95th percentile and maximum values of the spectral RMS error and CIEDE2000 values were used to evaluate the model accuracy. In addition, the speed performance of each optimisation algorithm was measured in terms of milliseconds (ms) per colour using computer with a 2.50 GHz processor and with 4 GB installed memory. This represents the time required to calculate the colour separations for the given test set.

Table 7.1 shows the performance of each algorithm for all ink sectors in terms of the spectral RMS error and the CIEDE2000 values. The SQP algorithm performed significantly better than the active-set algorithm. The 95th percentile and the maximum values for the active-set algorithm are notably higher than those for the SQP algorithm. This could be due to the fact that the SQP algorithm attempts to minimise the merit function by taking smaller steps within the defined constraints.

Table 7.1 Inversion of the YNSN model for each sector of the offset printing process using constrained optimization with the 1485 colour patches per sector.

Optimisation Algorithm	Ink Sector	CIEDE2000			Spectral RMS		
		Mean	95th percentile	Max	Mean	95th percentile	Max
SQP	CMYK	0.77	1.93	5.25	0.008	0.017	0.026
	Violet	1.01	2.46	4.14	0.008	0.018	0.028
	Green	1.26	3.25	4.33	0.013	0.028	0.044
	Orange	0.75	1.38	4.88	0.008	0.015	0.025
Active-Set	CMYK	6.11	21.18	33.43	0.020	0.053	0.125
	Violet	5.05	13.65	22.62	0.019	0.046	0.073
	Green	4.71	19.72	26.33	0.026	0.075	0.133
	Orange	3.82	13.30	28.05	0.016	0.039	0.123

The overall performance for the *n*-colour offset printing process (CMYKOGV) was evaluated by combining the results from all ink sectors. For each ink sector, there were 1485 colour patches of the ECI2002 test chart. By combining all ink sectors, there were a total of 5940 colour patches representing the complete 7-colour printing process. The overall performance of the optimisation algorithms for the 7-colour printing process is shown in Table 7.2.

Table 7.2 Accuracy of the optimisation algorithms for 7-colour offset printing process.

Optimisation Algorithm	CIEDE2000			Spectral RMS			Average Speed (ms per colour)
	Mean	95th percentile	Max	Mean	95th percentile	Max	
SQP	0.95	2.59	5.25	0.009	0.022	0.044	104.1
Active-Set	4.92	17.70	33.43	0.020	0.050	0.133	54.4

The active-set algorithm had the faster speed performance compared to the SQP algorithm, but its accuracy was considerably worse than that of the SQP algorithm.

Based on the accuracy and speed performance, the SQP algorithm was chosen for further evaluation with flexography and thermal sublimation printing processes using the ECI2002 test chart. This might seem a rather arbitrary choice but it was felt that the higher computation overhead was worth the improved colour accuracy obtained using this algorithm.

Measurement data sets for 7-colour flexography and thermal sublimation processes were produced. For each printing process, the inversion of the YNSN model was applied using the constrained nonlinear optimisation with the SQP algorithm. The results comparing the offset, flexography and thermal sublimation printing processes are given below.

Table 7.3 shows the overall results of the inversion of the YNSN model for all printing processes with the spectral RMS error and CIEDE2000 values between the measured colours and the model predictions.

Table 7.3 Overall results of the inversion of the YNSN model using the 7-colour printing processes.

Printing Technology	CIEDE2000			Spectral RMS			Average Speed (ms per colour)
	Mean	95th percentile	Max	Mean	95th percentile	Max	
Offset	0.95	2.59	5.25	0.009	0.022	0.044	104.1
Flexography	0.38	1.07	11.27	0.003	0.006	0.014	108.1
Thermal Sublimation	0.76	1.98	5.72	0.008	0.017	0.037	101.4

Figure 7.4 illustrates the performance of the inversion model for each of the four ink sectors for all printing processes. Figure 7.5 gives the histograms of the spectral RMS errors (left) and CIEDE2000 values (right) between the measured colours and the model predicted colours.
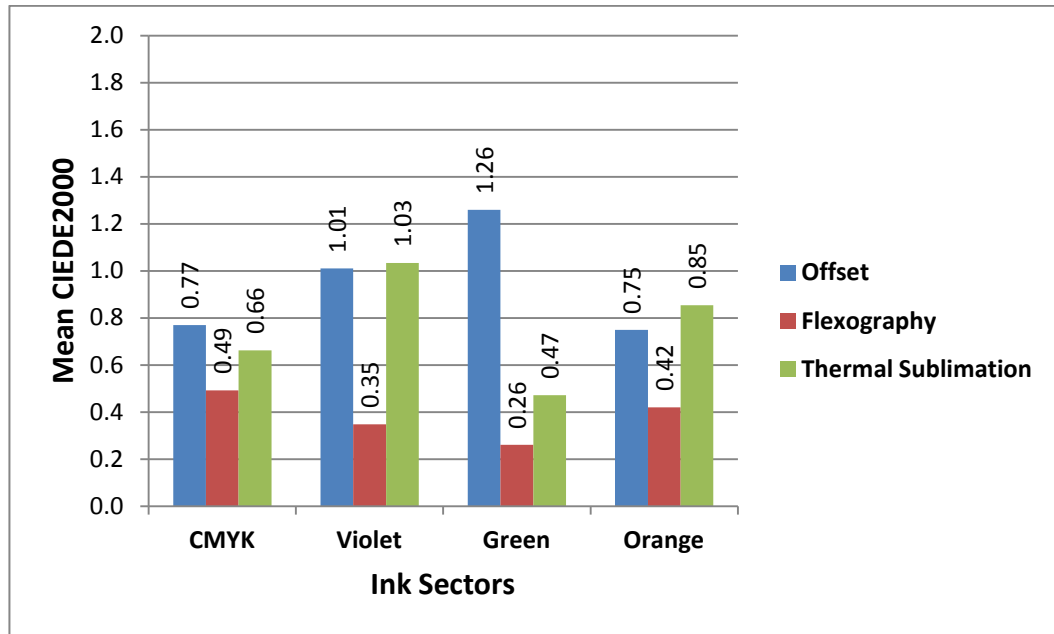
Figure 7.4 Results for each ink sector using different printing processes - mean CIEDE2000 values between the measured colours and the model predictions.
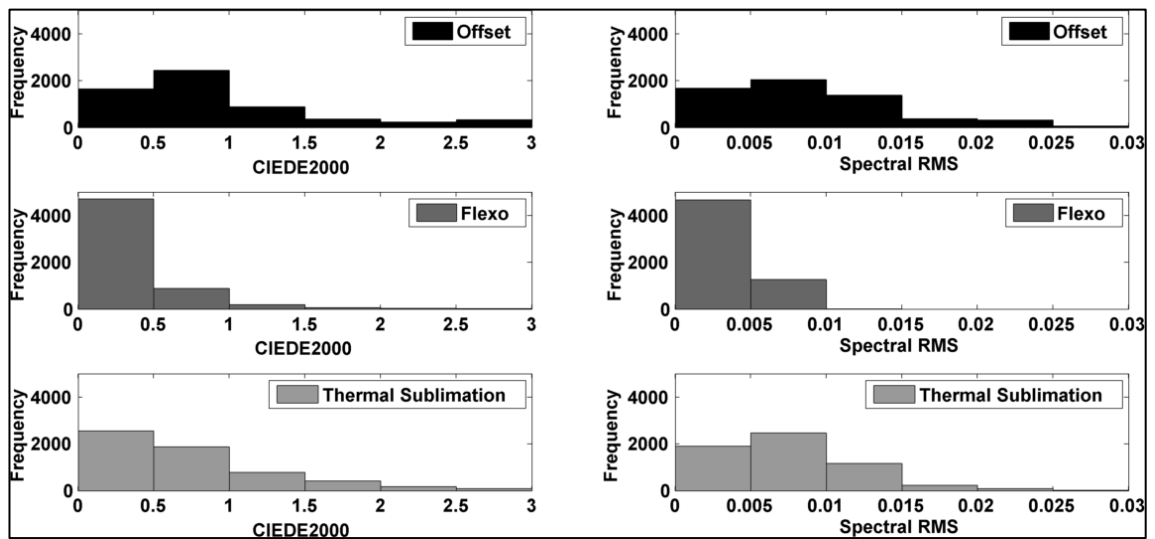
Figure 7.5 Histograms of the spectral RMS errors and CIEDE2000 values between the measured colours and the model predicted colours for 7-colour printing processes.

The overall accuracy of the inversion model for the three 7-colour printing processes was found to be very good with typical mean spectral RMS errors below 0.009 and the mean CIEDE2000 values below 1.0. Model predictions for the flexographic printing process were the best of all the three printing processes followed by thermal sublimation and offset printing. This may be due to fewer variables involved in flexographic printing process making it more stable than other processes. The maximum colour difference for the flexographic process however, was the highest (11.27) of the three processes considered, which could be an outlier. However the typical time required for inversion was 0.1 seconds per colour (pixel).

7.4   Lookup Table (LUT) based inversion

Colour separation can be implemented using a 3-dimensional lookup table (LUT) to map the device-independent colour values to device-dependent colorant values. This method is widely used in many applications including the ICC workflow (Kang, 2006).

Figure 7.6 illustrates the implementation of the inverse printer characterisation for the 4-colour printing process. CMY are populated as nodes of the lookup table. The inverse function for the 3-colour printing process is first calculated using the forward characterisation method to obtain colour separation for three chromatic colours. Then the black generation (see Section 7.4.2.1) is accomplished to provide the 4-colour separation CMYK. The black generation provides a unique transform from CMY to CMYK for the given printing system.

The inversion model based on the lookup table was applied using different interpolation methods. Initially the inversion model was tested on 3-colour offset CMY printing process using a subset of the CMYK sector dataset for offset printing process.
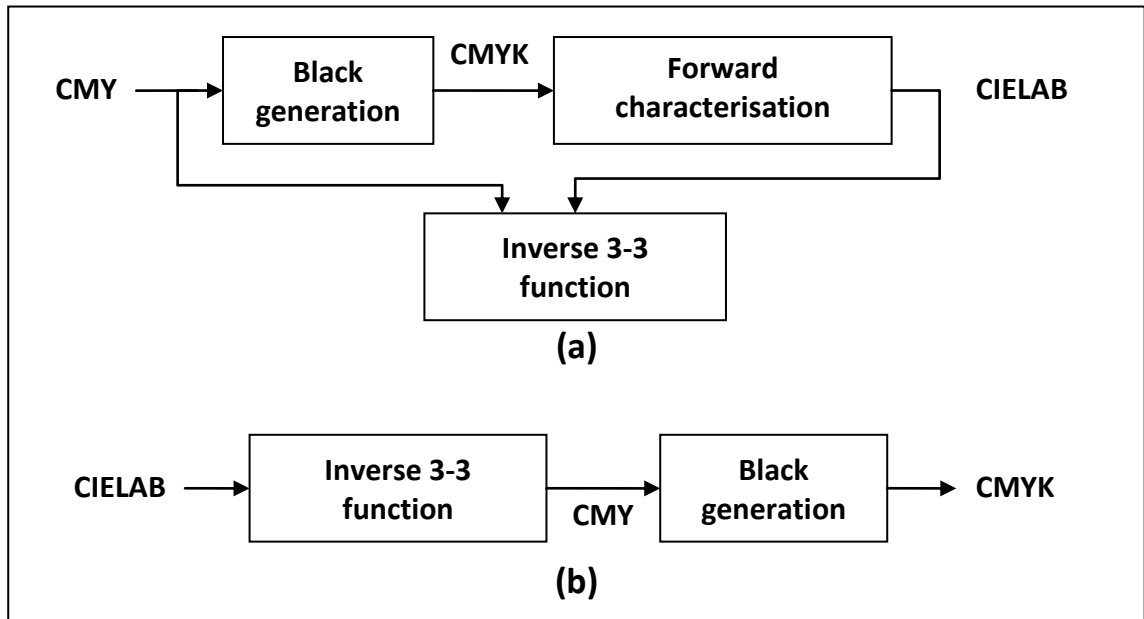
Figure 7.6 Inverse characterisation for the 4-colour printing process: (a) derivation of inverse 3-3 function and (b) combining inverse 3-3 function with black generation to obtain inverse function for 4-colour printing (Balasubramanian, 2003).

The coordinates lying outside the sector gamut were first mapped to the gamut surface using a gamut-mapping by using the minimum ΔE clipping algorithm (Section 7.2.2). If a colour was outside of the gamut, it was replaced by the nearest point on the gamut boundary to minimise the colour difference between the target colour and the reproduced colour.

7.4.1 Inversion for a 3-colour printing system

The forward YNSN model was used to generate a lookup table of training samples of CMY values and corresponding CIELAB values. The training set consisted of 729 coordinates of a 9-level uniform lookup table. An independent set of 794 samples was used as the test set. This test chart consisting of the test samples was printed and the colours of test samples were measured using a spectrophotometer to give a target data set consisting of CIELAB values. These CIELAB values were mapped by use of the lookup table to estimate the required CMY values. The following interpolation methods

were used to derive the inverse model: linear interpolation, nearest-neighbour interpolation and natural-neighbour interpolation (Sibson, 1981).

The estimated device values (CMY) were mapped through the forward printer model to obtain the CIELAB values. The colour difference values between the final CIELAB values and the corresponding values of the original 794 samples of the target were calculated, along with their mean, 95th percentile and maximum values.

To evaluate the accuracy of the inverse mode, it was also important to assess the difference, ΔD, between the estimated device values and the original device values in the device space (CMY). ΔD is defined as the Euclidean distance between the estimated CMY values and the original CMY values: these values were calculated for the 794 test samples.

Based on these results (see Section 7.4.3), linear interpolation was considered for the next stage of the inversion procedure for a 4-colour printing process.

7.4.2   Inversion for a 4-colour printing system

In addition to the chromatic C, M and Y colorants, usually a black colorant (K) is used in most printing processes. For the inverse model this becomes a one-to-many mapping issue since the same colour can be achieved by several different combinations of CMYK colorants i.e. metamers. Thus additional constraints were added to achieve the CMYK values for the given CIELAB colours. These are described in the next section (Section 7.4.2.1).

The forward YNSN model was used to generate a lookup table of training samples of CMYK values and corresponding CIELAB values. For the CMYK inversion, the training set consisted of a 9-level uniform lookup table resulting in 6561 coordinates. A set of 1485 samples was used as the test set. This test chart was printed using the offset printing process and the colours of the test samples were measured using a spectrophotometer. This provided the target data set consisting of CIELAB values.

These CIELAB values were mapped to estimate the CMY values by using the lookup table. This inversion is similar to the method described in the previous section (CMY inversion). A linear interpolation method was used to derive the inverse model with 5-level, 9-level and 17-level lookup table sizes.

7.4.2.1   Black generation

Next, the black generation and the grey component replacement (GCR) were applied to obtain a unique transform from CMY to CMYK. For a 3-colour printing process, there is a unique inverse mapping from CIELAB to CMY since the forward characterisation mapping is unique. Adding the black ink (K) enhances the perception of sharpness, increases the gamut in the dark regions of colour space and helps reducing the total amount and cost of ink required to produce the given colour. However, it introduces redundancy into the forward characterisation (Balasubramanian, 2003). A given colour can be achieved by varying the amount of black over a range of values. There are many different CMYK combinations that will result in the same colorimetric coordinates. Additional constraints become necessary to achieve a unique combination of CMYK for the given colour.

There have been several methods proposed for calculating of the amount of black, for example, Johnson (1996), Mahy (1999), Balasubramanian (2001). Green (2002) and Balasubramanian (2003) have described various methods of black generation. Generally the amount of black is determined by first calculating the CMY combinations and then finding the unique transform from CMY to CMYK (see Figure 7.6). This unique transform can be derived by under colour removal (UCR) and grey component replacement (GCR). The choice of black generation depends on various factors such as total area coverage, gamut volume and colour stability in neutral colours.

Under colour removal reduces the achromatic component of CMY in the neutral shadows and compensates the reduced amount by increasing the amount of K. Usually the reduction in CMY is proportional to the amount of K. This reduces the total area coverage and ink-film thickness.

Grey component replacement extends the scope of the under colour removal to chromatic areas in addition to the neutral areas. It replaces the neutral components of CMY with certain amount of K in both neutral and chromatic areas. The neutral component of CMY is given by the minimum of C, M, Y i.e. the least predominant of three chromatic inks. This neutral component is used to calculate the amount of K.

In this project, grey component replacement was implemented for calculating the amount of K using the following method. The neutral component was calculated as follows.

$$K = \begin{cases} \min{(C, M, Y)}, & \min{(C, M, Y)} \geq 20 \\ 0, & \min{(C, M, Y)} < 20 \end{cases}$$

(7.4)

Where K is the amount of black. If the minimum ink amount is below 20% threshold then $K = 0$ i.e. no black added. This is to avoid unwanted artefacts in pastel colours.

The reduced amounts of C, M and Y were computed using following equations:

$$C' = C - \alpha K$$
$$M' = M - \alpha K$$
$$Y' = Y - \alpha K$$

(7.5)

Where C', M' and Y' are the reduced amounts of C, M and Y respectively and α defines the level of the grey component replacement. The value of α ranges from 0 to 1.

To find the optimum value of α, the grey component replacement algorithm was performed in iterations with the increasing values of α for a set of colours. The estimated CMYK values were fed into the forward printer model to obtain the CIELAB values. The colour difference values (CIEDE2000) between the final CIELAB values and the original target CIELAB values were calculated. The α value of 0.6 gave the least average colour difference, hence this value was used for the grey component replacement.

Following additional constraint was used: total area coverage should be less than 320. This was based on the visual assessment of the printed chart for the total area coverage.

$$C + M + Y + K \leq 320$$

<div align="right">(7.6)</div>

Note that the objective was to reproduce the spot colours and not the continuous tone images. Hence some factors are trivial, for example, smoothness of gradations from grey to chromatic colours. It has been recognised that the methods for deriving the grey component function require a trade-off among competing requirements (Mestha, 2008).

The estimated device values (CMYK) obtained by the grey component replacement were mapped through the forward printer model to obtain the CIELAB values. The colour difference values between the final CIELAB values and the original target CIELAB values of 1485 samples were then calculated.

For the remaining ink-sectors, there exists an equivalency between the dominant ink and the two subordinate chromatic inks, for example, O – MY, G – CY and V – CM. The main criterion used for inversion was to maximise the dominant ink. For example, in case of OMYK ink-sector, inversion was based on maximisation of O, mainly at the expense of M and Y. It also minimises the number of inks used for reproducing the given colour. This method is similar to the paired component replacement proposed by Boll (1994) (See Section 2.4.3). Neutral colours were mainly reproduced by using black ink alone. Note that the objective was to reproduce spot colours rather than tonal gradations across the boundaries of the colour gamuts of ink-sectors, which was explored by Mahy (2011).

Finally, the 4-colour inversion model was applied to four ink-sectors to characterise the 7-colour printing process. As before, gamut mapping was applied before applying the inversion procedure. Each individual ink-sector was characterised using the inversions methods described in the above section using 5-level, 7-level and 17-level lookup table sizes.

The device values estimated by the inversion model were processed through the calibration function before printing. Inversion process for the 7-colour printing process and finding the best ink-sector for reproducing the target colour is described in Section 7.2.3.

7.4.3 Results – inversion using the YNSN model

3-colour printing process

Table 7.4, Figure 7.7 and Figure 7.8 show the results of the inversion models based on the lookup table for different levels using three interpolation methods. Linear and natural-neighbour interpolation methods performed equally well with the mean CIEDE2000 values below 2 and the mean ΔD values below 6 device units. The nearest-neighbour interpolation method showed poor performance.

Table 7.4 Accuracy of the LUT based inverse model for 3-colour CMY printing process.

LUT-levels	Interpolation method	CIEDE2000			Speed (mS per colour)
		Mean	95th percentile	Max	
5-level	Linear	1.66	6.12	9.31	0.11
	Nearest	4.91	8.44	11.00	0.14
	Natural	1.65	6.12	9.31	0.33
9-level	Linear	1.14	4.04	7.97	0.18
	Nearest	3.57	6.77	10.73	0.23
	Natural	1.14	4.02	7.97	0.47
17-level	Linear	0.79	2.84	5.76	0.64
	Nearest	2.65	4.20	6.26	0.49
	Natural	0.78	2.86	5.76	2.49
33-level	Linear	0.67	2.34	5.76	3.65
	Nearest	2.65	4.20	6.26	2.44
	Natural	0.67	2.32	5.76	17.68

As expected the lookup table based inversion is significantly faster than the constrained nonlinear optimisation method (see Table 7.1). Among three interpolation methods, the linear interpolation method was the fastest followed by the nearest-neighbour interpolation and the natural-neighbour interpolation methods. As the number of nodes of the lookup table was increased from 5-level through to 33-level, the computational speed decreases. It can be seen from Table 7.4 that the natural-neighbour interpolation gives almost exactly similar results to linear interpolation, but with considerable increase in computation overhead.
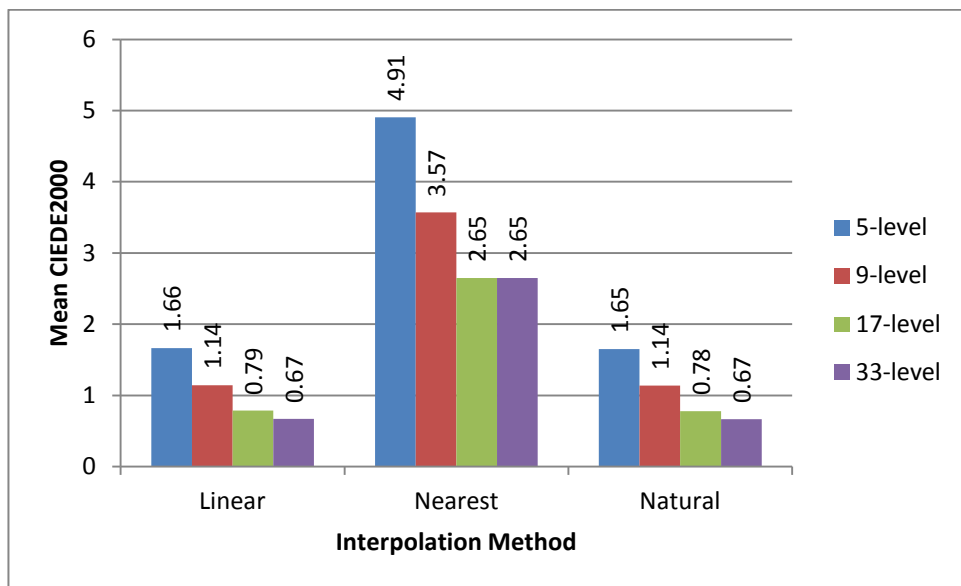
Figure 7.7 Mean CIEDE2000 values for lookup table based inverse model.

Although the accuracy of the inverse model increases with increasing levels or nodes of the lookup table, beyond the 17-level size there is no significant improvement.
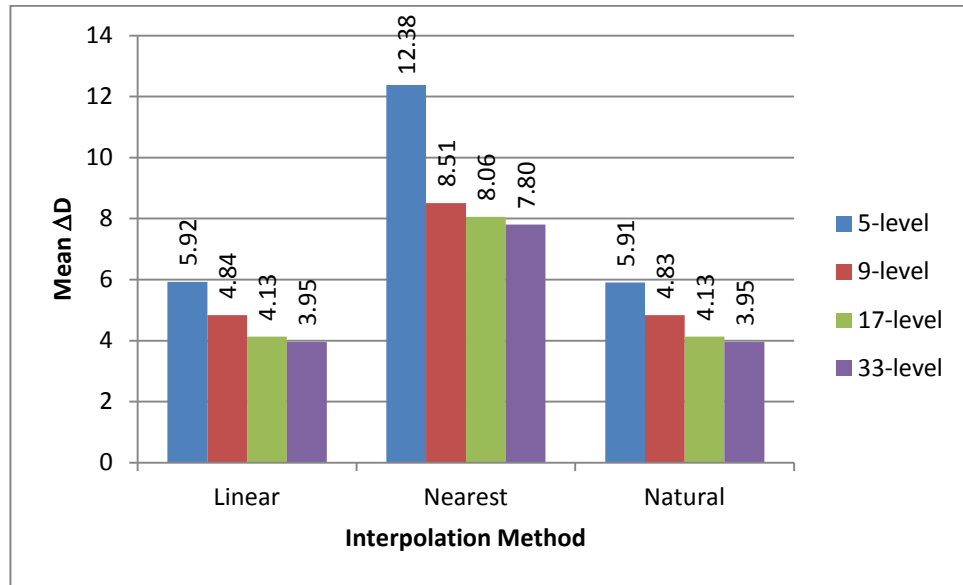
Figure 7.8 Mean ΔD values between the estimated CMY and the original CMY.

4-colour printing process

Table 7.5 shows the accuracy of the inversion model for the CMYK offset printing process. The oversell accuracy was found to be good. Figure 7.9 compares the speed performance against the mean CIEDE2000 values for all LUT sizes. Note that the increase in LUT size improves the accuracy but this is at the cost of speed performance, as might be expected. The processing time for the algorithm increases considerably with the increase in the LUT size beyond 9-levels.

Table 7.5 Accuracy of the inverse model for CMYK offset printing process.

LUT-levels	CIEDE2000			Speed (mS per colour)
	Mean	95th percentile	Max	
5-level	1.26	4.68	9.20	8.38
9-level	0.83	3.13	6.07	8.85
17-level	0.70	2.46	7.12	57.85
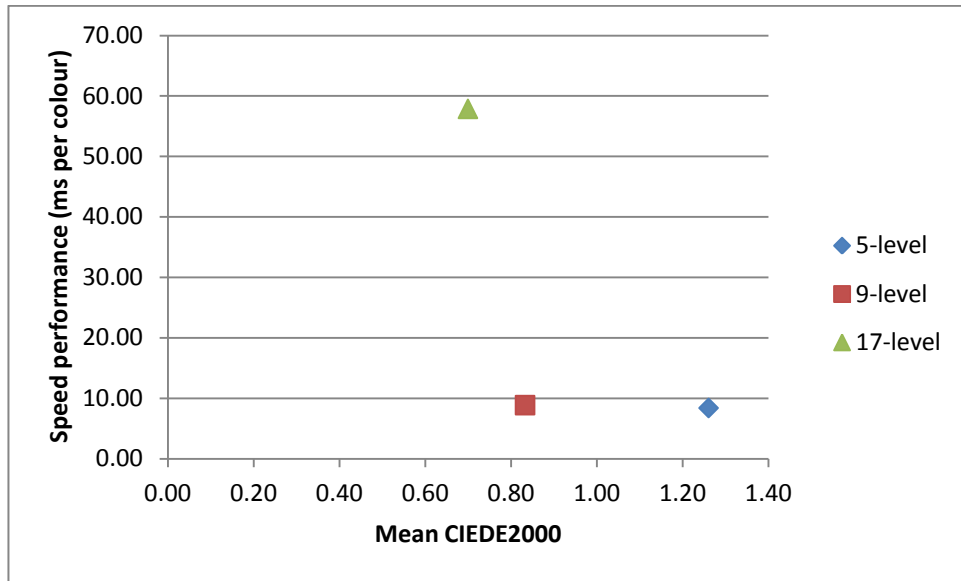
Figure 7.9 Speed performance and accuracy of the inverse model for the CMYK offset printing process.

Figure 7.10 illustrates the distribution of the CIEDE2000 values for the test samples across the lightness, chroma and hue angle axes. There is no peculiar trend suggesting that the inversion model is not biased towards any particular colour direction.
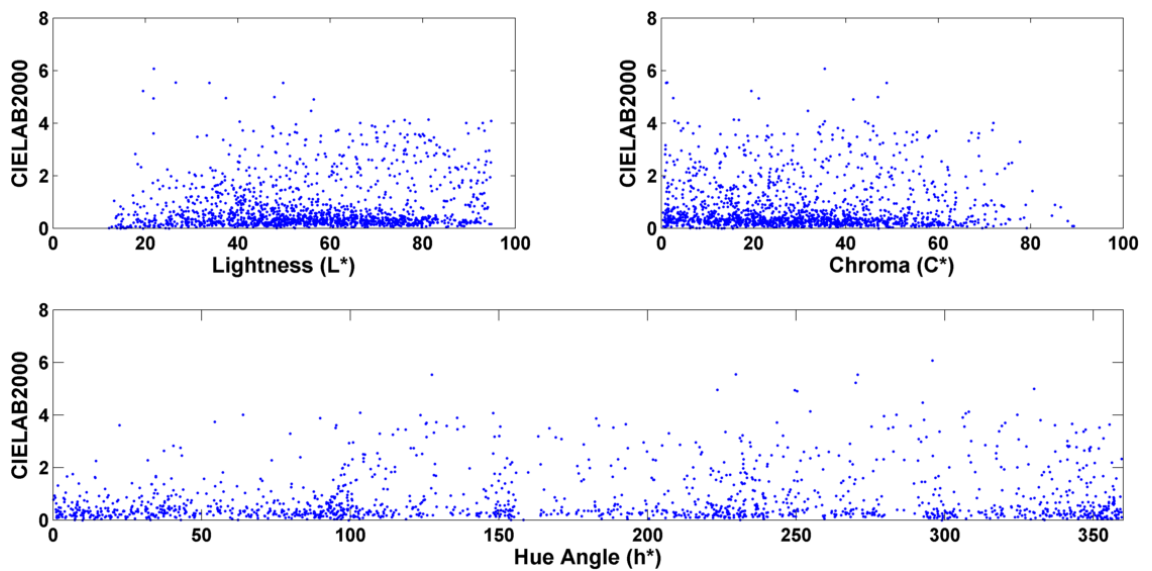
Figure 7.10 Distribution of the CIEDE2000 values of the test samples across lightness, chroma and hue axes for the CMYK offset printing process using the YNSN model.

Figure 7.11 shows the target colours and the model estimated colours for the CMYK ink-sector in *L*-C** plane for the 9-level LUT inversion method. Most of the estimated colours lie close to the target colours.
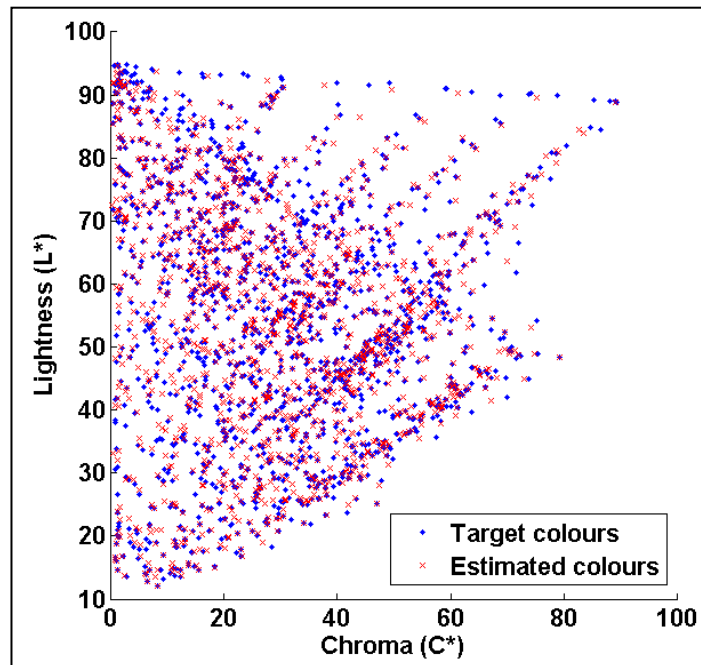
Figure 7.11 Distribution of the target colours and the estimated colours in Lightness – Chroma plane using 9-level LUT inversion model based on the YNSN model for CMYK sector.

Figure 7.12 shows the accuracy of the inverse model for all ink-sectors of the 7-colour offset printing process using different LUT sizes.
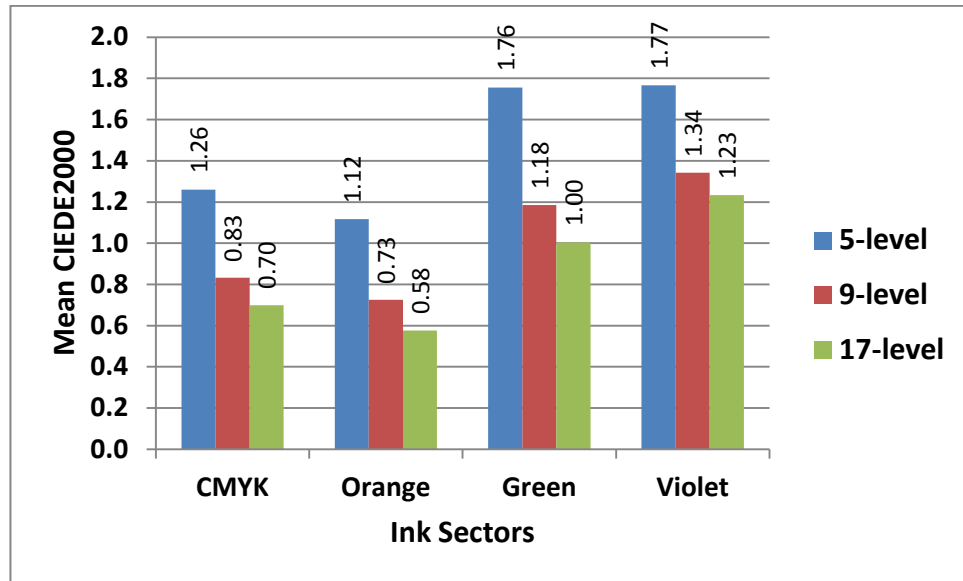
Figure 7.12 Mean CIEDE2000 values for the inverse model for all ink-sectors of the offset printing process for different LUT sizes using the YNSN model.

As expected the prediction accuracy increases with the number of nodes of the lookup table with the 17-level lookup table giving the best performance. The Green and Violet ink-sectors showed higher colour differences (1.18 CIEDE2000 and 1.34 CIEDE2000 respectively for the 9-level LUT) than the CMYK and orange ink-sectors (0.83 CIEDE2000 and 0.73 CIEDE2000 respectively for the 9-level LUT). However the mean CIEDE2000 values between the measured colours and the predicted colours were below 2.0 for all LUT sizes across all ink-sectors.

7-*colour printing process*

The mean, 95th percentile and the maximum values between the measured and the predicted colours are given in Table 7.6. This table also shows the speed performance of calculating the colour separation for the given target expressed in terms of milliseconds per colour. Comparing the accuracy and the speed performance of three LUT sizes, it is clear that the 9-level LUT size gives reasonably accurate prediction without a high computational overhead. It was found that the 17-level LUT size showed significantly slower performance than other two LUT sizes.

Table 7.6 Overall accuracy of the inverse model using the YNSN model for the 7-colour offset printing process.

LUT-levels	Mean CIEDE2000			Speed (mS per colour)
	Mean	95th percentile	Max	
5-level	1.47	5.01	10.64	8.62
9-level	1.02	3.56	9.90	9.01
17-level	0.88	3.21	9.90	57.61

Table 7.7 shows the overall accuracy and the speed performance of the 9-level LUT inverse model for all printing processes. Overall accuracy for all printing processes was found to be very good with typical mean CIEDE2000 values below 1.5 at the average speed of approximately 9 ms per colour.

Table 7.7 Overall accuracy and speed of the 9-level LUT inverse model using the YNSN model for the 7-colour printing processes.

Printing Process	CIEDE2000 between the measured colours and the model predictions			Average Speed (ms per colour)
	Mean	95th percentile	Max	
Offset	1.02	3.56	9.90	9.01
Flexography	0.70	2.41	11.00	8.88
Thermal Sublimation	0.85	3.09	10.57	9.03

7.4.4 Results – inversion using the SCOP model

4-colour printing process

Table 7.8 shows the accuracy of the inverse model for all ink sectors of the offset printing process using the SCOP model for forward characterisation. The mean CIEDE2000 values between the target colours and the estimated colours are typically below 2. The violet ink-sector showed worse performance than other ink-sectors with a mean value for CIEDE2000 colour difference of 3.08 for a 5-level LUT. It was found that the violet ink was less stable than other inks during press-runs. This may have contributed towards the worse performance of the violet ink-sector. As expected the model accuracy improved with the number of LUT-levels. However, there is no significant improvement from a 9-level to a 17-level LUT.

Table 7.8 Performance of the inverse model of the offset printing process using the SCOP model for different LUT sizes for all ink-sectors.

LUT-levels	Sector	CIEDE2000			Speed (mS per colour)
		Mean	95th percentile	Max	
5-level	CMYK	1.81	6.59	15.91	2.58
	Orange	1.40	5.12	14.16	2.55
	Green	1.04	4.09	10.62	2.64
	Violet	3.08	10.97	17.12	2.64
9-level	CMYK	1.30	4.93	9.62	5.74
	Orange	1.07	3.86	6.72	5.62
	Green	0.73	2.53	8.11	5.53
	Violet	1.80	6.86	12.36	5.65
17-level	CMYK	1.30	4.71	9.87	26.78
	Orange	1.00	3.50	6.89	26.75
	Green	0.71	2.20	8.00	26.87
	Violet	1.34	5.35	9.94	26.88

Figure 7.13 shows the target colours and the model estimated colours for the green ink-sector in the L*-C* plane. As shown to the right of the graph, some highly chromatic colours with lightness values between 40 and 50 are not estimated well. This could be improved by trying a different regression method than Eq. (6.2) for these highly chromatic colours.
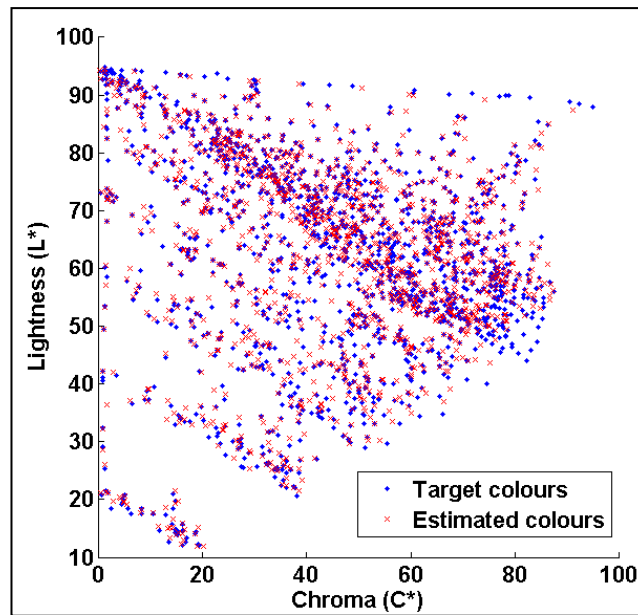

Figure 7.13 Distribution of the target colours and the estimated colours in an L*–C* plane using a 9-level LUT inversion model based on the SCOP model for the CGYK sector.

7-*colour printing process*

The overall combined accuracy and speed of the 9-level LUT inversion based on the SCOP model is shown in Table 7.9 for three printing technologies. Since the forward characterisation was based on the SCOP model using the CIEXYZ values, the speed performance is better than the 9-level LUT inversion based on the YNSN model (Table 7.7) which uses data in the spectral domain. The mean CIEDE2000 values between the target colours and the estimated colours for all printing technologies are reasonably good given that the inversion is based on a simple forward characterisation model.

Table 7.9 Overall accuracy and speed of the 9-level LUT inverse model for the 7-colour printing processes using the SCOP model.

Printing Technology	CIEDE2000			Average Speed (ms per colour)
	Mean	95th percentile	Max	
Offset	1.22	4.65	12.36	5.6
Flexography	1.66	5.80	12.13	5.4
Thermal Sublimation	2.21	8.88	28.77	5.9

7.5   Summary of results

The results of the inverse models are summarised in this section. The SQP optimisation and the 9-level LUT inversion methods based on the YNSN and the SCOP models are compared in Table 7.10 for the offset printing technology.

Table 7.10 Overall accuracy results of the inverse printer models for the 7-colour Offset printing process.

Inverse Printer Model	CIEDE2000 between the measured colours and the model predictions			Speed (ms per colour)
	Mean	95th percentile	Max	
SQP optimisation	0.95	2.59	5.25	104.1
YNSN 9-level LUT	1.02	3.56	9.90	9.0
SCOP 9-level LUT	1.22	4.65	12.36	5.6

Constrained optimisation using the SQP algorithm showed the best accuracy at the cost of computational overhead. All models performed well with the mean CIEDE2000 values between the target colours and the model predictions below 1.3. The 9-level LUT inversion based on the SCOP model performed worse than the other two methods,

particularly in terms of the 95th percentile and the maximum CIEDE2000 values; however, it was the fastest of the three methods with an average speed of 5.6 ms per colour.

Figure 7.14 shows the graphical representation of the overall accuracy of the inverse methods for three printing technologies. The SQP optimisation and the YNSN 9-level LUT methods showed very good performance across all printing technologies, flexographic printing showing the best results. All methods showed less than 2.5 mean CIEDE2000.
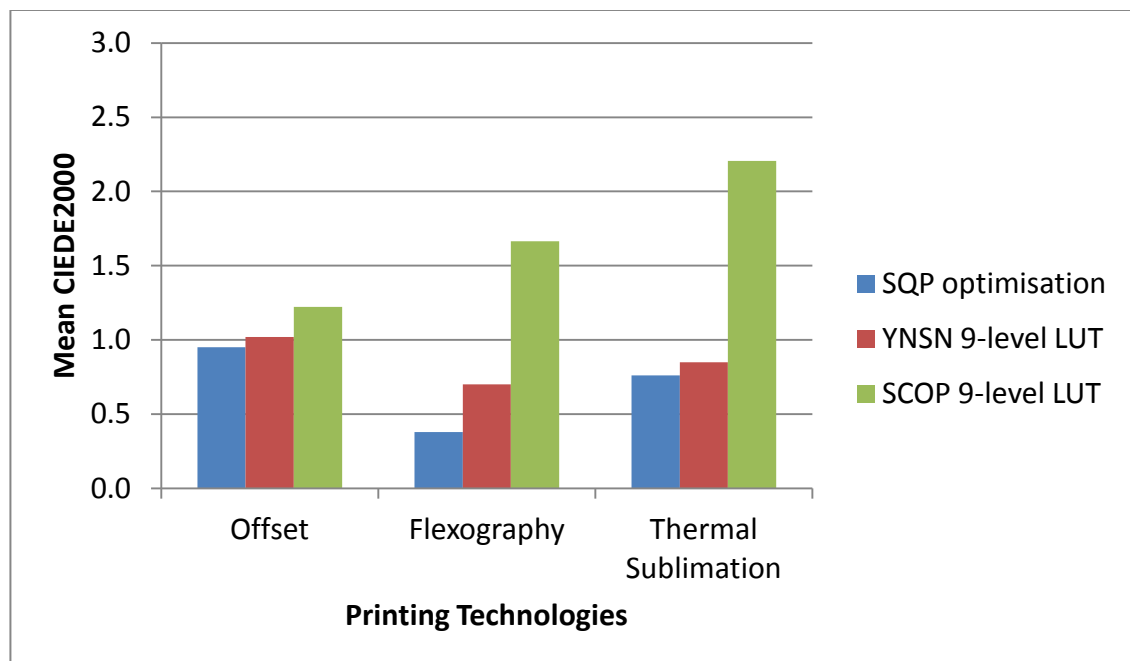
Figure 7.14 Overall accuracy of the inverse model for the 7-colour printing processes using different printing technologies.

7.6   Conclusion

Different inverse characterisation models were evaluated to derive the colour separation of 7-colour printing processes. Two approaches were compared: constrained optimisation and lookup table (LUT) based inversion. The challenge was to find a balance between the accuracy of the model and the computational cost. The LUT based methods were found to be significantly faster than the optimisation methods.

Three printing technologies were used: lithographic offset, flexographic and thermal sublimation printing process, consisting of 7 process inks. For the LUT based methods, two models were used separately as the forward characterisation models: the YNSN model which uses the spectral reflectance data and the SCOP model which uses the CIEXYZ tristimulus values. Each model can be successfully used as a forward printer model to populate the lookup table and to perform the inversion for all three printing technologies.

Although the constrained optimisation method based on the SQP algorithm was the most accurate, it was much slower than the LUT based methods. The YNSN 9-level LUT based method showed the best overall performance with the CIEDE2000 values between the target colours and the model predicted colours below 1.0 for all printing technologies. Although the accuracy of the SCOP 9-level LUT method was worse than other two methods, the main advantages of using this combination are the reduced computational cost due to the simplicity of the model and ink-based characterisation that does not require the printing of any combinations of multiple inks.

In the next chapter the real-world spot colours are reproduced using the 7-colour offset printing process. The colour separation for each of the target spot colours was calculated using the 9-level LUT based inverse methods based on the YNSN model and the SCOP model. The colours printed with 7 inks were measured and then compared against the colour measurements of the original spot colours to evaluate the accuracy.

Chapter 8 Evaluation of the *n*-colour separation using spot colours

Various methods of obtaining the colour separation for the *n*-colour printing process were discussed in the last chapter. This chapter evaluates the *n*-colour separation by reproducing the spot colours with the 7-colour printing process. The lookup table based method with 9-levels was selected for the colour separation. To generate the lookup table, two different forward characterisation models were used: the YNSN model and the SCOP model.

The success of the colour separation can be measured by reproducing the brand colours using the desired inverse characterisation method. Here, the *n*-colour separation is evaluated by converting a set of real-life spot colours to the 7-colour separation. The printed colours were compared to the original spot colours by calculating the CIEDE2000 between them. A psychophysical experiment was conducted to evaluate the quality of the reproduction of spot colours. The quantitative and qualitative evaluation is described in detail below.

8.1 Method

A set of 35 spot colours were selected as a test-set. They were the target colours to be reproduced with a 7-colour separation and they were real-life spot colours from a print production representing brand colours of various brand owners. The following criteria were used to select the spot colours: brand colours of key customers and the distribution of colours across the CIELAB colour space. As can be seen from Figure 8.1, the target spot colours are well distributed across the a^* - b^* plane and the lightness (L^*) – chroma (C^*) plane of CIELAB colour space to cover different hues and colour regions including pastel colours, saturated colours, neutral colours and dark colours. These spot colours were available from a master colour library. The spectral reflectance and the CIELAB colorimetric values of all the colours were measured using X-Rite i1 Pro 2 using the defined reference measuring conditions (Chapter 3, Section 3.1).
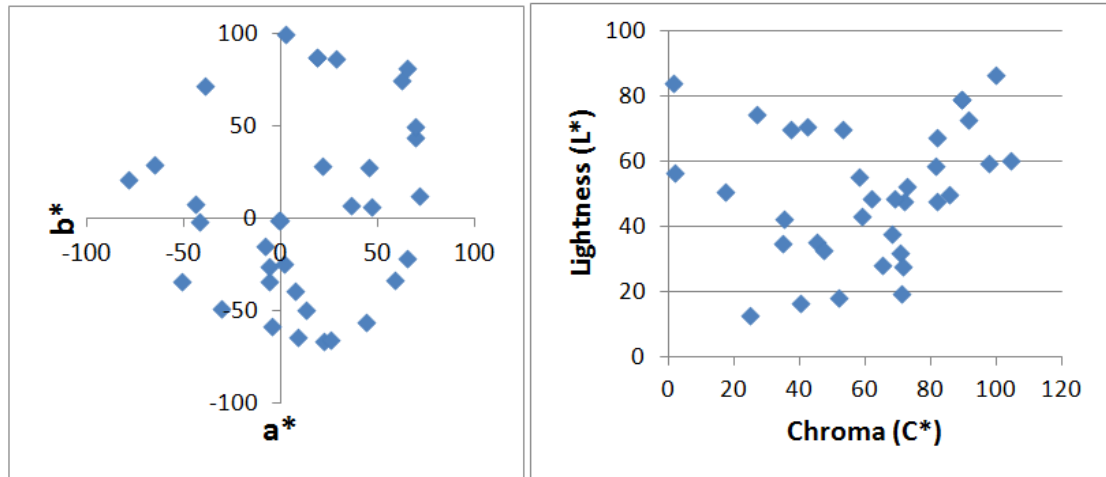
Figure 8.1 Distribution of the spot colours in the a* - b* plane and the L* - C* plane.

Lithographic printing with 7 inks, Cyan, Magenta, Yellow, Black, Orange, Green and Violet, was used, on a gloss coated substrate. The reproduction workflow including the colorant space division, screening method and calibration was the same as described in Chapter 3 (Section 3.2).

8.1.1   Training set

For each sector of 4 inks, the training set is required to optimise the model parameters, namely, the Yule-Nielsen factor (n) for the YNSN model and the scaling factors and the exponents for the SCOP model.

For the YNSN model, a subset of 60 colour patches from the ECI2002 test chart was selected which included the 16 Neugebauer primaries. This was used as a training set for optimising the Yule-Nielsen factor for each ink-sector. Thus a total of 240 colour patches were printed and measured.

The training set for the SCOP model consisted of the following colours: 33 colour patches for each primary chromatic ink – 11 patches (0%, 10%, 20%,…, 90%, 100%) printed on white (plain substrate), grey (50% black) and black (100% black) backgrounds. A total of 198 colour patches were used to provide input measurements to cover all sectors for the SCOP model.

All colour patches in each training set were measured using an X-Rite i1 Pro 2 spectrophotometer with the reference measuring conditions (Chapter 3, Section 3.1).

8.1.2   Colour separation

Characterisation of the 7-colour printing process was carried out as follows. The colorant space was divided into four sectors – CMYK, OMYK, CGYK and CMVK. Note that any target colour can be reproduced using a maximum of 4 inks belonging to the corresponding ink-sector.

Two inversion methods were used: the 9-level LUT inversion based on the YNSN model and the 9-level LUT inversion based on the SCOP model. These methods are explained in the previous chapter (Section 7.4). The YNSN model and the SCOP models were used as forward characterisation models to populate the lookup tables.

The forward characterisation model was applied to each ink sector to build a 9-level lookup table with 6561 coordinates in device space and corresponding CIELAB colour space.

For each 4-inks sector, the Yule-Nielsen value (n) is optimised by minimising the mean colour difference between the predicted and the measured colours of the training set (Chapter 4, Section 4.2.2). Similarly the coefficients of the SCOP model were optimised by data fitting (Chapter 6, Section 6.6)

The forward characterisation model was used to derive the gamut of each ink-sector as described in Chapter 5 (Section 5.3). This resulted in four sector-gamuts. The flow diagram for reproducing the target spot colour with the 7-colour printing process is given in Figure 8.2.
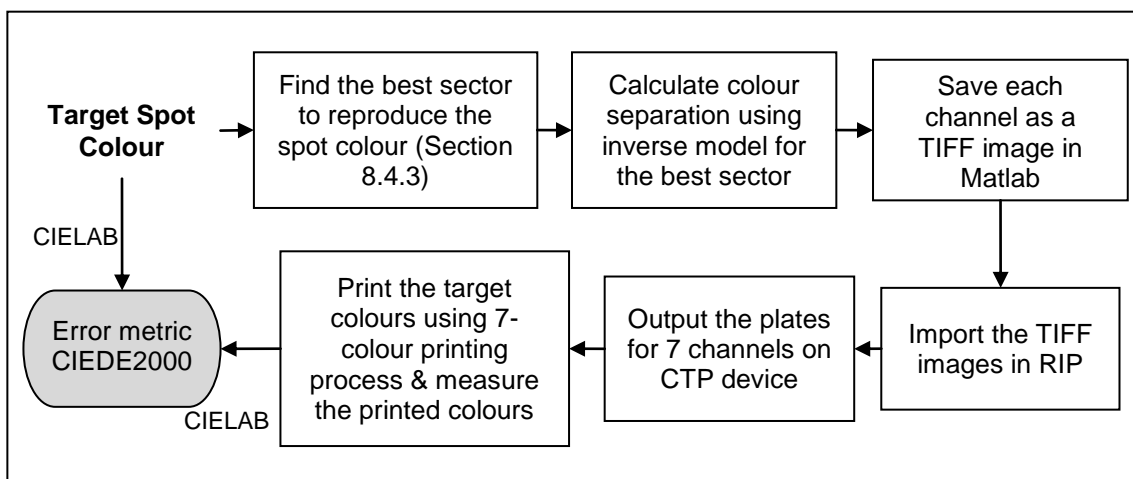
Figure 8.2 Flow diagram of reproducing the spot colour with 7-colour printing process.

A test form consisting of 35 spot colours was designed as a TIFF file with CIELAB colour mode and this file was read into Matlab using the 'imread' function. Each spot colour patch had multiple pixels with identical CIELAB values.

For each pixel (spot colour), the best sector of 4-inks was derived. In Matlab, the colour separation for each pixel was calculated by applying the inverse characterisation model for the best sector. This is described in Chapter 7 (Section 7.2.3). This resulted in 7 channels corresponding to each ink of the 7-colour printing process.

Each channel was saved as a separate TIFF file with 8-bits per pixel using the 'imwrite' function in Matlab. The TIFF file was input to the raster image processor (RIP) to produce the 1-bit data for each ink channel. All the colour management settings were turned off to avoid unwanted colour transformations.

Finally the plates were made using a computer-to-plate (CTP) device which had been pre-calibrated. The plates were used for printing the test form on a lithographic offset printing press. Process control parameters for the CTP device and the printing conditions during the press-run were recorded (Chapter 3, Section 3.4).

All the printed colour patches reproduced with the 7-colour printing process were measured using X-Rite i1 Pro 2 with the reference measuring conditions (Chapter 3, Section 3.1). The CIEDE2000 values between the printed colours and the original spot colours were calculated.

8.2   Results

The mean, 95th percentile and maximum values of the CIEDE2000 between the target spot colours and the printed colours are shown in Table 8.1. Both the inverse models showed good results. As expected, the YNSN LUT model (mean CIEDE2000 of 1.60) performed better than the SCOP LUT model (mean CIEDE2000 of 2.06) at the expense of reduced performance speed.

Note that these colour difference values are the results of accumulative error across the reproduction workflow. For example, the model prediction, error due to the process variables including the printing conditions, measurement uncertainty etc. Although process control was in place, there are inherent variability contributing to the final colour difference between the printed colours and the original target colours.

Table 8.1 Accuracy of the spot colours reproduced with the 7-colour separation on lithographic offset printing press.

Method	CIEDE2000 between the target colours and the printed colours after 7-colour separation			Speed (ms per colour)
	Mean	95th percentile	Maximum	
YNSN 9-level LUT	1.60	3.20	3.61	12.6
SCOP 9-level LUT	2.06	3.68	4.09	6.9

Figure 8.3 shows the target colours and the simulated spot colours across the lightness-chroma plane. Many of the target colours were closely matched although there were a few colours which could not be matched closely. No particular bias or trend towards specific colour region, chroma or hue was observed.
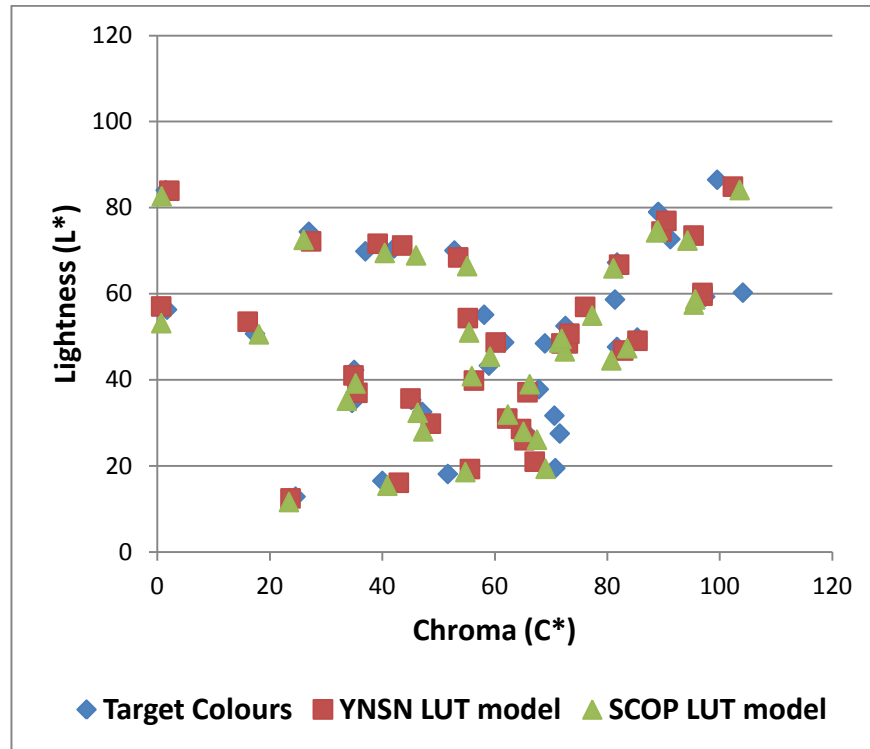
Figure 8.3 Target spot colours and the printed colours with 7-colour separation in L* - C* plane.

The frequency of occurrence of the various CIEDE2000 values is shown in Figure 8.4. Most of the colours were achieved within 3 CIEDE2000 units with the YNSN LUT model and within 4 CIEDE2000 units with the SCOP LUT model.
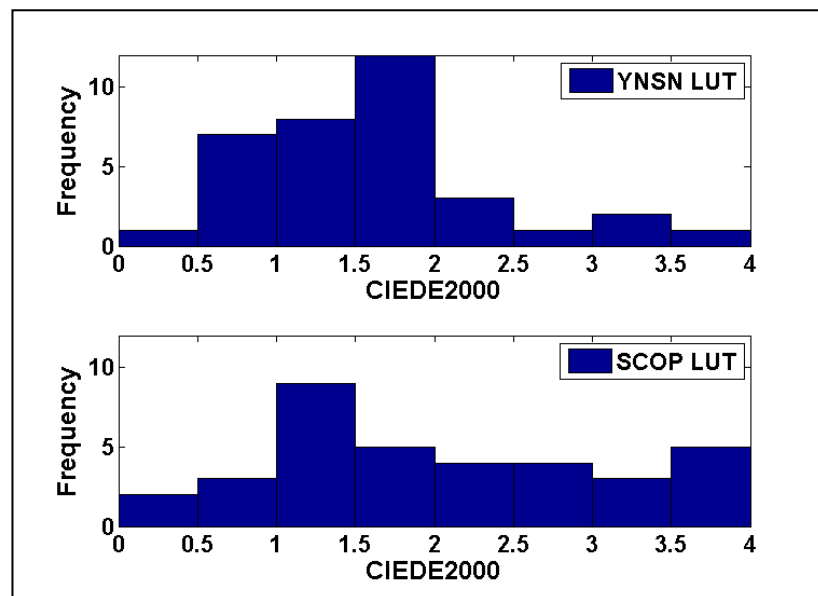
Figure 8.4 Histogram of the CIEDE2000 values between the target spot colours and the simulated spot colours on the 7-colour offset printing processes.

8.3   Psychophysical experiment

A psychophysical experiment was conducted to evaluate the quality of the reproduction of the spot colours reproduced using *n*-colour separation. The target spot colours originally approved by the customers were compared to the colours reproduced using two methods of *n*-colour separations – LUT based inversion using the YNSN model and LUT based inversion using the SCOP model. ISO 3664:2009 viewing condition P1 was used.

The original spot colours printed with special inks are called as the target colours and the spot colours reproduced with 7-colour printing process were called as the test colours. Verivide viewing booth simulating D50 illuminant was used. The light quality was measured using X-Rite i1 Pro 2 spectrophotometer. The correlated colour temperature was 5004K with illuminance of 2284 Lux and the colour rendering index of 95%.

The psychophysical experiment was based on the perceptibility and acceptability thresholds for the given set of colours using the category judgement method. The observers were presented the stimuli and asked to assign one of the six categories described below in the experimental procedure. This method yields multiple thresholds providing more trends about the samples.

8.3.1   Stimuli

The same set of 35 spot colours was used in the psychophysical experiment. For each spot colour, there were two stimuli – a target colour printed with a special ink and a test colour printed with 7-colour printing process. Size of the stimuli was 1.5 cm x 1.5 cm. This size is representative of the typical brand colour elements used in this sector of the pharmaceutical packaging market.

Printed samples of the target colours and the test colours were collected. Both target and test stimuli were prepared by cutting each sample to 1.5 cm x 1.5 cm size using a template. At the back of each sample the identification number of the colour was labelled.

8.3.2   Observers

A total of 25 observers participated in the psychophysical experiment. All observers were skilled persons with good experience of colour assessment in the printing industry, for example, print operators and pre-press personnel. The observers were familiar with the spot colour assessment due to their involvement in the print-job approval process on a daily basis. All observers had normal colour vision. They went through the Farnsworth-Munsell 100 hue test for colour vision. There were 70 judgements per observer – 35 each for the YNSN LUT based separation samples and the SCOP LUT based separation samples. A total of 1750 judgements were recorded.

8.3.3   Experimental procedure

For each colour, two stimuli were presented separated by 2 cm from each other in the middle of the booth. One stimulus was the target spot colour and another was the test colour reproduced with 7-colour printing process. Each observer was given a 5 minute time to adapt to the surround conditions before starting the experiment. To get acquainted with the task each observer was given training before starting the experiment. The following instruction sheet was given to each observer.

The purpose of this project is to evaluate the quality of different spot colours printed using n-colour separations. You will be asked to participate in a visual experiment to assess a number of pairs of spot colours. This will take about 15 to 20 minutes to complete. The observations you provide will help understanding the accuracy of spot colours reproduced with n-colour separations.

Please sit comfortably and look at the colour samples. You will be shown a series of pairs of colour samples. For each pair of samples, please tell me how close the colour of one sample is to that of another sample by assigning one of the following categories. When making a judgement for each pair of samples, please try to respond as quickly as possible.

0 = No perceptible difference (you cannot see the difference between colours)

1 = Barely perceptible difference (you can see just small degree of colour difference)

2 = Perceptible difference but acceptable (you can see the difference, but you would accept it)

3 = Barely acceptable difference (you can see the difference and it is just acceptable)

4 = Barely unacceptable difference (you can see the difference and it is just about unacceptable)

5 = Unacceptable difference (you can see the difference and you would not accept it)

The terms for the categories were chosen to have minimal ambiguity to the observers. All observers were experts in colour assessment with several years of experience in the industry. Although the categories were perceived differently by different users, this was better than inexperienced observers. The terms and explanation of different categories were easily understood by observers.

The first two categories show the degree of perceptibility, the next two categories show the degree of acceptability and the last two categories show the degree of unacceptability. This represents balanced representation of categories with respect to perceptibility, acceptability and unacceptability. A boundary between category 1 (Barely perceptible difference) and category 2 (Perceptible difference but acceptable) depicts the perceptibility threshold, whereas the boundary between category 3 (Barely acceptable difference) and category 4 (Barely unacceptable difference) depicts the acceptability threshold.

The observers did not have any information about the method of colour separation for any test sample, for example, the YNSN LUT method or SCOP LUT method. For the

given pair of stimuli, the observers were not told which one is the target colour and which is the test colour. Also the pairs of stimuli were presented in a random sequence for each observer to avoid any bias in the judgements. There was no time restriction imposed on observers. The time duration for a typical observer session of 35 colours was found to be 16 minutes.

8.3.4   Data analysis

Data analysis was based on Torgerson's Law of Category Judgement, condition D (Engeldrum, 2000) as follows:

$$t_g - S_j = z_{jg}\sqrt{\sigma_j^2 + \sigma_g^2 - 2\rho_{jg}\sigma_j\sigma_g}$$

(8.1)

where

t_g = the mean location of the gth category boundary,

S_j = the scale value of the jth sample,

z_{jg} = the unit normal deviate corresponding to the proportion of times stimulus j is sorted below category boundary g,

σ_g = the standard deviation of the gth category boundary,

σ_g = the standard deviation of the jth sample,

ρ_{jg} = the correlation between the momentary position of the category boundary g and stimulus j.

Data analysis was carried out according to the procedure described by Engeldrum (2000) for analysing data of category judgement. The judgements given by each observer were captured in an Excel spreadsheet. A frequency matrix of all judgements was prepared. For each pair of stimuli, this matrix provides the frequency with which each category was selected by observers. Thus the frequency matrix has the same number of rows as the number of pairs of stimuli and the same number of columns as the number of categories. A cumulative frequency matrix was calculated from the frequency matrix. The corresponding z-scores were calculated by finding the normal deviate (normal inverse) of the values in the cumulative proportion matrix. Finally the

mean z-scores, category boundaries and 95% confidence interval were computed. Matlab Colour Engineering Toolbox (Green, 2003b) was used for data analysis.

To find the correlation between the colour difference values and the psychometric scores, the CIEDE2000 values between the target and test stimuli were plotted against the mean scores. For each pair of stimuli, the mean score is calculated by averaging the scores assigned by all 25 observers. This method was used by Oicherman (2003) for psychometric data analysis with four categories.

In addition, the correlation between the visually perceived and the instrumentally measured colour differences were analysed by using a logistic regression. This was achieved by fitting a sigmoid (S-shaped) curve to all values of cumulative proportions for each category. For each pair of stimuli, the cumulative proportion values were plotted against the measured CIEDE2000 values between the target and test stimuli. A sigmoid curve was fitted to the scatter points using iterative approximations.

Observer repeatability: for each observer, three stimuli were repeated randomly. The difference between the two judgements of the same stimulus was calculated. Absolute difference between the two estimations is used as the statistical measure to evaluate the repeatability of the observers. For each observer, the mean of absolute difference values were calculated. Finally the mean from the mean from the mean of absolute difference values of all observers were calculated. The mean repeatability of all observers was found to be 0.88 for the YNSN LUT based samples and 0.95 for the SCOP LUT based sample. This suggests that the observers gave consistent judgements within +/- 1 category units.

8.3.5   Results

The results of the psychophysical experiments are given as *z*-scores below. Figure 8.5 shows the results for test samples printed with the colour separation based on the YNSN LUT model. Figure 8.6 shows the results for the samples printed with the colour separation based on the SCOP LUT model. Pairs of stimuli are given on *X*-axis whereas the *z*-scores are shown on *Y*-axis. Category boundaries are shown horizontally. The

boundary between category 1 and category 2 represents the perceptibility threshold. Similarly the boundary between category 3 and category 4 represents the acceptability threshold.
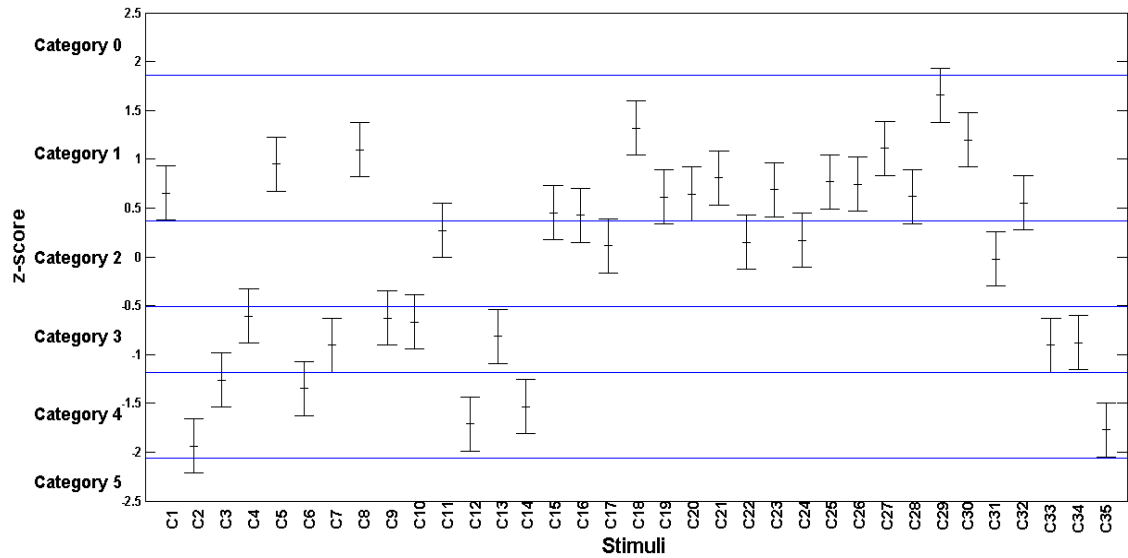
Figure 8.5 *z*-score results with 95% confidence interval - YNSN LUT model

For the samples printed using the YNSN LUT based colour separations, most of the scores were in category 1, 2 and 3 with few in category 4 and 5. This means only few colours printed with 7-colour separation were unacceptable to the observers when compared to the original spot colours. For the samples printed using the SCOP LUT based colour separations, similar trend was observed with slightly different category boundaries.
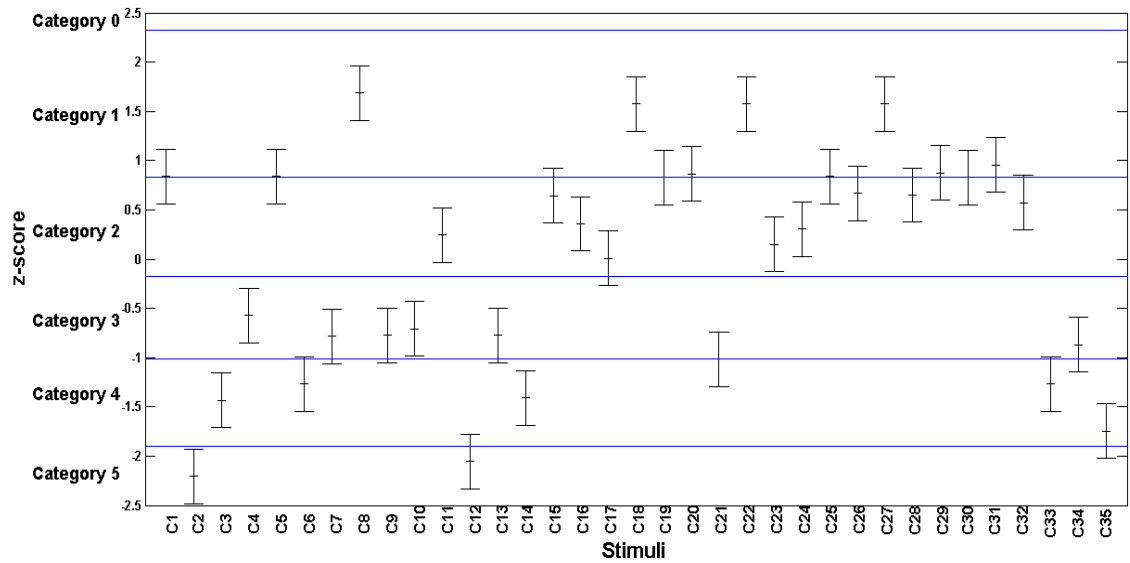
Figure 8.6 *z*-score results with 95% confidence interval – SCOP LUT model

Figure 8.7 and Figure 8.8 show the scatter plots of the CIEDE2000 values between the target and test stimuli against the mean scores for the YNSN LUT model and the SCOP LUT model respectively. Note that the mean score does not strictly reflect the overall psychometric results since the categories are subjective and the intervals may not be equal. But the terms of categories were chosen carefully to minimise ambiguity to the observers. These graphs also reveal useful information about the relationship between the CIEDE2000 value and the corresponding mean score for each pair of stimuli.
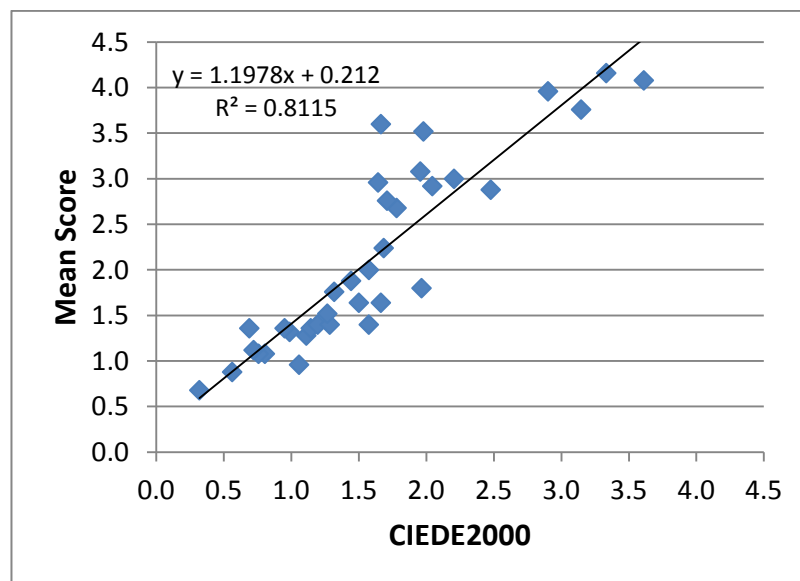
Figure 8.7 YNSN LUT model – the mean scores plotted against the CIEDE2000 values between the target and test stimuli
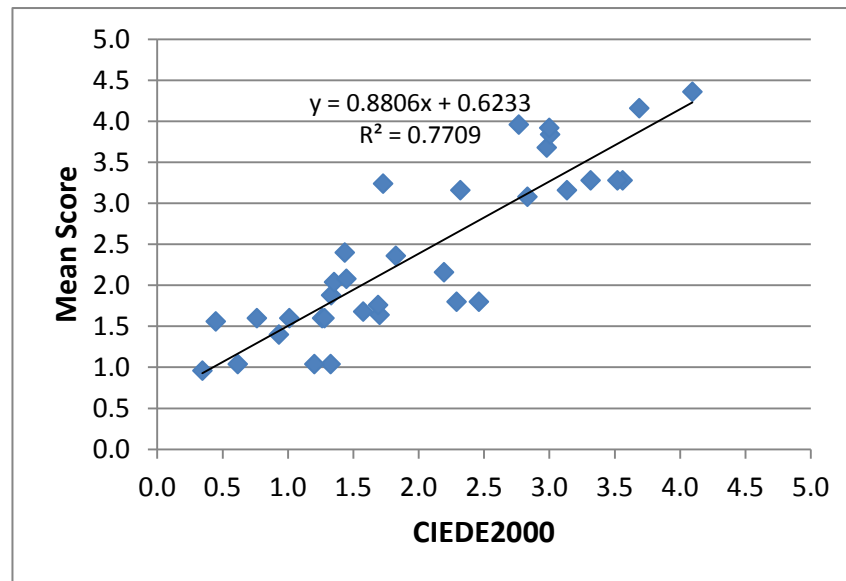
Figure 8.8 SCOP LUT model – the mean scores plotted against the CIEDE2000 values between the target and test stimuli

Both figures show good correlation between the CIEDE2000 values and the mean scores of the judgements. The correlation coefficients (R^2) were 0.8115 and 0.7709 for the YNSN LUT model and the SCOP model respectively. Thus the mean scores calculated from the observers' judgements are in agreement with the colour difference values between the target and test stimuli. One of the reasons for this strong agreement could be the colour assessment skills of all observers who have several years of experience in assessing the spot colours in the packaging printing environment.

The stimuli with the mean scores higher than 3.5, which reflects the "unacceptable" colour match, were found to be neutral colours (for example, light grey), pastel blues and dark purples.

Figure 8.9 shows the results of logistic regression with sigmoid curves. Cumulative proportion values of all observers for each category were plotted against the CIEDE2000 values between the target and test stimuli. Each sigmoid curve represents a category boundary and the categories are shown between the curves.
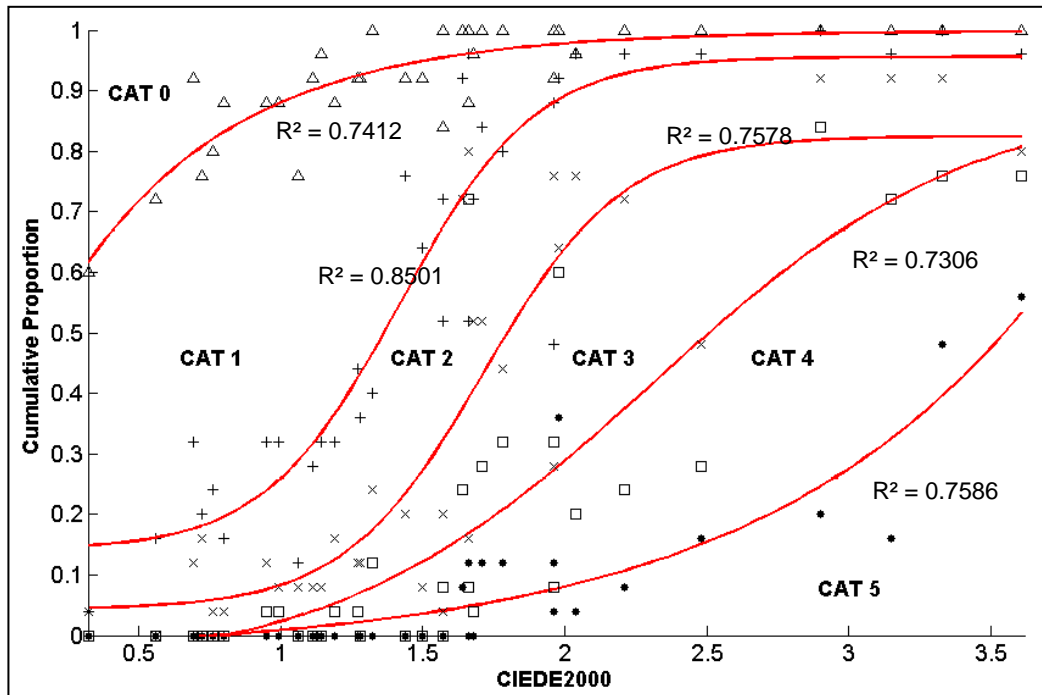
Figure 8.9 Sigmoid curves based on logistic regression for each category

The frequency with which each category was selected by the observers is shown in Figure 8.10 for both inversion models. This gives the overall histograms for categories selected by all observers. For the YNSN LUT model, category 1 shows the highest frequency; for the SCOP LUT model category 2 shows the highest frequency followed by category 1.
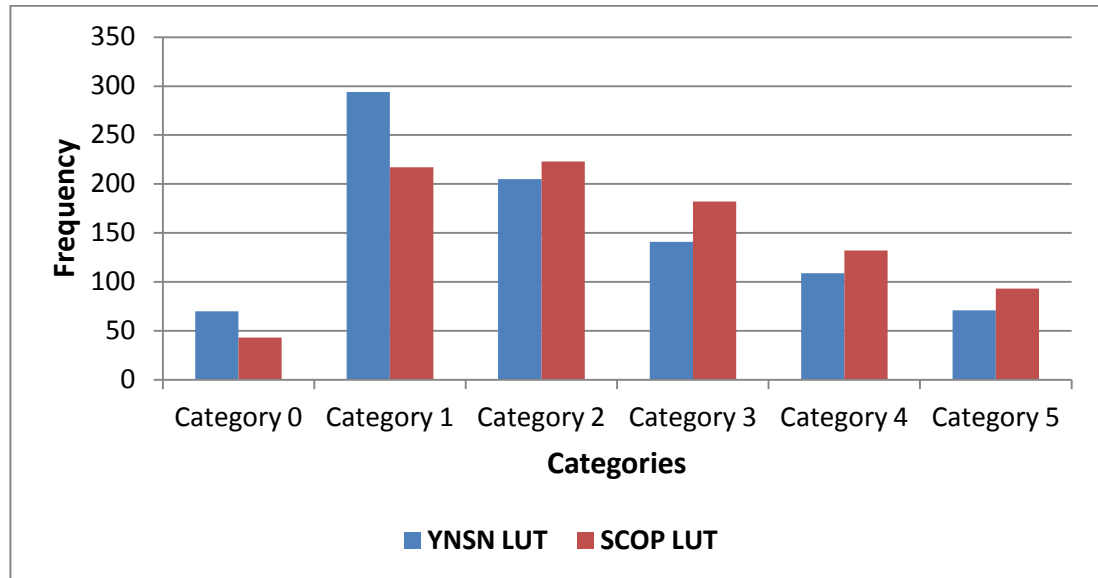
Figure 8.10 Frequency with which each category was selected by observers

The results of the psychophysical experiments confirm that the colours printed by 7-colour separation can be visually acceptable. Both inversion methods performed well though the YNSN LUT based colour separation performed better than the SCOP LUT based colour separation. The psychometric results agree with the quantitative results obtained from the instrumentally measured colour difference values.

8.4   Conclusion

A set of 35 spot colours were reproduced using a 7-colour lithographic offset printing process. Two different inversion methods were used for calculating the colour separations for the spot colours. Both were based on the use of a lookup table, one using the YNSN model and another using the SCOP model, to generate the lookup table lattice points.

The results show that both methods can be used successfully to reproduce the spot colours with good accuracy. The YNSN based LUT inversion showed better accuracy than the SCOP based LUT inversion. However, this is at the cost of increased computational overhead, more complexity and an increased number of model inputs.

Qualitative evaluation of the reproduced colours was done by conducting a psychophysical experiment using 25 skilled observers under controlled viewing conditions. Perceptibility and acceptability thresholds were determined using six categories. The results show that the visual judgements agree with the measured CIEDE2000 values between the target and test stimuli. The YNSN based and the SCOP based 9-level LUT methods which gave a good performance in the numerical evaluation (Chapter 7: Sections 7.4.3 and 7.4.4) have also been shown to perform well in psychophysical experiments.

The YNSN based and the SCOP based 9-level LUT methods can be effectively implemented to replace the spot coloured inks and achieve the target colours with the 7-colour printing process. This could save significant material, time and costs in those market sectors of the packaging industry where printing jobs mainly consist of solid spot colours.

The next chapter will conclude with the summary of the thesis, discussions and future work.

Chapter 9 Summary and Conclusion

Finally the contributions of the project are summarized in this chapter. A synopsis of the results, production strategies for the *n*-colour printing process and suggested directions for future research are discussed.

9.1 Overview

The main objective of the project was to reproduce spot colours accurately by use of *n*-colour separations. This goal is aimed at the packaging printing sectors where the majority of inks used are special inks to print solid spot colours.

Chapter 1 provides the background, industrial applications and significance and thesis overview. The literature and the previous research in the relevant fields consisting of the spectral printer models, inverse printer characterisation methods and the *n*-colour separation techniques are discussed in Chapter 2.

Chapter 3 describes the methodology and procedures used during the project including metrology, reproduction workflow, computational procedures and the process control requirements for the *n*-colour printing process.

A key part of the *n*-colour separation is the division of the device-dependent colorant space. The *n*-colour printing process is considered as an extension of the CMYK printing process (Chapter 3). In addition to the CMYK ink-sector, a new ink-sector for each intermediate ink (for example, orange, green and violet) is required. Each sector contains four inks with an achromatic colour (black) common among all the sectors. This allows extension of the principles and schema of the CMYK printing process to these additional sectors without the need for *n*-dimensional colour profiles. A 7-colour printing process was used as a representative, but the methods used can be generalised to any *n*-colour printing process by having sub-sets of 4-inks each containing a common black ink and three chromatic inks.

The spectral printer models were applied to 4-colour and 7-colour printing processes (Chapter 4). This provides comprehensive evaluation of the existing printer models for the *n*-colour printing process using different printing technologies, for example, lithographic offset, flexographic, inkjet and thermal sublimation printing. The YNSN model and the KM+YNSN models performed well. The results show that the printer models originally developed for halftone screening can be successfully applied to the digital printing techniques like inkjet. Another outcome was realisation of the range of optimised Yule-Nielsen values (*n* factors) for different printing technologies with different ink-sectors using the YNSN model and the KM+YNSN model.

A colour gamut of the 7-colour printing process, which is an important part of the characterisation process, was predicted and analysed using the spectral printer models (Chapter 5). A combination of the KM and YNSN models predicted the colour gamut reasonably well using the spectral reflectance measurements of the primary inks alone. This procedure can significantly reduce the time and cost of printing and materials for the *n*-colour printing, particularly when there are several ink-sets to be analysed.

Another contribution of the project is the gamut comparison index (GCI) which provides an objective metric to compare two colour gamuts and quantify the difference between them. This metric, along with additional gamut metrics, were used to evaluate the accuracy of the predicted gamut of the *n*-colour printing process. The gamut metrics can be used in various applications in the printing and imaging fields.

The spectral printer models may not be used in the existing workflows owing to their complexities and computational cost. This is particularly important in an imaging workflow where a large number of pixels are processed. To address this issue, a new method, called as the spot colour overprint (SCOP) model, was proposed for characterisation of the printing devices (Chapter 6). The SCOP model was evaluated for the 7-colour printing process with different printing technologies.

This is relatively simple and computationally inexpensive model based on the CIEXYZ colour space making it suitable for the existing standards like ICC workflow and PDF/X documents. This method can also be used for other application like previewing spot colour overprints on monitor using pre-media software and matching spot colour overprints on digital printing and proofing devices.

The colour separations were derived for a set of test colours using the inverse printer characterisation models (Chapter 7). The constrained optimisation and the lookup table (LUT) based inversion approaches were evaluated. The challenge was to find a balance between the accuracy of the model and the computational cost. The LUT based methods were found to be faster and more robust without compromising the accuracy.

Finally a set of real-world spot colours were converted using 7-colour separation and printed with the 7-colour lithographic offset printing process (Chapter 8). Two different inversion methods, based on the lookup table, were used for calculating the colour separations. The first method used the YNSN model and the second used the SCOP model to generate the LUT lattice points. A psychophysical experiment was performed using 25 skilled observers to assess the perceptibility and acceptability threshold between the printed colours and the original spot colours. The results indicate that both the methods can be effectively implemented to replace the spot coloured inks with the 7-colour printing process.

This project provides an efficient method of reproducing the spot colours with the *n*-colour printing process. This can save significant material, time, wastage and costs in those market sectors of the packaging industry where the printing jobs mainly consist of the solid spot colours. It will avoid the special inks thus saving the huge ink inventory.

The key considerations for implementing the *n*-colour printing process in the real-world are provided as practical guidelines in the next section.

9.2 Key considerations for the real-world implementation

During the evaluation stage of the project, many practical aspects of the *n*-colour printing process were recognised. The key considerations for the real-world implementation and production of the *n*-colour printing process are briefly described below. Although it is not a comprehensive list, it does provide some useful insights for the implementation of the *n*-colour printing process.

Process control and stability

Process parameters should be controlled across the print production workflow from the design stage through pre-press to the press conditions. The artwork specifications and the colour acceptability criteria should be in place. The pre-press devices should be calibrated and the plate-making process must be standardised. A small error in the pre-press, for example, un-calibrated plates, could result in relatively large variations in the final print quality. The press conditions, including the roller-settings, consumables and press maintenance will affect the implementation of the *n*-colour printing process. Stability and consistency of the printing system is critical. Unlike the spot coloured ink which is printed using a single print unit on the press, the *n*-colour printing involves reproducing the same spot colour with multiple inks using multiple print units. This adds considerably more variability and added complexity to the printing process.

Ink selection and optimisation

Selection of the inks is another important part of the implementation. Depending on the objectives of the *n*-colour printing, the ink-set can be optimised. For example, if the aim is to reproduce a specific set of spot colours with the *n*-colour printing process, then the ink-set can be optimised such that all, or at least a maximum number, of the spot colours are achieved within the overall gamut of the *n*-colour printing process. The gamut prediction and evaluation methods used in Chapter 5 can be used for this purpose.

Usually mono-pigment inks are suited to the *n*-colour printing process. However, multi-pigment inks can also be used in specific applications.

Calibration of inks

Calibration of each primary ink (colour), particularly the intermediate colours - orange, green and violet is essential. There are currently no standard targets for calibrating the inks which are used for the *n*-colour printing process. Even the CMYK inks used in the *n*-colour printing may be slightly more chromatic than the standard ink-set used for process colour printing. In this project, the existing standard calibration targets were used for all inks, for example, ISO 12647-2 (2007) for lithographic offset printing and ISO 12647-6 (2006) for flexographic printing. Other methods of calibration can be used, for example, the channel-independent calibration method described by Balasubramanian (2003). This method aims at achieving a visually linear response for each ink.

Spot colour consolidation

If the objective is to reproduce the spot colours with the *n*-colour printing process, then the spot colours in the library should be consolidated to remove the redundant spot colours. For example, there may be multiple versions of the same colour-name with different CIELAB values. The spot colour library can be analysed and rationalised to eliminate the duplicate and unwanted colours.

Screening method

Screening technique used for the *n*-colour printing process should be considered. Although the conventional screening with amplitude modulation (AM) is sufficient in many cases, it could produce the print artefacts for some elements of the print job. This also depends on the screen frequency (resolution). In the case of AM screening, the screen angles should be carefully selected to avoid the moiré effect and inaccurate reproduction of some spot colours. The frequency modulation (FM) and hybrid screening (combination of AM and FM screening) can be used if required, especially when the blue and violet spot colours show artefacts. The ink lay-down order should be

established earlier in the project. This is usually based on the reducing tack principle, starting with the high-tack ink in the first print unit to the lowest tack ink in the last print unit.

Colour measurements on press

If the printing press is equipped with an on-press colour measurement device, for example a scanning spectrophotometer, then this process may require changing. The colour patches and elements in the colour control bar should be changed in order to measure the solid colours and the tonal data for the *n*-colour printing process. The solid colours printed with the spot coloured inks represent the actual spot colour. But the solid colours printed with the *n*-colour printing process represent the solid colour of the primary ink, not the desired spot colour because this spot colour will now be reproduced with *n*-colour separation with multiple inks. For quality control purposes, it may be required to create brand-specific colour control patches which represent the final spot colour printed with the *n*-colour separations.

Metamerism

In addition to colorimetric accuracy, metamerism (see definition in Section 1.6) can be critical for brand colours. Although exact spectral matching of spot colours may not be achieved using the *n*-colour printing process, metamerism between the target colour and its reproduction should be reduced. As compared to the conventional 4-colour printing, the *n*-colour printing process adds the number of degrees of freedom to minimise metamerism. This was explored by Tzeng (1999 & 2000) and Taplin (2001).

Implementation scope

The scope of implementation may be initially restricted to a few spot colours or brand owners. For example, selecting the top 50 spot colours which represent a large volume of the business instead of the whole spot colour library is much more convenient.

The above mentioned key considerations should provide brief practical guides for those who wish to implement the *n*-colour printing process.

9.3   Production strategies for the *n*-colour printing process

The *n*-colour printing process can be implemented on different scales, for example, a single job, a product series, a complete brand or across multiple brands to cover the full production portfolio. It is essential to have an implementation strategy to ensure the success and to achieve the desired benefits. A family of products with high-volume recurring print jobs can be considered as a pilot project. Defining the project scope and team is an important part along with the training and education of team members.

Critical brand colour and a high-volume brand colour
There may be a critical brand colour which cannot be compromised or a brand colour which covers a large volume of the business. If possible, this colour can be used as an intermediate ink (see terminology in Section 1.6) of the *n*-colour printing process to provide better stability of reproduction. Alternately, if the printing press has an auxiliary print unit then the critical brand colour can be used as a solid colour in addition to *n* inks. This is usually decided after estimating the sustainability benefits.

Restrict the maximum number of inks to reproduce any given colour
In this project, the colorant space was divided into sectors each containing four inks. This means that any target colour (or pixel) can be reproduced by using a maximum of four inks. If the printing system is not stable enough then it may have adverse effects on the consistency of the colours reproduced with 4 inks. To improve the consistency, it may be better to restrict the separation of target colours to a maximum of three or two inks instead of four. But this may reduce the accuracy. The balance between the consistency and the accuracy should be considered.

Text and barcode elements

Although modern printing technologies are capable of achieving and maintaining tight registration on all colours, the colour of text and barcode elements should be considered carefully. These elements are best reproduced with single inks, particularly if there is a micro-text in the artwork as a security feature.

Production planning strategy

With the *n*-colour printing process, it is possible to combine different print jobs together in a single job. This is particularly valuable for a family of the same product, for example, a product printed with the same design but in different languages for different geographical locations. The merging of the jobs provides flexibility to the production planning and job scheduling which traditionally depends on the job-specific spot colour portfolio. It also saves the production time and waste material.

9.4   Future work

The natural next step for this research would be to extend the methodology to evaluate the overprints of the spot colours using the *n*-colour separations. This will be relevant to other packaging printing sectors where spot colour tonal overprint reproduction is important.

The objective of this project was to reproduce solid spot colours, but the schema presented in this project can be extended to contone images in future. The challenge is to achieve the desired smoothness of images. The smoothness is affected due to abrupt changes in colorant values particularly in regions where the colour gamuts of ink-sectors overlap.

The SCOP model can be used for different applications, for example previewing spot colour overprints on a monitor using pre-media software and matching spot colour overprints on digital printing and proofing devices. It would be useful, in the future, to determine the optical phenomena and physical properties underlying the mathematical

equations that comprise the model. The relation between the ink characteristics and the model coefficients should be explored. The effect of the dot area of the foreground colour on the accuracy of model should be investigated. The results of these investigations should lead to better accuracy and further simplification of the model.

Although several printer characterisation models were implemented and evaluated in this project, the scope can be widened to test other characterisation models, for example, the ink spreading enhanced YNSN model (Hersch, 2005), the extended EYNSN model (Rossier, 2010).

In this project, the spot colours lying outside the gamut of the n-colour printing process were mapped to the gamut surface using the minimum ΔE clipping method by finding the nearest coordinate on the gamut boundary (Section 7.2.2). Other methods of the gamut mapping should be investigated, for example, the hue preserving minimum ΔE method which maintains the hue angle while finding the minimum distance to the destination gamut boundary. For the inverse printer model based on the constrained optimisation method (Section 7.3), weighted RMS error (Imai, 2002) between the predicted spectra and the measured spectra should be tested.

In the future, the n-colour separation methods should be also evaluated using modern digital printing techniques, for example, different types of inkjet technologies, electrophotography, nanography etc.

The future direction for the n-colour separation can be envisaged as a context aware colour separation. For example, a brand logo element in a print job will have a different strategy for colour separation than the photographic image element. This may include the dynamic analysis of the image elements and their colour regions, hues and especially chroma values. It would allow the ability to further exploit the strengths of the n-colour printing process.

References

Abebe, M., Gerhardt, J. and Hardeberg, J. Y. (2011) Kubelka-Munk theory for efficient spectral printer modelling, *Proc. SPIE*, **7866**, 786614-1 to 786614-15.

Agar, A.U. and Allebach, J.P. (1998) An iterative cellular YNSN method for color printer Characterization, *IS&T/SID 6th Color Imaging Conference*, Scottsdale, Arizona, USA, 197-200.

Agar, A.U. (2001) Model based colour separation for CMYKcm printing, *IS&T/SID 9th Color Imaging Conference,* Scottsdale, Arizona, USA, 298-302.

Alman, D.H., Berns, R.S., Snyder, G.D. and Larsen, W.A. (1989) Performance testing of colour difference metrics using a colour appearance data set, *Color Res. Appl.*, **14**, 139-151.

Alsam, A., Gerhardt, J. and Hardeberg J.Y. (2005) Inversion of the spectral Neugebauer printer model, *AIC Colour 05*, 44-62.

ANSI/13A IT10.7666:2002 *Photography – Electronic Still Picture Imaging – Reference output medium metric RGB color encoding (ROMM-RGB)*.

ANSI IT8.7/4-2005 (R2010) *Graphic technology – Input data for characterisation of 4-colour process printing – Expanded data set*.

Balasubramanian, R. (1995) Colorimetric modelling of binary color printers, *Proc. IEEE International Conf. on Image Processing*, **2**, 327-330, Washington, DC.

Balasubramanian, R. and Dalal, E. (1997) A method for quantifying the colour gamut of an output device, *Proc. SPIE,* **3018**, 110-116.

Balasubramanian, R. (1999), Optimization of the spectral Neugebauer model for printer characterization, *J. Electron. Imag.*, **8** (2), 156–166.

Balasubramanian, R. and Esbach, R. (2001) Reducing multi-separation color moiré via a variable undercolor removal and gray-component replacement strategy, *J. Imag. Sci. Tech.*, **45** (2), 152–160.

Balasubramanian, R. (2003) Digital color imaging handbook. Sharma, G. (Ed.) CRC Press, Chapter 5.

Barber, C.B., Dobkin, D.P. and Huhdanpaa, H.T. (1996) The Quickhull algorithm for convex hulls, *ACM Transactions on Mathematical Software*, **22** (4), 469-483.

Bartleson, C.J. and Grum, F. (1984) Optical Radiation Measurements, Vol. 5: Visual Measurements, Academic Press, Orlando, FL.

Bastani B., Cressman B. and Shaw M. (1996) Sparse Cellular Neugebauer Model for N-ink Printers, *Proc. IS&T/SID 4th Color Imaging Conference: Color Science, Systems and Applications*, 58-60.

Berns, R.S., Alman, D.H., Reniff, L., Snyder, G.D. and Balonen-Rosen, M.R. (1991) Visual determination of suprathreshold colour-difference tolerances using probit analysis, *Color Res. Appl.*, **16**, 297-316.

Berns, R. S. (2000) *Billmeyer and Saltzman's Principles of Color Technology*, 3rd edn., New York: Wiley.

Berns R.S and Mohammadi M. (2007) Single-constant simplification of Kubelka-Munk turbid media theory for paint systems – a review, *Color Res. Appl.,* **32** (3), 201-207.

Boll H. (1994) A color to colorant transformation for seven ink process, *Proc. SPIE,* **2170**, 108-118.

Boyd, S. and Vandenberghe, L. (2004) Convex Optimization, Cambridge: Cambridge University Press.

Braun, G. and Fairchild, M.D. (1997) Techniques for gamut surface definition and visualization, *IS&T/SID 5ᵗʰ Color Imaging Conference,* 147-152.

Chen,Y., Berns, R. S. and Taplin, L. A. (2004a) Six color printer characterization using an optimized cellular Yule-Nielsen spectral Neugebauer model, Journal of Imaging Science and Technology, **48** (6), Nov. 2004. *IS&T/SID 6th Color Imaging Conference*, Scottsdale, Arizona, USA, 197-200.

Chen,Y., Berns, R. S. and Taplin, L. A. (2004b) Extending printing color gamut by optimizing the spectral reflectance of inks, *IS&T/SID 12ᵗʰ Color Imaging Conference: Color Science and Engineering Systems, Technologies, and Applications*, Scottsdale, Arizona, USA, 163-169.

Cholewo, Tomasz J., and Shaun Love. (1999) Gamut boundary determination using alpha-shapes, In *IS&T/SID 7th Color Imaging Conference*, 200-204.

Cholewo, T.J. (2000) Printer model inversion by constrained optimization, *Proc. IS&T/SPIE 12ᵗʰ Annual Symposium*, San Jose, California, USA, 349-357.

Chung, R., Riordan, M. and Prakhya S. (2008) Predictability of spot colour overprints. Advances in Printing and Media Technology, Vl. XXXV, 373-380.

CIE Technical report (1986) CIE Publication 15.2, Colorimetry, 2ⁿᵈ edition. Central Bureau of the CIE, Vienna, Austria.

CIE Technical Report (1993) *Parametric effects in colour-difference evaluation*, CIE Publication No. 101, Central Bureau of the CIE, Vienna, Austria.

CIE Technical Report (1995) *Industrial colour difference evaluation*, CIE Publication No. 116, Central Bureau of the CIE, Vienna, Austria.

CIE Technical Report (2005) *Criteria for the evaluation of extended-gamut colour encodings*, CIE Publication No. 168, Central Bureau of the CIE, Vienna, Austria.

Clarke, F., MacDonald, R. and Rigg, T. (1984) *Modifications to the JPC79 colour-difference formula*, J. Soc. Dyers Colourists, **100**, 117-148.

Clapper, F.R. and Yule, J.A.C. (1955) Reproduction of color with halftone images, *Proc. TAGA*, 1-12.

Clapper, F.R. (1961) An empirical determination of halftone color reproduction requirements, *Proc. TAGA Conf.*, 31-41.

de Berg, M., Cheong, O., van Kreveld, M. and Overmars, M. (2008) Computational Geometry: Algorithms and Applications, Berlin: Springer-Verlag.

Dennis, J.E. and Schnabel, R.B. (1983) Numerical methods for unconstrained optimization and nonlinear equations, Prentice-Hall.

Deshpande, K., Green P.J., MacDonald L. and Bayley T. (2009) Gamut prediction of *n*-colour printing processes, *Proc 11th Congress of the International Colour Association (AIC),* Sydney, Australia.

Deshpande, K. and Green, P.J. (2010) A simplified method of predicting the colorimetry of spot colour overprints, *IS&T/SID 18th Color Imaging Conference,* San Antonio, Texas, USA, 213-216.

Deshpande, K. and Green, P.J. (2011) Regression method for predicting the colorimetry of spot colour overprints, *Proc. 38th IARIGAI conf. Advances in Printing and Media Technology*, Budapest, Hungary.

Deshpande, K. and Green, P.J. (2012) Gamut comparison index: a metric for comparing colour gamuts, *AIC Interim Meeting*, Taipei.

Deshpande, K., Green, P.J. and Pointer, M.R. (2014a) Gamut evaluation of an *n*-colour printing process with the minimum number of measurements, *Color Res. Appl.* **40** (4), 408-415.

Deshpande, K., Green, P.J. and Pointer, M.R. (2014b) Metrics for comparing and analysing two colour gamuts, *Color Res. Appl.* doi: 10.1002/col.21930.

Deshpande, K., Green, P.J. and Pointer, M.R. (2014c) Characterisation of the *n*-colour printing process using the spot colour overprint model, *Optics Express*, **22** (26), 31786-31800, Dec. 2014.

Deshpande, K., Green, P.J. and Pointer, M.R. (2014d) Colour separation of *n*-colour printing process using inverse printer models, Proc. *IS&T/SID 22nd Color Imaging Conference,* Boston, Arizona, USA, 194-199.

Deshpande, K., Green, P.J. and Pointer, M.R. (2014e) Color separation of an *n*-color printing process using inverse printer models, *J. Imag. Sci. Techno.,* **58** (5), Sept. 2014, 50504-1-50504-8.

Dolezalek, F.K. (1994) Appraisal of production run fluctuations from color measurements in the image, *Proc. Tech. Assoc. Graphic Arts*, 154-164.

Doll, P. (2001) 3-Dimensional colour gamut quantification and comparison, *NIP17: International Conference on Digital Printing Technologies*, 804-807.

Edström, P. (2004), Comparison of the DORT2002 radiative transfer solution method and the Kubelka-Munk model, *Nordic Pulp and Paper Research Journal*, **19** (3), 397-403.

Edström, P. (2005), A fast and stable solution method for the radiative transfer problem, *SIAM Review*, **47** (3), 447-468.

Emmel, P. and Hersch, R. D. (1999) A model for colour prediction of halftoned samples incorporating light scattering and ink spreading, *IS&T/SID 7th Color Imaging Conference, Scottsdale, Arizona, USA,* 173-181.

Emmel, P. and Hersch, R. D. (2001) Prediction of the reflection spectra of three ink colour prints, *Proc. IS&T Int. Conference on Digital Printing Technologies, Fort Lauderdale, Florida, USA,* 465-468.

Emmel, P. and Hersch, R.D. (2002) Modeling ink spreading for color prediction, *J. Imag. Sci. Techno.,* **46** (3), 237-246.

Emmel, P. (2003) Digital color imaging handbook. Sharma, G. (Ed.) CRC Press, Chapter 3.

Engeldrum, P.G. (2000) Psychometric scaling: a toolkit for imaging systems development, Imcotek Press.

Fairchild, M.D. (2005) *Color Appearance Models*, 2nd edn., Chichester: Wiley.

FOGRA39L (2007) Characterization data for standardized printing conditions, http://www.fogra.org/en/fogra-standardization/fogra-characterizationdata/a-icc-en.html.

Gardner, J.L. (2000) Uncertainty estimation in colour measurement, *Color Res. Appl.*, **25**, 349-355.

Gerhardt, J. and Hardeberg, J.Y. (2006) Spectral colour reproduction by vector error diffusion, *Proc. 1st European Conference on Colour in Graphics, Imaging and Vision (CGIV)*, 469-473.

Gescheider, G.A. (1997) Psychophysics 3rd edition Mahwah, N.J. Lawrence Earlbaum Assoc.

Glynn E. F. (2007) http://www.efg2.com/Lab Overland Park, KS USA.

Gordon, I.E. (2004) *Theories of Visual Perception,* 3rd edn. Hove: Psychology Press.

Green, P.J. and Johnson, A.J. (2000) Issues of measurement and assessment in hard copy colour reproduction, *Proc. SPIE Conf. Col. Imag.: Device-Independent Color, Color Hardcopy and Graphic Arts*, **3963**, 281-292.

Green, P.J. (2001) A test target for defining media gamut boundaries, *Proc. SPIE,* **4300**, 105-113.

Green, P.J. and MacDonald, L.W. (2002) (eds) *Colour Engineering,* Chichester: Wiley.

Green, P.J. (2003) *Sources of variation in colorimetry: Uncertainty of measurement*, Course CD\Modules\Colour\Lecture\Uncertainty of measurement, Colour Imaging Group, LCC.

Green, P.J. (2003b) A colour engineering toolbox, http://www.color.org/resources/ColourEngineeringToolbox.zip.

Green P.J. (2013) Gamut mapping for the perceptual reference medium gamut, *Colour and Visual Computing Symposium* (*CVCS*), IEEE Sept 2013.

Guan, S.S. and Luo, M.R. (1999) Investigation of parametric effects using small colour differences, *Color Res. Appl.*, **24**, 331-343.

Guyler, K. (2001) Visualization of Expanded Printing Gamuts Using 3-Dimensional Convex Hulls, *American Ink Maker,* **79** (9), 36-56.

Hersch, R.D. and Crete, F. (2005) Improving the Yule-Nielsen modified spectral Neugebauer model by dot surface coverages depending on the ink superposition conditions, *IS&T/SPIE Electronic Imaging Symposium*, *Colour Imaging X: Processing, Hardcopy and Applications*, SPIE, **5667**, 434-445.

Hersch, R.D., Collaud, F., Crete, F. and Emmel, P. (2004) Spectral prediction and dot surface estimation models for halftone prints, *IS&T/SPIE Electronic Imaging Symposium, Conf. Imaging IX: Processing, Hardcopy and Applications*, *SPIE*, **5293**, 356-369.

Heuberger, K.J., Jing, Z.M. and Persiev, S. (1992) Color Transformations and lookup tables, *TAGA/ISCC Proc:1992*, 863-881.

Hua, C.C. and Huang, K.L. (1997) Advanced cellular YNSN printer model, *IS&T/SID 5th Color Imaging Conference,* 231-234.

Hunt, R.W.G. (1998) *Measuring Colour*, 3rd edn. Fountain Press.

Hunt, R.W.G. (2004) *The Reproduction of Colour*, 6th edn. Chichester: Wiley.

IEC 61966-2-1/Amd 1:2003 *Multimedia systems and equipment – Colour measurement and management – Part 2-1 Colour management – Default RGB colour space – sRGB.*

IEC 61966-2-1:1999 *Multimedia systems and equipment – Colour measurement and management – Part 2-1 Colour management – Default RGB colour space – sRGB.*

Imai, F.H., Rosen, M.R. and Berns, R.S. (2002) Comparative study of metrics for spectral match quality, *Proc. 1st European Conference on Colour in Graphics, Imaging and Vision (CGIV)*, 492-496.

ISO/TS 10128:2009 *Graphic technology – Methods of adjustment of the colour reproduction of a printing system to match a set of characterisation data*, Geneva, Switzerland: International Organisation for Standardisation.

ISO 12640-3:2007 *Graphic technology – Prepress digital data exchange – Part 3: CIELAB standard colour image data (CIELAB/SCID)*, Geneva, Switzerland: International Organisation for Standardisation.

ISO 12642-2: 2006/Rev:2009 *Graphic technology – Input data for characterisation of 4-colour process printing – Part 2 Expanded data set*, Geneva, Switzerland: International Organisation for Standardisation.

ISO 12647-2:2004/Amd.1:2007 *Graphic technology – Process control for the production of half-tone colour separations, proof and production prints – Part 2: Offset lithographic processes*, Geneva, Switzerland: International Organisation for Standardisation.

ISO 12647-2:2013 *Graphic technology – Process control for the production of half-tone colour separations, proof and production prints – Part 2: Offset lithographic processes*, Geneva, Switzerland: International Organisation for Standardisation.

ISO 12647-6:2006 Graphic technology – *Process control for the production of half-tone colour separations, proof and production prints – Part 6: Flexographic printing,* Geneva, Switzerland: International Organisation for Standardisation.

ISO 13655:2009 *Graphic technology – Spectral measurement and colorimetric computation for graphic arts images*, Geneva, Switzerland: International Organisation for Standardisation.

ISO DIS 15339-2 (2012) *Graphic technology — Printing from digital data across multiple technologies — Part 2: Characterized reference printing conditions,* Geneva, Switzerland: International Organisation for Standardisation.

ISO 15790:2000 *Graphic technology and photography – Reflection and transmission metrology – Certified reference materials – Documentation and procedures for use, including determination of combined standard uncertainty*, Geneva, Switzerland: International Organisation for Standardisation.

ISO 3664:2009 *Graphic technology and photography – Viewing conditions*, Geneva, Switzerland: International Organisation for Standardisation.

Johnson, A.J., Luo, M.R., Lo, M.C., Xin, J.H. and Rhodes, P.A. (1997) Aspects of colour management: Part I – Characterisation of three colour imaging devices, *Color Res. Appl.,* **22**, 000-000.

Johnson, A.J. (1995) Colour management in graphic arts and publishing, Pira International, Leatherhead.

Johnson, A.J. (1996) Methods for characterizing colour printers, *Displays*, **16**, 193-202.

Kang, H.R. (1993) Comparison of colour mixing theories for use in electronic printing, *IS&T/SID 1st Color Imaging Conference, Scottsdale, Arizona, USA,* 78-82.

Kang, H.R. (1997) Color technology for electronic imaging devices, SPIE Press, Bellingham, WA.

Kang, H.R. (2006) Computational color technology, SPIE Press, Bellingham, WA.

Kueppers, H (1989) Printing process where each incremental area is divided into a chromatic area and an achromatic area and wherein the achromatic areas are printed in black and white and the chromatic areas are printed in color sub-sections, *US Patent* 4,812,899, March 14, 1989.

Lundgren, J. (2010) Alpha shapes, Matlab Central File Exchange, Retrieved 10 January 2011 from http://www.mathworks.com/matlabcentral/fileexchange/28851.

Luo, M.R. (1996) The LLAB model for colour appearance and colour difference evaluation, *Proc. SPIE Conf. Color Imaging: Device-Independent Color, Color Hard Copy and Graphic Arts*, **2658**, 261-269.

Luo, M.R., Cui, G. and Rigg, B. (2001) The development of the CIE 2000 colour difference formula, CIEDE2000, *Color Res. Appl.*, **26**, 340-350.

MacEvoy, B. (2005) http://www.handprint.com/HP/WCL/color7.html#CIELAB.

Mahy, M., Van Eycken, L. and Osterlink, A. (1994) Evaluation of uniform colour spaced developed after the adoption of CIELAB and CIELUV, *Color Res. Appl.*, **19**, 105-121.

Mahy, M. and Delabastita, P. (1996a) Inversion of the Neugebauer equations, *Color Res. Appl.*, **21**, 404-411.

Mahy, M. (1996b) Gamut calculation of color reproduction devices, *IS&T/SID 4th Color Imaging Conference, Scottsdale, Arizona, USA,* 145-150.

Mahy, M. and De Baer, D. (1997a) HIFI color printing within a color management system, *IS&T/SID 5th Color Imaging Conference*, *Scottsdale, Arizona, USA,* 277-283.

Mahy, M. (1997b) Calculation of color gamuts based on the Neugebauer model, *Color Res. Appl.* **22** (6), 365-374.

Mahy, M. (1999) Color separation method and apparatus for same, U.S. Patent No. 5,878,195, March 2, 1999.

Mahy, M. and Verbeeck, F. (2011) Multicolorant separation system and method, U. S. Patent 8,054,504 November 8, 2011.

MathWorks (2014) Optimization Toolbox: User's Guide (R2013a), Retrieved 10 September 2014 from http://www.mathworks.co.uk/help/optim/ug/constrained-nonlinear-optimization-algorithms.html

Mestha, L.K. and Dianat, S.A. (2009) Control of Color Imaging Systems: Analysis and Design, CRC Press.

Morovič, J. (1998) To develop a universal gamut mapping algorithm, *Ph.D. Thesis*, University of Derby.

Morovič, J. and Luo, M. R. (2000) Calculating medium and image gamut boundaries for gamut mapping, *Color Res. Appl.,* **25**, 394-401.

Morovič, J. (2007) Fast computation of multi-primary color gamuts, *IS&T/SID 15th Color Imaging Conference, Albuquerque, New Mexico, USA*, 228-232.

Morovič, J. (2008) Colour Gamut Mapping, Barcelona: John Wiley & Sons.

Morovič, J., Morovič, P. and Arnabat, J. (2010) HANS – a new color separation and halftoning paradigm, *IS&T/SID 18th Color Imaging Conference, San Antonio, Texas, USA*, 359-364.

Morovič, P., Morovič, J. and García-Reyero J.M. (2011) Optimizing HANS color separation: meet the CMY metamers, *IS&T/SID 19th Color Imaging Conference, San Jose, California, USA*, 229-233.

Morovič, J., Morovič, P. and Arnabat, J. (2012a) HANS: Controlling ink-jet print attributes via Neugebauer primary area coverages, IEEE Transactions On Image Processing, **21** (2), 688-696.

Morovič, P., Morovič, J., Arnabat, J. and García-Reyero J.M. (2012b) Revisiting spectral printing: a data driven approach, *IS&T/SID 20th Color Imaging Conference, Albuquerque, New Mexico, USA*, 210-214.

Morovič, J., Morovič, P., Rius, M. and García-Reyero J.M. (2013) 8 vertex HANS: An ultra-simple printer color architecture, *IS&T/SID 21st Color Imaging Conference, Los Angeles, California, USA*, 335-340.

Mourad, S., Emmel, P., Simon, K. and Hersch, R. (2001) Extending Kubelka-Munk's theory with lateral light scattering, *IS&T International Conference on Digital Printing Technologies*, Fort Lauderdale, Florida, USA, 469-473.

Nelder, J.A. and Mead, R. (1965) *Computer Journal,* **17**, 308-313.

Neugebauer, H.E.J. (1937) Die Theoretischen Grandlagen des Mehrfarben-edruckes, Zeitschrift Wissenschaften Photography, 73-89.

Nocedal, J. and Wright, S.J. (2006) Numerical Optimization. Springer Series in Operations Research, Springer Verlag.

Ohta, N. and Robertson, A. (2006) Colorimetry: Fundamentals and Applications, Chichester: John Wiley & Sons.

Oicherman, B. (2003) To develop a procedure for visual evaluation of colour differences between printed complex images, MSc thesis, London College of Printing.

Ostromoukhov, V. (1993) Chromaticity gamut enhancement by heptatone multi-colour printing, In Device-independent Color Imaging and Imaging Systems Integration, *Proc. IS&T/SPIE*, **1909**, 139-151.

Perales, E., Martinez-Verdu, F.M., Viqueira, V., Fernandez-Reche, J., Diaz, J.A. and Uroz, J. (2009) Comparison of colour gamuts among several types of paper with the same printing technology, *Color Res. Appl.* **34** (4), 330-336.

Reel, R. and Penrod, M. (1999) Gamut visualisation tools and metrics, *IS&T/SID 7th Colour Imaging Conference,* Scottsdale, Arizona, USA, 247-251.

Rolleston, R. and Balasubramanian, R. (1993) Accuracy of various types of Neugebauer Models, *IS&T/SID 1st Color Imaging Conference, Scottsdale, Arizona, USA,* 32-37.

Rossier, R. and Hersch, R.D. (2010) Ink-dependent n-factors for the Yule-Nielsen modified spectral Neugebauer model, *Proc. 5th European Conference on Colour in Graphics, Imaging and Vision* (*CGIV*), Joensuu, Finland, 202-206.

Schittkowski, K. (1985) NLQPL: A FORTRAN-Subroutine Solving Constrained Nonlinear Programming Problems, *Annals of Operations Research*, **5**, 485-500.

Sharma, G. (2003) Digital color imaging handbook, CRC Press.

Sharma, G. and Trussell, H. (1997) Digital color imaging, *IEEE Transaction on Image Processing*, **6** (7), July 1997, 901-932.

Sharma, G., Wu, W. and Dalal, E. N. (2005) The CIEDE2000 colour-difference formula: implementation notes, supplementary test data, and mathematical observations, *Color Res. Appl.*, **30** (1), 21-30.

Sharma, G. and Rodriguez-Pardo, C.E. (2012) The dark side of CIELAB, *Proc. SPIE: Color Imaging XVII Displaying, Hardcopy, Processing, and Applications*. SPIE, **8292**, 1-9.

Sibson, R. (1981) A brief description of natural neighbor interpolation, in *Interpreting Multivariate Data*, V. Barnett (Ed.), Chichester: Wiley, 21-36.

Sigg, F., Viggiano, J.A.S. and Husain, K. (2011) Predicting the color of an overprint of two spot colors using a mathematical model, *Proc. TAGA,* 233-252.

Slavuj, R., Coppel, L.G., Olen, M. and Hardeberg, J.Y. (2014) Estimating Neugebauer primaries for multi-channel spectral printing modelling, *Proc. SPIE, 9018, Measuring, Modeling, and Reproducing Material Appearance*, 90180C.

Song, T. and Luo, M.R. (2000) Testing color-difference formulae on complex images using a CRT monitor, *IS&T/SID 8th Color Imaging Conference*, 44-48.

Spellucci, P. (1998) A new technique for inconsistent QP problems in the SQP method, *Journal of Mathematical Methods of Operations Research*, **47** (3), 355–400.

Stollnitz, E.J. (1998a) Reproducing color images with custom inks, Ph.D. dissertation, University of Washington.

Stollnitz, E.J., Ostromoukhov, V. and Salesin, D.H. (1998b) Reproducing colour images using custom inks, *Proc. SIGGRAPH*, 267-274.

Taplin, L.A. (2001) Spectral modelling of a six-colour inkjet printer, *M.S. Degree Thesis*, RIT.

Tone, K. (1983) Revisions of constraint approximations in the successive QP method for nonlinear programming problems, *Journal of Mathematical Programming*, **26** (2), 144–152.

Torgerson, W.S. (1958) Theory and Method of Scaling, New York: Wiley.

Tzeng, D., and Berns, R. S. (1998) Spectral-based ink selection for multiple-ink printing I. colorant estimation of original objects, *IS&T/SID 6th Color Imaging Conference*: *Color Science, Systems and Applications*, 106 -111.

Tzeng, D.Y. (1999) Spectral based color separation algorithm developed for multi-ink color reproduction, *Ph.D. thesis*, RIT.

Tzeng, D.Y. and Berns, R.S. (2000) Spectral based six-color separation minimizing metamerism, *IS&T/SID 8th Color Imaging Conference,* 342-347.

Urban, P. and Grigat, R.-R. (2006) Spectral-based colour separation using linear regression iteration, *Color Res. Appl.*, **31**, 229-238.

Van De Capelle, J.P and Meireson, B. (1997a) A new method for characterizing output devices and its fit into ICC and HIGI color workflows, *IS&T/SID 5th Color Imaging Conference,* 66-69.

Van de Capelle, J.P. and Meireson, B. (1997b) Method and device for determining the color appearance of color overprints, *U. S. Patent No. 5933578.*

Van de Capelle, J.P. and Meireson, B. (1999) A new method for characterising colour printing devices, in *Colour Imaging: Vision and Technology*, MacDonald L.W. and Luo, M.R. (Eds.), Chichester: Wiley, 179-188.

Van De Capelle, J.P., Sundermann, E., Meireson, B. and Geurts, W. (2002) Method and device for determining the colour appearance of colour overprints, United States Patent 10/143,543 December 19, 2002.

Viggiano, J.A.S. (1990) Modeling the color of multi-colored halftones, *Proc. TAGA,* 44-62.

Viggiano, J.A.S. And Hoagland. W.J. (1998) Colorant selection for six-color lithographic printing, *IS&T/SID 6ᵗʰ Color Imaging Conference*, 112-115.

Viggiano, J.A.S. (2005) The legacy of Hans Neugebauer in color imaging: a centennial remembrance, *IS&T/SID 13ᵗʰ Color Imaging Conference*, 153-158.

Viggiano, J.A.S. and Prakhya, S. (2008) Prediction of overprint spectra using trapping models: A feasibility study, *TAGA Proc.* 2008, Rochester, NY:2008 TAGA student chapter, 113-133.

Wang, H., Cui, G., Luo, M.R. and Xu, H. (2012) Evaluation of colour-difference formulae for different colour-difference magnitudes, *Color Res. Appl.*, **37** (5), 316-325.

Yule, J.A.C. and Nielsen, W.J. (1951) The penetration of light into paper and its effect on halftone reproduction, *Proc. TAGA*, 65-76.

Yule, J.A.C. and Colt, R. (1951) Colorimetric investigations in multicolor printing, *Proc. TAGA*,77-82.

Yule, J.A.C. (1967) Principles of Color Reproduction, New York: Wiley.

Zuffi, S., Schettini, R. and Mauri, G. (2005) Spectral-based printer modeling and characterization, *Journal of Electronic Imaging*, **14** (2), 023008.

Appendix A: CIEDE2000 calculations

The colour difference CIEDE2000 between two colours can be calculated as follows.

$$\Delta E_{00}^* = \sqrt{\left(\frac{\Delta L'}{k_L S_L}\right)^2 + \left(\frac{\Delta C'}{k_C S_C}\right)^2 + \left(\frac{\Delta H'}{k_H S_H}\right)^2 + R_T \frac{\Delta C'}{k_C S_C} \frac{\Delta H'}{k_H S_H}}$$

Calculation of *ΔL'*, *ΔC'* and *ΔH'*

.

$$\Delta L' = L_2^* - L_1^*$$

$$\bar{L} = \frac{L_1^* + L_2^*}{2}$$

$$\bar{C} = \frac{C_1^* + C_2^*}{2}$$

$$a_1' = a_1^* + \frac{a_1^*}{2}\left(1 - \sqrt{\frac{\bar{C}^7}{\bar{C}^7 + 25^7}}\right)$$

$$a_2' = a_2^* + \frac{a_2^*}{2}\left(1 - \sqrt{\frac{\bar{C}^7}{\bar{C}^7 + 25^7}}\right)$$

$$\bar{C}' = \frac{C_1' + C_2'}{2}$$

$$\Delta C' = C_2' - C_1'$$

where

$$C_1' = \sqrt{a_1'^2 + b_1^{*2}} \quad C_2' = \sqrt{a_2'^2 + b_2^{*2}}$$

$$h_1' = \begin{cases} \tan^{-1}(b_1/a_1') & \tan^{-1}(b_1/a_1') \geq 0 \\ \tan^{-1}(b_1/a_1') + 360° & \tan^{-1}(b_1/a_1') < 0 \end{cases}$$

$$h_2' = \begin{cases} \tan^{-1}(b_2/a_2') & \tan^{-1}(b_2/a_2') \geq 0 \\ \tan^{-1}(b_2/a_2') + 360° & \tan^{-1}(b_2/a_2') < 0 \end{cases}$$

$$\Delta h' = \begin{cases} h_2' - h_1' & |h_1' - h_2'| \leq 180° \\ h_2' - h_1' + 360° & |h_1' - h_2'| > 180°, h_2' \leq h_1' \\ h_2' - h_1' - 360° & |h_1' - h_2'| > 180°, h_2' > h_1' \end{cases}$$

$$\Delta H' = 2\sqrt{C_1' C_2'} \sin(\Delta h'/2)$$

$$\bar{H}' = \begin{cases} (h_1' + h_2' + 360°)/2 & |h_1' - h_2'| > 180° \\ (h_1' + h_2')/2 & |h_1' - h_2'| \leq 180° \end{cases}$$

Calculation of the weighting functions S_L, S_C, S_H

$$S_L = 1 + \frac{0.015\left(\bar{L} - 50\right)^2}{\sqrt{20 + \left(\bar{L} - 50\right)^2}}$$

$$S_C = 1 + 0.045\bar{C}'$$

$$S_H = 1 + 0.015\bar{C}'T$$

$$T = 1 - 0.17\cos(\bar{H}' - 30°) + 0.24\cos(2\bar{H}') + 0.32\cos(3\bar{H}' + 6°) - 0.20\cos(4\bar{H}' - 63°)$$

Calculation of the hue-chroma interaction factor R_T

Appendix B: Matlab codes for the spectral printer models

Neugebauer model

```
function XYZ = neugcmyk(XYZin, cmyk)

% neugcmyk applies the Neugebauer equations for 4-colour printing
% system.
%
% Input Arguments
% cmyk: m x 4 matrix for dot areas of c, m, y, k inks of the
% input colour patches for which XYZ is to be predicted.
%
% XYZin: 16 x 3 matrix for XYZ values of 16 Neugebauer primaries
% strictly in the following order.
% [white (paper),c,m,y,k,cm,cy,ck,my,mk,yk,cmy,cmk,cyk,myk,cmyk]
%
% Output Arguments
% XYZ: m x 3 matrix for the model-predicted XYZ values for the input
% CMYK
% values.
%
% Example: XYZ = neugcmyk (XYZin, cmykECI2002);
% See also: YNneugcmyk, YNSNcmyk, neugcmy
%
% Kolourprint Dynamic Toolbox
% Author: © Kiran Deshpande
% E-mail: kiranudeshpande@gmail.com
% Last modified: 06/08/2013
% Matlab version R2013a (8.1.0.604)

%% Define colorant values and normalise for 0-1
c = cmyk(:,1)/100;
m = cmyk(:,2)/100;
y = cmyk(:,3)/100;
k = cmyk(:,4)/100;

%% Calculate the relative areas
aw = (1-c).*(1-m).*(1-y).*(1-k);
ac = c.*(1-m).*(1-y).*(1-k);
am = m.*(1-c).*(1-y).*(1-k);
ay = y.*(1-c).*(1-m).*(1-k);
ak = k.*(1-c).*(1-m).*(1-y);
acm = c.*m.*(1-y).*(1-k);
acy = c.*y.*(1-m).*(1-k);
ack = c.*k.*(1-m).*(1-y);
amy = m.*y.*(1-c).*(1-k);
amk = m.*k.*(1-c).*(1-y);
ayk = y.*k.*(1-c).*(1-m);
acmy = c.*m.*y.*(1-k);
acmk = c.*m.*k.*(1-y);
acyk = c.*y.*k.*(1-m);
amyk = m.*y.*k.*(1-c);
acmyk = c.*m.*y.*k;

W=[aw ac am ay ak acm acy ack amy amk ayk acmy acmk acyk amyk acmyk];
```

```matlab
%% Input tristimulus values
Xin = XYZin(:,1);
Yin = XYZin(:,2);
Zin = XYZin(:,3);

%% Calculate the predicted values of XYZ
X = (W*Xin);
Y = (W*Yin);
Z = (W*Zin);
XYZ=[X Y Z];


end
```

Yule-Nielsen modified Neugebauer model

```matlab
function XYZ = YNneugcmyk(XYZin, cmyk, n)

% YNneugcmy applies the Yule-Nielsen modified Neugebauer equations
% for 4-colour printing system.
%
% Input Arguments
% cmyk: m x 4 matrix for dot areas of c, m, y, k inks of the
% input colour patches for which XYZ is to be predicted.
%
% XYZin: 16 x 3 matrix for XYZ values of 16 Neugebauer primaries
% strictly in the following order.
% [white (paper),c,m,y,k,cm,cy,ck,my,mk,yk,cmy,cmk,cyk,myk,cmyk]
% n: the Yule-Nielsen factor to account for optical dot gain.
% Default value of n is 1 which results in Neugebauer model.
%
% Output Arguments
% XYZ: m x 3 matrix for the model-predicted XYZ values for the input
% CMYK
% values.
%
% Example: XYZ = YNneugcmyk (XYZin, cmykECI2002, 1.66);
% See also: neugcmyk, YNSNcmyk, YNneugcmy
%
% Kolourprint Dynamic Toolbox
% Author: © Kiran Deshpande
% E-mail: kiranudeshpande@gmail.com
% Last modified: 06/08/2013
% Matlab version R2013a (8.1.0.604)

%% Default value of n-factor
if nargin < 3
    n = 1;
end

%% Define colorant values and normalise for 0-1
c = cmyk(:,1)/100;
m = cmyk(:,2)/100;
y = cmyk(:,3)/100;
```

262

```matlab
k = cmyk(:,4)/100;

%% calculate relative areas
aw = (1-c).*(1-m).*(1-y).*(1-k);
ac = c.*(1-m).*(1-y).*(1-k);
am = m.*(1-c).*(1-y).*(1-k);
ay = y.*(1-c).*(1-m).*(1-k);
ak = k.*(1-c).*(1-m).*(1-y);
acm = c.*m.*(1-y).*(1-k);
acy = c.*y.*(1-m).*(1-k);
ack = c.*k.*(1-m).*(1-y);
amy = m.*y.*(1-c).*(1-k);
amk = m.*k.*(1-c).*(1-y);
ayk = y.*k.*(1-c).*(1-m);
acmy = c.*m.*y.*(1-k);
acmk = c.*m.*k.*(1-y);
acyk = c.*y.*k.*(1-m);
amyk = m.*y.*k.*(1-c);
acmyk = c.*m.*y.*k;

W = [aw ac am ay ak acm acy ack amy amk ayk acmy acmk acyk amyk
acmyk];

%% Input tristimulus values
Xin = XYZin(:,1).^(1/n);
Yin = XYZin(:,2).^(1/n);
Zin = XYZin(:,3).^(1/n);

%% Calculate the predicted values of XYZ
X = (W*Xin).^n;
Y = (W*Yin).^n;
Z = (W*Zin).^n;
XYZ=[X Y Z];

end
```

Yule-Nielsen modified Spectral Neugebauer (YNSN) model

```matlab
function R = YNSNcmyk(Rin,cmyk,n)

% YNSNcmyk applies the Yule-Nielsen Spectral Neugebauer equations
% for 4-colour printing system.
%
% Input Arguments
% Rin: 16 x p matrix for spectral reflectance values of 16 Neugebauer
% primaries strictly in the order as follows:
% [white (paper),c,m,y,k,cm,cy,ck,my,mk,yk,cmy,cmk,cyk,myk,cmyk]
%
% cmyk: m x 4 matrix for dot areas (%) of c, m, y, k inks of the
% input colour patches for which reflectance R is to be predicted.
%
% p is the no. of reflection values for the given spectral
% reflectance., for example, p=36 for the wavelength range of 380 to
% 730 with 10 nm
% interval.
```

```matlab
%
% Output Arguments
% R: m x p matrix of the predicted spectra for CMYK dot areas.
%
% n: the Yule-Nielsen factor to account for optical dot gain.
% Default value of n is 1 which results in Spectral Neugebauer model.
%
% Example: R = YNSNcmyk (Rin, cmykECI2002, 1.7);
% See also: cellYNSNcmyk, neugcmyk, YNneugcmyk
%
% Kolourprint Dynamic Toolbox
% Author: © Kiran Deshpande
% E-mail: kiranudeshpande@gmail.com
% Last modified: 23/06/2014
% Matlab version R2013a (8.1.0.604)

%% Default value of n-factor
if nargin < 3
    n = 1;
end

%% Define colorant values and normalise for 0-1 range
c = cmyk(:,1)/100;
m = cmyk(:,2)/100;
y = cmyk(:,3)/100;
k = cmyk(:,4)/100;

%% Calculate relative area for each primary

aw = (1-c).*(1-m).*(1-y).*(1-k);
ac = c.*(1-m).*(1-y).*(1-k);
am = m.*(1-c).*(1-y).*(1-k);
ay = y.*(1-c).*(1-m).*(1-k);
ak = k.*(1-c).*(1-m).*(1-y);
acm = c.*m.*(1-y).*(1-k);
acy = c.*y.*(1-m).*(1-k);
ack = c.*k.*(1-m).*(1-y);
amy = m.*y.*(1-c).*(1-k);
amk = m.*k.*(1-c).*(1-y);
ayk = y.*k.*(1-c).*(1-m);
acmy = c.*m.*y.*(1-k);
acmk = c.*m.*k.*(1-y);
acyk = c.*y.*k.*(1-m);
amyk = m.*y.*k.*(1-c);
acmyk = c.*m.*y.*k;

W = [aw ac am ay ak acm acy ack amy amk ayk acmy acmk acyk amyk
acmyk];

%% Calculate the predicted spectra
Rin = Rin.^(1/n);
R = (W*Rin).^n;


end
```

Cellular YNSN model

```matlab
function R = cellYNSNcmyk(Rin,cmyk,nodes,n)
%
% cellYNSNcmyk applies the Cellular YNSN model for the 4-colour
% printing
% system.
%
% Input Arguments
% cmyk: m x 4 matrix for dot areas (%) of c, m, y, k inks of the
% input colour patches for which reflectance R is to be predicted.
%
% Rin: (nodes^4) x 36 matrix containing reflectance values of
% (nodes^4) Neugebauer primaries, where 'nodes' is the no. of nodes in
% each axis of c,m,y,k.
%, for example, if nodes=3 (i.e.0,0.5,1) then size(Rin)=81 by 3.
%
% Rin values must correspond to uniform table for cmyk values
% in which the first dimension (Cyan) varies most slowly and the last
% dimension (Black) varies fastest.
%, for example,  0    0    0      0
%       0    0    0     50
%       0    0    0    100
%       0    0   50      0
%       0    0   50     50
%       0    0   50    100
%       .    .    .      .
%       .    .    .      .
%
% n: is the Yule-Nielsen factor to account for optical dot gain.
% Default value of n is 1 which results in cellular Neugebauer model.
%
% Example: R = cellYNSNcmyk (Rin, cmykECI2002, 9, 1.7);
% See also: extract4d, YNSNcmyk, YNneugcmyk, neugcmyk
%
% Kolourprint Dynamic Toolbox
% Author: © Kiran Deshpande
% E-mail: kiranudeshpande@gmail.com
% Last modified: 23/06/2014
% Matlab version R2013a (8.1.0.604)

%% Default value of n-factor
if nargin < 4
    n = 1;
end
% check if the no. of rows of Rin are equal to (nodes^4).
r = size(cmyk,1);
rr = size(Rin,1);
if rr~=nodes^4
    error('No. of rows of Rin must be equal to (nodes^4)');
end


%% Define colorant values and normalise for 0-1 range
cmyk = cmyk/100;
c = cmyk(:,1);
m = cmyk(:,2);
```

```matlab
y = cmyk(:,3);
k = cmyk(:,4);

%% Extract bounding cube for each of the input cmyk values
lut_rows = extract4d(cmyk,nodes);     % index entries of bounding cell

%% Find 16 Neugebauer primaries for each bounding cell
% preallocate xyz primaries for each patch (i.e. each row of cmyk)
Rpri = zeros([16 36 r]);

for i = 1:r
    Rpri(:,:,i) = Rin(lut_rows(i,:),:);     % each page of xyzpri gives
16 primaries
end

%% Create cells (4D LUT) within cmyk colour space
nodes = linspace(0,1,nodes);
[x1,x2,x3,x4] = ndgrid(nodes,nodes,nodes,nodes);
M = [x4(:) x3(:) x2(:) x1(:)];

%% Effective (normalised) values for c,m,y,k
% find lower & upper limits of c,m,y,k for each input row
cmyklu = zeros([2 4 r]);  % preallocate 2 by 4 matrix for lower and
upper limits of c,m,y,k

% preallocate Cl: r by 1 vector showing lower limit for each input row
Cl = zeros(r,1);
Cu = Cl;Ml = Cl;Mu = Cl;Yl = Cl;Yu = Cl;Kl = Cl;Ku = Cl;

% 1st row gives lower limits and last row gives upper limits; see
'extract4d.m'
for i = 1:r
    cmyklu(:,:,i) = M(lut_rows(i,[1 end]),:);
    Cl(i) = cmyklu(1,1,i);
    Cu(i) = cmyklu(2,1,i);
    Ml(i) = cmyklu(1,2,i);
    Mu(i) = cmyklu(2,2,i);
    Yl(i) = cmyklu(1,3,i);
    Yu(i) = cmyklu(2,3,i);
    Kl(i) = cmyklu(1,4,i);
    Ku(i) = cmyklu(2,4,i);
end

%% Calculate effective values from lower and upper limits
ceff = (c-Cl)./(Cu-Cl);
meff = (m-Ml)./(Mu-Ml);
yeff = (y-Yl)./(Yu-Yl);
keff = (k-Kl)./(Ku-Kl);
cmykeff = cat(2,ceff,meff,yeff,keff);
cmykeff = cmykeff*100;
%% Apply YN modified Neugebauer model to each row
R = zeros(r,36);      % preallocate xyz output

% Apply YNSN model to each row of cmykeff using each page of xyzpri
for i = 1:r
    R(i,:) = YNSNcmyk(Rpri(:,:,i),cmykeff(i,:),n);
end
```

Kubelka-Munk model

```matlab
function R = km1cmyk(Rin, cmyk, k1, k2)

% km1cmyk applies Single Constant Kubelka-Munk model for CMYK process
% to determine reflection spectra for the given concentration of cmyk
% with Saunderson correction.
%
% Input Arguments
% Rin: 5 x p matrix for spectral reflectances of substrate and primary
% inks. 5 rows consist of spectral data of [white, c, m, y, k].
%
% p is the no. of reflection values for the given spectral
% reflectance., for example, p=36 for the wavelength range of 380 to
% 730 with 10 nm interval.
%
% cmyk: n x 4 matrix for dot areas of c, m, y, k with range 0-100.
%
% Output Arguments
% R: n x m matrix of predicted spectral reflectances for 'n' colour
% patches.
%
% Example: R = km1cmyk (Rin, cmykECI2002, 0.03, 0.6);
% See also: YNSNcmyk
%
% Kolourprint Dynamic Toolbox
% Author: © Kiran Deshpande
% E-mail: kiranudeshpande@gmail.com
% Last modified: 23/06/2014
% Matlab version R2013a (8.1.0.604)

%% Default values of k1 and k2
if nargin == 2
    k1 = 0;
    k2 = 0;
end

%% Measured reflectances of white, c, m, y, k

rw = Rin(1,:);
rc = Rin(2,:);
rm = Rin(3,:);
ry = Rin(4,:);
rk = Rin(5,:);


%% Apply Saunderson's correction

rw = (rw-k1)./(1-k1-k2+k2.*rw);
rc = (rc-k1)./(1-k1-k2+k2.*rc);
rm = (rm-k1)./(1-k1-k2+k2.*rm);
ry = (ry-k1)./(1-k1-k2+k2.*ry);
rk = (rk-k1)./(1-k1-k2+k2.*rk);

%% Apply clipping in case rw,rc,rm,ry,rk is zero
```

```
rw(rw==0) = 0.0001;
rc(rc==0) = 0.0001;
rm(rm==0) = 0.0001;
ry(ry==0) = 0.0001;
rk(rk==0) = 0.0001;

%% Normalize cmyk dot areas for 0-1 range

c = cmyk(:,1)/100;
m = cmyk(:,2)/100;
y = cmyk(:,3)/100;
k = cmyk(:,4)/100;

%% Calculate the K/S ratios

ksw = ((1-rw).^2)./(2*rw);
ksc = ((1-rc).^2)./(2*rc);
ksm = ((1-rm).^2)./(2*rm);
ksy = ((1-ry).^2)./(2*ry);
ksk = ((1-rk).^2)./(2*rk);

r1 = size(cmyk,1);

ksw = repmat(ksw,r1,1);
ks = ksw+c*ksc+m*ksm+y*ksy+k*ksk;

%% Calculate R from the single constant ratio K/S

R = 1+ks-((ks.^2)+(2*ks)).^0.5;

%% Apply Inverse of Saunderson's correction

R = k1+((1-k1)*(1-k2)*R)./(1-k2*R);
end
```

Van De Capelle and Meireson model

```
function R = meireson(colprm, Rbg, cmyk)

% meireson calculates the spectral reflectance by using a method
% proposed by Van de Capelle and Meireson (1997).
%
% Input Arguments
% colprm: m x n matrix containing colorant parameters Sp,up,ap for
% each colorant.
% Sp: scattering parameter
% up: interaction parameter
% ap: absorption parameter
%, for example, if the printing ink sequence is c-m-y-k then colprm
% consists of [Spc;upc;apc;Spm;upm;apm;Spy;upy;apy;Spk;upk;apk].
%
% 33 rows of Rin should be in the following order:
% R_100_w, R_100_g, R_100_k, R_90_w, R_90_g, R_90_k, ..., R_0_w,
% R_0_g, R_0_k.
```

```matlab
% where R: spectral reflectance values; (100, 90,..., 0): dot% of ink;
% (w, g, k): white, grey, black background on which ink is printed.
%
% Example: R = meireson (colprm, Rb, cmykECI2002);
% See also: inkprofile
%
% Kolourprint Dynamic Toolbox
% Author: © Kiran Deshpande
% E-mail: kiranudeshpande@gmail.com
% Last modified: 23/06/2014
% Matlab version R2013a (8.1.0.604)

%% Define colorant values and normalise for 0-1 range
c = cmyk(:,1);
m = cmyk(:,2);
y = cmyk(:,3);
k = cmyk(:,4);

% get no. of rows of colprm and divide by 12 i.e. no. of parameters
r = size(colprm,1)/12;

%% Extract the model coefficients from 'colprm' input
Spc = colprm(r:-1:1,:);
upc = colprm((2*r:-1:(r+1)),:);
apc = colprm((3*r:-1:(2*r+1)),:);
Spm = colprm((4*r:-1:(3*r+1)),:);
upm = colprm((5*r:-1:(4*r+1)),:);
apm = colprm((6*r:-1:(5*r+1)),:);
Spy = colprm((7*r:-1:(6*r+1)),:);
upy = colprm((8*r:-1:(7*r+1)),:);
apy = colprm((9*r:-1:(8*r+1)),:);
Spk = colprm((10*r:-1:(9*r+1)),:);
upk = colprm((11*r:-1:(10*r+1)),:);
apk = colprm((12*r:-1:(11*r+1)),:);

% prepare the matrix for the background spectra
Rbg = repmat(Rbg,size(cmyk,1),1);

%% Calculate the predicted spectra from coefficients
Rcpred = ((1-apc(c+1,:)).*(Rbg.^upc(c+1,:)))+Spc(c+1,:);
Rcmpred = ((1-apm(m+1,:)).*(Rcpred.^upm(m+1,:)))+Spm(m+1,:);
Rcmypred=((1-apy(y+1,:)).*(Rcmpred.^upy(y+1,:)))+Spy(y+1,:);
R = ((1-apk(k+1,:)).*(Rcmypred.^upk(k+1,:)))+Spk(k+1,:);
end


---


function [Sp,up,ap] = inkprofile(Rin)

% 'inkprofile' calculates the colorant parameters defined by Van de
% Capelle and Meireson (1997) as follows:
% Sp: scattering parameter
% up: interaction parameter
% ap: absorption parameter
%
% Rin: 33 x n matrix containing spectral measurements of the 11-steps
```

```matlab
% ink-profiling chart of Kaleidoscope® (EskoArtwork).
% n is the no. of reflection values for the given spectral
% reflectance., for example, p=36 for the wavelength range of 380 to
% 730 with 10 nm interval.
%
% 33 rows of Rin should be in the following order:
% R_100_w, R_100_g, R_100_k, R_90_w, R_90_g, R_90_k, ..., R_0_w,
% R_0_g, R_0_k.
% where R: spectral reflectance values; (100, 90,..., 0): dot% of ink;
% (w, g, k): white, grey, black background on which ink is printed.
%
%
% Example: [Sp,up,ap]=inkprofile(Rin);
% See also: meireson
%
% Kolourprint Dynamic Toolbox
% Author: © Kiran Deshpande
% E-mail: kiranudeshpande@gmail.com
% Last modified: 23/06/2014
% Matlab version R2013a (8.1.0.604)

%% Check the number of patches in Rin
s=size(Rin,1);

if s~=33
    if s~=303
        error('No. of rows for Rin must be either 33 or 303')
    end
end

% 11-step chart on three backgrounds
if s==33
    Rw=Rin(31,:);
    Rg=Rin(32,:);
    Rk=Rin(33,:);
    Rpiw=Rin(1:3:31,:);
    Rpig=Rin(2:3:32,:);
    Rpik=Rin(3:3:33,:);

% interpolate for intermediate dot areas, for example, 1%,2%,3% etc.
    x=(0:10:100)';
    xi=(0:1:100)';
    Rpiw=interp1(x,Rpiw,xi);
    Rpig=interp1(x,Rpig,xi);
    Rpik=interp1(x,Rpik,xi);
end

% 101-step chart on three backgrounds
if s==303
    Rw=Rin(101,:);
    Rg=Rin(202,:);
    Rk=Rin(303,:);
    Rpiw=Rin(1:101,:);
    Rpig=Rin(102:202,:);
    Rpik=Rin(203:303,:);
end

% size(Rpiw,1)=101 i.e. no. of rows (0,1,2,...,98,99,100)
Rw=repmat(Rw,size(Rpiw,1),1);
```

```matlab
Rg=repmat(Rg,size(Rpig,1),1);
Rk=repmat(Rk,size(Rpik,1),1);

% calculate Sp parameter
Sp=Rpik-Rk;
Sp(Sp<0)=0;

RRpiw=Rpiw-Sp;
RRpig=Rpig-Sp;

%% Normalise/clipping for RRpiw, RRpig, Rw, Rg

RRpiw(RRpiw<eps & RRpiw>-eps)=eps;
RRpig(RRpig<eps & RRpig>-eps)=eps;
Rw(Rw<eps & Rw>-eps)=eps;
Rg(Rg<eps & Rg>-eps)=eps;

up=(log(RRpiw./RRpig)./log(Rw./Rg));
%up(isnan(up))=1;         % to replace NaN (not-a-number) with 1
%up=real(up);             % to exclude imaginary part of up
%up(isinf(up))=1;         % to replace Inf nos. caused due to RRpig=0
or denominator=0
%up(up>1)=1;              % to normalize up for 0-1

%% Normalise/clipping for up
up(abs(RRpiw-RRpig)<0.0001)=1;
up(Rw==Rg)=1;
up(up<0.0001)=0.0001;
ap=1-((RRpiw./(Rw.^up)));

%% Normalise/clipping for ap
ap(abs(RRpiw-RRpig)<0.0001)=0.0001;
ap(ap<0.0001)=0.0001;
end
```

Spot colour overprint (SCOP) model

```matlab
function xyz = SCOPcmyk( xyzin, cmyk, inputdots )

% SCOPcmyk applies the spot colour overprint model with power
% regression to predict the L*a*b* values of the given colorant values
% 'inputdots'.
% (Deshpande, 2010). Deshpande, K. and Green, P. (2011) Regression
% method for predicting the colorimetry of spot colour overprints,
% Proc. 38th IARIGAI conf. Budapest, Hungary.
%
% Input Arguments
% xyzin: m x 3 matrix of the tristimulus values of training set
% colour patches. The training set is used for calculating the model
% coefficients.
% cmyk: m x 4 matrix of CMYK (or OMYK/CGYK/CMVK) from 0 to 100%. They
% are the colorant values for 'xyzin'. The last column should always
% represent black (K) ink. The ink-sequence for printing should always
% start with K-ink1-ink2-ink3, for example, K-C-M-Y or K-O-M-Y or K-C-
% G-Y or K-C-M-V
```

```matlab
% Together 'cmyk' and 'xyzin' forms the inkprofiling chart
% measurements.
% The training set need not to be the full inkprofiling chart. It can
% be any number of tints of the given ink, for example, 0%, 50% and
% 100% on three backgrounds or two backgrounds.
% inputdots: p x 4 colorant values for which the XYZ colours are to be
% calculated.
%
% Output Arguments
% xyz: p x 3 predicted colours (XYZ) for the given colorant values
% 'inputdots'.
%
% Example: lab = spotoverprint4col(it87cmyk, Rm_it87, input_cmyk);
% See also: powercoeffpxyz, powercoeffallxyz
%
% Kolourprint Dynamic Toolbox
% Author: © Kiran Deshpande
% E-mail: kiranudeshpande@gmail.com
% Last modified: 23/06/2014
% Matlab version R2013a (8.1.0.604)

%% Calculate the model coefficients
cmykxyz = [cmyk xyzin];

coef1 = powercoeffallxyz(xyzin, cmyk, 'ink1');
coef2 = powercoeffallxyz(xyzin, cmyk, 'ink2');
coef3 = powercoeffallxyz(xyzin, cmyk, 'ink3');

%% All XYZ for black - 0 to 100%
black = cmykxyz((cmyk(:,1)==0&cmyk(:,2)==0&cmyk(:,3)==0),:);
[C, ia] = unique(black(:,1:4),'rows');
black = black(ia,:);
black = interp1(black(:,4),black(:,5:7),(0:1:100)');

%% All XYZ for ink1 - 0 to 100%
ink1 = cmykxyz((cmyk(:,2)==0&cmyk(:,3)==0&cmyk(:,4)==0),:);
[C, ia] = unique(ink1(:,1:4),'rows');
ink1 = ink1(ia,:);
ink1 = interp1(ink1(:,1),ink1(:,5:7),(0:1:100)');

%% All XYZ for ink2 - 0 to 100%
ink2 = cmykxyz((cmyk(:,1)==0&cmyk(:,3)==0&cmyk(:,4)==0),:);
[C, ia] = unique(ink2(:,1:4),'rows');
ink2 = ink2(ia,:);
ink2 = interp1(ink2(:,2),ink2(:,5:7),(0:1:100)');

%% All XYZ for ink3 - 0 to 100%
ink3 = cmykxyz((cmyk(:,1)==0&cmyk(:,2)==0&cmyk(:,4)==0),:);
[C, ia] = unique(ink3(:,1:4),'rows');
ink3 = ink3(ia,:);
ink3 = interp1(ink3(:,3),ink3(:,5:7),(0:1:100)');

C = inputdots(:,1);
M = inputdots(:,2);
Y = inputdots(:,3);
K = inputdots(:,4);
```

```matlab
%% First iteration - K + ink1 (or K + Cyan)
xyzb = black(K+1,:);
xyzf = ink1(C+1,:);

jx = coef1(C+1,1); kx = coef1(C+1,2);
jy = coef1(C+1,3); ky = coef1(C+1,4);
jz = coef1(C+1,5); kz = coef1(C+1,6);

x = jx.*(xyzf(:,1).*xyzb(:,1)).^kx;
y = jy.*(xyzf(:,2).*xyzb(:,2)).^ky;
z = jz.*(xyzf(:,3).*xyzb(:,3)).^kz;

xyzb = [x y z];
ind = find(K==0);
xyzb(ind,:) = ink1(C(ind)+1,:);

%% Second iteration - (K+ink1) + ink2
xyzf = ink2(M+1,:);

jx = coef2(M+1,1); kx = coef2(M+1,2);
jy = coef2(M+1,3); ky = coef2(M+1,4);
jz = coef2(M+1,5); kz = coef2(M+1,6);

x = jx.*(xyzf(:,1).*xyzb(:,1)).^kx;
y = jy.*(xyzf(:,2).*xyzb(:,2)).^ky;
z = jz.*(xyzf(:,3).*xyzb(:,3)).^kz;

%% Third iteration - (K+ink1+ink2)+ink3
xyzb = [x y z];
xyzf = ink3(Y+1,:);

jx = coef3(Y+1,1); kx = coef3(Y+1,2);
jy = coef3(Y+1,3); ky = coef3(Y+1,4);
jz = coef3(Y+1,5); kz = coef3(Y+1,6);

x = jx.*(xyzf(:,1).*xyzb(:,1)).^kx;
y = jy.*(xyzf(:,2).*xyzb(:,2)).^ky;
z = jz.*(xyzf(:,3).*xyzb(:,3)).^kz;

xyz = [x y z];
end
```

```matlab
function coef = powercoeffallxyz(xyzin, cmyk, ink)

% 'POWERCOEFFALL' derives coefficients of all dot percentages for an
% ink, required for the spot colour overprint model with power
% regression

%% Check 'ink' input
if nargin < 3
    ink = 'ink1'; % default ink is ink1 (e.g. Cyan in case of CMYK)
end

% Check validity of 'ink'
validStrings = {'ink1','ink2','ink3'};
```

```matlab
ink = validatestring(ink, validStrings,'powercoeffall','ink');

%% Find the relevant ink-combinations & index of column for each ink
switch ink
    case 'ink1'
        inkdot = cmyk((cmyk(:,2)==0&cmyk(:,3)==0),:); % m=0 & y=0
        col = 1;      % column of ink1 is '1'
    case 'ink2'
        inkdot = cmyk((cmyk(:,1)==0&cmyk(:,3)==0),:);
        col = 2;
    case 'ink3'
        inkdot = cmyk((cmyk(:,1)==0&cmyk(:,2)==0),:);
        col = 3;
end

inkdot = unique(inkdot,'rows'); %remove duplicates
%% Find those dot percentages having at least 4 unique combinations
% with black ink, for example, [20 0; 20 100]. Each dot percentage
% will be used for calculating the individual coefficients
ind = unique(inkdot(:,col));      %unique dot percentage of the ink
n = histc(inkdot(:,col),ind);     %frequency of each dot percentage
p = ind(n > 4);   %check those dot percentages with more than 4
frequency

%% Apply 'powercoeffp.m' to find the model coefficients for each dot
% percentage
row = size(p,1);     % number of dot percentages (rows)
coef = zeros (row,6);    % pre-allocate the 'coefficients' matrix
for i = 1:row
    coef(i,:) = powercoeffpxyz(xyzin, cmyk, p(i), ink);
end

%% Interpolate for 0 to 100% from the existing coefficients
pi = (0:1:100)';
coef = interp1(p,coef,pi);
end
```

```matlab
function [coef,cp] = powercoeffpxyz(xyzin, cmyk, p, ink)

% 'POWERCOEFFP' derives coefficients of the given dot percentage 'p'
% for an ink, required for the spot colour overprint model with power
% regression

%% default ink is ink1 (e.g. Cyan in case of CMYK)
if nargin < 4
    ink = 'ink1';
end

% Check validity of 'ink'
validStrings = {'ink1','ink2','ink3'};
ink = validatestring(ink, validStrings,'powercoeffp','ink');

%% Find the ink-combinations required for calculating the coefficients
% for the given dot percentage 'p' of the required ink. Also prepare a
% matrix for foreground colour, for example, [50 0 0 0] in case of
% ink1.
```

```matlab
switch ink
    case 'ink1'
        cip=find(cmyk(:,2)==0&cmyk(:,3)==0&cmyk(:,1)==p);
        [fg,ic]=intersect(cmyk,[p 0 0 0],'rows');
    case 'ink2'
        cip=find(cmyk(:,1)==0&cmyk(:,3)==0&cmyk(:,2)==p);
        [fg,ic]=intersect(cmyk,[0 p 0 0],'rows');
    case 'ink3'
        cip=find(cmyk(:,1)==0&cmyk(:,2)==0&cmyk(:,3)==p);
        [fg,ic]=intersect(cmyk,[0 0 p 0],'rows');
end

%% Find the unique combinations (remove duplicates)
cp=cmyk(cip,:);
xyzmp=xyzin(cip,:);
[C,ia]=unique(cp(:,1:4),'rows');
cp=cp(ia,:);
xyzmp=xyzmp(ia,:);

%% Find the background colours
% For the given ink-combinations (cp), find the background colours
bg=cp(:,1:4);

switch ink
    case 'ink1'
        bg(:,1)=0;
    case 'ink2'
        bg(:,2)=0;
    case 'ink3'
        bg(:,3)=0;
end

[bg,ia]=intersect(cmyk,bg,'rows');
xyzb=xyzin(ia,:);

%% Find the foreground colours for the ink-combinations 'cp'
xyzf=repmat(xyzin(ic,:),size(cp,1),1);

%% Calculate the product of the background and the foreground colours
prod = xyzb.*xyzf;

%% Calculate the coefficients jxp, kxp, jyp, kyp, jzp, kzp
% Use power regression with 'polyfit'
coefx = polyfit(log(prod(:,1)),log(xyzmp(:,1)),1);
jxp=exp(coefx(2));kxp=coefx(1);

coefy = polyfit(log(prod(:,2)),log(xyzmp(:,2)),1);
jyp=exp(coefy(2));kyp=coefy(1);

coefz = polyfit(log(prod(:,3)),log(xyzmp(:,3)),1);
jzp=exp(coefz(2));kzp=coefz(1);

coef = [jxp, kxp, jyp, kyp, jzp, kzp];
end
```